

**HSCTM-2D, A FINITE ELEMENT MODEL FOR
DEPTH-AVERAGED HYDRODYNAMICS, SEDIMENT AND
CONTAMINANT TRANSPORT**

By

Earl J. Hayter^{1,4}, Mary A. Bergs², Ruochuan Gu³,
Steve C. McCutcheon⁴, S. Jarrell Smith^{1,5}, and Holly J. Whiteley¹

¹Department of Civil Engineering
Clemson University
Clemson, South Carolina 29634-0911

²Department of Civil Engineering
University of Toledo
Toledo, Ohio 43606

³Department of Civil Engineering
Iowa State University
Ames, Iowa 50010

⁴National Exposure Research Laboratory
Ecosystems Research Division
U. S. Environmental Protection Agency
Athens, Georgia 30605

⁵U.S. Army Engineer Waterways Experiment Station
Coastal Engineering Research Center
P.O. Box 631
Vicksburg, Mississippi 39180

NATIONAL EXPOSURE RESEARCH LABORATORY
OFFICE OF RESEARCH AND DEVELOPMENT
U. S. ENVIRONMENTAL PROTECTION AGENCY
ATHENS, GEORGIA 30605

DISCLAIMER

The information in this document has been funded wholly or in part by the United States Environmental Protection Agency under Cooperative Agreement CR819025-02-1 to Clemson University. It has been subjected to the Agency's peer and administrative review, and it has been approved for publication as an EPA document. Mention of trade names or commercial products does not constitute endorsement or recommendation for use.

FOREWORD

As environmental controls become more costly to implement and the penalties of judgement errors become more severe, environmental quality management requires more efficient analytical tools based on greater knowledge of the environmental phenomena to be managed. As part of this Laboratory's research on the occurrence, movement, transformation, impact, and control of environmental contaminants, the Assessment Branch develops management or engineering tools to help pollution control officials achieve water quality goals in impoundments, streams, and estuaries.

Clays and other cohesive sediments may influence water quality in estuaries by affecting aquatic life, by providing a large assimilative capacity, and by acting as a transporting mechanism for dissolved and particulate pollutants. In fact, the bulk of the pollution load in an estuary is quite often adsorbed to cohesive sediments rather than being dissolved in the water column. The assimilation and storage of contaminants in bottom sediments, then, is an important component of any water quality evaluation. The HSCTM-2D model addresses the movement (or non-movement) of bottom sediments and thereby assists in predicting the fate of pesticides and other organic chemicals, heavy metals, and other adsorbed contaminants.

Rosemarie C. Russo, Ph.D.
Director
National Exposure Research Laboratory
Ecosystems Research Division
Athens, Georgia

ABSTRACT

HSCTM-2D (**H**ydrodynamic, **S**ediment and **C**ontaminant **T**ransport **M**odel) is a finite element modeling system for simulating two-dimensional, vertically-integrated, surface water flow (typically riverine or estuarine hydrodynamics), sediment transport, and contaminant transport. The modeling system consists of two modules, one for hydrodynamic modeling (HYDRO2D) and the other for sediment and contaminant transport modeling (CS2D). One example problem is included. The HSCTM-2D modeling system may be used to simulate both short term (less than 1 year) and long term scour and/or sedimentation rates and contaminant transport and fate in vertically well mixed bodies of water.

HYDRO2D solves the equations of motion and continuity for nodal depth-averaged horizontal velocity components and flow depths. The effects of bottom, internal and surface shear stresses, horizontal salinity gradients, and the Coriolis force are represented in the equations of motion.

CS2D solves the advection-dispersion equation for nodal vertically-integrated concentrations of suspended sediment, dissolved and sorbed contaminants, and bed surface elevations. The processes of dispersion, aggregation, erosion, deposition, adsorption and desorption are simulated. A layered bed model is used in simulating bed formation and subsequent erosion. Sediment bed structure (density and shear strength profiles, thickness and elevation), net change in bed elevation and net vertical mass flux of sediment over an interval of time (e.g., over a certain number of tidal cycles), average amount of time sediment particles are in suspension, and the downward flux of sediment onto the bed are calculated for each element.

HSCTM-2D can be run in an uncoupled or semi-coupled mode. In the uncoupled mode, HYDRO2D is run separately from CS2D. In the semi-coupled mode, HYDRO2D and CS2D are run in the following fashion. First, HYDRO2D calculates the flow field for the current time step. Second, the predicted flow field is used in CS2D to calculate the transport of sediments and contaminants during the same time step. HYDRO2D is run at every time step to update the flow field to account for predicted changes in nodal flow depths due to erosion and deposition. In addition, HSCTM-2D has a default option that will allow the user to make relative comparisons between sites or designs with limited data. To obtain a quantitative analysis, the user must run the non-default option with a complete set of data.

This report was written cooperatively in partial fulfillment of cooperative agreement with Clemson University under the sponsorship of the U.S. Environmental Protection Agency. This report covers a period from October 1991 to September 1994, and work was completed as of May 1995.

TABLE OF CONTENTS

	<u>Page</u>
DISCLAIMER	ii
FOREWORD	iii
ABSTRACT	iv
FIGURES	ix
TABLES	xii
ABBREVIATIONS AND SYMBOLS	xiii
ACKNOWLEDGMENTS	xix
1 INTRODUCTION	1
1.1 EXPERIENCE REQUIRED TO USE HSCTM-2D	1
1.2 SEDIMENTATION-RELATED PROBLEMS IN SURFACE WATERS	2
1.3 CONTAMINATION PROBLEMS IN SURFACE WATERS	2
1.4 MODEL DESCRIPTION	4
1.4.1 Approach to the Problems	4
1.4.2 Overview of the Modeling System	5
1.5 ORGANIZATION OF THE DOCUMENT	8
2 MODEL DEVELOPMENT, DISTRIBUTION AND SUPPORT	9
3 THEORY	10
3.1 ESTUARIAL DYNAMICS	10
3.1.1 General Description	10
3.1.2 Governing Equations	11
3.1.2.1 Coordinate System	11
3.1.2.2 Equations of Motion	11
3.2 COHESIVE SEDIMENT TRANSPORT	14
3.2.1 Description and Properties of Cohesive Sediments	14
3.2.1.1 Composition	14
3.2.1.2 Structure	15
3.2.1.3 Interparticle Forces	15
3.2.1.4 Cation Exchange Capacity	16
3.2.2 Estuarial Cohesive Sediment Transport	17
3.2.2.1 Overview	17
3.2.2.2 Sediment Bed	19
3.2.2.3 Erosion	23
3.2.2.4 Advection and Dispersion	30
3.2.2.5 Dispersive Transport	31
3.2.2.6 Coagulation	34
3.2.2.7 Aggregation	38
3.2.2.8 Settling	39

	3.2.2.9 Deposition	39
	3.2.2.10 Consolidation	55
3.3	COHESIONLESS SEDIMENT TRANSPORT	59
3.4	CONTAMINANT TRANSPORT	63
4	FINITE ELEMENT METHOD	70
4.1	INTRODUCTORY NOTE	70
4.2	DESCRIPTION	71
	4.2.1 Interpolation Functions	71
	4.2.2 Method of Weighted Residuals	75
	4.2.3 Discretization of Physical System	75
4.3	FINITE ELEMENT FORMULATION	76
	4.3.1 Hydrodynamic Equations	76
	4.3.2 Sediment and Contaminant Transport Equations	78
	4.3.3 Boundary Conditions	79
	4.3.4 Equations Solver	80
5	DESCRIPTION OF THE MODELING SYSTEM	81
5.1	SYSTEM COMPONENTS	81
5.2	HYDRODYNAMIC MODULE	82
5.3	COHESIVE SEDIMENT TRANSPORT MODULE	82
	5.3.1 Bed Schematization	83
	5.3.2 Erosion Algorithm	87
	5.3.3 Dispersion Algorithm	90
	5.3.4 Deposition Algorithm	94
6	DATA COLLECTION AND MODEL CALIBRATION	99
6.1	DATA COLLECTION AND ANALYSIS	99
	6.1.1 Field Data Collection Program	99
	Hydrographic Survey	99
	Sediment Sampling Using Corers	101
	Measurement of Suspended Concentration, Salinity and Temperature	101
	Determination of Sediment Settling Velocity	103
	6.1.2 Laboratory Testing Program	103
	Properties of Undisturbed Sediment Cores	103
	Properties of Original Settled Bed	103
	Properties of New Deposits	104
	Aggregate Shear Strength and Density	104
	Fluid Composition	105
	Composition and Cation Exchange Capacity of the Sediment ..	105
6.2	MODEL CALIBRATION	106
	6.2.1 Hydrodynamic Module	106
	6.2.2 Sediment Transport Module	107

7	HSCTM-2D USER INSTRUCTIONS	108
7.1	MODELING SYSTEM LIMITATIONS	108
	7.1.1 Limitations of the Hydrodynamic Module	109
7.2	USER INSTRUCTIONS	110
7.3	DATA INPUT FOR MAIN PROGRAM OF HSCTM-2D	111
7.4	SYSTEM DATA OUTPUT	111
	7.4.1 Hydrodynamic Module	111
	7.4.2 Sediment Transport Module	111
	7.4.3 Contaminant Transport Module	112
8	DATA INPUT REQUIREMENTS	114
8.1	GRID GENERATION	114
8.2	DATA INPUT FOR MAIN PROGRAM OF HSCTM-2D	115
	8.2.1 Input/Output Filenames	115
8.3	HYDRODYNAMIC MODULE - DATA INPUT	117
8.4	SEDIMENT/CONTAMINANT TRANSPORT MODULE - DATA INPUT ..	117
	8.4.1 Data Set A: Job Control Cards	117
	8.4.2 Data Set B: Job Control Parameters	119
	8.4.3 Data Set C: Transient Problem Input	121
	8.4.4 Data Set D: Water and Sediment Properties	122
	8.4.5 Data Set E: Initial Concentration Field	126
	8.4.6 Data Set F: Original Settled Bed Profile	127
	8.4.7 Data Set G: Initial Velocity Field	128
	8.4.8 Data Set H: Initial Dispersion Coefficients	129
	8.4.9 Data Set I: Initial Settling Velocities	130
	8.4.10 Data Set J: Boundary Conditions	130
	8.4.11 Data Set K: New Salinities	131
	8.4.12 Data Set L: Dynamic Input	131
8.5	DATA MANAGEMENT	132
8.6	DEFAULT OPTION	132
9	EXAMPLE PROBLEM	135
	REFERENCES	143
	APPENDICES	
A	HSCTM-2D STRUCTURE	152
A.1	Subroutines in HYDRO2D	152
A.2	Subroutines in CS2D	153
B	LABORATORY SEDIMENT TESTING PROGRAM	156
B.1	Properties of Undisturbed Sediment Cores	156
B.2	Properties of Original Settled Bed	156
B.3	Properties of New Deposits	157

B.4	Fluid Composition	158
B.5	Composition and Cation Exchange Capacity of the Sediment	158
C	DATA OUTPUT FOR HSCTM-2D AND DATA INPUT FOR HYDRO2D	160
C.1	HSCTM-2D Binary Output File Format	161
C.2	Card Image Input Data Coding Instructions for HYDRO2D	162
C.3	Input Data Cards Description	173

FIGURES

<u>Fig. No.</u>	<u>Page</u>
1.1	Flowchart of HSCTM-2D Modeling System 7
3.1	Coordinate System 11
3.2	Schematic Representation of Transport and Shoaling Processes in the Mixing Zone of a Stratified Estuary (after Mehta and Hayter 1981). . 18
3.3	Time and Depth Variation of Suspended Sediment Concentration in the Savannah River Estuary (after Krone 1972). 20
3.4	Schematic Representation of the Physical States of Cohesive Sediments in Estuarial Mixing Zone (after Mehta <i>et al.</i> 1982a). 21
3.5	Bed Shear Strength Profiles as Functions of Salinity. 24
3.6	Relative Suspended Sediment Concentration versus Time for a Stratified Bed (after Mehta and Partheniades 1979). 27
3.7	Normalized Rate of Erosion versus Normalized Excess Shear Stress Using Kaolinite in Tap Water (after Mehta <i>et al.</i> 1982a). 28
3.8	Internal Circulation in a Partially Stratified Estuary. (a) A Transverse Section; (b) A Vertical Section (after Fischer <i>et al.</i> 1979). 36
3.9	Illustration of Wind-Induced Circulation (adapted from Fischer <i>et al.</i> 1979). 37
3.10	Comparison of the Collision Functions for Brownian, Shear and Differential-Sedimentation Coagulation (after Hunt 1980). 38
3.11	Ratio C/C_o versus Time for Kaolinite in Distilled Water (after Mehta and Partheniades 1975). 42
3.12	Ratio C_{eq}/C_o versus Bed Shear Stress τ_b (after Mehta and Partheniades 1975). 43
3.13	C_{eq}^* versus $\tau_b^* - 1$ (after Mehta and Partheniades 1975). 45
3.14	C^* in Percent versus t/t_{50} for Kaolinite in Distilled Water (after Mehta and Partheniades 1975). 46

3.15	Log t_{50} versus τ_b^* for Kaolinite in Distilled Water (after Mehta and Partheniades 1975).	48
3.16	Settling Velocity versus Concentration for San Francisco Bay Mud (after Krone 1962).	49
3.17	Settling Velocity versus Concentration (after Thorn 1981).	50
3.18	Effect of Size and Settling Velocity of Elementary Particles on the Coagulation Factor of Natural Muds (after Bellessort 1973).	52
3.19	Effect of Salinity on Settling Velocity of San Francisco Bay Mud (after Krone 1962).	53
3.20	Effect of Salinity on Settling Velocity of Avonmouth Mud (after Owen 1970).	54
3.21	Variation of Mean Bed Density with Consolidation Time (after Dixit 1982).	56
3.22	Variation of the Normalized Mean Bed Density versus Consolidation Time (after Dixit 1982).	56
3.23	Normalized Depth Below the Surface versus Normalized Bed Bulk Density for Avonmouth, Brisbane, Grangemouth and Belawan Muds (after Dixit 1982).	57
3.24	Normalized Depth Below the Bed Surface versus Normalized Bed Bulk Density for Consolidation Times (a) Less than 48 Hours and (b) Greater than 48 Hours (after Dixit 1982).	58
3.25	Normalized Bed Density Profiles for Different Bed Thicknesses.	60
3.26	Bed Shear Strength versus Distance Below the Initial Bed Surface for Various Consolidation Periods (after Dixit 1982).	61
3.27	Correlation of Bed Shear Strength with Bed Density (after Owen 1970).	62
4.1	Global and Local Coordinates	72
5.1	Bed Schematization Used in Bed Formation Algorithm	85
5.2	Hypothetical Shear Strength Profile Illustrating Determination of Bed Layer Thickness.	86
5.3	Apparent Settling Velocity Description in Domains Defined by Suspended Sediment Concentration and Bed Shear Stress	95

6.1	A Plot of Raw Viscometer Data Obtained from the U.S. Army Corps of Engineers Philadelphia District Sample (after Krone 1963).	106
9.1	Reach of Winyah Bay, South Carolina modeled.	138
9.2	Finite Element Grid used in the HSCTM-2D Modeling.	139
9.3	Velocity Vectors During Simulated Ebb Tide	140
9.4	Constant Length (indicate flow direction only) Velocity Vectors in the Marina During Ebb Tide	141
9.5	Sedimentation Contours (mm) after 5 Day Simulation	142

TABLES

	<u>Page</u>
3.1 Principal Factors Controlling Erosion of Saturated Cohesive Sediment Beds	25
4.1 Quadratic Shape Functions	73
5.1 Values of Erosion Rate Coefficients	91
5.2 Values of Deposition Rate Coefficients	97
8.1 Default Values Used for Listed Parameters when Using Default Option	139

ABBREVIATIONS AND SYMBOLS

ABBREVIATIONS

Ca	calcium (3.18)
Cd	cadmium
CEC	cation exchange capacity (§3.2.1.4)
Cl	chloride
cm	centimeter
CPU	central processing unit
CS2D	two-dimensional finite element sediment and contaminant transport module in HSCTM-2D
Cu	copper
erf	error function (eq. 3.23, eq. 3.26) (refer to a handbook of mathematical tables)
Fe	iron
FEM	Finite Element Method (§4.1)
g/l	grams per liter
HSCTM-2D	two dimensional finite element hydrodynamic and sediment & contaminant transport model
HYDRO2D	two-dimensional finite element hydrodynamic module in HSCTM-2D
Hz	hertz
K	potassium
kg	kilogram
kg/s	kilogram per second
kHz	kilohertz
km	kilometer
m	meter
meq	milliequivalent (§3.2.1.4)
m ³	cubic meter
Mg	magnesium (3.18)
Na	sodium (3.18)
NBC	number of boundary nodes with specified boundary conditions (FEM) (§4.3.2)
Ni	nickel
NLAYTM	number of UND layers (§5.3.1)
NP	number of nodes in the system (FEM) (§4.3.2)
Pb	lead
PCND	partially consolidated new deposit layers (§5.3.1)
ppt	parts per trillion
PVC	polyvinyl chloride
RMA2	two-dimensional finite element hydrodynamic model
SAR	sodium adsorption ratio (§3.2.2.3.1, 3.18)
TLAYM	thickness of each UND layer (§5.3.1)
UND	unconsolidated new deposit layers (§5.3.1)
Zn	zinc

SYMBOLS

Symbol	Definition (equation number, §section number where the symbol is first used)
α	empirical resuspension coefficient (3.11)
α_1	average empirical coefficient for the top PCND layer (5.4)
α_a	coefficient that describes the approximate (linear) function for the depth (4.10)
α_b	coefficient that describes the approximate (linear) function for the x velocity component (4.11)
α_c	coefficient that describes the approximate (linear) function for the y velocity component (4.12)
β	collision function (3.15)
β_b	collision function due to Brownian motion (3.16)
β_{ds}	collision function due to differential sedimentation (3.18)
β_{sh}	collision function due to internal shearing (3.17)
β_a	coefficient that describes the approximate (linear) function for the depth (4.10)
β_b	coefficient that describes the approximate (linear) function for the x velocity component (4.11)
β_c	coefficient that describes the approximate (linear) function for the y velocity component (4.12)
Γ	z/d (5.8)
ε	resuspension rate, rate of erosion (§3.2.2.3, 3.9, 3.10, 3.11)
ε	average erosion rate for the period Δt (5.3)
ε_{ij}	eddy viscosity acting in i direction on plane perpendicular to j direction (3.5)
ε_o	empirical resuspension coefficient (3.11)
ε_{o1}	average empirical coefficient for the top PCND layer (5.4)
$\varepsilon(t)$	erosion rate at time t (5.4, 5.5)
ε_v	kinematic eddy viscosity (§3.2.2.5)
ζ	variable length along the kth boundary (4.9)
η	local coordinate element (FEM) (§4.2.1)
η_i	nodal coordinate (FEM) (§4.2.1)
θ	degree of implicitness (4.17)
θ	$\frac{1}{2}(\theta(t) + \theta(t+\Delta t))$ where $\theta = C, t_{50}, C_{eq}^*$ and σ_2, τ_b^* , (5.19)
κ	von Karman turbulence constant = 0.40 (5.9)
Λ	function of d and P_d (3.22)
λ	$\Delta T \pm 0.02 \Delta T$ (5.1)
μ	dynamic viscosity of the fluid (3.16)
ν	kinematic viscosity of the fluid (3.18)
ξ	local coordinate element (FEM) (§4.2.1)
ξ_i	nodal coordinate (FEM) (§4.2.1)
π	$\pi = 3.141593$ (3.18)
ρ	fluid density (3.2, 3.3)
ρ_a	aggregate density (§6.1.2.4)
ρ_B	bed bulk density (§3.2.2.10)
ρ_f	floc density (3.18)
ρ_s	dry sediment density (3.9)

ρ_s	mean dry bed density (§3.2.2.10)
$\rho_{\infty s}$	fully consolidated mean dry bed density (Appendix B)
$\rho_s(Z)$	dry sediment density profile (§5.3.1)
σ_1	standard deviation of the log-normal relation given by eq. 3.23 (3.24)
σ_2	standard deviation of log-normal relationship of given by eq. 3.26 (3.27)
ζ	empirical wind shear coefficient (3.4)
τ_b	flow induced bed shear stress (§3.2.2.3, 3.10)
τ_b^*	τ_b/τ_{bmin} (3.24, 3.25, Figure 5.3)
τ_{bc}^*	specified characteristic value of τ_b^* (§5.3.4, Figure 5.3)
τ_{bmax}	maximum shear stress above which no sediment deposits (§3.2.2.9)
τ_{bmin}	minimum shear stress at which all sediment eventually deposits (p. 50, 3.25)
$\Delta\tau_b$	$= (\tau_b/\tau_c) - 1$ (§3.2.2.3)
τ_c	bed shear strength (§3.2.2.2.2, 3.10, 3.31, 5.6)
τ_c	average bed strength over Z_* (5.4)
τ_{cd}	critical shear stress above which no deposition occurs (3.20)
τ_{bi}	flow induced bed shear stress in i dir. (3.2, 3.3, 3.6)
τ_i^s	surface wind shear stress in i direction (3.2, 3.3, 3.4)
τ_{ij}	depth-averaged turbulent shear stress acting in i-direction on a plane perpendicular to j-direction (3.2, 3.3, 3.5)
τ_s	aggregate shear strength (§6.1.2.4)
ϕ	local latitude (§3.1.2.2.2)
ψ	angle between the positive x-axis and the wind direction (3.4)
ω	angular velocity of the earth (§3.1.2.2.2)
Ω	Coriolis parameter $= 2\omega\sin\phi$ (§3.1.2.2.2)
Ωv	Coriolis acceleration in Northern Hemisphere in x-direction (3.2)
$-\Omega u$	Coriolis acceleration in Northern Hemisphere in y-direction (3.3)
A_e	element subdomain (4.9)
[b]	element node matrix used to evaluate eq. 4.14
C	mass of sediment per unit volume of water and sediment mixture (§3.2.2.3, 3.9, 3.13, 3.19, 3.22, 5.12, 5.16, 5.20)
C	average concentration between times t and (t + Δt) (5.17, 5.18, 5.19)
{c}	vector of unknown nodal concentrations (4.14)
{C}	unknown nodal concentrations for the system (4.15)
C^*	variation of suspended sediment concentration with time, fraction of depositable sediment at any time t $C^* = (C_o - C)/(C_o - C_{eq})$ (3.26, 3.28)
C_{eq}	steady state equilibrium concentration (p. 49, 5.3.4)
C_{eq}^*	C_{eq}/C_o (p. 49, 3.23)
C_i	nodal point concentration (§4.2.1, 4.1)
C_j	approximate suspended sediment concentration at any location inside the jth element (4.1)
C_o	initial suspended sediment concentration (3.21)
C_z	Chezy coefficient (3.6)
C_1	concentration at lower limit of mutual interference range (§5.3.4, Figure 5.3, 5.13, 5.14)
C_2	value at which hindered settling begins (§5.3.4, Figure 5.3, 5.14, 5.15)

d	depth of flow (3.1)
d_e	thickness of sediment deposited per time step (§5.3.4)
\bar{d}_e	refer to equation between 5.17 and 5.18 (5.17)
d_i, d_j	effective diameter of a suspended sediment particle (3.15)
dN_i	number of particles with sizes between d_i and $[d_i + \Delta(d_i)]$ (3.15)
dN_j	number of particles with sizes between d_j and $[d_j + \Delta(d_j)]$ (3.15)
D	mean particle diameter in microns (§3.2.2.9)
D_{ij}	(where i and j are replaced by x or y) effective sediment dispersivity tensor (3.13, 5.7)
\bar{E}	mean value of the scalar turbulent diffusion coefficient in the vertical direction E_z (5.7, §5.3.3, 5.10)
E'	E_z/\bar{E} (5.8)
E_z	vertical turbulent diffusion coefficient (5.9, §5.3.3, 5.10)
f	0.845; empirical coefficient used in the consolidation algorithm to be determined by performing laboratory consolidation tests
$\{f\}$	element source/sink vector (4.14)
F	flocculation factor (3.30, Figure 3.19)
$\{F\}$	system source/sink array (4.15)
FC	collision frequency for suspended sediment particles (3.15)
g	constant of acceleration due to gravity (3.2, 3.3)
G	local shearing rate = du/dz (3.17, §3.2.2.6)
H	thickness of bed in Dixit experiment (Figure 3.24-Figure 3.26)
H	height of water in outer cylinder (Figure 6.1)
H_o	suspension depth (Figure 3.26)
i	counter (4.1, 7.1)
I_{ii}	refer to equation 5.8 (5.7); often assumed to be a constant (§5.3.3)
j	counter (4.9 - 4.13, 7.1)
J	current time step ($t = J\Delta t$) indicator (4.17)
$J+1$	next time step ($t = (J+1)\Delta t$) indicator (4.17)
$ J $	Jacobian (4.3, 4.4, 4.5)
k	Boltzmann constant (3.16)
$[k]$	element steady-state coefficient matrix (4.14)
K	inverse of the hypothetical, fully settled sediment concentration (5.15)
$[K]$	system steady-state coefficient matrix (4.15)
K_e	empirical constant (3.29, 5.14)
L	counter (4.9)
m	empirical power coefficient (3.29, 5.14)
M	erodibility constant (§3.2.2.3, Table 5.1)
$M(1)$	erodibility constant for the first layer (5.5)
M'	$M \cdot \tau_c$ (2.13.10)
$\{M\}$	shape function representing flow depth (4.10)
M_D	dry sediment mass deposited per unit bed area per element per time step (§5.3.1, 5.17)
M_R	sediment mass per unit bed area that is redispersed during one time stop (§5.3.2, 5.2)

n_x	direction cosine between the boundary normal and the x-direction (4.11, 4.12)
n_y	direction cosine between the boundary normal and the y-direction (4.11, 4.12)
nn	number of nodes forming the jth element (4.1)
$\{N\}$	shape function representing velocity (4.11)
N_{sub}	shape function for node 'sub' in a given element (FEM) where sub = any subscript (§4.2.1, 4.1, 4.3, 4.4)
NE	total number of elements in grid (4.9)
NEC	number of elements in which at least one erosion-deposition cycle occurred (7.1)
NL	number of element interfaces and external boundaries (4.8)
NOCR	number of erosion-deposition cycles that occur in the i^{th} element over the entire simulation period (7.1)
P_d	probability of deposition (3.19, 3.20)
q_i^+	outward normal flux from one element (4.8)
q_i^-	outward normal flux from one element (4.8)
q_{sub}^s	normal flux from source/sink on the 'sub' boundary where sub = any subscript (4.8, 4.13)
Q	$\partial C/\partial t - S_T = \text{constant}$ (4.13)
r	residual that results from applying the governing equations to the element subdomain using the approximate value instead of the actual value (§4.2.2, 4.9)
R	residual that results from the use of \bar{C} in eq. 4.8 (4.9)
R_{ij}	collision radius between d_i and d_j size particles = $d_i + d_j$ (3.17)
S	salinity (§3.2.2.9, 5.6)
S_e	boundary of element for line integral (4.11, 4.12)
S_L	localized source/sink term for dredging and dumping (3.14)
S_T	source/sink term (3.13, 3.14)
t	time (3.1)
[t]	temporal matrix (4.14)
Δt	time increment (4.16)
$(\Delta t_{E-D})_j$	jth time period from occurrence of either redispersion or resuspension to occurrence of deposition in the ith element. (7.1)
t_{ave}	the average amount of time sediment particles are in suspension for the entire model simulation (7.1)
t_{50}	time at which $C^* = 50\%$ (3.27)
T	refer to eq. 3.27 (3.26)
[T]	system temporal matrix (4.15)
ΔT	thickness of the bed formed for each element (§5.3.1, 5.1)
T_{dc}	consolidation time (§3.2.2.10)
T_k	absolute temperature (3.16)
u	depth-averaged water velocity component in the x-direction (3.1)
\bar{u}	depth-averaged velocity component in the x-direction (§5.3.3)
u'	$u(z) - \bar{u}$ (5.7); velocity deviation over depth from the depth-averaged value u (5.7, §5.3.3)
u''	u'/\bar{u} (5.8)
u_f	shear velocity (5.9)
$u(z)$	vertical velocity profile (§5.3.3)

U	root-mean-square value of u' over the depth d (5.7); the intensity of u' (§5.3.3)
v	depth-averaged velocity component in the y -direction (3.1)
\bar{v}	depth-averaged component of the velocity in the y -direction (5.7)
v'	$v(z) - \bar{v}$ (5.7); velocity deviation over depth from the depth-averaged value \bar{v} (5.7, §5.3.3)
$v(z)$	vertical velocity profile (§5.3.3)
V	root-mean-square value of v' over the depth d (5.7); the intensity of v' (§5.3.3)
w	integration variable (Figure 3.13, Figure 3.14)
W	wind speed (3.4)
W_r	reference settling velocity (5.15)
W_s	[median] sediment settling velocity (3.19, 3.29)
W'_s	effective settling velocity, $P_d \cdot W_s$ (§5.3.4, 5.12)
W_{sA}	median settling velocity of aggregates (3.30)
W_{sP}	median settling velocity of sediment particles (3.30)
W_{s1}	median sediment settling velocity in the free settling range (5.13)
W'_{s1}	effective settling velocity in Range I as defined on Figure 5.3 (5.13, 5.14, 5.15)
x	global coordinate in a horizontal direction (§3.1.2.1)
\bar{x}	approximation of the global coordinate x (4.2)
x_i	global nodal point coordinate (4.2)
y	global coordinate in a horizontal direction (§3.1.2.1)
\bar{y}	approximation of the global coordinate y (4.2)
y_i	global nodal point coordinate (4.2)
Y_a	see eq. 3.24 (3.23)
z	global coordinate in the vertical direction following the right-hand rule (§3.1.2.1)
z_b	bed elevation (3.2, 3.3)
z_e	depth of erosion (§3.2.2.3)
Z_*	the bed depth at which $\tau_c(z_b) = \tau_b$ (§5.3.2)
Z	depth below the initial bed surface (§3.2.2.2.2)

ACKNOWLEDGMENTS

The development of a numerical model is a time-consuming task that normally extends over a number of years. There are significant periods in the evolution of a computer code, but rarely is there a definitive end to the development. Such is the case with the HSCTM-2D code that simulates vertically-integrated hydrodynamics and the transport of both cohesionless and cohesive (silts and clays) sediment, and (at present) one inorganic contaminant.

Work on HSCTM-2D originated in 1980 with the dissertation studies of Earl Hayter in the University of Florida's Coastal & Oceanographic Engineering Department under the advisement of Professor A.J. Mehta. Mr. Hayter's research was first supported by a grant from the U.S. EPA Environmental Research Laboratory at Athens, Georgia (AERL), and later by a U.S. Geological Survey thesis support grant.

After his arrival at Clemson University in South Carolina in 1984, Dr. Hayter was further supported by EPA, starting in 1985 with Mr. Robert Ambrose serving as the project manager, to develop documentation for HSCTM-2D and to improve the model algorithm efficiency. This initiated what was to become the significant involvement of AERL in the development of HSCTM-2D. We are pleased with the technical leadership Mr. Ambrose provided in this development and with EPA's wider effort to understand the fate of sorbed contaminants in surface waters. During this period Dr. Hayter conducted a case study using HSCTM-2D to simulate potential sedimentation in a proposed marina on Daufuskie Island, South Carolina. In 1986 during the end of this development phase, Dr. Steve McCutcheon became associated with AERL and followed the initial efforts of Mr. Ambrose to arrange drafting of this documentation. Dr. Winston Lung of the University of Virginia and Dr. Tien Sheunn Wu, then of the Northwest Florida Water Management District, reviewed and critically commented on the initial draft. Mr. Mike Bell, an engineering aide with Dr. McCutcheon assisted in addressing the review comments and rewriting this report. Mr. Bell tested the use of the code on AERL's VAX system with assistance from Mr. Dave Disney and other contractors at AERL.

In 1991 AERL began a cooperative agreement with Clemson University to support the final development of HSCTM-2D and to demonstrate the application of the program to Superfund sites. Mr. Robert Ambrose served as the Project Officer at AERL and Dr. Earl Hayter was the Principal Investigator. EPA Region 8 Superfund office through Ms. Julie Dalsogio, Remedial Project Manager (RPM) for the Milltown Reservoir site, provided initial funding for the agreement that lead to case study investigations of downstream contamination from a catastrophic release (usually large flood or dam break) for arsenic and heavy metal contaminated sediments deposited in Milltown Reservoir during mining activities upstream. During the initial period of the cooperative agreement, Dr. McCutcheon was assigned to Clemson University through an Interpersonal Agreement with the State of South Carolina. During the period from August 15, 1991 to May 15, 1992 Dr. McCutcheon, while at Clemson, assisted in the studies at Milltown. After this period he returned to AERL. The Studies at Milltown are notable for the way Dr. Hayter conducted his investigations. He met with the site RPM, interested citizens

groups, and the responsible party and its contractors. Although it was not the purpose of his investigations, Dr. Hayter's case studies of contaminated sediments had the impact of demonstrating the level of understanding of contaminated sediment transport and flood modeling that could be applied. The contractors for the responsible party adopted elements of the case study by Dr. Hayter. The end result was that the RPM and the responsible party had available information developed from more advanced methods by the contractors for the responsible party and EPA. After his return to AERL, Dr. McCutcheon formulated a framework for integrating simulations and estimates of potential contaminated sediment deposition into risk assessment calculations. The framework was used by contractors for EPA Region 8 to conclude a risk assessment.

The final phase of cooperative agreement, which ended September 30, 1994, was funded by EPA's Region 2 Superfund Office. This phase focused on application of HSCTM-2D to understanding the fate of arsenic contaminated sediments in Blackwater Branch, the Maurice River, and Union Lake near Vineland, New Jersey. Mr. Matt Westgate was the Remedial Project Manager for Region 2 during this period. This work sprung from an innovative approach to integrate contaminated sediment modeling into the Superfund decision making process. The original Vineland site RPM and Mr. Ambrose of AERL developed a new paradigm for using simulation of environmental processes in decisions on cleaning up hazardous waste sites. Rather than attempt contaminated sediment simulations during the site characterization phase when time constraints are very tight and data to calibrate and test complex hydrodynamic and sediment transport models are extremely limited, Mr. Ambrose and the Region 2 RPM formulated a new policy to use existing data and supplemental monitoring plans for site characterization to support a record of decision. The record of decision then targeted clean up of source areas and existing arsenic hotspots but recognized the mobile nature of contaminated sediments that endangers downstream swimming and fishing during the initiation source clean up. To best resolve downstream risks that may occur during normal sediment transport conditions and in the event of extreme flooding, modeling investigations were devised to predict transport of contaminants during certain scenarios. Region 2 arranged necessary data collection over a two-year period to collect sufficient data to calibrate a model with adequate predictive capabilities. Since the contractors for Region 2 reported that they and most consulting firms were not able to apply predictive contaminated sediment models, AERL was asked by Region 2 to establish sufficient case studies to serve as a guide for these types of Superfund site investigations, and funded for this purpose. Part of the funding was employed in Cooperative Agreement with Clemson University where Dr. Hayter proposed to simulate sediment and arsenic transport. Although Dr. Hayter is free to use any appropriate data set, the general purpose data collection program designed for Blackwater Branch Maurice River, and Union Lake in consultation with AERL promises to be a more ideal setting for testing the use of more complex models in aiding decision making on whether additional clean up or containment will be necessary to ensure the health of the public and the ecological system of the river and lake involved. In order to ensure that advanced modeling technology is available to support contractors and others, AERL is documenting the HSCTM-2D model and other computer codes.

To assist in developing case studies on the use of the HSCTM-2D, Dr. Hayter engaged Dr. Rouchuan Gu as a research assistant professor at Clemson from October 1, 1992 until August 12, 1993. Dr. Gu is presently an assistant professor at Iowa State University at Ames.

To also support the model development and case study application, a part of the Region 2 funding was used to support a National Research Council associate at AERL in looking at wider issues involving arsenic mobility and sediment transport. Dr. Mary Bergs proposed to look at the wider issues and she was selected to work with Dr. Steve McCutcheon at AERL. Dr. Bergs assisted Dr. Hayter and others involved by using the data collected by the U.S. Geological Survey and the contractors supporting Region 2 to investigate arsenic mobility. Dr. Bergs also took the lead in finishing this documentation. Her work on arsenic mobility will be reported elsewhere.

The final version of this documentation was reviewed and critically commented upon Dr. Viadimir Novonty of Marquette University and Dr. Tien Sheunn Wu, who reviewed the first draft. Dr. Novonty acknowledges the theoretical development as a well organized presentation of the latest theory for fine sediment transport, but he cautions the authors and readers alike that the predictive capabilities of a model of this type is governed by the degree to which the model can be calibrated. Where data are spatially limited, and not available for extensive periods of time, the calibration can be expected to be more uncertain.

The AERL support contractor, CSDI, converted the report figures to a WordPerfect format that allows the documentation to be printed from disk. The leadership of Dr. Bergs in getting this document to the final stages of publication is gratefully acknowledged. Dr. Bergs' determination that this report be highly useful and understandable by engineers and scientists will significantly improve the impact that this work can have.

Steven C. McCutcheon, Ph.D., P.E.
U.S. Environmental Protection Agency
National Exposure Research Laboratory
Ecosystems Research Division
Athens, Georgia

SECTION 1

INTRODUCTION

This report documents the finite element hydrodynamic and sediment and contaminant transport modeling system, HSCTM-2D. The modeling system consists of HYDRO2D, a two-dimensional, depth-averaged finite element hydrodynamic model; and CS2D, a two-dimensional, depth-averaged finite element sediment and contaminant transport model. HSCTM-2D can be used by engineers/scientists to predict the movement and fate of sediments and contaminants in riverine and estuarine environments. Output from the modeling system includes the two-dimensional (depth-averaged) flow field, suspended sediment concentration-time record and spatial distribution, contaminant distribution and fate (dissolved concentrations in the water column, sorbed concentrations on suspended sediments, and sorbed concentrations on bed sediments), and changes in bed elevations throughout the modeled water body due to erosion and deposition.

1.1 EXPERIENCE REQUIRED TO USE HSCTM-2D

This report provides the information needed to use the modeling system. The prerequisites for using the system are: (1) a working knowledge of the finite element method; (2) an understanding of the logical structure of the programs, including data requirements and input format; and (3) an awareness of the limitations inherent in the theory on which the models are based and the limitations associated with the use of spatially averaged (in this case depth-averaged) numerical models in simulating three-dimensional processes such as tidal flow and sediment transport in estuaries. **IT IS RECOMMENDED THAT SECTION 7.1 BE READ**

BEFORE USING THE MODEL. This introductory section discusses the sedimentation and contamination problems typically encountered in rivers and estuaries and the modeling approach used in investigating these problems. Then an overview of the modeling system is presented.

1.2 SEDIMENTATION-RELATED PROBLEMS IN SURFACE WATERS

Estuaries are often centers of population and industry, and as such are used as commerce routes to the sea, convenient dump sites for waste products, as well as areas for man's recreational enjoyment. They also serve as sinks for sediment and pollutants transported by rivers from inland sources.

As man's activity in, and hence dependence upon, estuaries has increased with the growth of population and commerce, the need to manage estuarial resources becomes apparent. Included in estuarial management are maintenance of navigable waterways and control of water pollution, both of which are affected to varying degrees by the load of suspended and deposited sediment. These two tasks are discussed next.

Under low flow velocities, sometimes coupled with turbulent conditions that favor the formation of large aggregates, cohesive sediments have a tendency to deposit in areas such as dredge cuts, navigation channels, basins (e.g., harbors and marinas), and behind pilings (Einstein and Krone 1962; Ariathurai and Mehta 1983). In addition, the estuarial mixing zone between upland fresh water and sea water is a favorable site for bottom sediment accumulation. The amounts and locations of the deposits are also affected by development projects, such as construction of port facilities or dredging of navigation channels. Because estuaries are often used as transportation routes, accurate estimates of the amount of dredging required to maintain navigable depths is desired.

1.3 CONTAMINATION PROBLEMS IN SURFACE WATERS

Contamination of surface waters by point and non-point sources is a critical water quality problem that has drawn the concentrated attention of, among others, environmental scientists and engineers. This concern is based on the increased awareness of contaminants such as metals, radionuclides and pesticides on humans and aquatic ecosystems. The potential impacts contaminants have on aquatic environments and possible remediation alternatives can be evaluated

only if the transport and fate of such contaminants are known. In turn, the ability to predict future contaminant distributions, including accumulation on bottom sediments, and their possible effect on indigenous biological communities is requisite to mitigating pollution in surface waters.

A necessary component of the assessment and prediction of environmental effects of contaminants such as metals in surface waters is evaluating the transport rates and fates of the contaminants in the system. In order to simulate the transport of contaminants it is necessary to reproduce not only the physical-chemical processes of contaminants in aquatic environments (e.g., adsorption/desorption), but also changes in the various factors (e.g., pH) that govern them. The latter requires an ability to predict the hydraulics, water quality, and sediment transport in the water system, because the movement of surface waters, sediments and contaminants are highly coupled. For example, the role of sediments in accumulating contaminant levels in depositional environments such as reservoirs, lakes, and marina basins has been revealed in several studies (Bauer 1981; Reese *et al.* 1978; Abernathy *et al.* 1984; Medine and McCutcheon 1989; Brown *et al.* 1990). In particular, in an investigation of the bottom sediments from several coastal marinas in Florida, two interesting observations were made (Weckmann 1979; Bauer 1981). First, when comparing sediment particle size inside the basin with that obtained immediately outside in the main body of water, the sediment inside the basin was measurably finer than that outside the basin in the majority of the marinas investigated. Second, a similar comparison was made in terms of heavy metal (e.g., Cu, Pb, Ni, Cd and Zn) content within the basin and immediately outside the basin. Measurably higher concentrations of the heavy metals were found inside the basin. These two observations exemplify the role of cohesive sediments in accumulating contaminant levels in depositional environments such as marina basins. This assimilation and storage of contaminants in bottom sediments may prove to be an acceptable means of waste disposal although even a relatively small change in the chemical composition of the water may sometimes cause desorption of contaminants from sediment particles.

Cohesive sediments (in particular clays, which can adsorb pollutants) have a large surface area to volume ratio, net negative electrical charges on their surfaces, and exchangeable cations. (Refer to Section 3.2.1.) Cohesive sediments may influence water quality by affecting aquatic life, by providing a large assimilative capacity, and by acting as a transporting mechanism for dissolved and particulate pollutants. Turbidity caused by suspended sediment particles restricts the

penetration of light, and thereby reduces the depth of the photic zone. This, in turn, may result in a decrease in production of phytoplankton and other algae leading to a reduction in the amount of food available for fish. Deposited sediments can damage spawning areas for fish and eliminate invertebrate (e.g., oyster) populations.

1.4 MODEL DESCRIPTION

1.4.1 Approach to the Problems

Physical and mathematical models or combinations of these two types (hybrid approach) are usually used in predicting cohesive sediment transport. Physical hydraulic models have their limitations due to spatial and temporal scaling problems, lack of an appropriate model sediment, poor model reproduction of estuarial mixing processes and internal shear stresses (Owen 1977), and limited time scales. Mathematical models have been generally more practical and successful in simulating mixing processes and the processes governing the transport of cohesive sediments in estuarial waters.

To simulate the motion of the three main constituents in an estuarial environment mathematically, the full three-dimensional forms of the equations for the conservation of momentum, conservation of mass for water, and conservation of mass for dissolved salt and suspended sediment must be solved numerically. The horizontal length scales relative to the transport of cohesive sediments are often one to three orders of magnitude greater than the vertical length scales in many estuaries. As a result, and because horizontal transport distances are usually of primary interest in ascertaining the magnitude of sedimentation or the fate of adsorbed contaminants, vertically integrated transport equations can be used for most modeling purposes. Depth-averaged flow and sediment transport models are appropriate for use in modeling vertically well mixed (non-stratified) bodies of water. For stratified waters, laterally averaged equations or the full three-dimensional equations should be used for modeling flow and sediment transport.

A complete model of the depth-averaged motion of water and sediment, even using two-dimensional forms of the governing equations, must still solve some five to seven coupled equations. As a result, modeling of surface water flow is commonly performed separately from the sediment transport modeling. For example, a two-dimensional hydrodynamic model, which solves the coupled momentum and continuity equations, is used to model the movement of water. Then a

two-dimensional cohesive sediment transport model is used to predict the motion of sediment using the results from the hydrodynamic model. This approach assumes that sedimentation and/or erosion during the simulation does not affect the flow field.

1.4.2 Overview of the Modeling System

The modeling system HSCTM-2D consists of two coupled models designed for analysis of two-dimensional, depth-averaged flow, sediment transport, and contaminant transport in estuaries and other surface waters. The coupled models are a finite element hydrodynamic module (HYDRO2D) and a finite element sediment and contaminant transport module (CS2D). The program HYDRO2D is a modified version of model RMA2 developed by Resource Management Associates, Lafayette, California. The modifications made to RMA2 are described in Section 5.2.

The two-dimensional, depth-averaged hydrodynamic module HYDRO2D solves the shallow water equations using the finite element method to determine the horizontal, depth-averaged velocities and flow depth at each node. The model includes the effects of bottom friction, turbulent stresses, wind-induced surface stresses, horizontal salinity gradients, and the Coriolis force. Output from the model consists of the two-dimensional flow field that is required by CS2D.

The sediment and contaminant transport module CS2D solves the two-dimensional, depth-averaged advection-dispersion equation with source/sink term by the finite element method. The transport processes of dispersion, erosion, settling, and deposition are simulated in CS2D. The output from the model consists of nodal values of the bed elevation, the depth-averaged suspended sediment concentration, the dissolved and sorbed contaminant concentrations, and the sorbed contaminant concentration in the bed.

HYDRO2D and CS2D output one or more solution files, which include the water surface elevation, flow velocity, salinity field, suspended sediment concentration, bed contaminant concentration, and bed elevation change at each node in the mesh.

A schematic representation of the modeling system is shown in Figure 1.1. As indicated in this figure, the system can be operated in either an uncoupled or semi-coupled mode. In the former, HYDRO2D is run to generate the simulated flow field for the entire model period, and then CS2D is run using the data set generated by HYDRO2D to predict the movement of cohesive sediments. In the semi-coupled mode, HYDRO2D is called from CS2D and used to update the

flow field at each time step during model execution. This allows the changes in bed elevations and the resulting changes in flow depths due to erosion and deposition to be incorporated into flow field predictions at subsequent time steps.

The HSCTM-2D modeling system may be run using either a default option or a non-default option. In the former, default values (contained in the program) for certain sediment-related input parameters are used, whereas in the non-default mode all the input parameters have to be included in the input data set. The default option of HSCTM-2D is discussed in Section 8.6. The purpose of the default option is to allow model use even when all the required sediment-related parameters (e.g., erosion/deposition rate coefficients) are not available. **THE DEFAULT OPTION SHOULD BE USED FOR QUALITATIVE ANALYSIS ONLY.** The default option will allow the modeler to make relative comparisons among various sites or designs.

A pre-processor and post-processor such as contained in the Surface Modeling System (SMS) developed by the Engineering Graphics Laboratory at Brigham Young University will save considerable time in generating and modifying the finite element grid of the system to be modeled. SMS also generates the boundary condition file required by HYDRO2D, and reads in the binary solutions files generated by HSCTM-2D for post-processing.

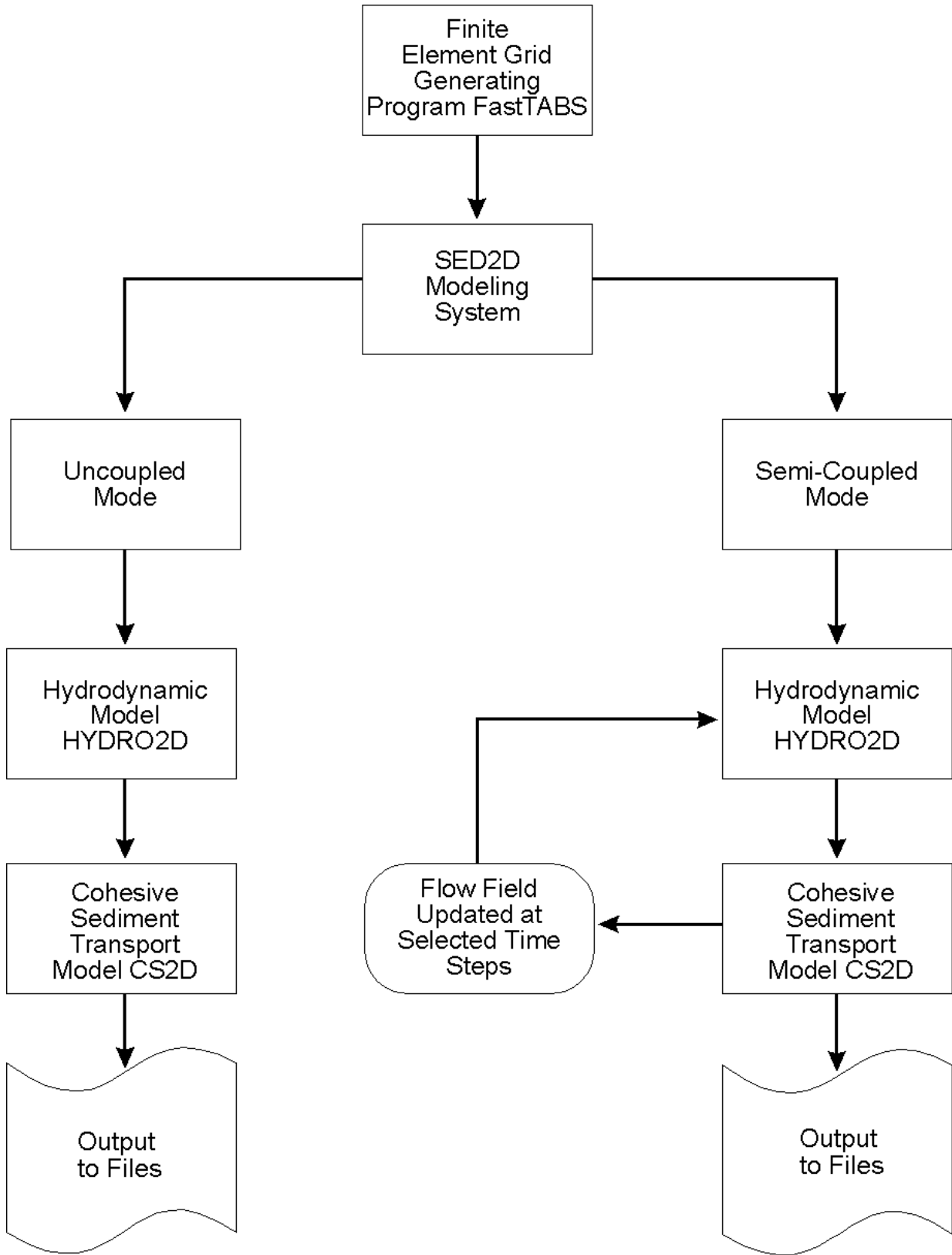


Figure 1.1 Flowchart of HSC TM-2D Modeling System

1.5 ORGANIZATION OF THE DOCUMENT

Section 2 provides information on availability of the program, and installation and run time requirements. In Section 3 a brief description of estuarial hydrodynamics and a detailed description of the mechanics of cohesive sediment transport are given. Section 4 includes a brief introduction to the finite element method and the finite element formulation of the governing equations for surface water flow and cohesive sediment transport. A detailed description of the modeling system is given in Section 5. Section 6 discusses application of the modeling system including limits for use, data collection and analysis, and model calibration. Section 7 has user instructions and data input requirements, while Section 8 discusses data input requirements. Section 9 describes two example problems. The Appendices include information about the program such as flow charts of the program structure and subroutines, a laboratory sediment testing program, and the data input manual for HYDRO2D.

SECTION 2

MODEL DEVELOPMENT, DISTRIBUTION AND SUPPORT

The user should refer to the file READ.ME for the latest supplemental information, changes, and or addendum to the HSCTM-2D model system and its related documentation. A copy of the READ.ME file is distributed with the HSCTM-2D model package by the U.S. Environmental Protection Agency (US EPA) Center for Exposure Assessment Modeling (CEAM). For the latest information concerning the location, version number, and availability of the HSCTM-2D model system, users should call the CEAM HelpDesk at 706/355-8400.

NOTE: The file READ.ME is an ASCII text (non-binary) file that can be displayed on the monitor screen with the DOS TYPE command or printed using the DOS PRINT command.

The READ.ME file contains the following information:

- Introduction
- Abstract
- Documentation
- Distribution Diskette(s)
- File Name and Content
- Development System
- Routine Execution
- Run Time and Performance
- Minimum File Configuration
- Modification
- Technical Help Contact
- Electronic Support and Distribution
- Disclaimer

SECTION 3

THEORY

3.1 ESTUARIAL DYNAMICS

3.1.1 General Description

The hydrodynamic regime in an estuary is governed by the interaction among fresh water flow, astronomical tides, surface (i.e., wind) stresses, wind-generated surface waves, the Coriolis force, the geometry of the water body, and roughness characteristics of the sedimentary material composing the bed (Dyer 1973). Fresh water flow and the next four factors mentioned are the driving forces. Geometry includes the shape and bathymetry of the estuary. The geometry and bed roughness interact with the driving forces to control the pattern of water motion (in particular the shear stress and turbulence structure near the bed), frictional resistance, tidal damping, and degree of tidal reflections (Ippen 1966).

The magnitude of tidal flow relative to fresh water inflow governs, to a large extent, the intensity of vertical mixing of sea water with less dense fresh water. There exists in all estuaries a longitudinal salinity profile that decreases from the mouth to the upper reaches of the estuary. The existence of a longitudinal salinity gradient or baroclinic force implies that there could be a gravity driven upstream transport of a high density sediment suspension in the lower portion of the water column (Officer 1981; Mehta and Hayter 1981).

Winds affect the hydrodynamic regime and mixing in an estuary by generating surface shear stress and waves. The surface stress is capable of generating a surface current (whose magnitude will be approximately 3 percent of the wind speed at 9.1 m elevation (Hughes 1956)) and a super-elevation of the water surface along a land boundary located at the downwind end of

the estuary (Ippen 1966). The latter effect increases the degree of vertical mixing by causing a vertical circulation cell with landward flow at the surface and seaward flow along the bottom.

Wave action, and in particular wave breaking, substantially increases the intensity of turbulence and mixing in the upper portion of the water column. Along the banks and in shallow areas, surface waves generated by the wind are capable of eroding bottom sediments. A tidal current of sufficient strength to transport sediment eroded by other mechanisms is generally present. Although the tidal current may not necessarily have enough force by itself to erode sediment, it will cause suspended material to be advected and dispersed both longitudinally with the main tidal flow and laterally by secondary currents towards the deeper sections of the estuary.

The Coriolis force, caused by the earth's rotation, has both a radial (horizontal) and a tangential (vertical) component. The latter is generally negligible as it is linearly proportional to and smaller than the vertical component of the flow velocity, which is typically an order of magnitude smaller than the horizontal velocity components. The magnitude of the radial component depends upon the size of the water body. Most extra-tropical estuaries are relatively large and therefore the effect of this force on the hydrodynamic regime is measurable. Estuarial hydrodynamics are described in detail elsewhere (Ippen 1966; Barnes and Green 1971; Dyer 1973; Officer 1976; Fischer *et al.* 1979).

3.1.2 Governing Equations

3.1.2.1 Coordinate System

A right-handed Cartesian coordinate system (Figure 3.1) is used in the governing equations. The positive z-axis points upward with $z=0$ located at a mean water level datum selected by the user of the model. The x- and y-axes are in the horizontal plane.

3.1.2.2 Equations of Motion

The equations that govern the two-dimensional, depth-averaged unsteady turbulent movement of an incompressible viscous fluid are based on the principles of conservation of mass (continuity equation) and conservation of

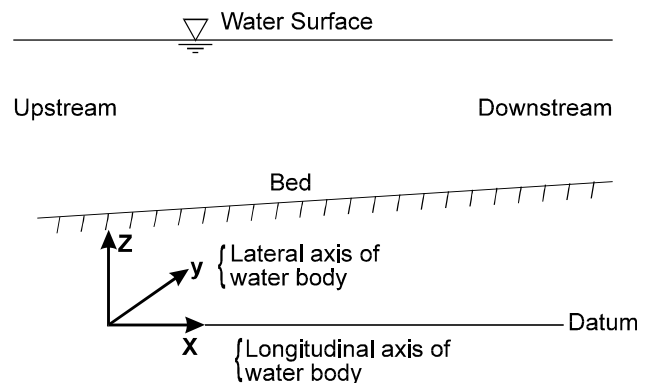


Figure 3.1 Coordinate System

momentum (equations of motion). These equations are solved numerically in order to simulate the velocity field in an estuary or other water body of interest.

3.1.2.2.1 Continuity -- The conservation of mass, as expressed by the continuity equation, states that the mass of an incompressible fluid entering a control volume per unit time is equal to the sum of the fluid mass leaving the control volume plus the change in volume of the control volume. The depth-averaged continuity equation for an incompressible fluid is

$$\frac{\partial d}{\partial t} + \frac{\partial}{\partial x} (u \cdot d) + \frac{\partial}{\partial y} (v \cdot d) = 0 \quad (3.1)$$

where d = depth of flow, t = time, and u, v = depth-averaged water velocity components in the x - and y -directions, respectively.

3.1.2.2.2 Conservation of Momentum -- The conservation of momentum for an incompressible fluid states that the product of the fluid mass and acceleration is equal to the sum of the body (gravitational) forces and the normal (pressure) and tangential (friction) surface forces that act on the boundaries of the water body. The two-dimensional, depth-averaged equations of motion for an incompressible viscous fluid are given by

$$\begin{aligned} \frac{\partial u}{\partial t} + u \frac{\partial u}{\partial x} + v \frac{\partial u}{\partial y} = & -g \frac{\partial d}{\partial x} - g \frac{\partial z_b}{\partial x} + \Omega v \\ & + \frac{1}{\rho d} \left[\frac{\partial}{\partial x} (d \tau_{xx}) + \frac{\partial}{\partial y} (d \tau_{xy}) + \tau_x^s - \tau_x^b \right] \end{aligned} \quad (3.2)$$

in the x -direction, and

$$\begin{aligned} \frac{\partial v}{\partial t} + u \frac{\partial v}{\partial x} + v \frac{\partial v}{\partial y} = & -g \frac{\partial d}{\partial y} - g \frac{\partial z_b}{\partial y} - \Omega u \\ & + \frac{1}{\rho d} \left[\frac{\partial}{\partial x} (d \tau_{yx}) + \frac{\partial}{\partial y} (d \tau_{yy}) + \tau_y^s - \tau_y^b \right] \end{aligned} \quad (3.3)$$

in the y -direction, where g is the gravitational acceleration; z_b is the bed elevation; ρ is the water density; Ω is the Coriolis parameter; τ_x^s and τ_y^s are wind-induced shear stresses at the water surface in the x - and y -directions, respectively; τ_x^b and τ_y^b are flow induced bed shear stresses in the x -

and y-directions, respectively; and τ_{ij} (with $i, j = x, y$) is the depth-averaged turbulent shear stress acting in the i-direction on a plane that is perpendicular to the j-direction.

Equations 3.1-3.3 are referred to as the shallow water equations and are applicable to estuarial and other surface water flow problems in which the vertical (i.e., z) components of the flow velocity and acceleration are small relative to the horizontal (i.e., x and y) components of the flow velocity and acceleration. The three terms on the left hand side of equations 3.2 and 3.3 represent the substantive fluid acceleration in the x- and y-directions, respectively. The Coriolis parameter Ω is equal to $2\omega\sin\phi$, where ω is the angular velocity of the earth and ϕ is the local latitude. The terms Ωv and $-\Omega u$ represent the Coriolis acceleration in the Northern Hemisphere in the x- and y-directions, respectively. The surface wind shear stresses are given by

$$\tau_x^s = \frac{\zeta}{d} W^2 \cos \psi \quad \text{and} \quad \tau_y^s = \frac{\zeta}{d} W^2 \sin \psi \quad (3.4)$$

where ζ is an empirical wind shear coefficient; W is the wind speed; and ψ is the angle between the positive x-axis and the wind direction. The depth-averaged turbulent shear stresses are determined using Boussinesq's eddy viscosity model:

$$\tau_{ij} = \epsilon_{ij} \frac{\partial u_i}{\partial x_j} \quad \text{for } i, j = x, y \quad (3.5)$$

in which $x_i, x_j = x, y$, and $u_i, u_j = u, v$; and ϵ_{ij} is the eddy viscosity acting in the i-direction on a plane that is perpendicular to the j-direction. Values of the eddy viscosities are dependent on both fluid properties and the level of fluid turbulence.

The bottom shear stresses are given by two relationships:

$$\tau_x^b = \frac{g u}{C_z^2 d} (u^2 + v^2)^{1/2} \quad \text{and} \quad \tau_y^b = \frac{g v}{C_z^2 d} (u^2 + v^2)^{1/2} \quad (3.6)$$

where C_z is the Chezy coefficient.

Substituting equations 3.4-3.6 into equations 3.2 and 3.3 gives the following form of the depth-averaged equations of motion:

$$\frac{\partial u}{\partial t} + u \frac{\partial u}{\partial x} + v \frac{\partial u}{\partial y} = -g \frac{\partial d}{\partial x} - g \frac{\partial z_b}{\partial x} + 2v\omega \sin\phi + \frac{1}{\rho d} \left[\frac{\partial}{\partial x} \left(\epsilon_{xx} d \frac{\partial u}{\partial x} \right) + \frac{\partial}{\partial y} \left(\epsilon_{xy} d \frac{\partial u}{\partial y} \right) + \zeta W^2 \cos\psi - \frac{gu}{C_z^2 d} (u^2 + v^2)^{1/2} \right] \quad (3.7)$$

$$\frac{\partial v}{\partial t} + u \frac{\partial v}{\partial x} + v \frac{\partial v}{\partial y} = -g \frac{\partial d}{\partial y} - g \frac{\partial z_b}{\partial y} - 2u\omega \sin\phi + \frac{1}{\rho d} \left[\frac{\partial}{\partial x} \left(\epsilon_{yx} d \frac{\partial v}{\partial x} \right) + \frac{\partial}{\partial y} \left(\epsilon_{yy} d \frac{\partial v}{\partial y} \right) + \zeta W^2 \sin\psi - \frac{gv}{C_z^2 d} (u^2 + v^2)^{1/2} \right] \quad (3.8)$$

in the x- and y-directions, respectively. Equations 3.1, 3.7, and 3.8 are solved numerically using the finite element method by the hydrodynamic module HYDRO2D.

3.2 COHESIVE SEDIMENT TRANSPORT

3.2.1 Description and Properties of Cohesive Sediments

3.2.1.1 Composition

Cohesive sediments consist primarily of terrigenous clay-sized particles composed of clay and non-clay mineral components and organic material (Grim 1968). Clay particles are generally less than 2 micrometers (μm) in size. As a result they are termed colloids and in water possess the properties of plasticity, thixotropy and adsorption (van Olphen 1963). The most abundant types of clay minerals are kaolinite, montmorillonite, illite, chlorite, vermiculite, and halloysite. The non-clay minerals consist of, among others, quartz, carbonates, feldspar, and mica (Grim 1968). This component of clay material is generally larger than 2 μm in size. The amount of non-clay minerals present in a clay material currently cannot be determined with a high degree of accuracy.

The organic material often present in clay materials may be discrete particles of matter, adsorbed organic molecules, or constituents inserted between clay layers (Grim 1968). Additional possible components of clay materials are water-soluble salts, and adsorbed exchangeable ions and contaminants.

3.2.1.2 Structure

Clay minerals are primarily hydrous aluminum silicates with magnesium or iron occupying all or part of the aluminum positions in some clays, and with alkalines (e.g., sodium, potassium) or alkaline earths (e.g., calcium, magnesium) also present in others (Grim 1968). Most clays are composed of one or two atomic structural units or combinations of the two basic units.

Ions of one kind are sometimes substituted by ions of another kind with the same or different valence. This process does not necessarily involve replacement. The tetrahedral and octahedral cation distributions develop during initial formation of the mineral and not by later substitution (Mitchell 1976). Substitution in all the clay materials, except for kaolinite, gives clay particles a negative electric charge that is of great significance in coagulation of clays and in adsorption of contaminants. Another cause of net particle charge is the preferential adsorption of peptizing ions on the surface of the particle (van Olphen 1963).

3.2.1.3 Interparticle Forces

For particles in the colloidal size range, surface physicochemical forces exert a distinct influence on the behavior of the particles due to the large specific area, i.e., ratio of surface area to volume. As stated previously, most clay particles fall within the colloidal range in terms of both their size (2 μm or less) and the controlling influence of surface forces on the behavior. In fact, the average surface force on one clay particle is several orders of magnitude greater than the gravitational force (Partheniades 1962).

The relationships between clay particles and water molecules are governed by interparticle electrochemical forces. The different configurations and groupings as well as electric charges of clay particles affect their association with water molecules (Grimshaw 1971).

Interparticle forces are both attractive and repulsive. The attractive forces present are the London-van der Waals and are due to the nearly instantaneous fluctuation of the dipoles, which result from the electrostatic attraction of the nucleus of one atom for the electron cloud of a neighboring atom (Grimshaw 1971). These electrical attractive forces are weak and are only significant when interacting atoms are very close together. The electrical attractive forces are strong enough to cause structural build-up as they are additive between pairs of atoms. The magnitude of these forces decreases with increasing temperature; they are only slightly dependent on the salt concentration (i.e., salinity) of the medium (van Olphen 1963).

The repulsive forces of clay materials, which are due to negatively charged particle forces, increase in an exponential fashion with decreasing particle separation. An increase in the salinity, however, causes a decrease in the magnitude of the repulsive forces. This dependence on salinity can best be explained using the concept of the electrical double layer and the surrounding diffuse layer. van Olphen (1963) states that the double layer is composed of the net electrical charge of the elementary clay particle and an equal quantity of ionic charge of opposite sign located in the medium near the particle surface. The ions of opposite charge are called the counter-ions, i.e., cations. The counter-ion concentration increases with decreasing distance from the particle surface. The layer of counter-ions is referred to as the diffuse layer. A clay particle and associated double layer is referred to as a clay micelle (Partheniades 1971). When the salinity is increased, the diffuse layer is compressed toward the particle surface (van Olphen 1963). The higher the salinity, as well as the higher the valence of the cations that compose the diffuse layer, the more this layer is compressed and the greater the repulsive force is decreased.

3.2.1.4 Cation Exchange Capacity

The cation exchange capacity (CEC) is an important property of clays by which they adsorb certain cations and anions in exchange for those already present and retain them in an exchangeable state. The CEC of different clays varies from 3 to 15 milliequivalents per 100 grams (meq/100 gm) for kaolinite to 100 to 150 meq/100 gm for vermiculite. Higher CEC values indicate greater capacity to adsorb other cations. The negative surface charge caused by isomorphous substitution is neutralized by adsorbed cations located on the surfaces and edges of a clay particle. These cations remain in an exchangeable position and may in turn be replaced by other cations.

Two factors are the causes of cation exchange: (1) substitution within the lattice structure results in unbalanced electrical charges in structural units of some clays, and (2) broken bonds around the edges of tetrahedral-octahedral units give rise to unsatisfied charges. In both cases, the unbalanced charges are balanced by adsorbed cations. The number of broken bonds and hence the CEC increases with decreasing particle size.

The ability of particles to replace exchangeable cations depends on the concentration of the replacing cation, the number of available exchange positions, and the nature of the ions in the replacing solution. Increased concentration of the replacing cation results in greater cation

exchange. The release of an ion depends on the nature of the ion, the nature of the other ions filling the remaining exchange positions, and the number of unfilled exchange sites. The higher the valence of a cation, the greater is its replacing power and the more difficult it is to displace when adsorbed on a clay. Some of the predominantly occurring cations in sediments are sodium, potassium, calcium, aluminum, lead, copper, mercury, chromium, cadmium, and zinc.

3.2.2 Estuarial Cohesive Sediment Transport

3.2.2.1 Overview

In water with a very low salinity (less than about 1 part per thousand), the elementary cohesive sediment particles are usually found in a dispersed state. Small amounts of salts, however, are sufficient to repress the electrochemical surface repulsive forces among the elementary particles, with the result that the particles coagulate to form flocs. A systematic "build up" of flocs is defined as aggregation. An aggregate is the structural unit formed by the joining of flocs. Each aggregate may contain thousands or even millions of elementary particles. The transport properties of aggregates are affected by the hydrodynamic conditions and by the chemical composition of the suspending fluid. Most estuaries contain abundant quantities of cohesive sediments, which usually occur in the coagulated form in various degrees of aggregation. Therefore, an understanding of the transport properties of these sediments in estuaries requires knowledge of the manner in which aggregates are transported.

Cohesive sediment transport in estuaries is a complex process involving a strong coupling among tides, baroclinic circulation, and the coagulated sediment. For an extensive description of this process, the reader is referred to Postma (1967), Partheniades (1971), Barnes and Green (1971), Krone (1972), Kirby and Parker (1977), Kranck (1980) and Dyer (1986). Figure 3.2 is a schematic depiction. The case considered is one in which the estuary is stratified, and a stationary saline wedge is formed. Various phases of suspended fine sediment transport are shown, assuming a tidally averaged situation. In the case of a partially mixed estuary, the description will be modified, but since relatively steep vertical density gradients are sometimes present even in such a case, the sediment transport processes will generally remain qualitatively similar to that depicted. [NOTE: HSCTM-2D is depth averaged and should not be applied to a stratified estuary. The information in this section is provided for background information.]

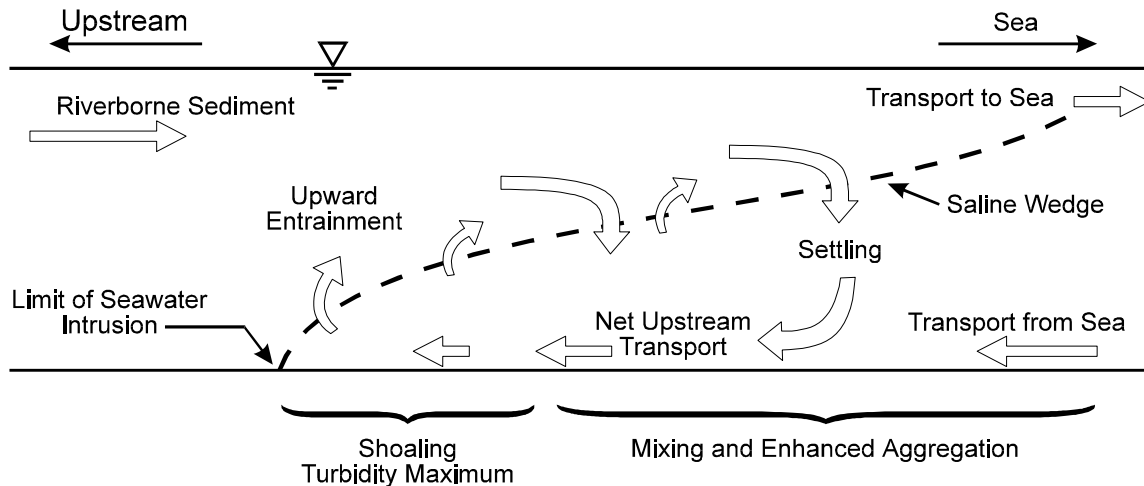


Figure 3.2 Schematic Representation of Transport and Shoaling Processes in the Mixing Zone of a Stratified Estuary (after Mehta and Hayter 1981).

As indicated in Figure 3.2, riverborne sediments from upstream fresh water sources arrive in the estuarial mixing zone. The comparatively high level of turbulence, the associated shearing rates, and the increasingly saline waters will cause aggregates to form and grow in size as a result of frequent interparticle collisions and increased cohesion. The large aggregates will settle to the lower portion of the water column because of their high settling velocities. Results from laboratory experiments show that aggregate settling velocities can be up to four orders of magnitude larger than the settling velocities of elementary particles (Bellessort 1973). Some of the sediment will deposit; the remainder will be carried upstream near the bottom until periods close to slack water when the bed shear stresses decrease sufficiently to permit deposition, after which the sediment starts to undergo self-weight consolidation. The depth to which the new deposit scours when the currents increase after slack will depend on the bed shear stresses imposed by the flow and the shear strength of the deposit. Net deposition, i.e., shoaling, will occur when the bed shear during flood, as well as during ebb, is insufficient to resuspend all of the material deposited during preceding slack periods. Some of the sediment that is resuspended will be re-entrained throughout most of the length of the mixing zone to levels above the sea water-fresh water interface and will be transported downstream as before. At the seaward end, some material may be transported out of the system, a portion of which could ultimately return with the net upstream bottom current.

In the mixing zone of a typical estuary, the sediment transport rates often are an order of magnitude greater than the rate of inflow of "new" sediment derived from upland or oceanic sources. The estuarial sedimentary regime is characterized by several periodic (or quasi-periodic) macro-time-scales, the most important of which are the tidal period (diurnal, semi-diurnal, or mixed) and one-half the lunar month (spring-neap-spring cycle). The tidal period is the most important since it is the fundamental period that characterizes the basic mode of sediment transport in an estuary. The lunar month is often significant in determining net shoaling rates.

From an Eulerian point of view, the superposition of oscillating tidal flows on the quasi-steady state transport phenomenon depicted in Figure 3.2 results in corresponding oscillations of the suspended sediment concentration with time as shown in Figure 3.3. Such a variation of the suspended load ultimately results from a combination of advective and dispersive transport, erosion, and deposition. Because of the complexity of the phenomenon, more than one interpretation is possible as far as any schematic representation of these phenomena is concerned. One such representation is shown in Figure 3.4. According to this description, cohesive sediments can exist in four different physical states in an estuary: mobile suspension, stationary suspension, partially consolidated bed, and settled bed. The last two are formed as a result of consolidation of a stationary suspension. Stationary here implies little horizontal movement. A stationary suspension, a partially consolidated bed and a settled bed may erode if the shear stress exceeds a certain critical value. Erosion of a stationary suspension is referred to as redispersion or mass erosion, whereas erosion of a partially consolidated bed or a settled bed is termed either resuspension or surface erosion.

To summarize, the sedimentary regime in an estuary is controlled by the hydrodynamics, chemical composition of the fluid, and physicochemical properties of the cohesive sediments. These factors affect the processes of erosion, advection, dispersion, aggregation, settling, deposition, and consolidation. A description of these processes follows that of cohesive sediment beds.

3.2.2.2 Sediment Bed

A flow-deposited bed of cohesive sediment aggregates possesses a vertical density and shear (i.e., yield) strength profile. The profile changes in time primarily due to consolidation and

secondarily due to thixotropy and associated physicochemical changes affecting inter-particle forces. Consolidation is caused by the gravitational force (overburden) of overlying deposited aggregates that crushes, and thereby decreases the order of aggregation of, the underlying sediment. The average values of bed density and bed shear strength increase and their vertical profiles change during the consolidation process. Consolidation changes the erosive behavior of cohesive sediment beds in two ways: (1) as the shear strength of the bed increases due to consolidation, the susceptibility of the bed to erosion decreases, and (2) the vertical shear strength profile determines the level to which a bed will erode when subjected to excess shear, i.e., an applied bed shear stress in excess of the bed surface shear strength.

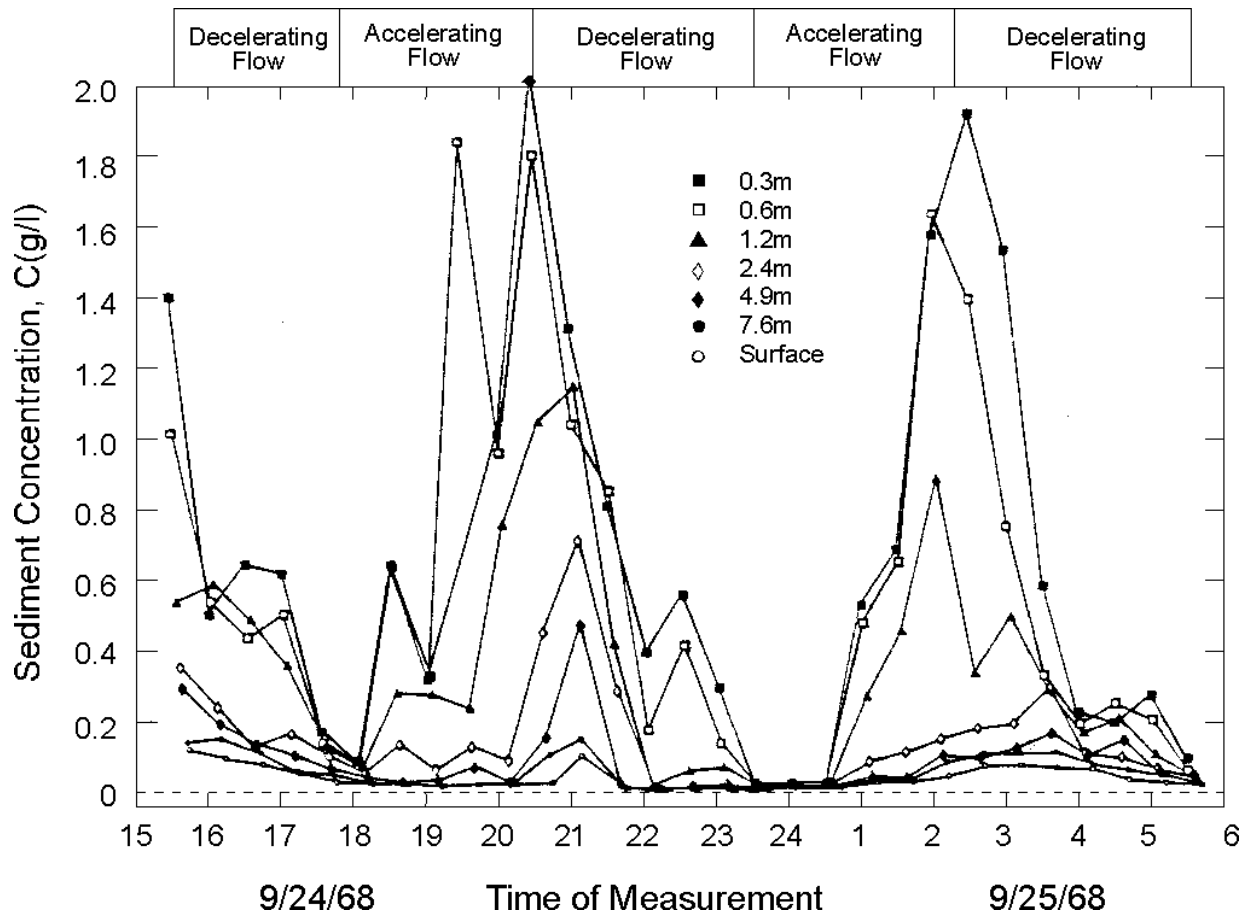


Figure 3.3 Time and Depth Variation of Suspended Sediment Concentration in the Savannah River Estuary (after Krone 1972).

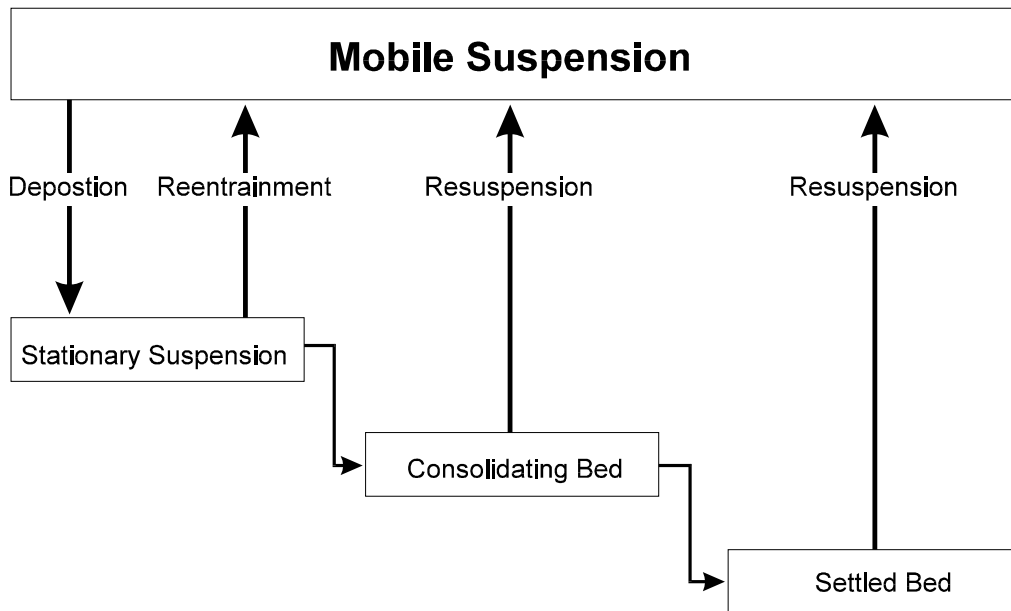


Figure 3.4 Schematic Representation of the Physical States of Cohesive Sediment in Estuarial Mixing Zone (after Mehta *et al.* 1982a).

3.2.2.2.1 Bed Structure -- Estuarial sediment beds, typically composed of flow-deposited cohesive sediments, occur in three different states: stationary suspensions, partially consolidated beds, and settled (or fully consolidated) beds. Stationary suspensions are defined by Parker and Lee (1979) as assemblages of high concentrations of sediment particles that are supported jointly by the water and developing skeletal soil framework and have no horizontal movement. These suspensions develop whenever the settling rate of concentrated mobile suspensions exceeds the rate of self-weight consolidation (Parker and Kirby 1982). They tend to have a high water content (therefore low bulk density) and a very low, but measurable, shear strength that must be at least as high as the bed shear that existed during the deposition period (Mehta *et al.* 1982a). Thus, they exhibit a definite non-Newtonian rheology. Kirby and Parker (1977) found that the stationary suspensions they investigated had a surface bulk density of approximately 1050 kg/m^3 and a layered structure. Krone (1963) found that, in addition to the bed shear, the structure of these suspensions depends on the aggregate order (see Section 3.2.2.7) in the following manner. If aggregates deposit without being broken up by the bed shear, the top layers of these suspensions

will be composed of an aggregate network whose aggregation order is one higher than that of the individual settling aggregates; therefore, these layers will have lower bulk densities and shear strengths than those of the aggregates that form them.

Whether redispersion of these suspensions occurs during periods of erosion depends upon the mechanical shear strength of this aggregate network. That portion remaining on the bed undergoes: (1) self-weight consolidation, and (2) thixotropic effects, defined as the slow rearrangement of deposited aggregates attributed to internal energy and unbalanced internal stresses (Mitchell 1961), both of which reduce the order of aggregation of sub-surface bed layers. This implies that the bed becomes stratified with respect to density and shear strength, with both properties typically increasing monotonically with depth, at least under laboratory conditions (Mehta *et al.* 1982a).

Continued consolidation eventually results in the formation of settled mud, defined by Parker and Lee (1979) as "assemblages of particles predominantly supported by the effective contact stresses between particles as well as any excess pore water pressure." This portion of the bed has a lower water content, lower order of aggregation, and higher shear strength. The settled mud in the Severn Estuary and Inner Bristol Channel, United Kingdom, was found to possess a bulk density ranging from 1300 to 1700 kg/m³ (Kirby and Parker 1983).

The nature of the density and shear strength profiles typically found in flow-deposited cohesive sediment beds has been revealed in laboratory tests by, among others, Richards *et al.* (1974), Owen (1975), Thorn and Parsons (1980), Parchure (1980), Bain (1981), Dixit (1982), and Burt and Parker (1984). A review of this subject is given by Hayter (1983).

3.2.2.2.2 Effect of Salinity on Bed Structure -- For most cohesive soils the inter-particle and inter-floc contact is considered to be the only significant region between particles where normal stresses and shear stresses can be transmitted (Mitchell *et al.* 1969). In particular, it seems very likely that the primary role of the double-layer interaction and other physicochemical forces is to control the structure of the soil and to alter the transmitted stresses from what they would be due to the flow-induced shear and overburden normal stresses alone. Hayter and Mehta (1982) discuss the effect of swelling and permeability (including the effect of salinity) on the structure of a cohesive soil. They also discuss the effect of the salinity of the pore fluids on bed density.

Using the method described by Mehta *et al.* (1982a), the bed shear strength, τ_c , of mud from Lake Francis, Nebraska, as a function of depth below the initial bed surface, Z , was determined as a function of salinity for salinities from 0 to 10 ppt (Figure 3.5). This mud, of which 50% was finer than $2\mu\text{m}$ (clay-sized particles), with montmorillonite, illite, kaolinite and quartz being the predominant minerals, had a CEC of 100 meq/100 g. Two trends are observed in this graph. First, τ_c increases with depth in the upper part of the bed for all salinities (no definite data could be obtained for the lower part of the bed, i.e., for $Z > 0.5$ cm, inasmuch as this portion of the bed did not erode during these experiments). Second, τ_c increases with increasing salinity from 0 to 2 ppt; thereafter, for salinities up to 10 ppt, no measurable increase in τ_c occurred.

3.2.2.3 Erosion

Erosion of cohesive soils occurs whenever the shear stress induced by fluid flow over the bed is great enough to break the electrochemical interparticle bonds (Partheniades 1965; Paaswell 1973). When this happens, erosion takes place by the removal of individual sediment particles and/or aggregates. This type of erosion is time dependent and is defined as surface erosion or resuspension. In contrast, another type of erosion occurs more or less instantaneously by the removal or entrainment of relatively large pieces of soil. This process is referred to as mass erosion or redispersion occurs when the flow induced shear stresses on the bed exceed the soil bulk strength along some deep seated plane.

A number of laboratory investigations were carried out in the 1960's and 1970's in order to determine the rate of resuspension, ϵ , defined as the mass of sediment eroded per unit bed surface area per unit time as a function of bed shear in steady, turbulent flows. An important conclusion from these tests was that the usual soil indices such as liquid and plastic limit do not adequately describe the erosive behavior of these soils (Mehta 1981). For example, Partheniades (1962) concluded that the bed shear strength as measured by standard tests, e.g., the direct-shear test (Terzaghi and Peck 1960), has no direct relationship with the soil's resistance to erosion, which is essentially governed by the strength of the interparticle and interaggregate bonds. Shown in Table 3.1 are various physicochemical factors known to govern the erosive properties of cohesive soils. These factors must be specified to properly characterize the erosive behavior. The hydrodynamic factors define the erosive forces; the bed and fluid physicochemical properties determine the resistivity of the bed to erosion.

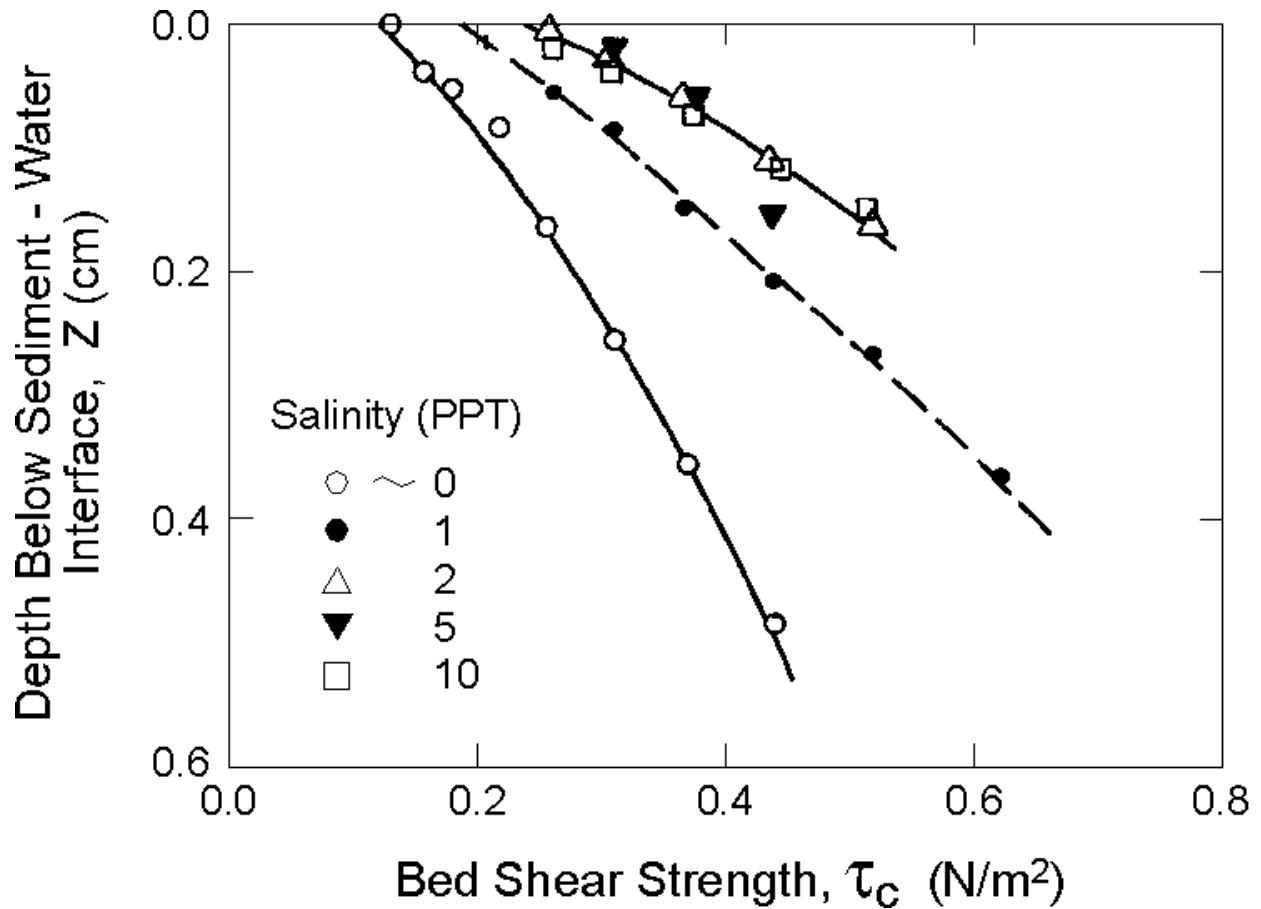


Figure 3.5 Bed Shear Strength Profiles as Functions of Salinity.

The sediment composition, pore and eroding fluid compositions, and structure of the flow-deposited bed at the onset of erosion must be determined in order to properly define the erosion resistance of the bed. Sediment composition is specified by the grain size distribution of the bed material (i.e., weight fraction of clays, silts), the type of clay minerals present, and the amount and type of organic matter. The compositions of the pore and eroding fluids are specified by the temperature, pH, total amounts of salts and type and abundance of ions present, principally Cl^- , Na^+ , Ca^{2+} , and Mg^{2+} . Cementing agents such as iron oxide can significantly increase the resistance of a sediment bed to erosion. Measurement of the electrical conductivity is used to determine the total salt concentration. The effect of the bed structure, specifically the vertical sediment density and shear strength profiles, on the rate of erosion is discussed by Lambermont and Lebon (1978) and Mehta *et al.* (1982a).

Table 3.1 Principal Factors Controlling Erosion of Saturated Cohesive Sediment Beds

HYDRODYNAMIC FACTORS (Erosive Force)		
BED SHEAR STRESS	Flow Characteristics	
	Bed-Fluid Interface	
BED AND FLUID PROPERTIES (Resistive Force)		
PROPERTY	FACTOR	INDICATOR
SEDIMENT COMPOSITION	Clay Mineral Type	Ion Exchange Capacity
	Clay Percentage by Weight	
	Organic Matter	
PORE FLUID COMPOSITION	Mono- and Di-valent Cation Concentrations	Conductivity (Na ⁺ , Ca ²⁺ , Mg ²⁺)
	Relative Abundance of Mono- and Di-valent Cations	SAR
	Temperature	
	pH	
ERODING FLUID COMPOSITION	Salinity (NaCl, CaCl ₂ , MgCl ₂)	
	Temperature	
	pH	
	Cementing Agents (Iron Oxide, etc.)	
BED STRUCTURE	Stress History	Placed Bed
		Deposited Bed

The erosive forces, characterized by the flow-induced instantaneous bed shear stress, are determined by the flow characteristics and the surface roughness of the fluid-bed interface. Several different types of relationships between the rate of erosion, ε , and the time-mean value of the flow-induced bed shear stress, τ_b , have been reported for non-stratified beds. These include statistical-mechanical models (Partheniades 1965; Christensen 1965), a rate process model (Paaswell 1973; Kelley and Gularte 1981), and empirical relationships (Ariathurai and Arulanandan 1978).

The resuspension rate, ε , is related to the time-rate of change of the suspension concentration, dC/dt , and to the time-rate of change of the depth of erosion, z_e , with respect to the original bed surface elevation by two expressions:

$$\varepsilon = d \frac{dC}{dt}; \quad \frac{dC}{dt} = \frac{1}{d} \rho_s(z_e) \frac{dz_e}{dt} = \left. \frac{dC}{dt} \right|_e \quad (3.9)$$

where:

$\rho_s(z_e)$ is the dry sediment density at the elevation corresponding to z_e ,

C = mass of sediment per unit volume of water and sediment mixture.

Ariathurai and Arulanandan (1978) found the following general relationship for consolidated beds:

$$\varepsilon = M' \left(\frac{\tau_b - \tau_c}{\tau_c} \right) \quad (3.10)$$

where $M' = M \cdot \tau_c$, where M is termed the erodibility constant, τ_b is the flow induced bed shear stress and τ_c is the bed shear strength.

Figure 3.6 shows the measured variation of C with time typically found by several investigators (Partheniades 1962; Mehta and Partheniades 1979; Mehta *et al.* 1982a) in laboratory resuspension tests with flow-deposited (stratified) beds under a constant τ_b . As observed, dC/dt is high initially, decreases monotonically with time, and appears to approach zero. The value of τ_c at the depth of erosion at which dC/dt , and therefore ε becomes essentially zero has been interpreted to be equal to τ_b (Mehta *et al.* 1982a). This interpretation is based on the hypothesis that erosion continues as long as $\tau_b > \tau_c$. Erosion is arrested at the bed level at which $\tau_b - \tau_c = 0$. This interpretation, coupled with measurement of $\rho_s(z_b)$ and the variation of C with time results in an

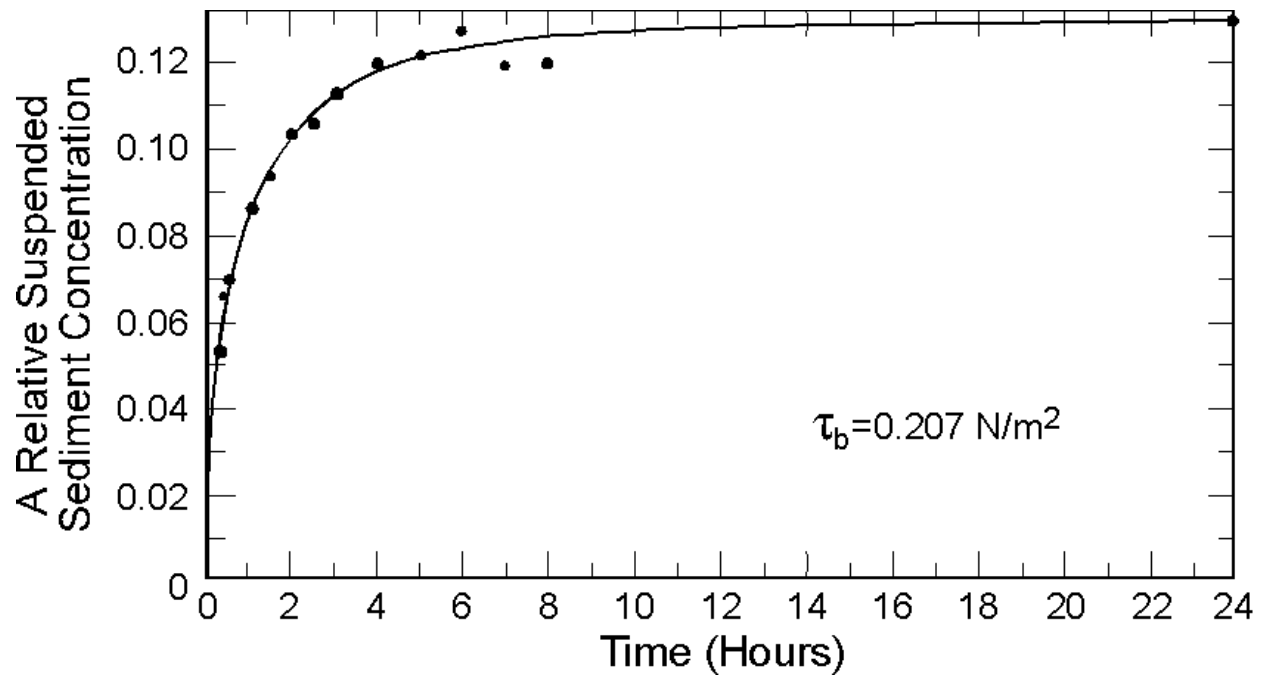


Figure 3.6 Relative Suspended Sediment Concentration versus Time for a Stratified Bed (after Mehta and Partheniades 1979)

empirical relationship for the rate of erosion of stratified beds.

Utilizing the above approach, resuspension experiments with deposited beds were performed by Parchure (1980) in a rotating annular flume and by Dixit (1982) in a recirculating straight flume. The following empirical relationship between ε and $\tau_b - \tau_c(z_b)$ was derived from these experiments:

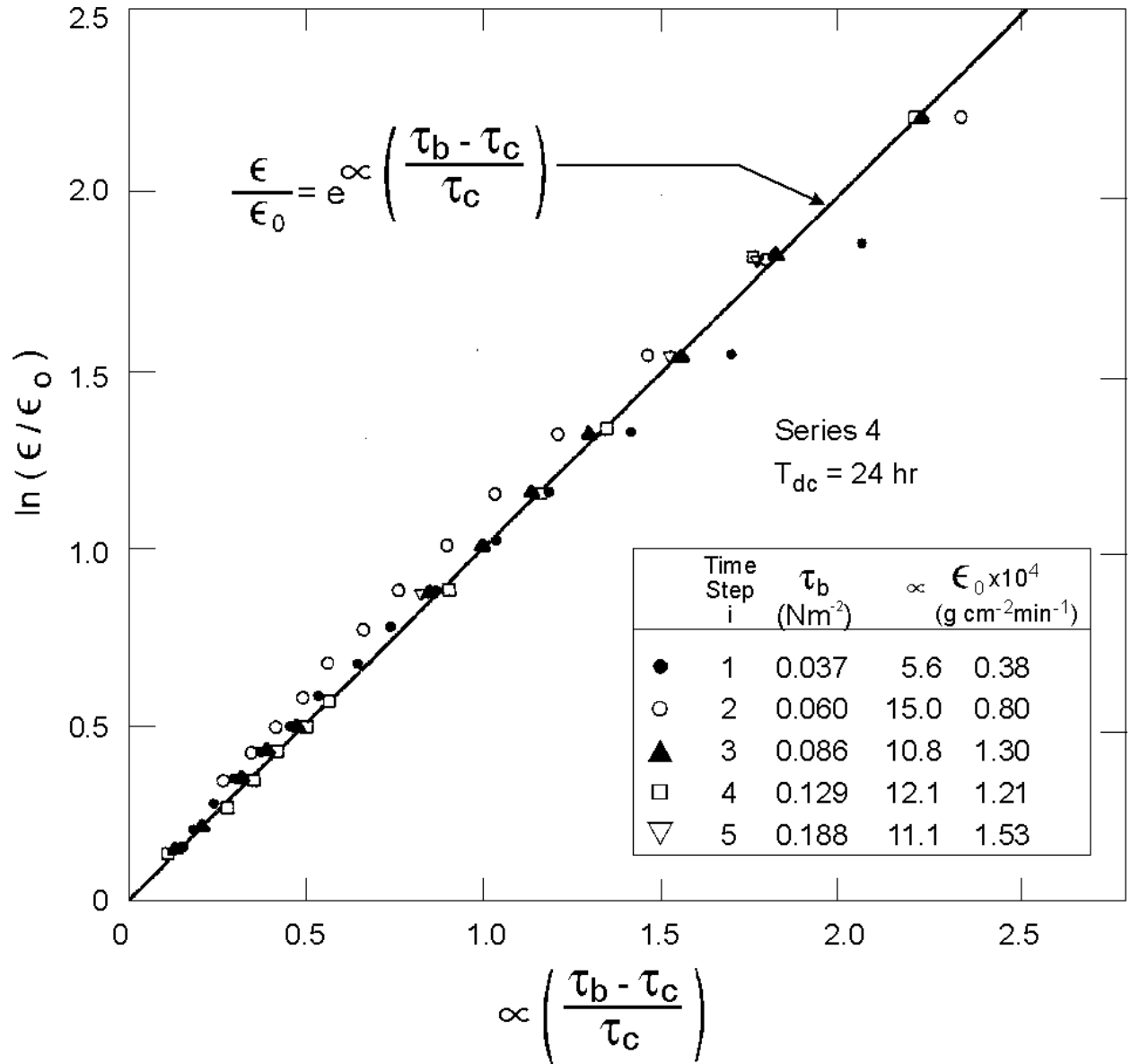


Figure 3.7 Normalized Rate of Erosion versus Normalized Excess Shear Stress Using Kaolinite in Tap Water (after Mehta *et al.* 1982a).

$$\varepsilon = \varepsilon_0 \exp \left[\alpha \frac{\tau_b - \tau_c(z_b)}{\tau_c(z_b)} \right] \quad (3.11)$$

where ε_0 and α are empirical resuspension coefficients. Figure 3.7 shows this relationship for tests in tap water. This relationship is analogous to the rate expression that results from a heuristic interpretation of rate process theory for chemical reactions (Mehta *et al.* 1982a). Christensen and Das (1973), Paaswell (1973) and Kelley and Gularte (1981) have used the rate process theory in explaining the erosional behavior of cohesive sediment beds. By analogy, ε is a quantitative measure of the work done by τ_b on the system, i.e., the bed, and ε_0 and $\alpha/\tau_c(z_b)$ are measures of the system's internal energy, i.e., bed resistance to an applied external force.

An important conclusion reached from these experiments was that new deposits should be treated separately from consolidated beds (Mehta *et al.* 1982a). The rate of surface erosion of new deposits may be evaluated using equation 3.11, while the erosion rate for settled beds may be suitably determined using equation 3.10, in which ε varies linearly with the normalized excess bed shear stress. The reasons for this differentiation in determining ε are twofold: 1) typical τ_c and ρ_s profiles in settled beds vary less significantly with depth than in new deposits, and may even be nearly invariant. Therefore, the value of $(\tau_b/\tau_c) - 1 = \Delta\tilde{\tau}_b$ will be relatively small. For $\Delta\tilde{\tau}_b \ll 1$, the exponential function in equation 3.11 can be approximated by $\alpha \cdot (1 + \Delta\tilde{\tau}_b)$, which represents the first two terms in the Taylor series expansion of $\exp(\alpha(\Delta\tilde{\tau}_b))$. Thus, for small values of $\Delta\tilde{\tau}_b$ both expressions for ε vary linearly with $\Delta\tilde{\tau}_b$ and, therefore, the variation of ε with depth in settled beds can be just as accurately and more simply determined using equation 3.10. 2) The laboratory resuspension tests required to evaluate the coefficients ε_0 and α for each partially consolidated bed layer cannot be practically or easily performed using vertical sections of an original settled bed (obtained from cores). A simpler laboratory test has been described by Ariathurai and Arulanandan (1978) to evaluate the variability of M with depth.

3.2.2.3.1 Effect of Salinity on Resuspension - Sea salt is a mixture of salts, with monovalent sodium ions and divalent calcium and magnesium ions prevalent as natural electrolytes. The sodium adsorption ratio (SAR), defined as,

$$\text{SAR} = \frac{\text{Na}^+}{\left[\frac{1}{2}(\text{Ca}^{2+} + \text{Mg}^{2+})\right]^{1/2}} \quad (3.12)$$

is a measure of the relative abundance of the three mentioned salts. The cation concentrations in equation 3.18 are in milliequivalents per liter (Arulanandan 1975).

Sherard *et al.* (1972) have shown that the susceptibility of a cohesive sediment bed to erosion depends on two factors: 1) pore fluid composition, as characterized by the SAR, and 2) salinity of the eroding fluid. It was found that, as the eroding fluid salinity decreases, soil resistivity to resuspension decreases. In addition, Kandiah (1974) and Arulanandan *et al.* (1975) found that the erosion resistance decreased and the rate of resuspension increased with increasing SAR (and therefore decreasing valency of the cations) of the pore fluid.

3.2.2.4 Advection and Dispersion

Once eroded from the bed, cohesive sediment is transported entirely as suspended load (not as bed load) by the estuarial barotropic and baroclinic circulation. Such transport is the result of three processes: (1) advection -- the sediment is assumed to be transported at the speed of the local mean flow; (2) turbulent diffusion -- driven by spatial suspended sediment concentration gradients, the material is diffused laterally across the width of the flow channel, vertically over the depth of flow, and longitudinally in the direction of the transport; and (3) longitudinal dispersion -- the suspended sediment is dispersed in the flow direction by spatial velocity gradients (Ippen 1966).

The principle of conservation of mass with appropriate source and sink terms describes the advective and dispersive transport of suspended sediment in a turbulent flow field. In this law, expressed by the advection-dispersion equation, the time-rate of change of mass of sediment in a stationary control volume is equated to the spatial rate of change of mass due to advection by an external flow field plus the spatial rate of change of mass due to diffusion and dispersion processes. The two-dimensional, depth-averaged form of the advection-dispersion equation is given here:

$$\begin{aligned} \frac{\partial C}{\partial t} + u \frac{\partial C}{\partial x} + v \frac{\partial C}{\partial y} = \frac{\partial}{\partial x} \left[D_{xx} \frac{\partial C}{\partial x} + D_{xy} \frac{\partial C}{\partial y} \right] \\ + \frac{\partial}{\partial y} \left[D_{yx} \frac{\partial C}{\partial x} + D_{yy} \frac{\partial C}{\partial y} \right] + S_T \end{aligned} \quad (3.13)$$

where D_{ij} = effective sediment dispersivity tensor, and S_T = source/sink term. Implicit in equation 3.13 is the assumption that suspended material has the same velocity as the water. Sayre (1968) verified the reasonableness of this assumption for sediment particles less than about 100 μm in diameter. Rolling and saltation of sediment, which occurs during bed load transport, can cause a significant difference between the water and sediment velocities. Therefore, this assumption is not applicable to sediment transported as bed load. As mentioned previously, cohesive sediment in an estuary is believed to be transported as suspended load only. The source/sink term in equation 3.13 is expressed as

$$S_T = \left. \frac{dC}{dt} \right|_e + \left. \frac{dC}{dt} \right|_d + S_L \quad (3.14)$$

where $\left. \frac{dC}{dt} \right|_e$ is the rate of sediment addition (source) due to erosion from the bed, and $\left. \frac{dC}{dt} \right|_d$ is the

rate of sediment removal (sink) due to deposition of sediment. Expressions for $\left. \frac{dC}{dt} \right|_e$ and $\left. \frac{dC}{dt} \right|_d$

are given in Sections 3.2.2.3 and 3.2.2.9 respectively. S_L accounts for removal (sink) of a certain mass of sediment, for example, by dredging in one area (e.g., navigational channel) of a water body, and dumping (source) of sediment as dredge spoil in another location.

3.2.2.5 Dispersive Transport

Taylor (1953, 1954) proved that a one-dimensional dispersion equation can be used to represent the longitudinal dispersion of a quantity (e.g., sediment) in turbulent pipe flow. Taylor's analysis has since been extended to shear flow in both rivers and estuaries. There have been numerous studies on the dispersion of a quantity in a bounded shear flow in the years since

Taylor's work. In this section, a brief review of dispersive transport theory precedes that of estuarial dispersion.

The governing equation (eq. 3.13) derived for the two-dimensional, depth-averaged transport of suspended sediment in a turbulent flow field includes dispersive transport terms that account for transport of sediment by processes other than advective transport. Some of these processes include the effects of spatial (i.e., transverse and vertical) velocity variations in bounded shear flows and turbulent diffusion. Thus, the effective sediment dispersion coefficients in equation 3.13 must include the effect of all processes whose scale is less than the grid size of the model, or, in other words, what has been averaged over time and/or space (Fischer *et al.* 1979). For example, the effect of the vertical concentration gradient would have to be (at least approximately) incorporated in the dispersion coefficients in depth-averaged transport models.

Diffusion is defined as "the transport in a given direction at a point in the flow due to the difference between the true advection in that direction and the time average of the advection in that direction," and dispersion is defined as "the transport in a given direction due to the difference between the true advection in that direction and the spatial average of the advection in that direction" (Holley 1969). Holley delineates the fact that diffusion and dispersion are both actually advective transport mechanisms, and that in a given flow field, the relative importance of one mechanism over the other depends on the magnitude of the concentration gradient. In equation 3.13, the effective sediment dispersion coefficients are equal to the sum of the turbulent diffusion and dispersion coefficients. This approach follows the analysis of Aris (1956) that showed that the coefficients due to turbulent diffusion and shear flow (dispersion) were additive. Thus, the analytic expressions to be used for the effective sediment dispersion tensor would include, at least in some sense, both diffusion and dispersion.

Fischer (1966) showed that the dispersion of a given quantity of tracer injected into a natural stream is divided into two separate phases. The first is the convective period in which the tracer mixes vertically, laterally, and longitudinally until it is completely distributed across the stream. The second phase is the diffusive period during which the lateral and possibly the vertical (depending on the nature of the tracer) concentration gradient is small, and the longitudinal concentration profile is highly skewed. Equation 3.13 is strictly valid only in the diffusive period. The criterion for determining whether the dispersing tracer is in the diffusive period is if it has

been in the flow longer than the Lagrangian time scale and has spread over a distance wider than the Lagrangian length scale (Fischer *et al.* 1979). The latter scale is a measure of the distance a particle travels before it forgets its initial conditions (i.e., initial position and velocity).

Analytic expressions for the sediment (mass) diffusion coefficients can be obtained by analogy with the kinematic eddy viscosity. Specifically, the Reynolds analogy assumes that the processes of momentum and mass transfer are similar, and that the turbulent diffusion coefficient, and the kinematic eddy viscosity, ϵ_v , are in fact linearly proportional. Jobson and Sayre (1970) verified the Reynolds analogy for sediment particles in the Stokes range (less than about 100 μm in diameter). They found that the "portion of the turbulent mass transfer coefficient for sediment particles which is directly attributable to tangential components of turbulent velocity fluctuations: (a) is approximately proportional to the momentum transfer coefficient and the proportionality constant is less than or equal to 1; and (b) decreases with increasing particle size." Therefore, the effective sediment mass dispersion coefficients for cohesive sediments may be justifiably assumed to be equal to those for the water itself.

Fischer *et al.* (1979) define four primary mechanisms of dispersion in estuaries: 1) gravitational circulation, 2) shear-flow dispersion, 3) bathymetry-induced dispersion and 4) wind-induced circulations. Gravitational or baroclinic circulation in estuaries is the flow induced by the density difference between fresh water at the landward end and sea water at the ocean end. There are two types of gravitational circulation. Transverse gravitational circulation is depth-averaged flow that is predominantly seaward in the shallow regions of a cross-section and landward in the deeper parts. Figure 3.8 depicts this net depth-averaged upstream (landward) and downstream (seaward) transport and the resulting transverse flow from the deeper to shallower parts of the cross-section. The interaction between the cross-sectional bathymetry and baroclinic flow causes the transverse circulation. Vertical gravitational circulation is schematically illustrated in Figure 3.8, which shows the predominantly seaward flow in the upper part of the flow and landward flow in the lower part. Fischer (1972) believed that vertical gravitational circulation is more important than transverse circulation only in highly stratified estuaries.

The mechanism of shear-flow dispersion is thought to be the dominant mechanism in long, fairly uniform sections of well-mixed and partially stratified estuaries (Fischer *et al.* 1979). Holley *et al.* (1970) applied the dispersion analysis of Taylor (1954) to oscillating flow in estuaries. They

concluded that, for wide estuaries, the effect of the vertical velocity distribution on shear-flow dispersion is dominant over that of the transverse velocity distribution. The exact opposite situation was found for relatively narrow estuaries.

The joint influence of bathymetry and density differences on dispersion has already been mentioned in reference to baroclinic circulation. Other examples of bathymetry-induced dispersion include: intrusion of salinity or sediment in certain parts of a cross-section caused by channelization of flood and ebb tides in tidal inlets or narrow estuaries (Fischer *et al.* 1979) and enhanced dispersion of a quantity (e.g., pollutant) or intrusion of salinity in tidal flats and side embayments, which serve as storage areas for these constituents, caused by the out of phase flow that occurs between the main channel and such features (Okubo 1973).

An example of wind-induced circulation is shown in Figure 3.9. The steady onshore wind causes a circulation in the wind direction in the shallow bay, where the smaller water mass per unit surface area results in a higher acceleration and therefore quicker response to wind-induced surface stresses, and in the opposite direction in deeper sections of the channel. Such a circulation can cause significant dispersion (Fischer *et al.* 1979).

3.2.2.6 Coagulation

Coagulation of suspended cohesive sediments depends upon interparticle collision and cohesion. Cohesion and collision, discussed in detail elsewhere (Kruyt (1952), Einstein and Krone (1962), Krone (1962), Partheniades (1964), O'Melia (1972), and Hunt (1980)) are briefly reviewed here.

The collision frequency, FC, for suspended sediment particles of effective diameters d_i and d_j is given by (Hunt 1980):

$$FC = \beta(d_i, d_j) dN_i dN_j \quad (3.15)$$

where $\beta(d_i, d_j)$ = collision function determined by the collision mechanism (discussed below), dN_i = number of particles with sizes between d_i and $d_i + \Delta(d_i)$ per unit volume of the fluid and dN_j = number of particles with sizes between d_j and $d_j + \Delta(d_j)$ per unit volume of the fluid.

There are three principle mechanisms of interparticle collision in suspension, and these influence the rate at which elementary sediment particles coagulate. The first is due to Brownian motion resulting from thermal motions of molecules of the suspending ambient medium. The collision function corresponding to this mechanism is given by (Hunt 1980):

$$\beta_b(d_i, d_j) = \frac{2}{3} \frac{kT_k}{\mu} \frac{(d_i + d_j)^2}{d_i d_j} \quad (3.16)$$

where k = Boltzmann constant, T_k = absolute temperature and μ = dynamic viscosity of the fluid. Generally, coagulation rates by this mechanism are too slow to be significant in estuaries unless the suspended sediment concentration exceeds 10 g/l as it sometimes does in fluid mud (a high density near-bed layer). Aggregates formed by this mechanism are weak, with a lace-like structure, and are easily fractured by shearing, especially in the high shear environment near the bed, or are crushed easily when deposited (Krone 1962).

The second mechanism is due to internal shearing produced by local velocity gradients in the fluid. Collision will occur if the paths of the particles' centers in the velocity gradient are displaced by a distance that is less than the sum of their radii (referred to as the collision radius, R_{ij} , between d_i and d_j size particles). The collision function is given as

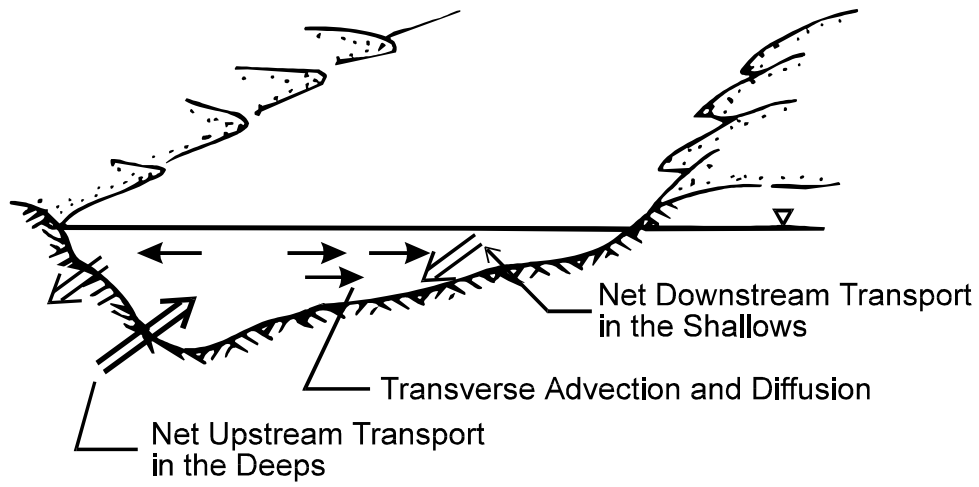
$$\beta_{sh}(d_i, d_j) = \frac{G}{6} R_{ij}^3 \quad (3.17)$$

where G is the local shearing rate and $R_{ij} = d_i + d_j$. Aggregates produced by this mechanism tend to be spherical, and are relatively dense and strong because only those bonds that are strong enough to resist the internal shearing due to local velocity gradients can survive.

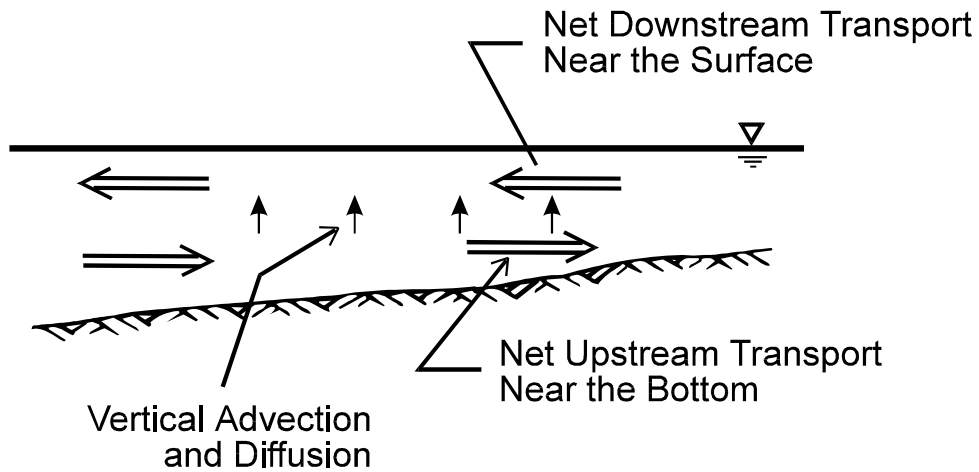
The third mechanism, differential sedimentation, results from particles of different sizes having different settling velocities. A larger particle, due to its higher settling velocity, will collide with smaller, more slowly settling particles and will have a tendency to "pick up" these particles. The collision function is expressed as

$$\beta_{ds}(d_i, d_j) = \frac{\pi g}{72 \nu} \left(\frac{\rho_f - \rho}{\rho} \right) (d_i + d_j)^2 |d_i^2 - d_j^2| \quad (3.18)$$

where ν = kinematic viscosity of the fluid, ρ_f = floc density and ρ = fluid density. This mechanism produces relatively weak aggregates and contributes to the often observed rapid clarification of estuarial waters at slack.



(a) A Transverse Section



(b) A Vertical Section

Figure 3.8 Internal Circulation in a Partially Stratified Estuary (after Fischer *et al.* 1979).

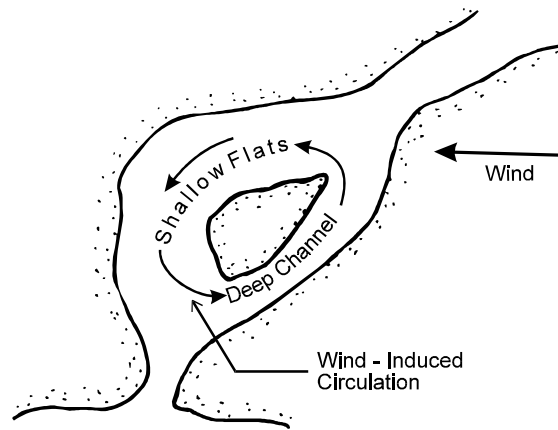


Figure 3.9 Illustration of Wind-Induced Circulation (adapted from Fischer *et al.* 1979).

All three collision mechanisms operate in an estuary, with internal shearing and differential sedimentation generally being predominant in the water column, excluding perhaps fluid mud where Brownian motion is likely to contribute significantly. The collision efficiency is less than 100%, so not all collisions result in coagulation.

Hunt (1980) compared the values of the three collision functions (eqs. 3.15-3.17) for collisions of a $d_i = 1 \mu\text{m}$ size particle with varying sizes, d_j , of the colliding particle under the following conditions: temperature 14°C , shearing rate $G = 3 \text{ sec}^{-1}$, and $(\rho_f - \rho) = 0.02$. The comparison is shown in Figure 3.10 and reveals that each collision mechanism is dominant over a certain particle size range. Hunt states that the same ordering of the dominant collision mechanisms with increasing d_j would be achieved for collisions with other d_i sizes.

3.2.2.6.1 Effect of salinity on coagulation - Cohesion or particle destabilization of colloidal particles is caused by the presence of net attractive electrochemical surface forces on the particles. Particle destabilization is promoted by an increased concentration of dissolved ions and/or an increased ratio of multivalent to monovalent ions. In both cases, the double layer around micelles is depressed and the attractive London-van der Waals and coulombic forces predominate (Krone 1963). The CEC, salinity and SAR all serve to determine the net interparticle force and thus the potential for micelles to become cohesive.

Kandiah (1974) found that the boundary between dispersed and coagulated states for the three main clay groups, kaolinite, illite and montmorillonite, varied with the SAR, total salt concentration and Ph of the solution. Kaolinite becomes cohesive at a salinity of 0.6 ppt, illite at 1.1 ppt and montmorillonite at 2.4 ppt (Ariathurai 1974). Whitehouse *et al.* (1960) and Edzwald *et al.* (1974) reported that the cohesiveness of these micelles develops quickly at the given salt concentrations, and that little increase in coagulation occurs at higher salt concentrations, which implies that the micelles must have attained the maximum degree of cohesion. The rapid development of cohesion and the low salinities at which the main clay types become cohesive indicates that cohesion is primarily affected by salinity variations near the landward end of an estuary where salinities are often less than about 3 ppt.

3.2.2.7 Aggregation

The rate and degree of aggregation are important factors that govern the transport of cohesive sediments. Factors, besides the water chemistry and magnitude of surface forces, known

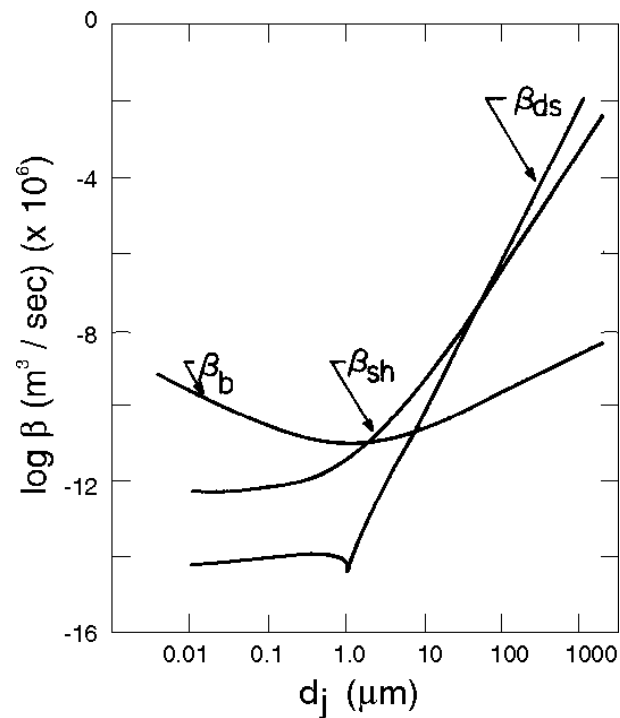


Figure 3.10 Comparison of the Collision Functions for Brownian, Shear and Differential-Sedimentation Coagulation (after Hunt 1980).

to govern coagulation and aggregation include: sediment size grading, mineralogical composition, particle density, organic content, suspension concentration, water temperature, depth of water through which the flocs have settled, and turbulence intensity (represented by the shearing rate G) of the suspending flow (Owen 1971). Bioflocculation is assumed to be negligible in this discussion.

The order of aggregation, which characterizes the packing arrangement, density and shear strength of aggregates, is determined by: (1) sediment type, (2) fluid composition, (3) local shear field, and (4) concentration of particles available for aggregation. Krone (1962) found that aggregate structure is dependent on salinity for salinities less than about 10 ppt.

Primary or 0-order flocs are highly packed arrangements of elementary particles, with each floc consisting of perhaps as many as a million particles. Typical values of the void ratio (volume of pore water divided by volume of solids) have been estimated to be on the order of 1.2. This is equivalent to a porosity of 0.55 and is a more "open" structure than commonly occurs in cohesionless sediments (Krone 1963). Continued aggregation under favorable shear gradients can result in the formation of first or higher order aggregates composed of loosely packed arrays of 0-order flocs. Each succeeding order consists of aggregates of lower density and lower shear strength. A range of aggregates of different shear strengths and densities are typically formed, with the highest order determined by the prevailing shearing rate, $G = du/dz$, provided that: (1) the sediment and fluid composition remain invariant, and (2) sufficient number of suspended particles are available for promoting coagulation and aggregation.

3.2.2.8 Settling

The settling rate of coagulated sediment particles depends on, in part, the size and density of the aggregates and as such is a function of the processes of coagulation and aggregation (Owen 1970a). Therefore, the factors that govern these two processes also affect the settling rate of the resulting aggregates. The settling velocities of aggregates can be several orders of magnitude larger than those of individual clay particles (Bellessort 1973).

3.2.2.9 Deposition

Deposition of aggregates occurs relatively quickly during slack water. Deposition also occurs in slowly moving and decelerating flows, as was observed in the Savannah River Estuary (see Figure 3.3) during the second half of flood and ebb flows (Krone 1972). Under such

conditions only those aggregates with shear strengths of sufficient magnitude to withstand the highly disruptive shear stresses in the near bed region will actually deposit and adhere to the bed. Thus, deposition is governed by the bed shear stresses, turbulence structure above the bed, settling velocity, type of sediment, depth of flow, suspension concentration and ionic constitution of the suspending fluid (Mehta and Partheniades 1973). Results of extensive laboratory erosion and deposition experiments, using a wide range of cohesive sediments under steady flow conditions, showed that erosion and deposition do not appear to occur simultaneously as they do in cohesionless sediment transport (Mehta and Partheniades 1975; 1979; Parchure 1984).

Deposition has been defined to occur when τ_b is not high enough to resuspend sediment material that settles onto and bonds with the bed surface. This process, therefore, involves two other processes, settling and bonding. Laboratory studies on the depositional behavior of cohesive sediment in steady turbulent flows have been conducted by, among others, Krone (1962), Rosillon and Volkenborn (1964), Partheniades (1965), Partheniades *et al.* (1966), Migniot (1968), Lee (1974), Mehta and Partheniades (1975) and Mehta *et al.* (1982b). The results from these and other studies on the settling rates of cohesive sediments pertinent to the deposition algorithm described in Section 5.3.4 are summarized below.

In laboratory flumes, the depositional behavior is usually investigated by allowing sediment suspended at a high shear stress to deposit by reducing the shear stress. Since the sediment concentration gradient in the direction of flow is usually small, the observed time-rate of change of the depth-averaged concentration, C , is due to the deposition of suspended material. The conservation of sediment mass can be expressed as (Einstein and Krone 1962):

$$\frac{dC}{dt} = - \frac{P_d W_s C}{d} \quad (3.19)$$

where t = time, d = flow depth, W_s = sediment settling velocity, and P_d = probability of deposition, or the probability of a sediment particle or floc bonding to the bed and not being instantly resuspended. Krone postulated that P_d increases linearly with a decrease in τ_b according to

$$P_d = 1 - \frac{\tau_b}{\tau_{cd}} \quad (3.20)$$

where τ_{cd} = critical shear stress for deposition, above which no deposition occurs. The value of τ_{cd}

was found to be equal to 0.06 N/m^2 for San Francisco Bay mud with $C < 0.3 \text{ g/l}$. Krone found that when $C < 0.3 \text{ g/l}$, W_s was independent of C . In this case, integration of equation 3.19 gives

$$\frac{C}{C_o} = \exp\left[-\frac{P_d W_s}{d} t\right] \quad (3.21)$$

where C_o is the initial suspended sediment concentration. Thus, all the suspended sediment will eventually deposit when $\tau_b < \tau_{cd}$.

For the range $0.3 \text{ g/l} < C < 10 \text{ g/l}$ and for $C > 10 \text{ g/l}$, logarithmic laws of the following form were derived:

$$\log C = -\Lambda \log(t) + \text{Constant} \quad (3.22)$$

where Λ was found to be a function of d and P_d . Krone attributed the variation of the depositional properties with suspension concentration to different forms of settling. Various forms of settling of coagulated cohesive sediments are discussed later in this section.

Partheniades (1965) conducted deposition tests in an open recirculating flume using San Francisco Bay mud. He noted that for flows above a certain critical bed shear, an initial period of rapid deposition was followed by the suspended sediment concentration approaching an equilibrium concentration, C_{eq} . The ratio $C_{eq}/C_o = C_{eq}^*$ was found to be a constant for given flow conditions, regardless of the value of C_o . Whereas for bed shears even slightly less than this critical value, all the sediment eventually deposited.

Partheniades *et al.* (1966) concluded that C_{eq} represents the amount of sediment broken up and resuspended because it could not withstand the high shear stresses present in the near bed region where it settled. In addition, the equilibrium concentration that stays in suspension appears not to be the result of an interchange between suspended and bed material, as it is for cohesionless sediment, because if such were the case, C_{eq} would not be dependent on C_o . Therefore, it follows that C_{eq} does not represent the maximum sediment carrying capacity of the flow, as it does in the case of cohesionless sediment, but instead may be considered to be the steady state concentration (Mehta and Partheniades 1973).

As noted by Mehta and Partheniades (1975), Krone did not observe C_{eq} in his tests because most of them were conducted at $\tau_b < \tau_{cd}$, where C_{eq} would be expected to be equal to zero. It is apparent that the definition of P_d must be extended to include bed shear stresses greater than τ_{cd} .

Mehta and Partheniades (1975) investigated the depositional properties of a commercial grade kaolinite in distilled water and in salt water at seawater salinity (35 ppt) in a rotating annular flume. Figure 3.11 shows typical suspended sediment concentration-time plots found in these tests. It is evident that a steady state concentration was reached in each test, and that for bed shears above approximately 0.16 N/m^2 , the value of C_{eq} was greater than zero, and in fact increased monotonically with increasing τ_b . Figure 3.12 shows the ratio $C_{eq}^* = C_{eq}/C_o$ plotted against τ_b for all the tests with kaolinite in distilled water. Two important conclusions are obtained from this figure: (1) C_{eq}^* is a constant for a given τ_b (and type of sediment) and is not a function of flow depth or C_o , and (2) for $\tau_b < \tau_{bmin}$, $C_{eq}^* = 0$. The first conclusion is based on the observation that the data points for the different flow conditions are almost randomly scattered about a "best fit" line. The minimum bed shear, τ_{bmin} , observed in Figure 3.12 may be interpreted to be the same as the τ_{cd} value defined by Krone (1962) and the critical bed shear obtained by Partheniades (1965). As observed in this figure, τ_{bmin} was found to be approximately 0.18 N/m^2 for kaolinite in distilled water. In Figure 3.13 the data of Figure 3.12 are plotted on log-normal coordinates as C_{eq}^* in percent against $\tau_b^* - 1$, where $\tau_b^* = \tau_b/\tau_{bmin}$. The straight line through the data points gives the following relationship between the two dimensionless parameters given by equations 3.23 and 3.24 on the next page.

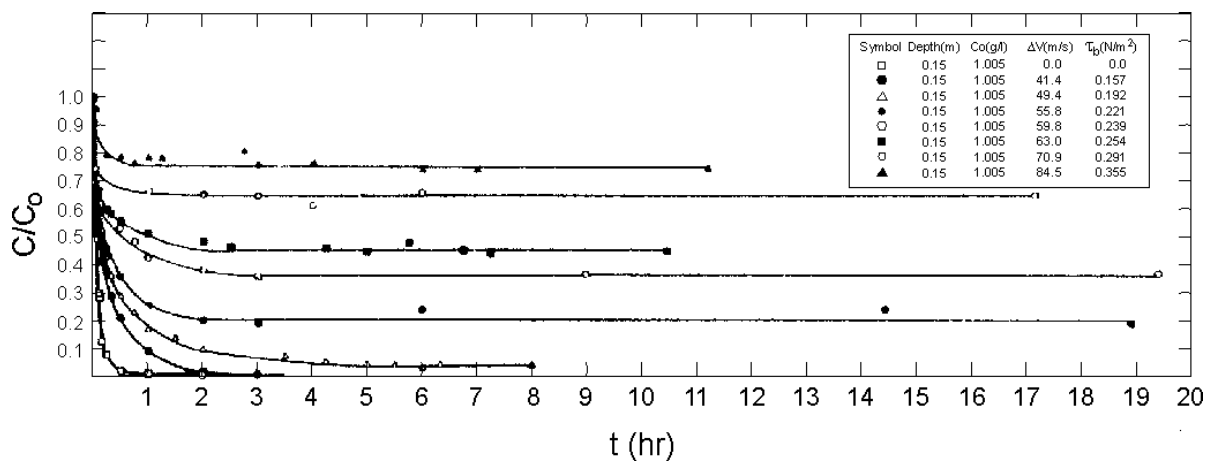


Figure 3.11 Ratio C/C_o versus Time for Kaolinite in Distilled Water (after Mehta and Partheniades 1975).

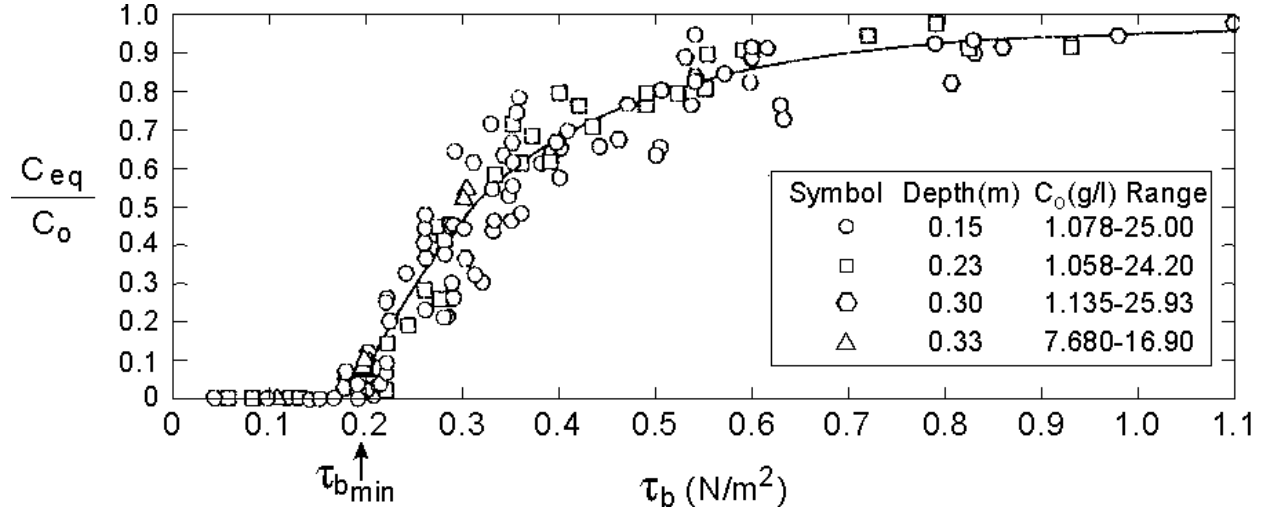


Figure 3.12 Ratio C_{eq}/C_o versus Bed Shear Stress τ_b (after Mehta and Partheniades 1975).

$$C_{eq}^* = \frac{1}{2} \left(1 + \operatorname{erf} \left(\frac{Y_a}{\sqrt{2}} \right) \right) \quad (3.23)$$

with

$$Y_a = \log_{10} \left[\frac{(\tau_b^* - 1)^{1/\sigma_1}}{(\tau_b^* - 1)_{50}} \right] \quad (3.24)$$

where σ_1 is the standard deviation and $(\tau_b^* - 1)_{50}$ is the geometric mean of the log-normal relationship given by equation 3.23 and erf is the error function. The value of σ_1 was found to be 0.49 for all tests conducted by Mehta and Partheniades (1975) and for the reanalyzed deposition tests of Rosillon and Volkenborn (1964), Partheniades (1965) and Partheniades *et al.* (1968).

Therefore, C_{eq}^* is dependent solely on the value of the ratio $(\tau_b^* - 1)/(\tau_b^* - 1)_{50}$. Mehta and Partheniades (1973) found for deposition tests in salt water the following relationship between τ_{bmin} and $(\tau_b^* - 1)_{50}$:

$$(\tau_b^* - 1)_{50} = 4 \exp(-1.27 \tau_{bmin}) \quad (3.25)$$

Mehta and Partheniades (1975) found the following dimensionless log-normal relationship for the variation of suspended sediment concentration with time:

$$C^* = \frac{1}{2} \left[1 + \operatorname{erf} \left(\frac{T}{\sqrt{2}} \right) \right] \quad (3.26)$$

where

$$T = \log_{10} \left(\frac{t}{t_{50}} \right)^{1/\sigma_2} \quad (3.27)$$

and where: $C^* = (C_o - C)/(C_o - C_{eq})$ represents the fraction of depositable sediment, $C_o - C_{eq}$, deposited at any given time t , σ_2 is the standard deviation of the log-normal relationship, and t_{50} is the geometric mean (i.e., the time at which $C^* = 50\%$). Figure 3.14 shows a comparison between

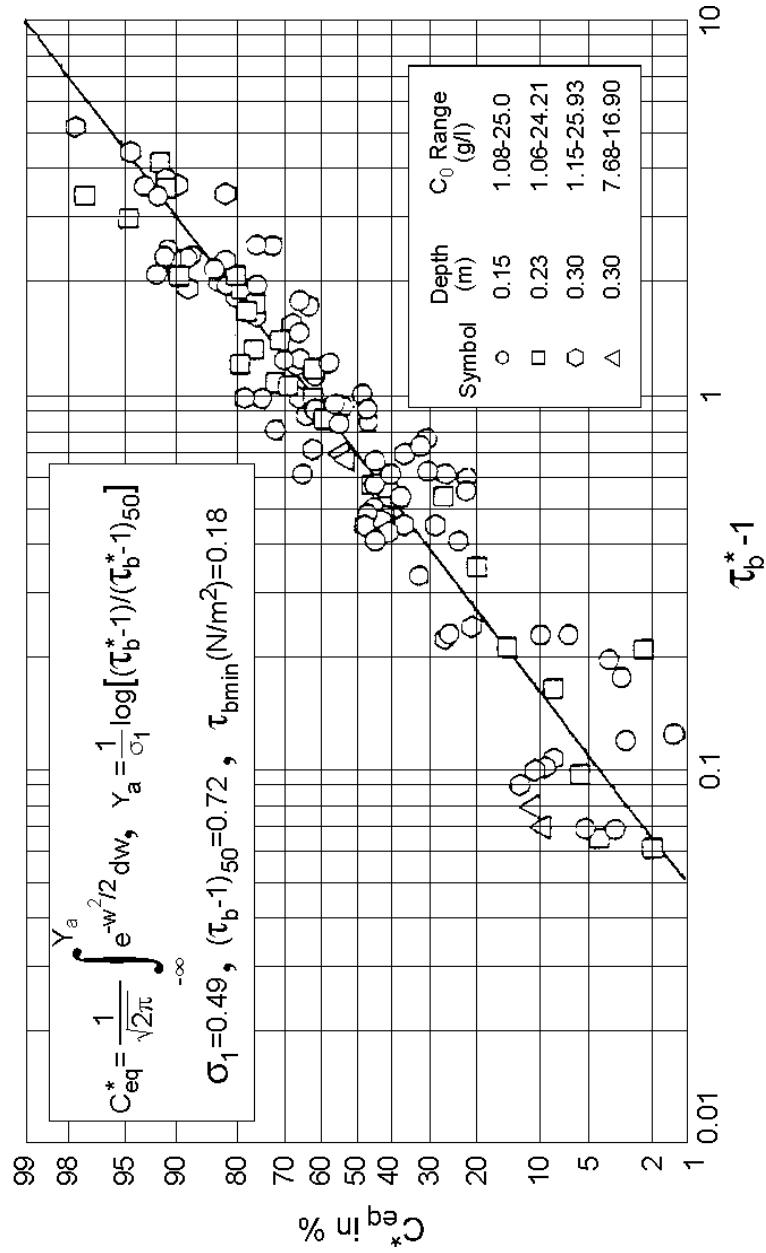


Figure 3.13 C_{eq}^* , vs $\tau_b^* - 1$ (after Mehta and Partheniades 1975).

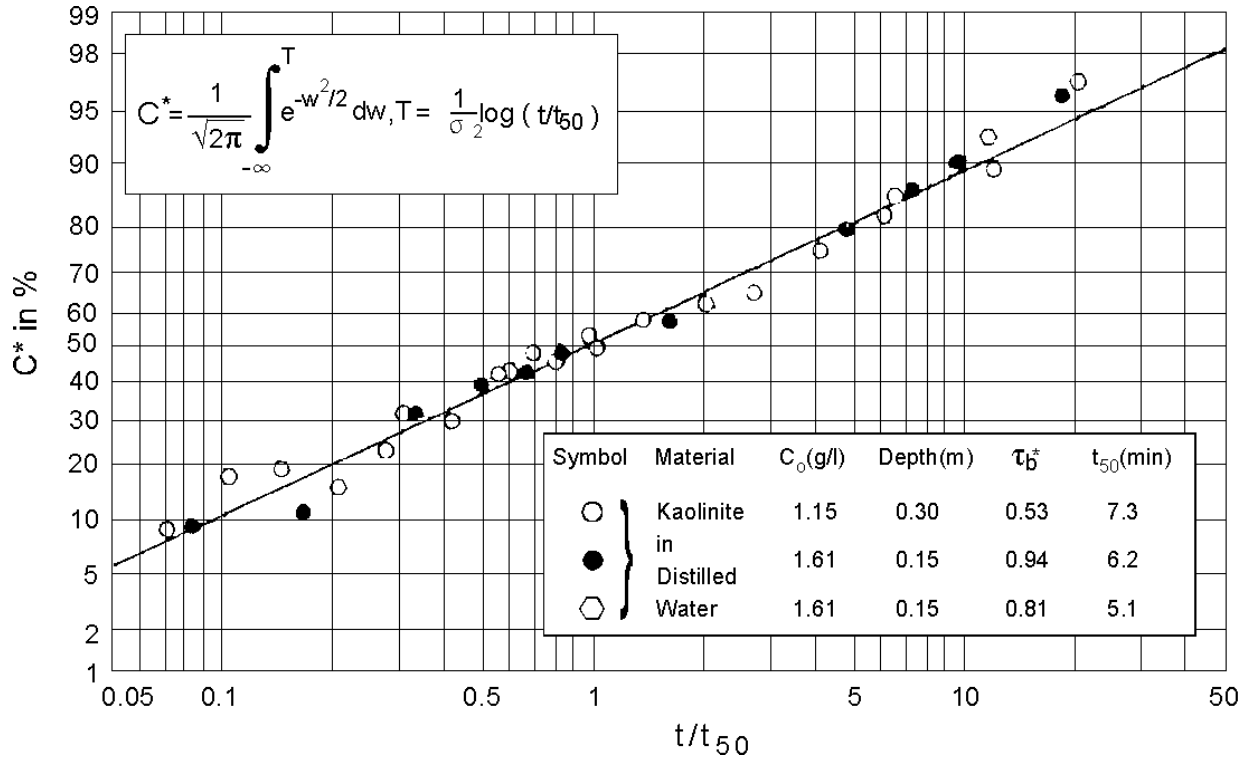


Figure 3.14 C* in Percent versus t/t₅₀ for Kaolinite in Distilled Water (after Mehta and Partheniades 1975).

some typical depositional data for kaolinite in distilled water and the log-normal relationship given by equation 3.26 and the equivalent equation on the figure. This relationship was found to hold for all values of τ_b* greater than approximately 0.25, with the exception that for very high C₀ values (around 20-25 g/l) with τ_b* < 1, an acceptable agreement between equation 3.26 and the measured data was not obtained. Good agreement was obtained between equation 3.26 and the data sets mentioned previously in this section.

Taking the derivative of equation 3.26 with respect to time gives the following expression for the rate of change of C* with time:

$$\frac{dC^*}{dt} = \frac{0.434}{\sqrt{2\pi}\sigma_2} \frac{\exp(-T^2/2)}{t} \quad (3.28)$$

The standard deviation, σ_2 , and the geometric mean, t_{50} , were found to be functions of τ_b^* and C_o . Shown in Figure 3.15 are examples of the relationships found between these parameters. Two conclusions were drawn by Mehta (1973). First, for a specific value of τ_b^* , the deposition rate was minimum. The rate of deposition increased for τ_b^* values both less than and greater than this specific value, but not as significantly for higher values as for the lower values. However, for $\tau_b > \tau_{bmax}$ no deposition of suspended sediment occurred. For San Francisco Bay mud in sea water, τ_{bmax} was determined to be 1.69 N/m^2 . Second, for $\tau_b^* < 1$, the rate of deposition increased with an increase in depth, while for $\tau_b^* > 1$, the effect of depth on the deposition rate was minimal. As previously described, the settling velocity of suspended cohesive sediment particles has been found to be a function of, among other parameters, the suspension concentration (Krone 1962). Three types of settling are: (1) no mutual interference, (2) mutual interference, and (3) hindered settling. For very low suspension concentrations, on the order of $0.1\text{-}0.7 \text{ g/l}$, the aggregates or elementary particles settle independently without much mutual interference, and therefore the settling velocity is independent of C . For concentrations higher than $5 \text{ to } 10 \text{ g/l}$, the settling velocity decreases with increasing concentration (Figure 3.17); this is referred to as hindered settling. At such high concentrations, the sediment suspension, referred to as fluid mud (Bellessort

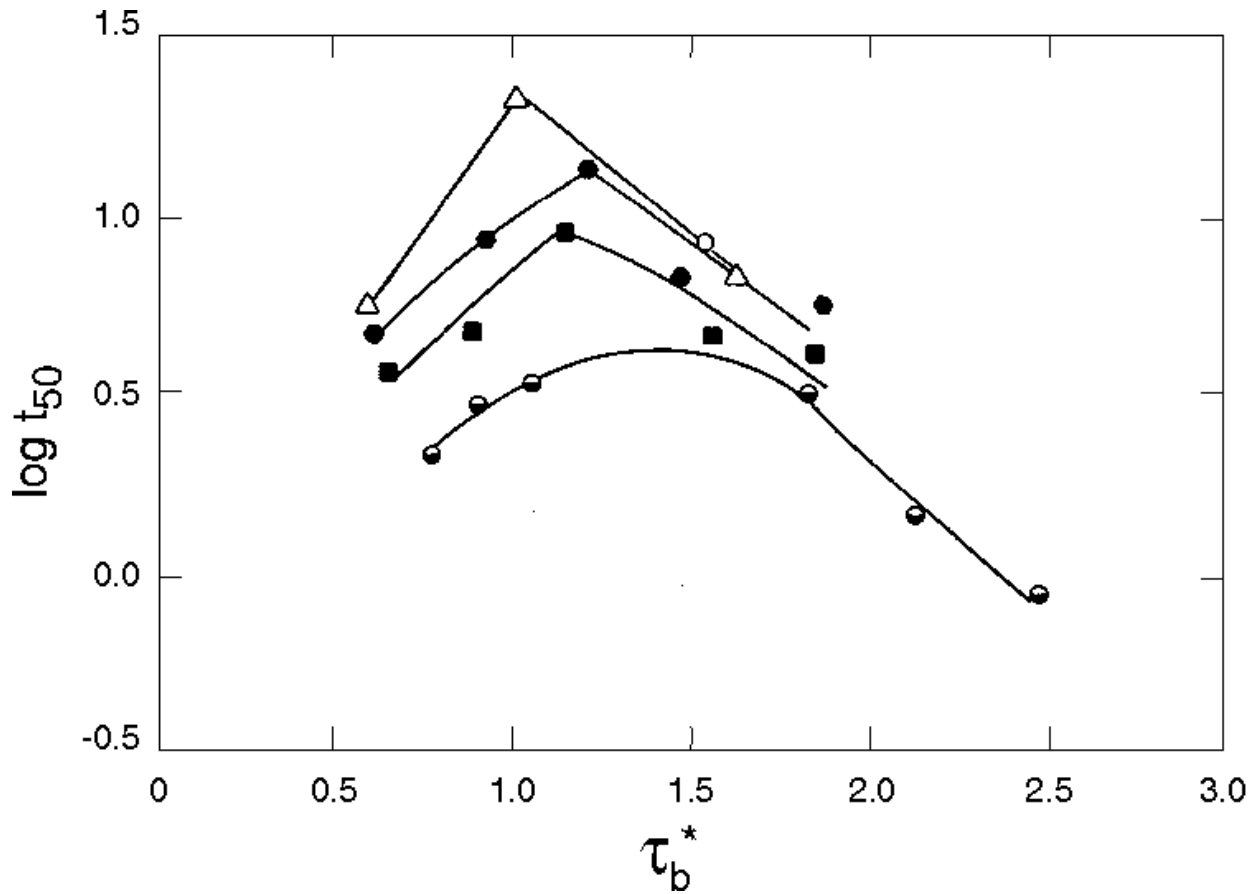


Figure 3.15 Log t_{50} versus τ_b^* for Kaolinite in Distilled Water (after Mehta and Partheniades 1975).

1973), hinders the upward flux of water expelled by consolidation of the lower suspension (Krone 1962).

In the mutual interference range, Krone (1962) and Owen (1971) have found the following empirical relationship between the median settling velocity, W_s , and C :

$$W_s = K_e C^m \quad (3.29)$$

where K_e and m are empirical constants that depend on sediment type and turbulence intensity of the fluid. Krone found m to be equal to 1.33 for San Francisco Bay mud in laboratory

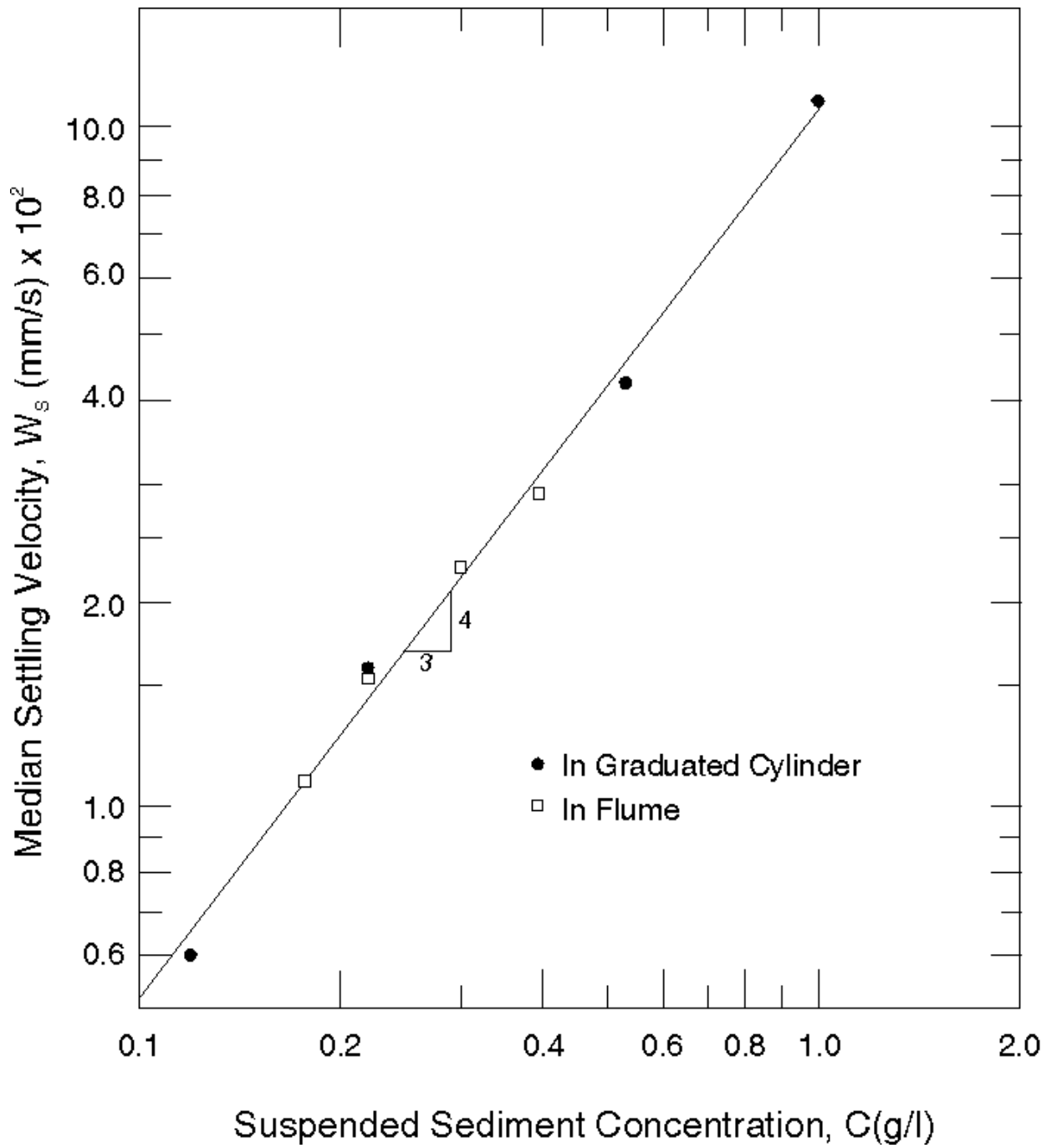


Figure 3.16 Settling Velocity versus Concentration for San Francisco Bay Mud (after Krone 1962).

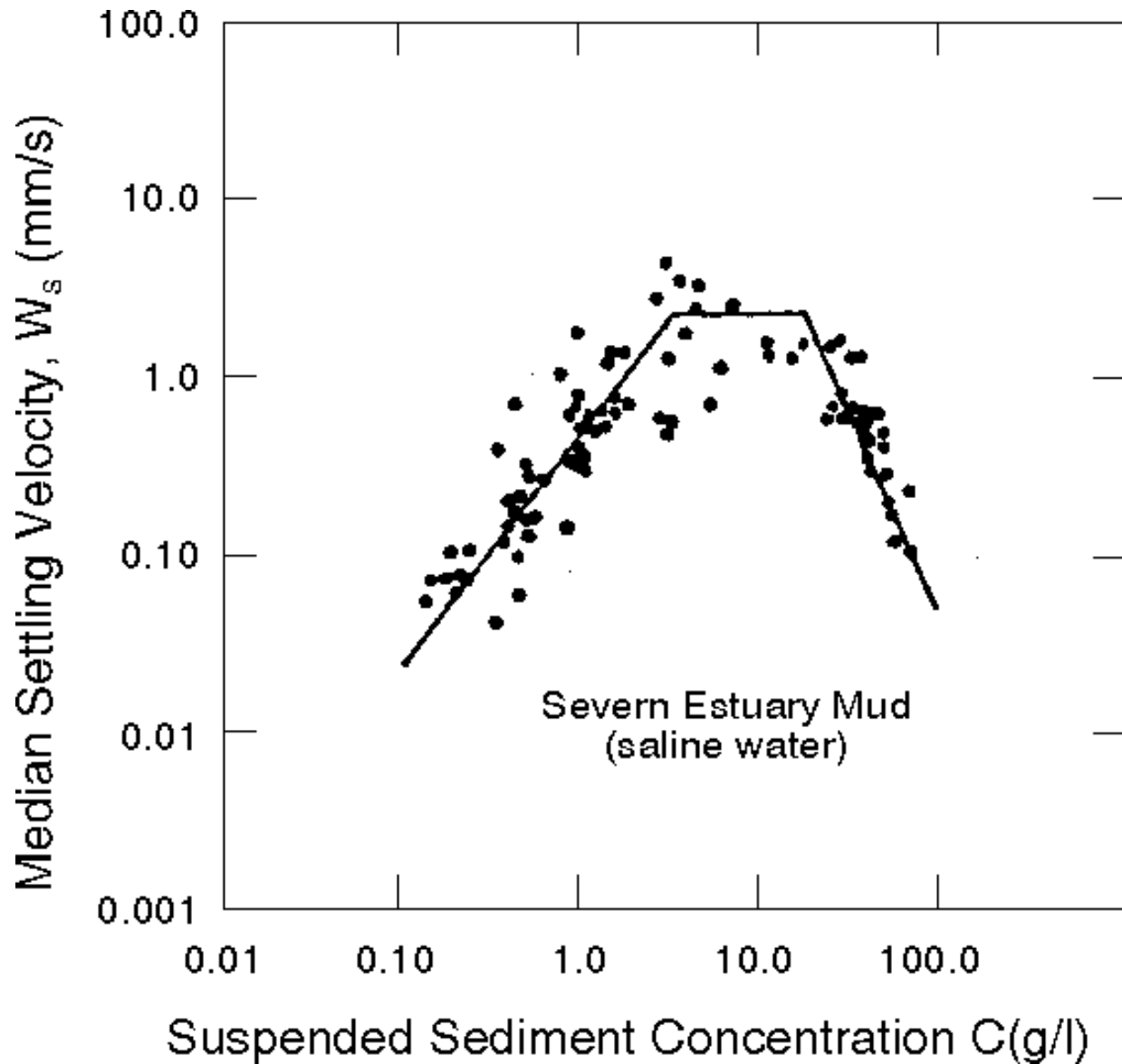


Figure 3.17 Settling Velocity versus Concentration (after Thorn 1981).

experiments (see Figure 3.16). Teeter (1983) found m to be less than 1.0 for sediment from Atchafalaya Bay, Louisiana.

Owen (1971) studied the effect of turbulence on settling velocities of natural mud. The value of m was found to be equal to 1.1 and 2.2 for sediment collected during spring and neap tides, respectively. The turbulence intensity during a spring tide is generally greater than during a neap tide. Owen postulated that m was greater (and therefore W_s as well) during neap tide because the lower level of turbulence did not cause as much breakage of the aggregates; thus relatively

large aggregates with higher settling velocities were formed. During spring tide, the higher internal shearing rates resulted in breakage of a higher portion of the aggregates. Thus, small aggregates with lower settling rates, and therefore lower values of m , were formed.

Migniot (1968) defined a flocculation (coagulation) factor, F , to quantify the effect of aggregation intensity on W_s :

$$F = \frac{W_{sA}}{W_{sP}} \quad (3.30)$$

where W_{sA} is the median settling velocity of the aggregates and W_{sP} is the median settling velocity of the elementary sediment particles. Bellessort (1973) found that F varied with grain size according to $F \approx 250D^{-1.8} \approx W_{sP}^{-0.9}$ where D is the mean diameter of the particles in micrometers and W_s is measured in mm/s. Figure 3.18 shows the effect of particle size on F and W_{sA} for numerous sediment samples at $C_o = 10$ g/l and salinity $S = 30$ ppt. Also plotted in this figure is the variation of F with D found by Dixit *et al.* (1982) using mud from Atchafalaya Bay, Louisiana. In these data, however, C_o varied from 1.2 to 11 g/l and $S \sim 0.0$ ppt. Another important difference between the two data sets is that Bellessort measured W_{sA} under quiescent conditions, whereas Dixit *et al.* (1982) measured the settling velocity under turbulent flow in a rotating annular flume. As observed, these data have the same slope between F and D as found by Bellessort. This suggests that, in general, F may be proportional to $D^{-1.8}$, albeit with different intercept values, at least for suspension concentrations with $C_o = 1.2-11$ g/l and $0 < S < 30$ ppt.

3.2.2.9.1 Effect of Salinity on Deposition - The larger, stronger aggregates of natural muds formed in a saline medium have been found to result in higher settling velocities (Krone 1962; Owen 1970a). Thus, the effect of salinity on deposition of cohesive sediments may be quantified in terms of a relationship between salinity and median settling velocity, W_s .

Krone (1962) studied the effect of salinity and suspended sediment concentration on W_s of San Francisco Bay sediment. The results from settling tests performed under quiescent conditions in 1-liter cylinders showed the effect of both salinity and suspension concentration on W_s (Figure 3.19). The influence of salinity on W_s is especially significant in the range of 0

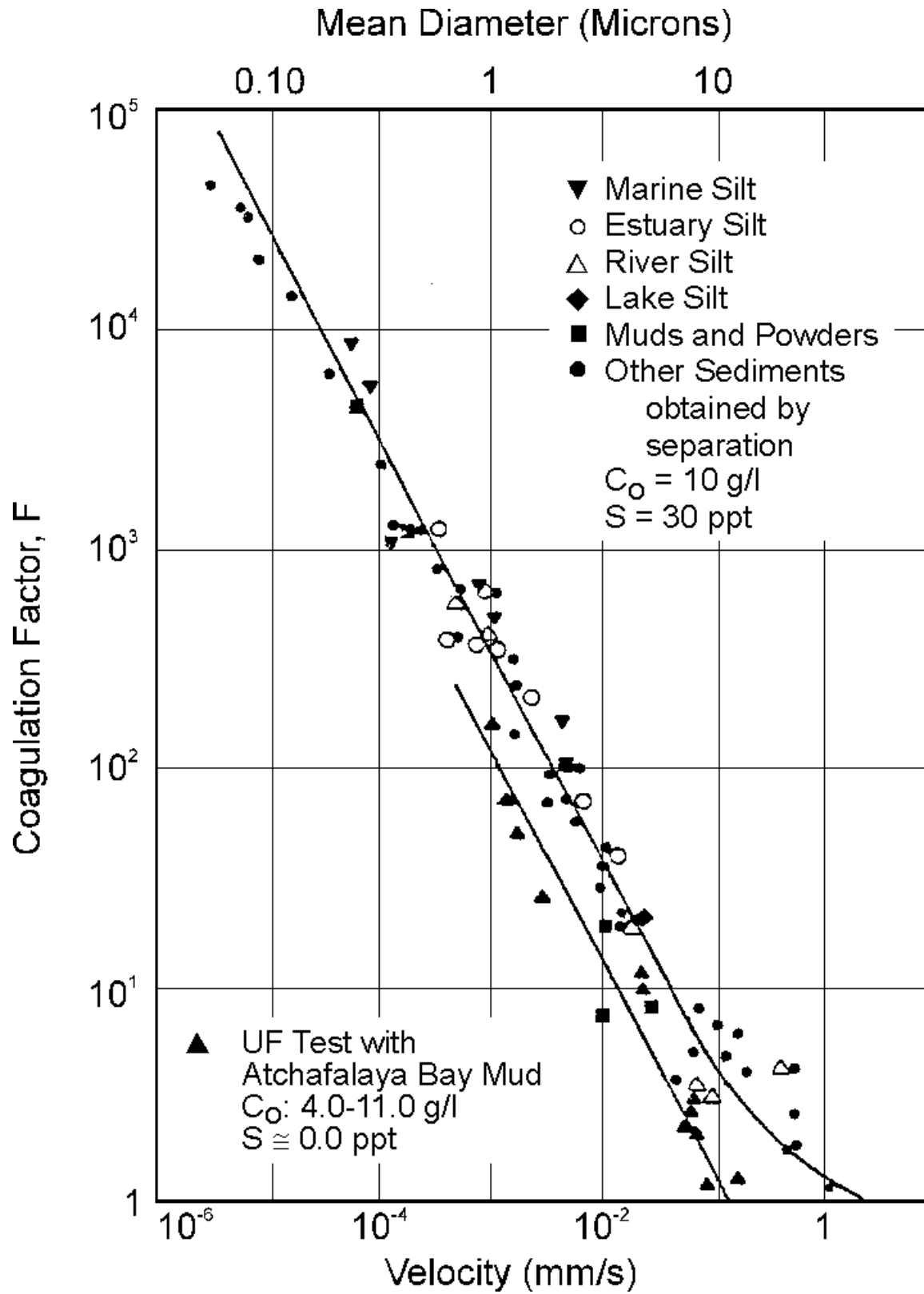


Figure 3.18 Effect of Size and Settling Velocity of Elementary Particles on the Coagulation Factor of Natural Muds (after Bellessort 1973).

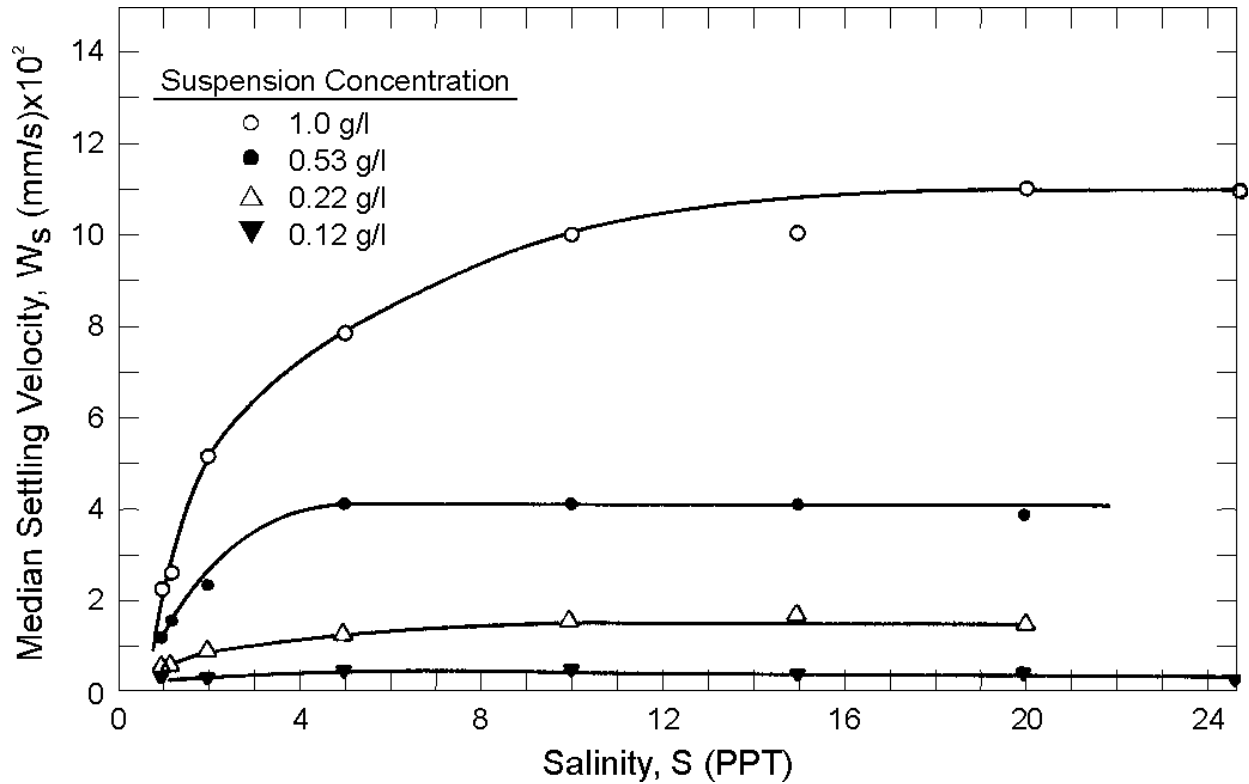


Figure 3.19 Effect of Salinity on Settling Velocity of San Francisco Bay Mud (after Krone 1962).

to 2 ppt, particularly for the 1.0 and 0.53 g/l suspension concentrations. An explanation for the apparent increasing influence of salinity on W_s with increasing suspension concentration is that as the suspension concentration increases, the number of collisions increases and larger aggregates with higher settling velocities form. The lowest order aggregate that could be formed would be limited by the suspension concentration, so that even with an increase in salinity (and therefore a corresponding increase in cohesive forces), lower order aggregates could not form due to insufficient concentration of suspended particles.

Owen (1970a) studied the variation of W_s of a natural mud with salinity and suspension concentration using a two meter high bottom withdrawal settling tube. The results of Owen's tests are shown in Figure 3.20. This figure shows that, in general, as the salinity and suspension concentration are increased, increased cohesion and interparticle collision result in higher coagulation rates with accompanying higher settling velocities. This trend corroborates that found by Krone (1962), except that no "leveling off" of W_s above a certain salinity value was found in

these tests. The decrease in W_s above a given salinity and concentration, as observed in Figure 3.20, represents the onset of hindered settling.

Owen (1971) found a negligible effect of salinity on the settling velocity of natural aggregates at two different locations in the Thames River estuary. The salinities at two

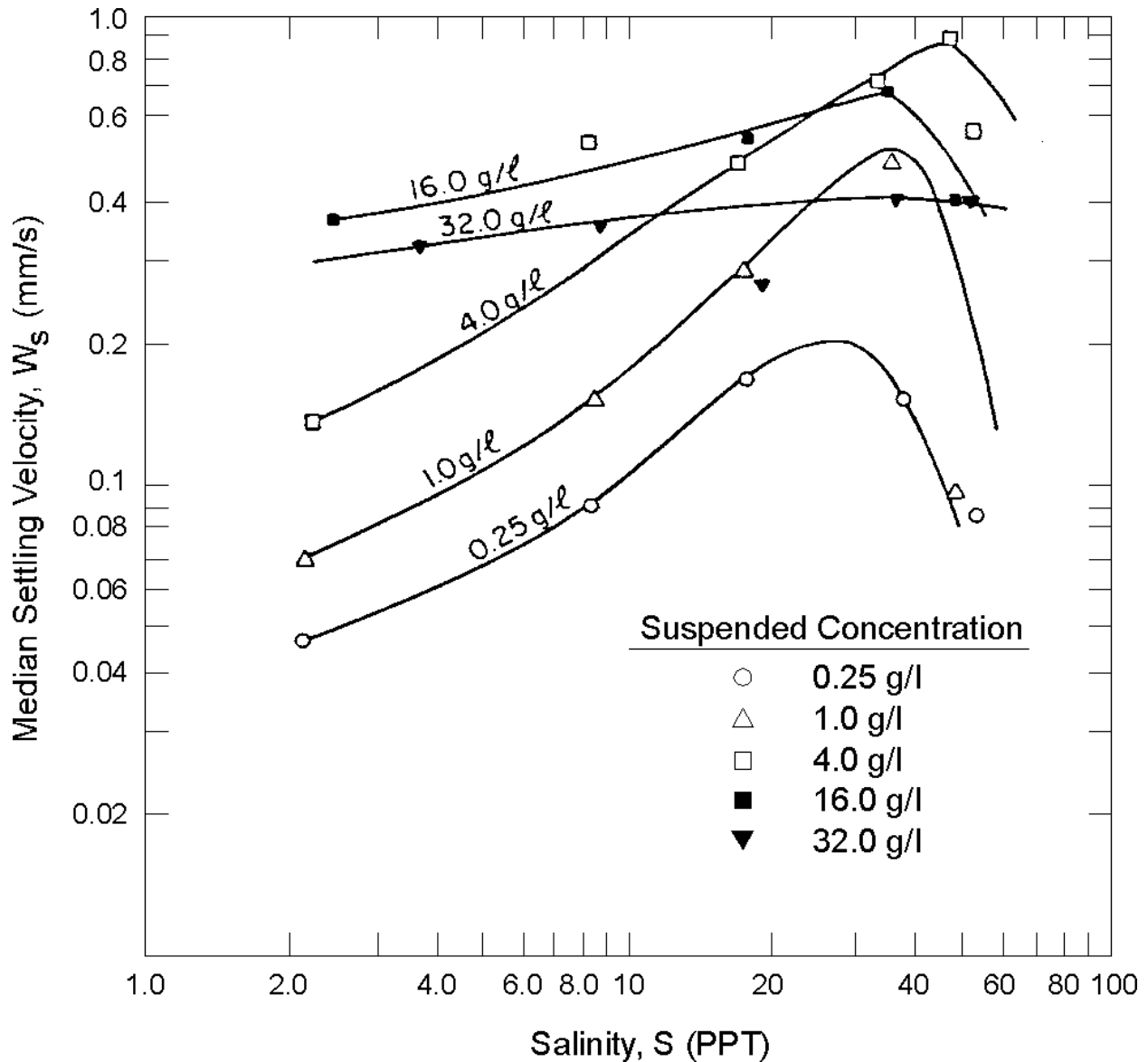


Figure 3.20 Effect of Salinity on Settling Velocity of Avonmouth Mud (after Owen 1970a).

sampling stations varied between 6 and 10 ppt and 26 and 32 ppt, respectively. Evidently, the effect of salinity on W_s at these salinities in a turbulent flow field is much less than that under

quiescent conditions. This implies that increased cohesion caused by higher salinities is counter-balanced by high internal shear rates that cause the aggregates to be broken apart. (Also refer to the discussion of the work of Mehta and Partheniades (1975) in the previous section.)

3.2.2.10 Consolidation

An estuarial sediment bed is formed when deposited sediment particles and/or aggregates comprising a stationary suspension begin to interact and form a soil that transmits an effective stress by virtue of particle-to-particle contacts. The self-weight of the particles, as well as deposition of additional material brings the particles closer together by expulsion of pore water between the particles. A soil is formed when the water content of the sediment-water suspension decreases to the fluid limit. Unfortunately, there is not a unique water content value for cohesive soils at which the suspension changes into a soil (Been and Sills 1981).

During the transition from suspension to soil, an extremely compressible soil framework or skeleton develops (Been and Sills 1981). The strains involved in this first stage of consolidation are relatively large and may continue for several days or even months. The straining and upward expulsion of pore water gradually decreases as the soil skeleton continues to develop. Eventually this skeleton reaches a state of equilibrium with the normal stress of the overlying sediment (Parker and Lee 1979).

During the early stages of consolidation, the self-weight of the soil mass near the bed surface is balanced by the seepage force induced by the upward flow of pore water from the underlying sediment. As the soil continues to undergo self-weight consolidation and the upward flux of pore water lessens, the self-weight of this near surface soil gradually turns into an effective stress. This surface stress and the stress throughout the soil may first crush the soil aggregate structure and then crush the flocs themselves.

Primary consolidation is defined to end when the excessive pore water pressure has completely dissipated (Spangler and Handy 1982). Secondary consolidation, which may continue for many weeks or months, is the result of plastic deformation of the soil under an overburden.

Figure 3.21 shows the variation of the mean dry bed density, $\bar{\rho}_s$ with consolidation time for Avonmouth mud (Owen 1977), for commercial grade kaolinite in salt water ($S=35$ ppt) (Parchure 1980), and for kaolinite in tap water ($S=0$ ppt) (Dixit 1982). Figure 3.23 shows the variation of the normalized mean bed density with consolidation time for the

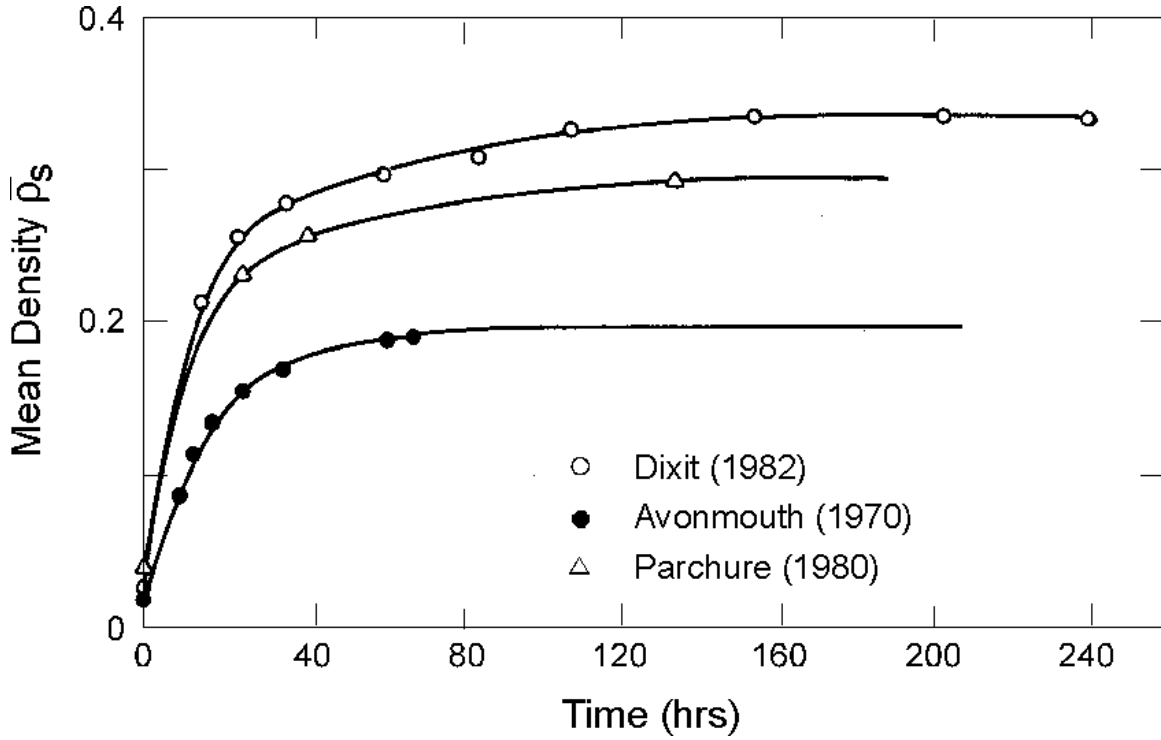


Figure 3.21 Variation of Mean Bed Density with Consolidation Time (after Dixit 1982).

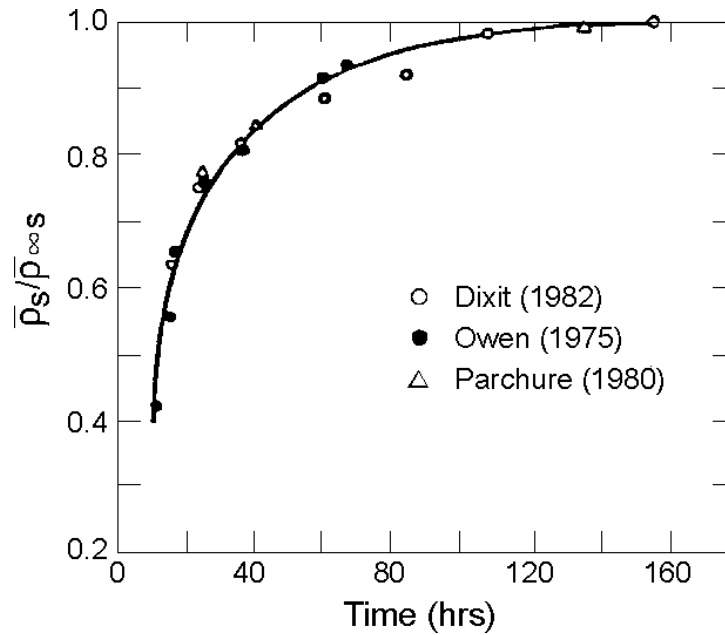


Figure 3.22 Variation of the Normalized Mean Bed Density versus Consolidation Time (after Dixit 1982).

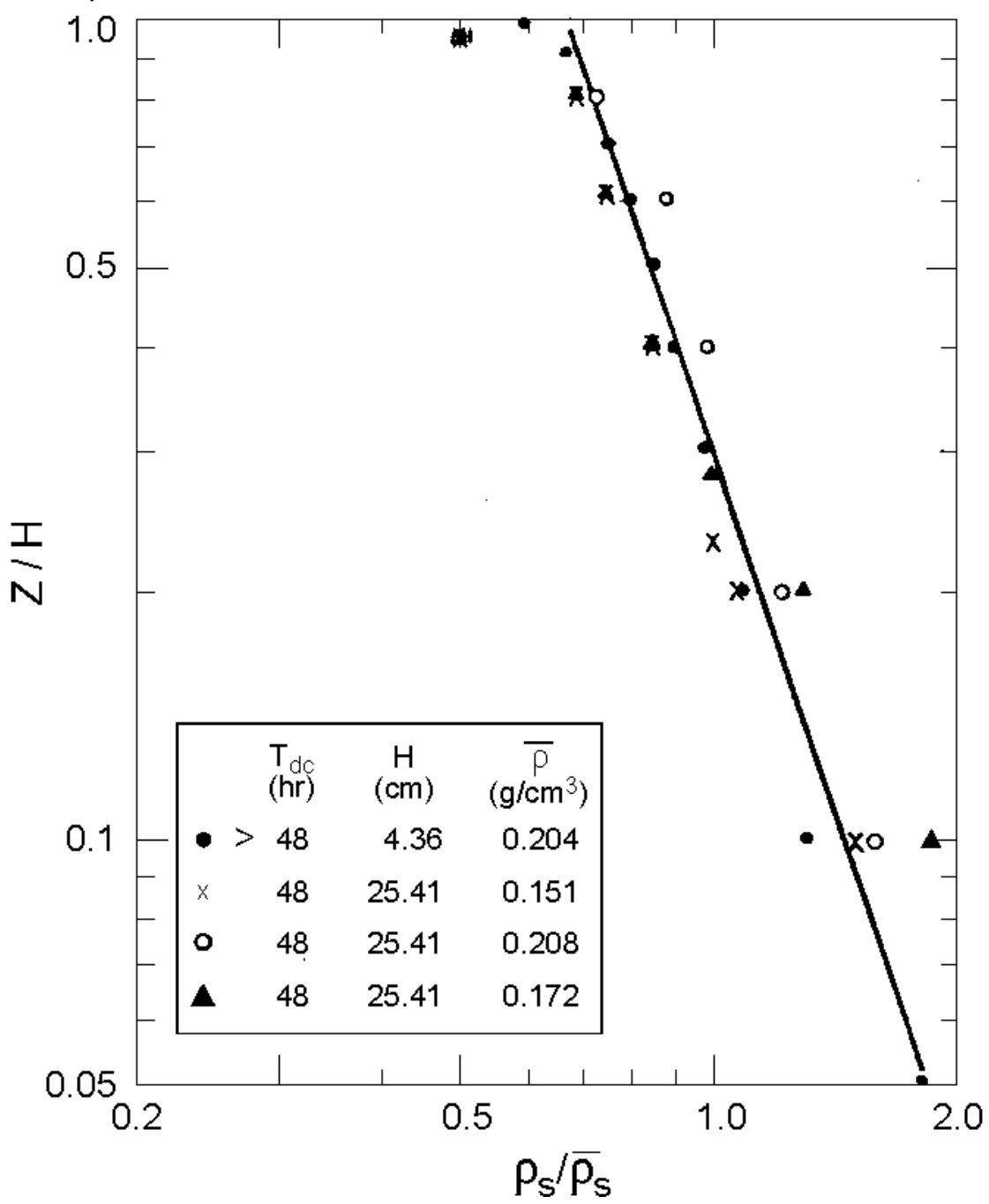


Figure 3.23 Normalized Depth Below the Surface versus Normalized Bed Bulk Density for Avonmouth, Brisbane, Grangemouth and Belawan Muds (after Dixit 1982).

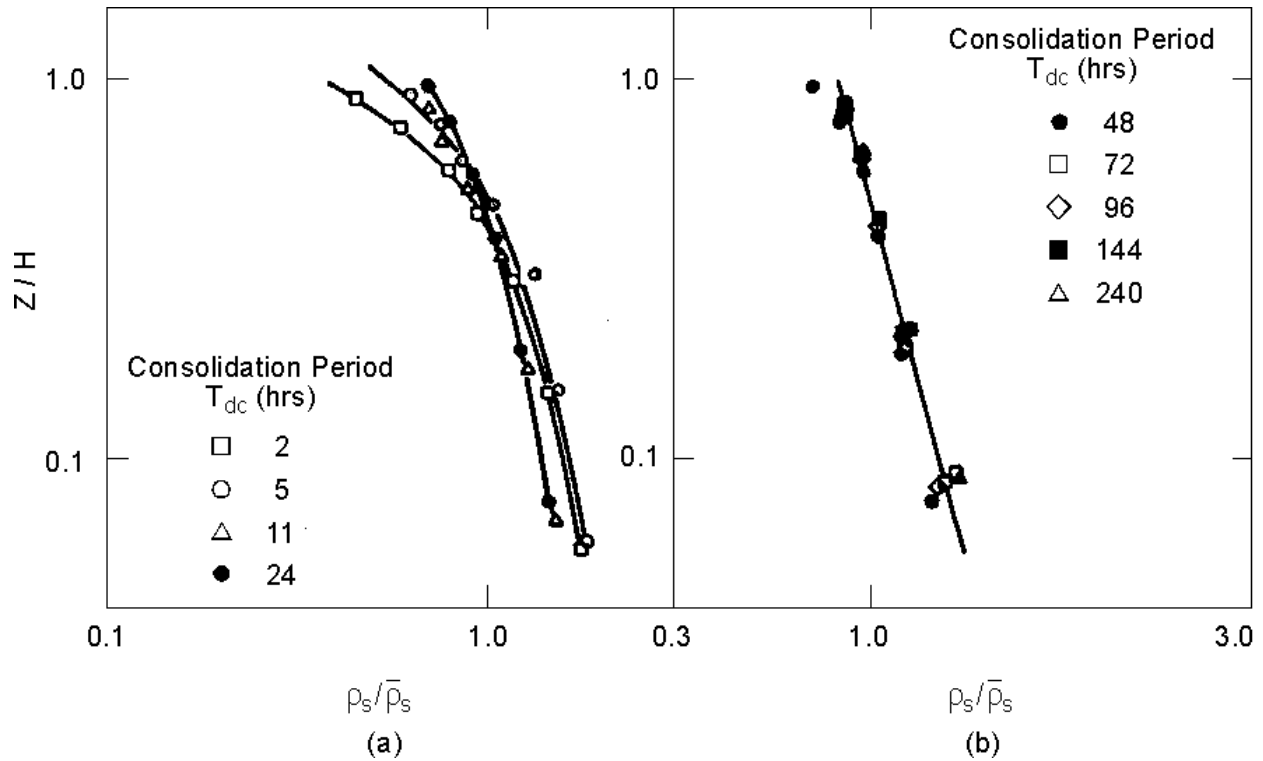


Figure 3.24 Normalized Depth Below the Bed Surface versus Normalized Bed Bulk Density for Consolidation Times (a) Less than 48 Hours and (b) Greater than 48 Hours (after Dixit 1982).

same three mud beds. This figure shows that the time-variation of the degree of bed consolidation with time for these three beds was approximately equal.

Figure 3.23 shows the dimensionless relationship found between the bed bulk density, ρ_B , and depth below the bed surface, Z , for consolidation times, T_{dc} , on the order of 48 hours for four natural muds. Figure 3.24a and Figure 3.24b show the dimensionless relationship found by Dixit (1982) for T_{dc} up to 24 hours and greater than 48 hours, respectively, for kaolinite beds in tap water. Figure 3.25 shows normalized density profiles for different bed depths. In these figures, H is the thickness of the bed in the experimental flume.

The shear strength of clays is due to the frictional resistance and interlocking between particles (physical component), and interparticle forces (physicochemical component) (Karcz and Shanmugam 1974; Parchure 1980). Consolidation results in increasing bed density and shear

strength (Hanzawa and Kishida 1981). Figure 3.26 shows the increase in the shear strength profile with consolidation time for flow-deposited kaolinite beds in tap water.

As mentioned previously, the nature and effect of consolidation on shear strength profiles of cohesive sediment beds are not well known at present, and the limited information that has been obtained is often contradictory (Parchure 1980). Figure 3.27 shows the correlation found by Owen (1970b) between the dry sediment density and shear strength for statically deposited beds of Avonmouth mud. Least squares analysis of the data plotted in this figure gave a slope of 2.44 and a coefficient of determination of $r^2 = 0.83$. The power expression relating τ_c and ρ_s is of the form:

$$\tau_c = 6.85 \times 10^{-6} \rho_s^{2.44} \quad (3.31)$$

Owen considered that the correlation obtained between τ_c and ρ_s was satisfactory, considering the experimental error involved in the measurement of both these parameters.

3.3 COHESIONLESS SEDIMENT TRANSPORT

Cohesionless sediment transport occurs when the hydrodynamic forces (i.e., bed shear) acting on sediment particles at the bed surface exceed the resisting forces of interparticle friction and gravity. Thus, estimation of sediment transport requires calculation of the flow induced bed shear stress (or shear velocity). The equation used in this module to calculate the bed shear stress is the following Darcy-Weisbach type relationship:

$$\tau_c = \frac{1}{2} \rho f_c |V| V \quad (3.32)$$

where V = current speed, and f_c = current friction factor, given by the well known relationship from turbulence theories (Christoffersen 1982):

$$\left(\frac{2}{f_c} \right)^{1/2} = 2.5 \ln \left(\frac{11.04h}{k_N} \right) \quad (3.33)$$

in which k_N is Nikuradse's roughness.

Two methods for predicting the non-cohesive sediment transport rate are incorporated in this module. These are the Einstein methodology (Simons and Senturk 1976) and the Ackers-White algorithm (Ackers and White 1973). The latter is used only when the median

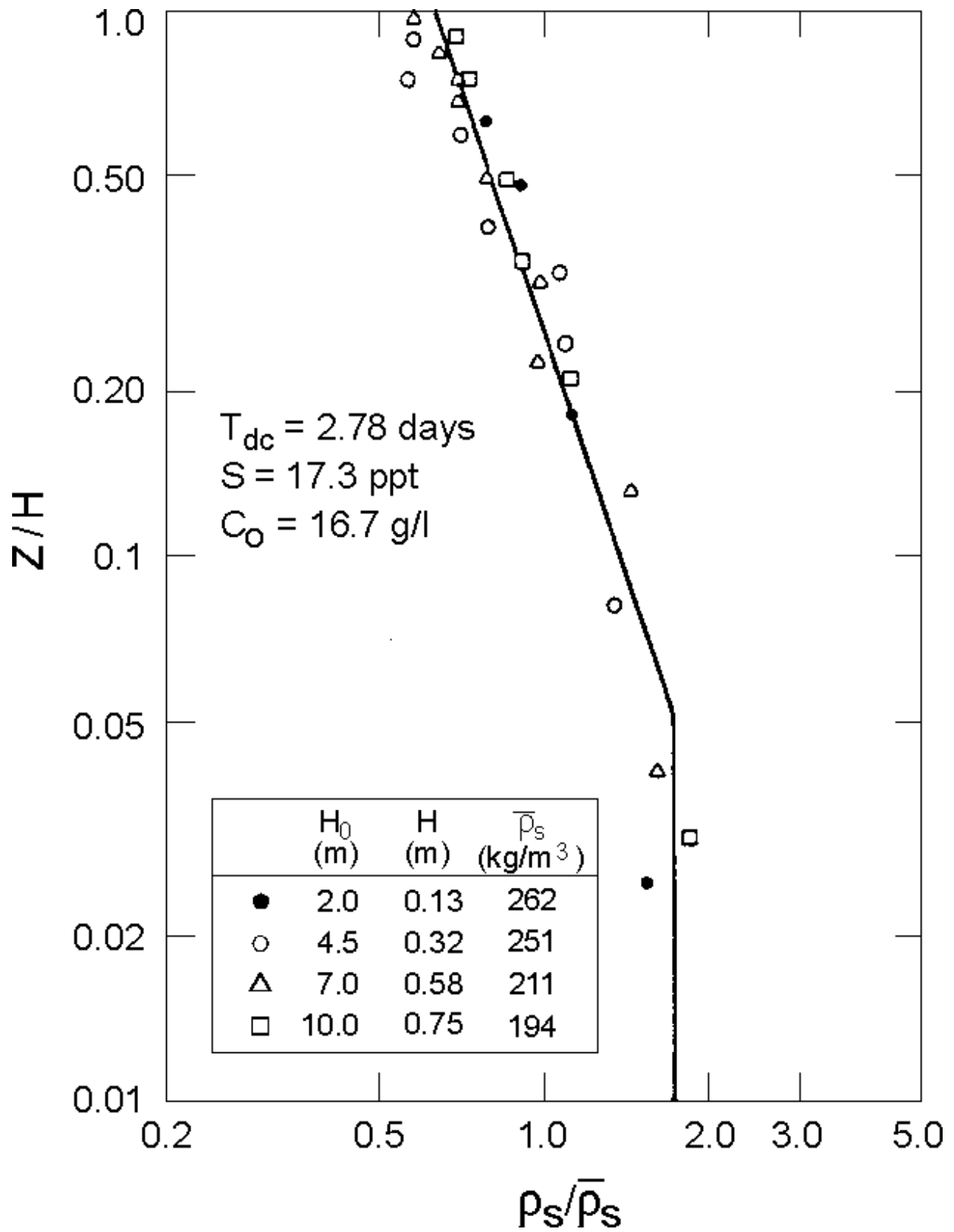


Figure 3.25 Normalized Bed Density Profiles for Different Bed Thicknesses.

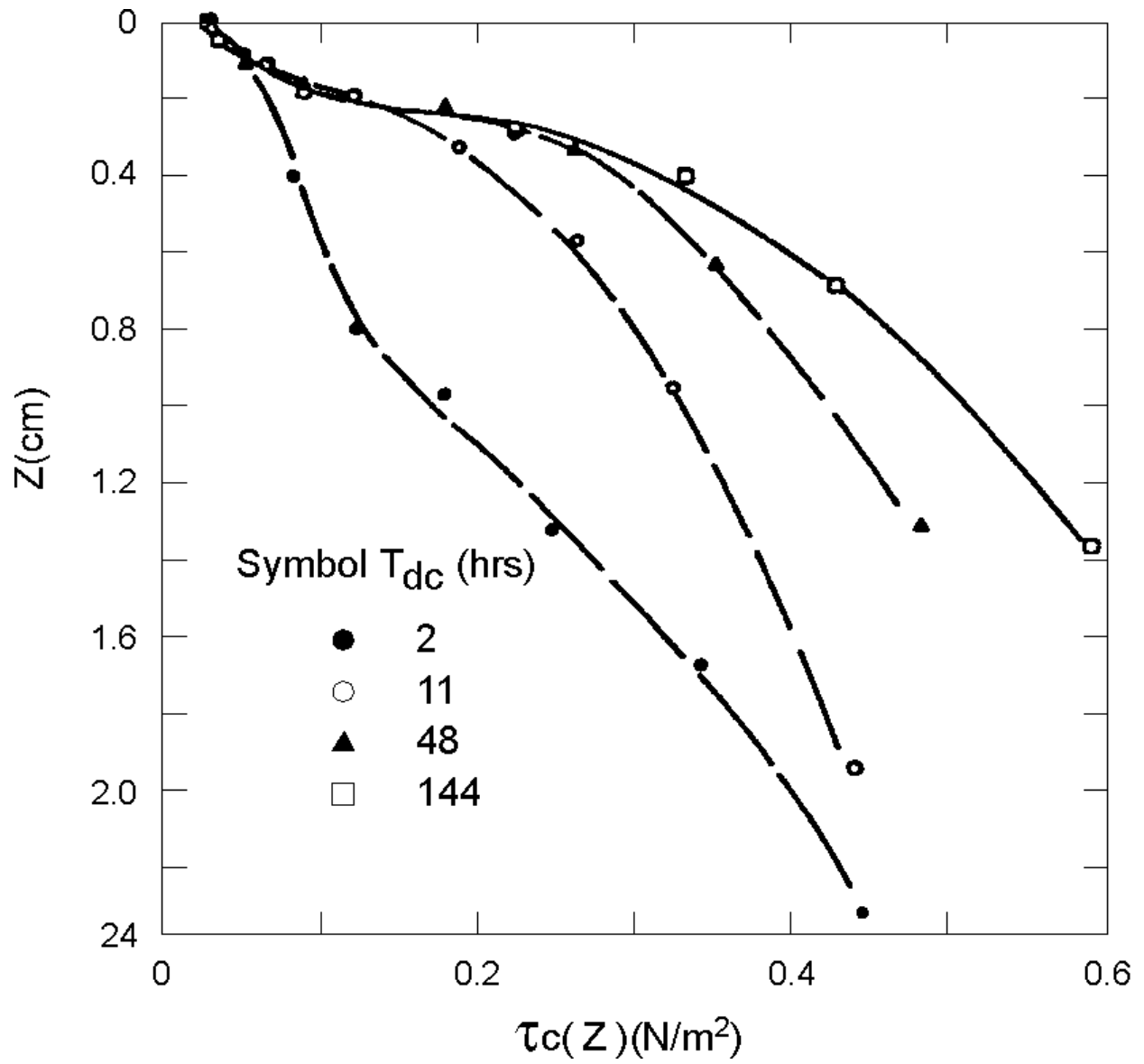


Figure 3.26 Bed Shear Strength versus Distance Below the Initial Bed Surface for Various Consolidation Periods (after Dixit 1982).

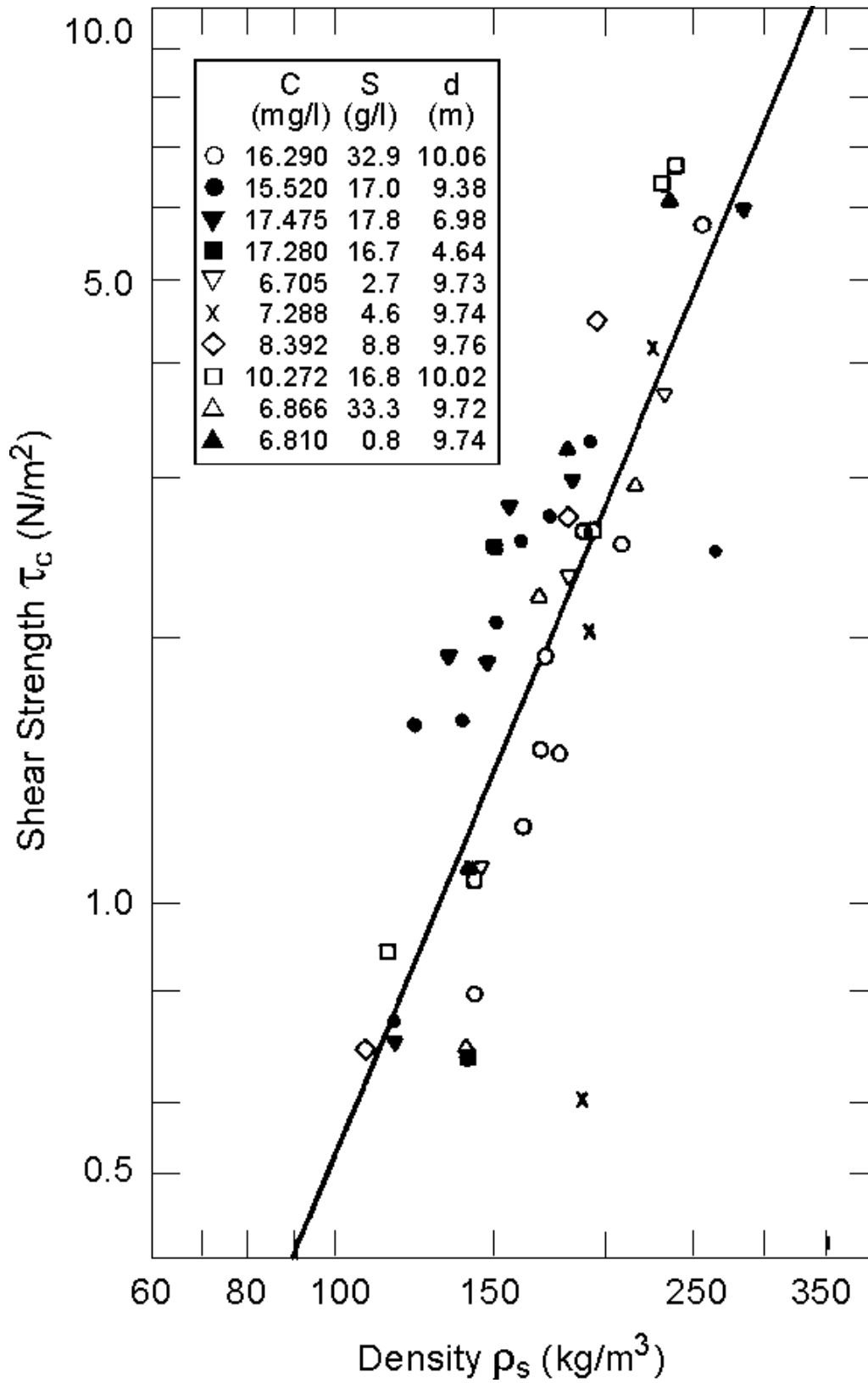


Figure 3.27 Correlation of Bed Shear Strength with Bed Density (after Owen 1970b).

diameter, d_{50} , is greater than 0.04 mm. When d_{50} is greater than 0.04 mm, the normal procedure is to alternatively use both methods and compare the results.

When sediment transport away from a point is not equal to that towards the same point, erosion or deposition will occur causing changes in the bottom elevation. Erosion will result if there is a net transport of sediment away from the point, while deposition will occur if there is a net sediment transport towards it. Using a control volume approach in two horizontal dimensions, Fahien (1983) presented a differential balance of sediment volume flux and accretion/scour. The sediment volume conservation equation is given by

$$\frac{\partial b}{\partial t} + \frac{\partial q_x}{\partial x} + \frac{\partial q_y}{\partial y} = 0 \quad (3.34)$$

where b = local bed surface elevation, and q_x , q_y = components of the sediment load (dry weight) transport per unit width in the x- and y-directions, respectively, as determined using either the Einstein or Ackers-White equation. Equation 3.34 is used in the sediment transport module to estimate the local (i.e., at each node) bottom elevation change resulting from net sediment transport to or away from a given location. The elevation change at each node during a single time step is computed after the hydrodynamic and sediment transport computations are completed. The predicted bathymetric changes at a given time step are used in the hydrodynamic module during the next time step to predict the new flow field.

3.4 CONTAMINANT TRANSPORT

The transport of both cohesionless sediments (i.e., medium size silts and larger particles) and fine grain cohesive sediments (i.e., mostly composed of terrigenous clay size particles and fine silts; sometimes includes small quantities of biogenic detritus, algae, and organic matter) must be modeled to account for adsorption and desorption of contaminants onto and from sediments of all sizes. The properties of clays which cause the sorption of contaminants are their large specific area, surficial negative electrical charge, and their cation exchange capacity. Particulate contaminants may be sorbed on the mineral, oxide or hydrous oxide surfaces; bonded in humic materials; precipitated as metal sulfides; sorbed on the exchange sites of clay minerals; or incorporated in the detrital organic or mineral phase associated with all sizes of sediment particles.

The bulk of the contaminant load in surface waters is in fact quite often transported sorbed to cohesive sediments rather than in the desorbed state (Kirby and Parker 1973). In addition, the portion of the contaminant load adsorbed to cohesionless sediments is often less than that sorbed to cohesive sediments. This follows from studies that have shown that increasing metal concentrations typically correlate positively with decreasing sediment particle size, increasing sediment specific area, and increasing concentrations of organic matter and manganese and iron oxides (Horowitz and Elrick 1987). However, there are exceptions to this trend. Studies by Moore *et al.* (undated) and Brook and Moore (undated), found weak correlation between percent of fine grained sediment (less than 63 microns) and trace metal concentrations in the Clark Fork River in Montana, while coarse grain sediments contributed significantly to bulk metal concentrations. This emphasizes the need to consider the transport of both cohesive and cohesionless sediments in contaminant transport modeling.

Processes that affect the association of inorganic contaminants with aquatic sediments include adsorption/desorption, complexation, and organic coatings (Dzombak and Morel 1987). These processes have been the subject of several studies, and are covered in detail elsewhere (e.g., Stumm and Morgan 1981). The processes of sorption and desorption are discussed below. Biological factors (e.g., presence of organic coatings on sorbents), which often have a significant effect on adsorption processes, are not discussed.

Sorption of contaminants generally refers to both adsorption and absorption (Elzerman and Coates 1987). Adsorption of a sorbate to a sorbent occurs at a surface or interface, while absorption continues beyond the interface and involves incorporation of the sorbate into the interior of the sorbent. Distinction between these two processes is usually not precise, thus explaining the use of the collective term sorption. Sorption of inorganic compounds is described as a chemical coordination process involving certain reactions between absorbents and the inorganic adsorbate (Dzombak and Morel 1987). Adsorption models for inorganic contaminants should simulate these chemical reactions and account for interaction between electrical surface charges and ion adsorption. Such adsorption models are highly empirical in nature due to the complex electrochemical interactions, and are generally applicable for a specific sorbent-sorbate pair only (Dzombak and Morel 1987). Desorption is the reverse of sorption. Typically, a geochemical-metals speciation model (such as MINTEQA2; Brown and Allison 1987), is used to

compute metals precipitation and sorption/desorption for the geochemical conditions at the site of interest.

A partition coefficient, K_p , is used to define the distribution of a contaminant between the particulate and dissolved phase concentration. Reported values of K_p usually correspond to equilibrium conditions, at which rates of desorption and sorption are equal. Despite typically high partition coefficients, the total mass of contaminants sorbed to suspended sediments is usually lower than that in the dissolved phase because of relatively low concentrations of suspended sediment. In addition, the sorbed contaminant mass on bed sediments, which can be large, has to be considered. Contaminants that are sorbed on bed sediments either sorbed directly onto the deposited sediments or sorbed onto suspended sediments which subsequently settled to the bed. In general, there are few limitations to benthic exchange, with the bed acting like a capacitor that tends to maintain elevated concentrations in the water column (Medine and McCutcheon 1989).

The partition coefficient is given by:

$$K_p = \frac{C_p}{C_d C_s} = \frac{f_p}{f_d C_s} \quad (3.35)$$

with C_p = particulate contaminant concentration [kg/m^3] (adsorbed contaminant mass/total volume of water);

C_d = dissolved contaminant concentration [kg/m^3] (dissolved contaminant mass/total volume of water);

C_s = mass concentration of suspended sediment [kg/m^3] (mass of sediments/total volume of water);

f_p = fraction of contaminant in the particulate phase = C_p/C_t ;

f_d = fraction of contaminant in the dissolved phase = C_d/C_t ; and

C_t = total contaminant concentration [kg/m^3] = $C_p + C_d$.

Values for partition coefficients can be determined through laboratory testing using the most prevalent or critical dissolved contaminant and environmental parameters (e.g., pH, temperature, conductivity) representative of field conditions. However, field studies are preferred to yield values that more realistically represent the actual field environment.

Sorption of contaminants onto both suspended and deposited sediments is usually treated as a process in thermodynamic equilibrium that occurs rapidly compared to transformation processes such as hydrolysis, microbial transformation, photolysis, volatilization, and chemical oxidation. These slower processes should be simulated using a kinetic approach (Baughman and Burns 1980). The rates at which sorption and desorption take place have been found to vary inversely with the partition coefficient, and therefore are slower for chemicals which more strongly sorb onto particular sorbents, e.g., cohesive sediments. It is often assumed that sorption/desorption occurs instantaneously, or within one time step in a contaminant transport model. The validity of this assumption is dependent on sorption rates between the contaminant and sediment.

Factors which collectively control the distribution and fate of a contaminant in an aquatic environment have been classified according to system, sorbent (sediment), and sorbate (contaminant) characteristics (Elzerman and Coates 1987). System characteristics include, among others, the following : a) transport of water; transport and fate of sediment; nature or contaminant loading to the system; and b) temperature; pH; ionic strength; concentration gradient of contaminant; and competing sorbates and sorbents. The items listed under a) are macro-system factors, while those given under b) are defined as micro-system factors that are important close to the sorbent surface. The item listed as 'nature of contaminant loading' refers to quantity, location, timing, and mode (i.e., point or non-point source) of contaminant release. Sorbent characteristics include the following: composition; size; shape; pore structure; and surface electrochemical charges. Sorbate characteristics include molecular structure, which itself is controlled by polarity, size, shape and electric charge. The effects of each of these components on contaminant transport and transformations in aquatic systems are discussed in detail by Karickhoff (1981), Lyman (1985), Elzerman and Coates (1987), and Dzombak and Morel (1987).

In HSCTM-2D, adsorption of dissolved contaminants onto suspended sediments and onto the bed surface and desorption of particulate contaminants from these surfaces into the water column are the modeled physico-chemical processes that affect the distribution and fate of contaminants. Other processes that typically affect the fate and transport of contaminants in surface water environments such as volatilization, bioconcentration, biouptake, and bioturbation are not incorporated in HSCTM-2D. The adsorption module used in HSCTM-2D is a so-called thermodynamic equilibrium model that assumes constant partitioning between the dissolved

(solute) phase and particulate (solid) phase. Equilibrium models that use a single "black box" partition coefficient are typically used to avoid the complexities of the kinetics of the adsorption and desorption processes. However, consistent relationships between the partition coefficients and environmental parameters such as temperature, conductivity and pH have not yet been found. Thus, equilibrium adsorption/desorption models such as the one in HSCTM-2D are based on the following assumptions:

- a. Local equilibrium between solute and solid phases is instantaneously achieved. Thomann and DiToro (1983) found that equilibrium is usually attained within minutes. Thus, assuming that equilibrium is achieved over one time-step in the model is very reasonable.
- b. The relationship between dissolved and particulate concentrations given by the adsorption isotherm is approximately linear for low contaminant concentrations (O'Connor 1980). Hence, a single partition coefficient can be used in an equilibrium adsorption model. This coefficient can be inferred from either the Freundlich or Langmuir isotherms (Schnoor et al. 1987).
- c. The adsorption and desorption processes are completely reversible. Thus, a single partition coefficient can be used to represent both processes.

The total contaminant concentration, C_t [kg/m³], is given by:

$$C_t = C_p + C_d = C_d(1 + K_p C_s) \quad (3.36)$$

Partition coefficients can be determined in laboratory experiments using sorbent species most prevalent in the field and environmental conditions representative of field conditions (Thomann and DiToro 1983). Ideally, however, field studies should be performed to determine partition coefficient values that more realistically represent natural conditions (HydroQual, Inc. 1982).

Dissolved Contaminant Transport Module - The following processes are accounted for in modeling the advective and dispersive transport of a maximum of three dissolved contaminants: sorption, desorption, chemical degradation or decay, and local (point) sources of contaminants. Contaminant-sediment interaction, by the processes of sorption and desorption is simulated to occur between dissolved contaminants and sediments in suspension and deposited on the bed.

The governing equation for dissolved contaminant transport is equation 3.13 with $C = C_d$ (where C_d = dissolved contaminant mass concentration) and S_T given by

$$S = - \sum K_i(K_{pi}C_dC_{si} - C_{pi}) - \sum K_i\gamma_i(1-P)\frac{D_i}{h}K_dC_d + \sum K_i\gamma_i(1-P)\frac{D_i}{h}(C_p)_B + S_d - \lambda C_d \quad (3.37)$$

where K_i = sorption or desorption rate to approach equilibrium with the i th sediment fraction; K_{pi} = partition coefficient between particulate contaminant associated with i th sediment and dissolved contaminant; C_{si} = suspended mass concentration associated with i th sediment; C_{pi} = particulate contaminant concentration associated with i th sediment; P = porosity of the sediment bed; D_i = diameter of the i th sediment in the bed [m]; γ_i = density of i th sediment in the bed [kg/m^3]; $(C_p)_{Bi}$ = particulate contaminant concentration associated with the i th sediment in the bed; λ = bio-chemical degradation rate or radionuclide decay rate [s^{-1}]; and S_d = source strength of dissolved contaminant [$\text{kg}/\text{m}^3\text{s}$]. The two terms inside the first summation on the right hand side of equation 3.37 represent the adsorption rate of dissolved contaminants and the desorption rate of particulate contaminants onto and from suspended sediments, respectively. The next two terms represent the rate of absorption of dissolved contaminants onto bed sediments (i.e., sink) and the rate of desorption of particulate contaminants from bed sediments into the water column (i.e., source), respectively.

Particulate Contaminant Transport Module - The following processes are accounted for in modeling the transport of up to three particulate contaminants: adsorption, desorption, local sources/sinks, and chemical degradation. Sorption occurs when a dissolved contaminant bonds to a sediment particle, at which time it becomes a particulate contaminant. When the latter desorbs from the sediment it again becomes a dissolved contaminant. The transport of contaminants sorbed to sediments is determined separately for each of the three size fractions.

The governing equation for particulate contaminant transport is equation 3.13 with $C = C_{pi}$ and S_T given by

$$S = \sum [-K_i(C_{pi} - K_{pi}C_{si}C_d) + \frac{d}{h}C_{pi} + \frac{e}{h}(C_{pi})_B + S_{pi} - \lambda C_{pi}] \quad (3.38)$$

where S_{pi} = source strength of particulate contaminant associated with the i th sediment fraction [$\text{kg}/\text{m}^3\text{s}$]. The first two terms on the right hand side of equation 3.38 represent the desorption rate of particulate contaminants and the adsorption rate of dissolved contaminants from and onto suspended sediments, respectively. The third and fourth terms represent the deposition rate and resuspension rate of particulate contaminants, respectively.

SECTION 4

FINITE ELEMENT METHOD

4.1 INTRODUCTORY NOTE

The finite element method (FEM) is used to solve the shallow water flow equations (eqs. 3.1, 3.7 and 3.8) and the advection-dispersion equation (eq. 3.12). The discretization procedures used in the FEM reduce the equations to be solved to ones with a finite number of dependent variables by dividing the continuous solution domain into a number of elements and by expressing the dependent variables in terms of approximating interpolation (i.e., shape) functions within each element. The values of the dependent variables at node points are used to define the interpolation functions. Node points are usually located on the boundaries of elements and are used to define the connection between adjacent elements. The number and location of node points must be chosen such that continuity of the dependent variables across common boundaries of adjacent elements is achieved (Zienkiewicz 1977). The behavior of the dependent variables within each element is defined by the values of the dependent variables at the nodes and the shape function. Then the errors which results from use of the approximate dependent variables are minimized. This procedure results in a set of simultaneous equations which are solved for the unknown nodal dependent variables at the next time step. A detailed description of the method is presented by Zienkiewicz (1977).

4.2 DESCRIPTION

4.2.1 Interpolation Functions

The global and local element coordinate systems are shown in Figure 4.1a and Figure 4.1b, respectively. The global x,y coordinate system is continuous over the entire solution domain, whereas the local element ξ, η coordinate system applies only within an element. The local coordinate systems for a quadratic quadrilateral and a quadratic right triangular element are shown in Figure 4.1b.

Because three nodes are used along each side of the triangular and quadrilateral elements in HSCTM-2D, quadratic shape functions are required. The quadratic shape functions in HSCTM-2D determine the values of both the dependent variables and element geometry. Thus, the elements are isoparametric (Zienkiewicz 1977). There is one shape function, N_i , for every node in a given element. Thus, for triangular elements there are six shape functions; for quadrilateral elements, there are eight. The shape functions are functions of the local coordinates ξ and η and the values of ξ and η at the nodal points. The quadratic shape functions for quadrilateral and triangular elements are given in Table 4.1. The parameters ξ_i and η_i in this table are the nodal coordinates.

A dependent variable, e.g., C , is approximated as the following function of the unknown nodal point concentrations, C_i , and the shape functions, N_i :

$$\tilde{C}_j \cong \sum_{i=1}^{i=nn} N_i C_i \quad (4.1)$$

where \tilde{C}_j = approximate suspended sediment concentration at any location inside the jth element, and nn = number of nodes forming the jth element.

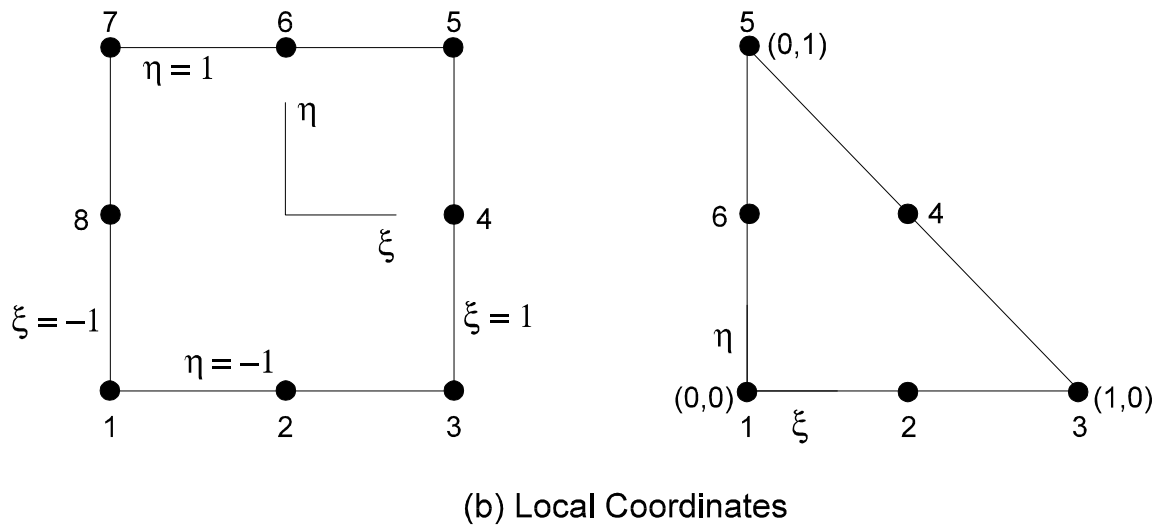
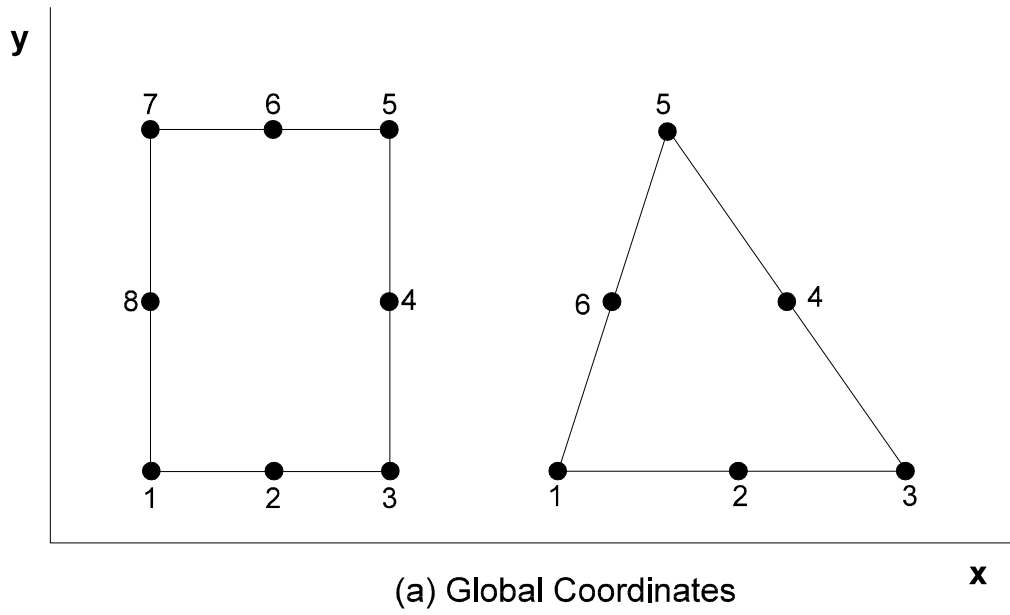


Figure 4.1 Global and Local Coordinates

Table 4.1 Quadratic Shape Functions

Quadrilateral Element		
Shape Function		Node Number
$N_i = (1+\xi\xi_i)(1+\eta\eta_i) (\xi\xi_i+\eta\eta_i-1)/4$		Corner Nodes 1,3,5,7
$N_i = (1-\xi^2)(1+\eta\eta_i)/2$		Midsection Nodes 2,6
$N_i = (1-\eta^2)(1+\xi\xi_i)/2$		Midsection Nodes 4,8
Triangular Element		
Shape Function		Node Number
$N_i = 4\xi_i(1-\eta_i)(1-\xi_i-\eta_i)$		Midsection Node 2
$N_i = 4\xi_i\eta_i /(\xi_i+\eta_i)$		Midsection Node 4
$N_i = 4\eta_i(1-\xi_i-\eta_i)(1-\xi_i)$		Midsection Node 6
$N_i = (1-\xi_i-\eta_i)\{1-2(\xi_i+\eta_i-2\xi_i\eta_i)\}$		Corner Node 1
$N_i = 2\xi_i\{1/2-2\eta_i-\xi_i+\eta_i^2+\eta_i\xi_i+\eta_i/(\xi_i+\eta_i)\}$		Corner Node 3
$N_i = -2\eta_i\{1/2-2\xi_i-\eta_i+\xi_i^2+\xi_i\eta_i+\xi_i/(\xi_i+\eta_i)\}$		Corner Node 5

Likewise, the global coordinates x and y are approximated as the following functions of the global nodal point coordinates, x_i and y_i , and the shape functions, N_i :

$$\tilde{x} = \sum_{i=1}^{i=nn} N_i x_i \quad \text{and} \quad \tilde{y} = \sum_{i=1}^{i=nn} N_i y_i \quad (4.2)$$

The shape functions are used for two additional purposes: (1) to transform from the global coordinate system to the local element coordinate system and (2) to transform the derivatives of C with respect to x and y to the local element coordinates. To perform these transformations, the derivatives of N_i with respect to x and y are needed. The derivatives of N_i with respect to x and y are given in terms of the derivatives of N_i with respect to the local coordinates ξ and η using the chain rule of partial differentiation (Zienkiewicz 1977).

$$\frac{\partial N_i}{\partial y} = \left[\frac{\partial \tilde{x}}{\partial \xi} \cdot \frac{\partial N_i}{\partial \eta} - \frac{\partial \tilde{x}}{\partial \eta} \cdot \frac{\partial N_i}{\partial \xi} \right] \cdot |J|^{-1} \quad (4.3)$$

$$\frac{\partial N_i}{\partial x} = \left[\frac{\partial \tilde{y}}{\partial \eta} \cdot \frac{\partial N_i}{\partial \xi} - \frac{\partial \tilde{y}}{\partial \xi} \cdot \frac{\partial N_i}{\partial \eta} \right] \cdot |J|^{-1} \quad (4.4)$$

where $|J|$ is the Jacobian given by:

$$|J| = \begin{vmatrix} \frac{\partial \tilde{x}}{\partial \xi} & \frac{\partial \tilde{y}}{\partial \xi} \\ \frac{\partial \tilde{x}}{\partial \eta} & \frac{\partial \tilde{y}}{\partial \eta} \end{vmatrix} \quad (4.5)$$

The four components of the Jacobian given by equation 4.5 are equal to

$$\begin{aligned} \frac{\partial \tilde{x}}{\partial \xi} &= \sum_{i=1}^{i=nn} \frac{\partial N_i}{\partial \xi} x_i & \frac{\partial \tilde{x}}{\partial \eta} &= \sum_{i=1}^{i=nn} \frac{\partial N_i}{\partial \eta} x_i \\ \frac{\partial \tilde{y}}{\partial \xi} &= \sum_{i=1}^{i=nn} \frac{\partial N_i}{\partial \xi} y_i & \frac{\partial \tilde{y}}{\partial \eta} &= \sum_{i=1}^{i=nn} \frac{\partial N_i}{\partial \eta} y_i \end{aligned} \quad (4.6)$$

Likewise, the derivatives of \tilde{C}_j with respect to ξ and η are equal to

$$\frac{\partial \tilde{C}}{\partial \xi} = \sum_{i=1}^{i=nn} \frac{\partial N_i}{\partial \xi} C_i \quad \frac{\partial \tilde{C}}{\partial \eta} = \sum_{i=1}^{i=nn} \frac{\partial N_i}{\partial \eta} C_i \quad (4.7)$$

4.2.2 Method of Weighted Residuals

The Galerkin weighted residual method is used to solve the governing equations in the modeling system. This method requires that the summation of weighted residuals over the solution domain be equal to zero when the shape functions are used for the nodal weighting factors. The residual, r , results from applying the governing equations to the element subdomain using, for example, the approximate suspension concentration \tilde{C} instead of the actual concentration C . In order for \tilde{C} to satisfy all the stipulated boundary conditions, the sum of normal concentration fluxes from adjacent elements and any source or sink must be equal to zero on all internal and external boundaries in the solution domain. This condition for the advection-dispersion equation is expressed mathematically as (Ariathurai and Krone 1976):

$$q_i^+ + q_i^- + q_i^s = 0 \quad \text{for } i = 1, \dots, NL \quad (4.8)$$

where q_i^+ is the outward normal flux from one element, q_i^- is the inward normal flux from adjacent element, q_i^s is the normal flux from source/sink on the i th boundary, and NL is the number of element interfaces and external boundaries.

The formulation of the Galerkin method can be expressed mathematically as

$$\sum_{j=1}^{j=NE} \int_{A_e} N_j r \, dA_e + \sum_{L=1}^{L=NL} \int_{\zeta} N_L R \, d\zeta = 0 \quad (4.9)$$

where NE is the total number of elements in the grid, A_e is the element subdomain, r as defined in the previous paragraph, R is the residual that results from the use of \tilde{C}_j in equation 4.8, and ζ is the variable length along the k th boundary.

4.2.3 Discretization of Physical System

The first step involved in the use of the finite element method is discretizing the water body to be modeled by dividing the study area into a network of finite elements. The objective of this process is to represent the continuous physical system with a discretized system that is sufficiently detailed to provide a "reasonably" accurate solution of the governing equations. In

general, the more detailed the finite element grid, i.e., the more elements used, the higher the computational costs. Thus, there is a trade-off between solution accuracy and cost involved in obtaining the solution. An understanding of the physical processes being modeled is essential in evaluating this trade-off.

The steps involved in discretizing the physical system, as well as a few guidelines to follow in this process, are listed below. For an in-depth discussion of these three steps, the reader is referred to any of the numerous books on the FEM (e.g., Huebner and Thornton 1982).

1. Define the boundaries of the area to be modeled. Water boundaries should be located where hydrodynamic conditions (e.g., discharges or water surface elevations) and water quality conditions (e.g., sediment concentrations) can be measured. If the required boundary conditions cannot be well defined, the water boundaries should be located as far away as possible from the main areas of interest. This will minimize the effects of errors caused by incomplete boundary specification.
2. Divide the identified area into triangular and/or quadrilateral elements. Elements with curved sides can be used to represent complex geometries. The size of each element should depend on the spatial behavior (i.e., gradient) of the dependent variables. In areas where the gradients are expected to be small, larger element sizes can be used. In regions where large gradients are anticipated, smaller element sizes should be used. Examples of regions where smaller elements may be needed include confluences of streams, locations of sediment inflows, and constricted openings, such as the entrance channel of a harbor or marina.
3. Number the nodes and elements comprising the grid network. Then a preprocessor should be used to reorder the elements to obtain the most efficient solution order.

4.3 FINITE ELEMENT FORMULATION

4.3.1 Hydrodynamic Equations

Without derivation, applying the Galerkin method of weighted residuals to the continuity equation (eq. 3.1) and momentum equations (eqs. 3.7 and 3.8) yields

$$\sum_{j=1}^{j=NE} \int \int_{A_e} \{M\} \left[(\alpha_a d + \beta_a) + \frac{\partial}{\partial x}(d \cdot u) + \frac{\partial}{\partial y}(d \cdot v) \right] dx dy = 0 \quad (4.10)$$

for the continuity equation, and

$$\begin{aligned} & \sum_{j=1}^{j=NE} \int \int_{A_e} \left[\{N\} \left[(\alpha_b u + \beta_b) + u \frac{\partial u}{\partial x} + v \frac{\partial u}{\partial y} + g \frac{\partial z_b}{\partial x} - 2v\omega \sin\phi - \zeta W^2 \cos\psi \right. \right. \\ & \left. \left. + \frac{gu}{C_z^2 d} (u^2 + v^2)^{1/2} \right] + \frac{\partial \{N\}}{\partial x} \left[\frac{\epsilon_{xx}}{\rho} \frac{\partial u}{\partial x} - g d \right] + \frac{\partial \{N\}}{\partial y} \left[\frac{\epsilon_{xy}}{\rho} \frac{\partial u}{\partial x} \right] \right] dx dy \\ & + \sum_{j=1}^{j=NE} \int_{S_e} \{N\} g d n_x dS_e - \sum_{j=1}^{j=NE} \int_{S_e} \{N\} \left[\frac{\epsilon_{xx}}{\rho} \frac{\partial u}{\partial x} n_x + \frac{\epsilon_{xy}}{\rho} \frac{\partial u}{\partial y} n_y \right] dS_e = 0 \end{aligned} \quad (4.11)$$

for the momentum equation in the x-direction, and

$$\begin{aligned} & \sum_{j=1}^{j=NE} \int \int_{A_e} \left[\{N\} \left[(\alpha_c v + \beta_c) + u \frac{\partial v}{\partial x} + v \frac{\partial v}{\partial y} + g \frac{\partial z_b}{\partial y} - 2u\omega \sin\phi - \zeta W^2 \sin\psi \right. \right. \\ & \left. \left. + \frac{gv}{C_z^2 d} (u^2 + v^2)^{1/2} \right] + \frac{\partial \{N\}}{\partial y} \left[\frac{\epsilon_{yy}}{\rho} \frac{\partial v}{\partial y} - g d \right] + \frac{\partial \{N\}}{\partial x} \left[\frac{\epsilon_{yx}}{\rho} \frac{\partial v}{\partial x} \right] \right] dx dy \\ & + \sum_{j=1}^{j=NE} \int_{S_e} \{N\} g d n_y dS_e - \sum_{j=1}^{j=NE} \int_{S_e} \{N\} \left[\frac{\epsilon_{yx}}{\rho} \frac{\partial v}{\partial x} n_x + \frac{\epsilon_{yy}}{\rho} \frac{\partial v}{\partial y} n_y \right] dS_e = 0 \end{aligned} \quad (4.12)$$

for the momentum equation in the y-direction, where C_z is the Chezy coefficient; α and β are coefficients that describe the approximate linear function for the velocity components; $\{M\}$ and $\{N\}$ are the shape functions representing flow depths and velocities, respectively; and n_x and n_y are direction cosines between the boundary normal and x- and y-directions, respectively. The approximate signs, \sim , over the dependent variables d , u and v have been dropped for convenience.

Equations 4.11 and 4.12 are nonlinear due to the convective acceleration terms. Newton's

iterative method for solving systems of nonlinear equations is used in HYDRO2D to solve the assembled set of finite element equations (eqs. 4.10-4.12). Convergence is generally achieved in three iterations for unsteady flow problems.

4.3.2 Sediment and Contaminant Transport Equations

Again, without derivation, applying the Galerkin method of weighted residuals to the advection-dispersion equation (eq. 3.12) gives

$$\sum_{j=1}^{j=NE} \int \int_{A_e} \left[N_j \left(Q + u \frac{\partial C}{\partial x} + v \frac{\partial C}{\partial y} \right) + v \frac{\partial N_j}{\partial x} \left(D_{xx} \frac{\partial C}{\partial x} + D_{xy} \frac{\partial C}{\partial y} + \frac{\partial N_j}{\partial y} \left(D_{yx} \frac{\partial C}{\partial x} + D_{yy} \frac{\partial C}{\partial y} \right) \right] dx dy + \sum_{L=1}^{L=NL} \int_{\zeta} N_L q_L^s d\zeta = 0 \quad (4.13)$$

where $Q = \partial C / \partial t - S_T$ is taken to be an instantaneous constant. This approach, which transforms equation 3.12 into an elliptic equation, results in a more efficient computation scheme. Equation 4.13, derived by Hayter (1983), may be expressed for a singular element by the element matrix differential equation

$$[k] \{c\} + [t] \frac{\partial \{c\}}{\partial t} + \{f\} = 0 \quad (4.14)$$

where $[k]$ is the element steady-state coefficient matrix, $[t]$ is the temporal matrix, $\{c\}$ is the vector of unknown nodal concentrations, and $\{f\}$ is the element source/sink vector.

Equation 4.14 is evaluated for each element with the element load matrix $[b] = 0$ for interior elements. The element coefficient matrix is modified to account for prescribed nodal boundary conditions by eliminating the row and column corresponding to that nodal unknown. For those boundary nodes at which no boundary conditions (i.e., concentrations or fluxes) are prescribed, the normal concentration fluxes across those nodes are set equal to zero.

Next, the element matrix differential equations (eq. 4.14) are assembled to form the system matrix differential equation

$$[K] \{C\} + [T] \frac{\partial \{C\}}{\partial t} + \{F\} = 0 \quad (4.15)$$

where all the matrices and arrays are the system equivalents of those given in equation 4.14.

Rearranging equation 4.15 and replacing the partial derivative with a finite difference gives

$$\left\{ \frac{[T]}{\Delta t} [K] \right\} \{C\} + \{F\} = 0 \quad (4.16)$$

Applying a Crank-Nicolson type representation to temporally discretize this equation gives

$$\left\{ \frac{[T]}{\Delta t} + \theta [K]^{J+1} \right\} \{C\}^{J+1} = \left\{ \frac{[T]}{\Delta t} - [(1-\theta) [K]^J] \right\} \{C\}^J - \theta \{F\}^{J+1} - (1-\theta) \{F\}^J \quad (4.17)$$

where θ is the degree of implicitness ($\theta = 1$, fully implicit; $\theta = 0$, fully explicit), and the superscripts J and $J+1$ indicate the values of the arrays and vectors at the current time step ($t = J\Delta t$) and at the next time step ($t = (J+1)\Delta t$), respectively. The value of θ is specified by the user. For stability reasons, θ should be greater than or equal to 0.50. Using the specified initial and boundary conditions, equation 4.17 is solved for the NP-NBC unknown nodal concentrations at $t = (J+1)\Delta t$, where NP is the number of nodes in the system, and NBC is the number of boundary nodes with specified boundary conditions. The method used to solve equation 4.17 is discussed later in this section.

4.3.3 Boundary Conditions

Both HYDRO2D and CS2D account for solid, or land, boundaries and open, or water, boundaries. Along land boundaries, a zero normal flux condition is automatically applied in both models. Thus, for example, in HYDRO2D there is no transport of water through these boundaries. In HYDRO2D, a tangential "slip" solid boundary condition is used that allows for parallel flow along these boundaries. Although this imposed condition obviously would not result in an accurate representation of the lateral velocity profile of a viscous fluid in open channel flow, the slip condition is accepted for practical reasons to reduce the number of elements in the system. If a no-slip condition were to be imposed at solid boundaries, a dense grid would have to be placed adjacent to all solid boundaries in order to accurately represent the large lateral velocity gradients present at solid boundaries.

Both models have the capability of simulating drying and rewetting of nodes (and elements). This allows for simulation of flooding and draining of tidal marshes during flood and ebb tides, respectively, and the emergence and submergence of, for example, mud flats over the

course of a tidal cycle.

The open or water boundary conditions that have to be specified in HYDRO2D are either the water surface elevations or unit discharges at all nodes across the boundary. The depth-averaged suspension concentrations have to be specified at open boundary nodes in HSCTM-2D or zero concentration gradients are automatically applied to those boundary nodes.

4.3.4 Equations Solver

The finite element modeling system HSCTM-2D uses the frontal solution program for unsymmetric matrices developed by Hood (1976) to solve the assembled systems of finite element equations. The frontal algorithm was developed specifically for applications to boundary value problems. Although it is based on the Gaussian elimination technique, it has advantages over conventional banded matrix techniques in that computer storage requirements and computation times may be considerably reduced in certain applications.

SECTION 5

DESCRIPTION OF THE MODELING SYSTEM

5.1 SYSTEM COMPONENTS

The finite element modeling system HSCTM-2D, a flowchart of which is given in Figure 1.1, is a set of computer programs written in FORTRAN 77 that have been integrated into a single package for modeling two-dimensional, depth-averaged surface water flows and transport of cohesive sediments. The programs are a hydrodynamic model, HYDRO2D, and a cohesive sediment transport model, CS2D. SMS, obtained separately, is used for pre- and post-processing.

The modeling system can be operated in either an uncoupled or semi-coupled mode (see Figure 1.1). In the former, HYDRO2D is used to specify the nodal water depths and velocities for the entire period of simulation and then CS2D solves for the spatial and temporal variations in the suspension concentration and bed surface elevations using the output from HYDRO2D. Operated in the semi-coupled mode, the modeling system runs both models during the first time step, CS2D at all subsequent time steps, and HYDRO2D at specified time steps. The semi-coupled mode allows predicted changes in flow depths resulting from deposition and erosion to be incorporated in the predicted flow field.

The following two subsections describe the structure of the two computer programs included in the HSCTM-2D modeling system. A detailed description of the algorithms included in HSCTM-2D, which simulate the processes of erosion, dispersion, and deposition, are given in Section 5.3. A description of the default option of the HSCTM-2D is given in Section 8.6.

5.2 HYDRODYNAMIC MODULE

The hydrodynamic module HYDRO2D simulates two-dimensional, depth-averaged flow of surface waters. The governing equations, eqs. 3.1, 3.7 and 3.8, are solved by the Galerkin method of weighted residuals using the finite element method, as described in Section 4. The depth-averaged velocities in the two horizontal directions and the flow depth are computed at each node. In addition, continuity can be checked across multiple cross-sections. The effects of bottom, internal, and surface shear stresses and the Coriolis force are simulated in HYDRO2D. Bottom and surface stresses are due to friction; internal stresses are the results of turbulence.

The module can simulate both steady state and dynamic flows. Boundary conditions at system "water" boundaries may be specified as either (a) the total discharge across the boundary in a specified direction, (b) the water surface elevation along the boundary, or (c) as a stage-discharge relationship. The data input routine in HYDRO2D reads the output (finite element grid) file generated by SMS. HYDRO2D has the ability to handle drying and wetting of nodes, thus simulating emergence and/or submergence of a particular portion of the water system, e.g., mud flats, over a tidal cycle. User instructions and a brief description of the function of each subroutine in HYDRO2D are included in Section 8. A synopsis of the operations performed during model operation is given below.

After the input data file is read, the finite element grid is examined for compatibility (with dimensioned arrays) and consistency (of node and element order). The system of finite element equations is established and then solved by the frontal elimination method. Newton's method is used to obtain an iterative solution of the nonlinear finite element equations by multiple calls to the frontal routine. The results are printed out after the specified number of iterations. For dynamic (time-dependent) problems, boundary conditions are updated at each time-step.

5.3 COHESIVE SEDIMENT TRANSPORT MODEL

The cohesive sediment transport model CS2D is a time varying, two-dimensional finite element model that is capable of predicting the horizontal and temporal variations in the depth-averaged suspended cohesive sediment concentrations and bed surface elevations in an estuary, coastal waterway or river (Hayter and Mehta 1986). In addition, it can be used to predict the steady-state or unsteady transport of any conservative or non-conservative constituent if the

reaction rates are known. CS2D simulates the advection and dispersion of suspended constituents, aggregation, and deposition to and erosion from the bed of cohesive sediments. Hayter (1983) describes a series of experiments that were used to partially validate the model. User instructions including a list of the data required to specify initial concentration and bed conditions, and subsequent dynamic conditions, and a brief description of the function of each subroutine are included in Section 8. A synopsis of the operations performed by CS2D during each time step is given below.

The average bed shear stress induced by the turbulent flow is calculated for each element. Then the amount of sediment that is predicted to be deposited onto or resuspended from the bed in each element during the current time-step is determined. The dispersion algorithm then calculates the values of the four components of the two-dimensional sediment dispersivity tensor. Using these values and the prescribed velocity field (input from HYDRO2D) and concentration boundary conditions, equation 4.17 is solved for the nodal suspended sediment concentrations for the next time-step. The new bed elevation in each element is determined by adding the thickness of sediment deposited onto, or subtracting the thickness of sediment resuspended from, the bed elevation that exists during the current time-step. Next, detailed descriptions of the algorithms included in HSCTM-2D are given.

5.3.1 Bed Schematization

To facilitate the modeling of changes in the bed surface elevation due to erosion and deposition the sediment bed is treated in the following manner: (1) it is discretized into a number of horizontal layers and (2) the bed properties, e.g., thickness, are assumed to be spatially (in the x-y plane) invariant within each element, but variant from element to element in order to account for inter-element spatial variances in shoaling and/or scouring patterns. These two factors are expounded upon below.

The bed in each element is considered to be composed of two sections: (1) the original, settled bed that is present at the start of modeling and (2) new deposits located on top of the settled bed that are initially present or result from deposition during model operation. Each of these two sections is divided into a number of horizontal layers in order to represent the bed shear strength and density profiles. The new deposit bed section is divided into two sub-sections, the top referred to as unconsolidated new deposit (UND) layers and the bottom as partially consolidated new

deposit (PCND) layers (see Figure 5.1). The former sub-section, which represents a stationary suspension, is considered to undergo redispersion; the latter, i.e., partially consolidated bed, undergoes resuspension when subjected to an excess shear stress. The settled bed as well is simulated to resuspend. The number of layers indicated in Figure 5.1 for each of the three bed sections are not fixed, as each section can be assigned any number of layers.

Stationary suspensions are represented in the depth-averaged model as being the top section of the layered bed model, even though they are not a true bed or soil, in order to account for the subsequent redispersion of these suspensions. The time-varying bed thickness in each element, however, is taken to be equal to the thickness of the PCND layers and settled bed layers only. The following bed-related parameters are required for bed schematization:

- 1) The bed shear strength, τ_c , profile of a stationary suspension. This can be ascertained from laboratory erosion tests using samples of sediment from the water body being modeled (see Section 6.1). The τ_c values at the NLAYTM+1 nodes, where NLAYTM is the number of UND layers, (see Figure 5.2) need to be included in the data input file.
- 2) The number of UND layers (NLAYTM) and the thickness of each layer (TLAYM(I), I= 1,NLAYTM). These parameters should be determined using the shear strength profile. For example, Figure 5.2 shows a hypothetical τ_c profile and illustrates how this bed section should be divided such that the variation of τ_c within each layer is approximately linear.
- 3) The dry sediment density, ρ_s , values at the NLAYTM+1 nodes. The ρ_s profiles may be determined using the laboratory freeze-drying method described by Parchure (1980), the pumping method described by Thorn and Parsons (1977), a gamma-ray nuclear transmission densitometer (Whitmarsh 1971), or a nondestructive X-ray technique (Been and Sills 1981).

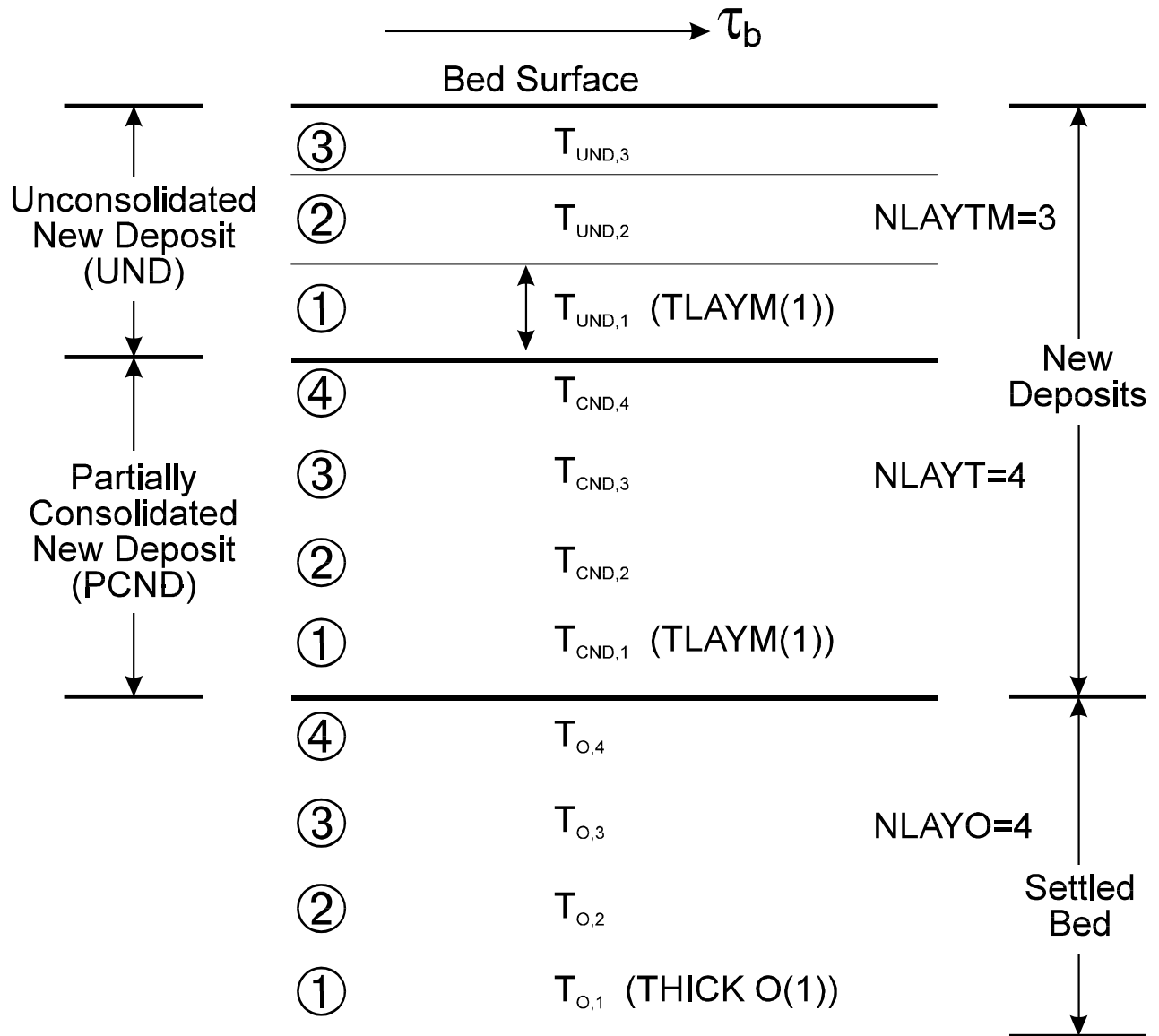


Figure 5.1 Bed Schematization Used in Bed Formation Algorithm

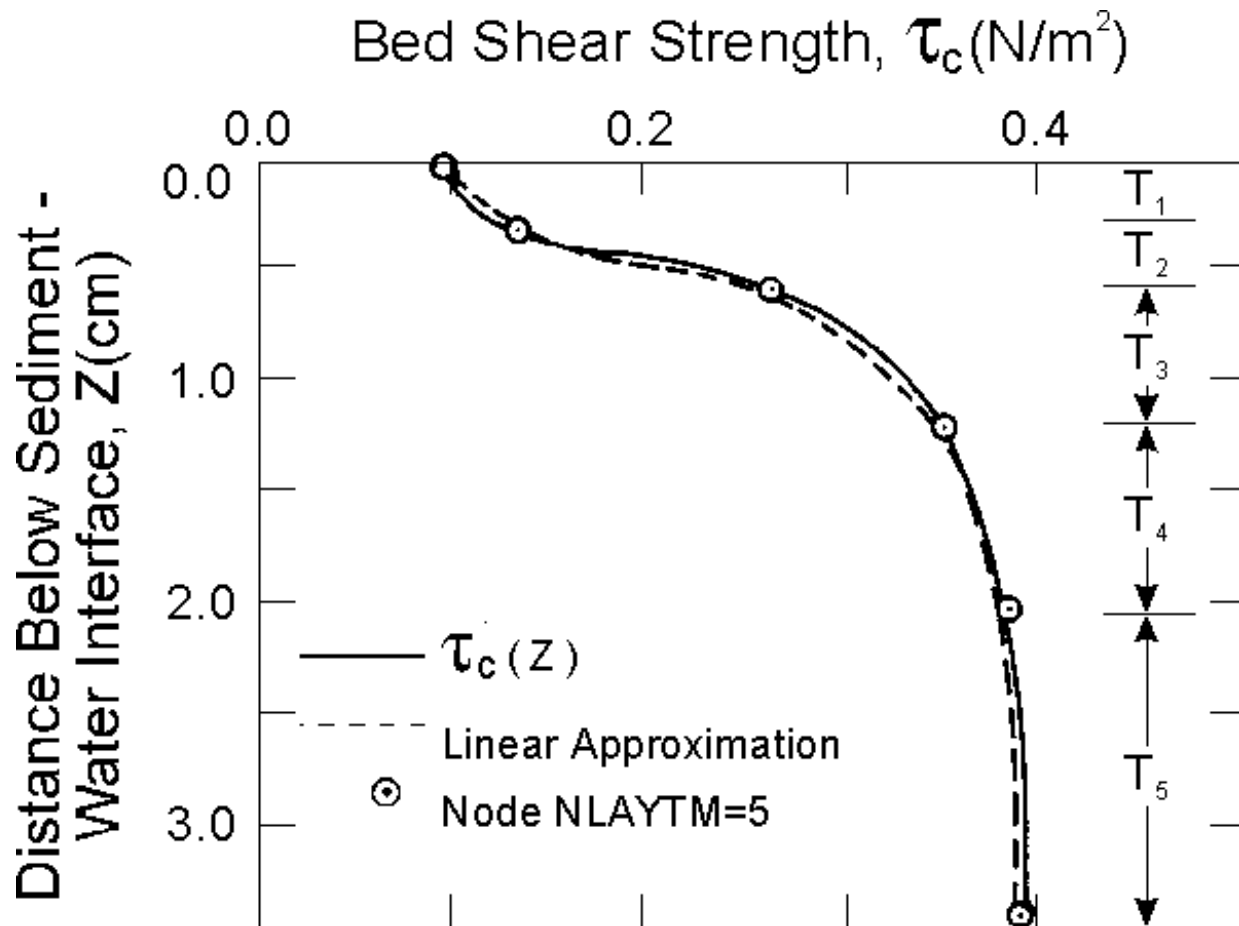


Figure 5.2 Hypothetical Shear Strength Profile Illustrating Determination of Bed Layer Thickness.

- 4) The corresponding parameters as in steps 1 to 3 above must be determined for the PCND layers and the settled bed layers. The settled bed parameters have to be determined for each element (where an original bed exists), but the parameters for the UND and PCND layers are assumed to be constants for all elements.
- 5) A stationary suspension and/or partially consolidated bed (i.e., new deposit) present on top of the settled bed at the start of the modeling is simulated by specifying the dry sediment mass per unit bed area of such new deposits in every element.

The bed level at which the dry sediment density is approximately 480 kg/m^3 is usually taken to be the top of the settled bed. Thus, the sediments located above this level are considered to be new deposits. Another method that may be used to differentiate between new deposits and the settled bed is described in Section 6.1.

Included in Section 6.1 is a brief description of how these various bed properties can be determined through the use of a field data collection program and a laboratory testing program. Other parameters characterizing the rate of resuspension that each layer undergoes when subjected to an excess shear must be evaluated as well; these are discussed in Section 5.3.2.

The following procedure is used to form the new deposit bed layer(s) that result from new deposits initially present on top of the settled bed and/or deposited during modeling. The dry sediment mass per unit bed area per element, M_D , either the initial amount or the amount deposited during modeling, is used in conjunction with the UND and PCND properties to solve iteratively for the thickness of the bed formed for each element where $M_D > 0$. This thickness, ΔT , depends on the dry sediment density profile, $\rho_s(Z)$, for the UND and PCND layers, where Z is the coordinate that defines the depth below the bed surface. The thickness ΔT is determined using the following relationship:

$$\Delta T = \frac{\int_0^{\lambda} \rho_s(Z) Z dZ}{M_D} \quad (5.1)$$

where $\lambda = \Delta T \pm 0.02\Delta T$. If ΔT is greater than $TLAYM(1)$ (see Figure 5.1), then more than one layer of UND is added. The assumed linear variation of ρ_s within each layer is used in the above equation. When the UND layers are filled, the same procedure is used to fill up the PCND layers below the UND layers. The bottom PCND layer can never completely fill up; therefore, continuing deposition is accounted for by increasing the thickness of this layer, while the thickness of the overlying UND and PCND layers remain the same.

5.3.2 Erosion Algorithm

A description of the redispersion and resuspension algorithms is given below. In both algorithms, the rate of erosion is calculated on an element by element basis.

A portion of the unconsolidated new deposit (UND), when present, will redisperse (mass erode) when τ_b is greater than the surface shear strength, i.e., $\tau_c(Z=0)$. The thickness of the UND that fails and is instantly redispersed is equal to Z_* , where Z_* is the bed depth at which $\tau_c(Z) = \tau_b$. The value of Z_* is determined from the linearly varying $\tau_c(z_b)$ profile in each UND layer. The value of Z_* may be greater than the thickness of the top layer, $TLAYM(1)$, in which case more than

one layer is re-entrained. The sediment mass per unit bed area that is redispersed, M_R , during one time-step, ΔT , is calculated according to

$$M_R = \int_0^{Z_*} \rho_s(Z) dz \quad (5.2)$$

The contribution to the source term in the governing equation (eq. 3.12) caused by redispersion is given by M_R divided by the product of the element-averaged water depth and time-step size Δt . New UND layer(s) thicknesses and $\tau_c(Z)$ and $\rho_s(Z)$ profiles are calculated at each time-step when redispersion occurs by subtracting Z_* and resetting $\tau_c(Z=0)$ and $\rho_s(Z=0)$ equal to their respective initial values at $Z = Z_*$. If Z_* is calculated to be greater than the thickness of the entire UND, then all of the stationary suspension is redispersed.

For both redispersion and resuspension algorithms, erosion is considered to occur only during accelerating flows, i.e., $\tau_b(t+\Delta t) > \tau_b(t)$. Thus, even though $\tau_b(t+\Delta t)$ may be greater than $\tau_c(Z=0)$, no erosion will occur if $\tau_b(t) > \tau_b(t+\Delta t)$. This stipulation for occurrence of erosion and an analogous one for deposition (as will be discussed in Section 5.3.4), are based on an interpretation of typically observed Eulerian time-concentration profiles in an estuarial environment. For example, Figure 3.3 shows a time-concentration profile from the Savannah River estuary (Krone 1972). Also indicated is the observed correlation between accelerating flows and increasing suspension concentration, and between decelerating flows and decreasing suspension concentration. Laboratory evidence (Mehta and Partheniades 1975; Partheniades 1977; Mehta *et al.* 1982a; Parchure 1984) suggests that under accelerating flows, erosion occurs without re-deposition of the eroded sediment. Likewise, during decelerating flows, sediment is deposited with re-entrainment of the deposit. During periods of steady flows, erosion or deposition may occur. These two processes do not, however, occur simultaneously (except as noted below) even in this case (Parchure 1984). The initial condition at the inception of the steady flow period determines whether erosion or deposition occurs. For example, if the antecedent phase was one of acceleration, the sediment will continue to erode under the steady flow condition. In both cases, however, relatively short transient periods of simultaneous erosion and deposition sometimes occur (Yeh 1979). For modeling purposes, however, these periods are ignored without introducing any significant errors.

Resuspension of partially consolidated beds (PCND) occurs when: (1) the entire UND has been redispersed, (2) $\tau_b(t+\Delta t) > \tau_b(t)$ and (3) $\tau_b(t+\Delta t) > \tau_c(Z=0)$, where $Z=0$ is now at the water-PCND interface. The resuspension rate expression (eq. 3.11) found by Mehta *et al.* (1982a) is used in the manner shown below to determine the bed thickness Z_* that is resuspended during one time-step, Δt . The iterative procedure used to calculate Z_* during any given time-step is described by Hayter (1983).

The average erosion rate, $\bar{\epsilon}$, for the period Δt is calculated as:

$$\bar{\epsilon} = \frac{1}{2} [\epsilon(t) + \epsilon(t + \Delta t)] \quad (5.3)$$

in which

$$\epsilon(t + \Delta t) = \epsilon_{o_1} \exp \left[\alpha_1 \left(\frac{\tau_b(t + \Delta t)}{\bar{\tau}_c} - 1 \right) \right] \quad (5.4)$$

where ϵ_{o_1} and α_1 are the average empirical coefficients for the first (i.e., top) PCND layer, and $\bar{\tau}_c$ is the average bed strength over Z_* . As in the redispersion routine, new PCND layer thickness(es) and $\tau_c(Z)$, and $\rho_s(Z)$ profiles are determined. As before, Z_* may be greater than the thickness on the top layer. Laboratory tests required to evaluate $\tau_c(Z)$, $\rho_s(Z)$, and the average values of ϵ_o and α for each PCND layer are described in Section 6.1. Values for ϵ_o and α reported in the literature are given in Table 5.1.

Once the entire new deposit bed section has been eroded, the original settled bed will undergo resuspension when the following two conditions occur: 1) $\tau_b(t+\Delta t) > \tau_b(t)$ and 2) $\tau_b(t+\Delta t) > \tau_c(Z=0)$, where $Z=0$ is now at the top of the settled bed. The surface erosion rate expression (eq. 3.10) given by Ariathurai and Arulanandan (1978) is used to evaluate the thickness, Z_* , of the settled bed that is eroded during each time-step. The iterative procedure used for the PCND is again used to solve for Z_* , with only the expression for ϵ being different. The following equation is used instead of equation 5.4.

$$\varepsilon(t + \Delta t) = M(1) \left(\frac{\tau_b(t + \Delta t)}{\bar{\tau}_c} - 1 \right) \quad (5.5)$$

where $M(1)$ is the erodibility constant for the first layer. Values for M reported in the literature are listed in Table 5.1.

The contribution to the source term in equation 3.12 caused by resuspension is given by equation 5.3 divided by the average elemental water depth, with equation 5.4 used for the partially consolidated bed section and equation 5.5 used for the original settled bed section.

The bed shear strength profiles, shown in Figure 3.5, were analyzed by determining the weighted depth-averaged value (weighted with respect to spacing, i.e., depth, among adjacent data points) of τ_c at the five different salt concentrations, S . The following relationship was found:

$$\begin{aligned} \tau_c(S) &= \left(\frac{S}{2} + 1 \right) \cdot \tau_c|_{(S=0)} & \text{for } 0 \leq S < 2 \\ \tau_c(S) &= 2 \cdot \tau_c|_{(S=0)} & \text{for } S \geq 2 \end{aligned} \quad (5.6)$$

where S is in ppt. The method used to include the effect of salinity on bed shear strength profiles, and hence on the erosion rate of that bed is described by Hayter (1983).

5.3.3 Dispersion Algorithm

The most important, and possibly the most difficult, task in modeling dispersion is to determine which of the dispersion mechanisms are important in the water body being modeled. For example, if the estuary has only a few tidal flats and shore irregularities, and has a fairly uniform cross-section (e.g., the Delaware River), shear flow dispersion may be the dominant mechanism. However, if the estuary is relatively deep and the river discharge is large (e.g., the Mississippi River), gravitational circulation may be just as (or even more) important than shear flow dispersion. Unfortunately, none of the existing dispersion models, most of which

Table 5.1 Values of Erosion Rate Coefficients

Coefficient	Value	Sediment Type	Salinity (ppt)	Consolidation Time (hrs)	CEC (meq/100gm)
ϵ_o ($\text{kg m}^{-2}\text{s}^{-1}$) ($\times 10^5$)	0.50	kaolinite	0	24-72	5.85
	0.63	kaolinite	0	144	NR
	1.4	kaolinite	35	24-240	5.85
	0.79 (0.50-1.53)	kaolinite	0	2-240	12.0
	0.40 (0.20-0.54)	kaolinite	35	24-120	12.0
	3.2	Lake Francis, Nebraska	0.35	NR	93.8
	0.42	Grangemouth Harbor, Scotland	26	48	NR
	1.86	Belawan mud	33	48	NR
α	9.3 (5.5-19.8)	kaolinite	0	2-240	12.0
	5.9 (5.8-6.0)	kaolinite	35	24-120	12.0
M ($\text{kg m}^{-2}\text{s}^{-1}$)	0.03-0.30	natural & made-up soils	NR	NR	2-27
			NR	NR	NR
	0.0023	Grangemouth Harbor, Scotland			

NR - Not reported

are two-dimensional, can represent the combined effects of irregular shoreline configuration, bathymetry, shear flow dispersion and baroclinic flow. Because of these problems in identifying, describing and modeling the various dispersion mechanisms that occur in estuaries, the dispersion algorithm in HSCTM-2D simulates shear flow dispersion only, and thus is most applicable to a wide, vertically well-mixed estuary. Following the analysis of Holley *et al.* (1970), it is assumed that dispersion in wide estuaries is associated primarily with the vertical shear. The limitations,

which determine the applicability of such a dispersion algorithm, are consistent with those associated with a two-dimensional, depth-averaged transport model.

The dispersion tensor derived by Fischer (1978) for two-dimensional, depth-averaged bounded shear flow is used in the dispersion algorithm. The four components of this tensor are

$$\begin{aligned}
 D_{xx} &= \left(U^2 d^2 / \bar{E} \right) I_{xx} \\
 D_{xy} &= \left(UV d^2 / \bar{E} \right) I_{xy} \\
 D_{yx} &= \left(UV d^2 / \bar{E} \right) I_{yx} \\
 D_{yy} &= \left(V^2 d^2 / \bar{E} \right) I_{yy}
 \end{aligned} \tag{5.7}$$

in which U and V are the root-mean-square values of u' and v' over the depth d ; $u' = u(z) - \bar{u}$, where \bar{u} is the depth-averaged component of the velocity in the x-direction; $v' = v(z) - \bar{v}$, where \bar{v} is the depth-averaged component of the velocity in the y-direction; \bar{E} is the mean value of the scalar turbulent diffusion coefficient in the vertical direction, E_z ; and

$$I_{ij} = \int_0^1 u_i'' \int_0^\Gamma \frac{1}{E'} \int_0^\Gamma u_j'' d\Gamma' d\Gamma d\Gamma \tag{5.8}$$

in which $E' = E_z / \bar{E}$, $u_i'' = u_i' / u$, and $\Gamma = z/d$. The quantities u' and v' are the velocity deviations over depth from the respective depth-averaged values, u and v . The values U and V represent the "intensity" of u' and v' , respectively (Fischer *et al.* 1979). The physical interpretation of the cross product dispersion coefficients D_{xy} and D_{yx} is that a velocity gradient in the x (or y) direction can produce mass (dispersive) transport in the y (or x) direction.

Fischer (1978) notes that, since in most investigations the vertical velocity profile, i.e., $u(z)$ and $v(z)$, and the vertical turbulent diffusion coefficient, E_z , are not known with a high degree of accuracy, it usually suffices to assume that the value of I_{ij} in equation 5.8 is a constant. The value of I_{ij} in various parallel shear flows ranges from 0.054 for turbulent pipe flow to 0.10 for laminar flow with a linear velocity profile over d (Fischer *et al.* 1979). Therefore, Fischer recommends that a value of 0.10 be used for I_{ij} .

The following expression for E_z , derived by Elder (1959) for flow down an infinitely wide inclined plane, is used in this analysis:

$$E_z = \kappa u_f z \left(1 - \frac{z}{d} \right) \quad (5.9)$$

where κ is the von Karman turbulence constant, and u_f is the shear velocity. Therefore, \bar{E} is given by

$$\bar{E} = \frac{1}{d} \int_0^d E_z dz = \frac{\kappa u_f d}{6} = 0.067 u_f d \quad (5.10)$$

with $\kappa = 0.40$. The values of κ obtained by Gust (1976) from the slopes of measured clay suspension velocity profiles varied between 0.3 and 0.4. Gust considered this variation a result of experimental error and not due to the presence of suspended sediments. Therefore, he assumed $\kappa = 0.40$ in his analysis.

Fischer (1966) found, in both laboratory experiments and in real streams, that the mean value of U^2/\bar{u}^2 was equal to 0.2. Substituting this value, $I_{ij} = 0.1$, and equation 5.10 into equation 5.7 gives:

$$\begin{aligned} D_{xx} &= \frac{0.2\bar{u}^2 d^2}{0.067u_f d} (0.10) = 0.30 \frac{\bar{u}^2 d}{u_f} \\ D_{xy} &= \frac{0.2\bar{uv} d^2}{0.067u_f d} (0.10) = 0.30 \frac{\bar{uv} d}{u_f} \\ D_{yx} &= \frac{0.2\bar{uv} d^2}{0.067u_f d} (0.10) = 0.30 \frac{\bar{uv} d}{u_f} \\ D_{yy} &= \frac{0.2\bar{v}^2 d^2}{0.067u_f d} (0.10) = 0.30 \frac{\bar{v}^2 d}{u_f} \end{aligned} \quad (5.11)$$

These are the coefficients used in the dispersion algorithm to model shear flow dispersion of cohesive sediments in a wide, well mixed estuary. Values of D_{ij} are calculated at each time step in the model using the specified nodal values of \bar{u} and \bar{v} and d .

5.3.4 Deposition Algorithm

The product $P_d \cdot W_s$ in equation 3.19 defines an effective settling velocity, W_s' , that is, in general, smaller in magnitude than W_s since the range of P_d is between 0 and 1. The rate of deposition given by equation 3.19 may, therefore, be written as

$$\frac{dC}{dt} = \frac{W_s' C}{d} \quad (5.12)$$

For the dimensionless bed shear stress τ_b^* less than a certain characteristic value, τ_{bc}^* , with the range $\tau_b^* < \tau_{bc}^* < 1$ designated as Range I (see Figure 5.3), the following empirical relationships for W_s' are assumed:

$$W_{s1}' = P_d W_r (1 - KC)^5 \quad \text{for } C > C_2 \quad (5.13)$$

$$W_{s1}' = P_d K_e C^m \quad \text{for } C_1 < C < C_2 \quad (5.14)$$

$$W_{s1}' = P_d W_{s1} \quad \text{for } C < C_1 \quad (5.15)$$

where W_{s1} is the median sediment settling velocity in the free settling range; W_r is the reference settling velocity; K is the inverse of the hypothetical, fully settled sediment concentration; and P_d is defined by equation 3.20. W_r is found by equating equations 5.13 and 5.14 at $C = C_2$.

Therefore, depending upon the value of C , the rate of deposition in Range I (see Figure 5.3) is given by equation 5.13, 5.14, or 5.15. These three expressions for W_{s1}' are based upon the experimental results of Krone (1962), Owen (1971) and Bellessort (1973). Typical values for C_1 and C_2 are 0.1 to 0.7 g/l and 5 to 10 g/l, respectively. The values W_{s1} , K_e , m and C_1 can vary widely, depending upon the particle diameter, D , the type of sediment and salinity. These parameters must be determined in laboratory settling tests (further discussion of this aspect is given by Delo (1988) and in Section 6.1). Values of these parameters reported in the literature are given in table 5.2. The effect of salinity on W_{s1}' is included in equations 8.1 through 8.4.

For $\tau_{bc}^* < \tau_b^* < \tau_{bmax}/\tau_{bmin}$ and the concentration range $C > C_1$, designated as Range IIB, the rate of deposition is determined using the log-normal relationship derived by Mehta and Partheniades (1975):

$$\frac{dC}{dt} = \frac{-0.434}{2\sqrt{2\pi}\sigma_2} \frac{\exp\left(\frac{-T^2}{2}\right)}{t} C_o \left(1 - \operatorname{erf} \left(\frac{2.04}{\sqrt{2}} \log_{10} \left[\frac{(\tau_b^* - 1)}{4 \exp(-1.27\tau_{bmin})} \right] \right) \right) \quad (5.16)$$

For $\tau_b^* < 1$, the argument of the error function is set equal to zero. Values of deposition rate coefficients reported in the literature are included in Table 5.2. Equation 5.16 is assumed to be valid for $C > C_1$ because the phenomenon of hindered settling was not observed in the steady-state deposition tests performed by Mehta (1973) for concentrations up to about 20 g/l. Evidently, the higher τ_b^* values Mehta used in his tests prevented the occurrence of this mode

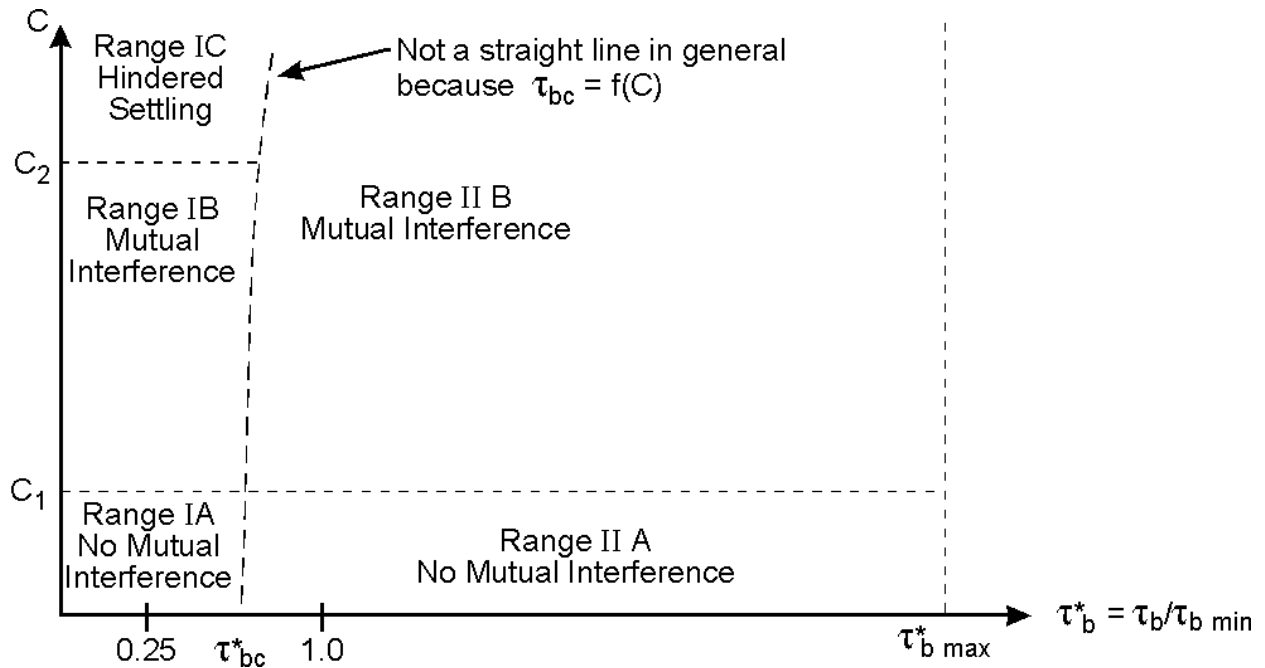


Figure 5.3 Apparent Settling Velocity Description in Domains Defined by Suspended Sediment Concentration and Bed Shear Stress

of settling, inasmuch as Krone (1962) did observe hindered settling in his tests, most of which were conducted at lower values of τ_b^* .

Deposition tests with $0.25 < \tau_b^* < 1$ using San Francisco Bay mud in sea water and kaolinite in distilled water revealed that for suspension concentrations less than $C_1 \approx 0.1-0.7$ g/l, the exponential law given by equation 5.12 was valid. Therefore, for $C < C_1$ in Range IIA, the rate of deposition is given by equations 5.12 and 5.13 with P_d defined such that dC/dt is continuous for all concentrations in Range II (Hayter and Mehta 1982).

Likewise, the parameter τ_{bc}^* is defined to be the value of τ_b^* at which the expression for W_s' in Range I is equal to the same in Range II. Thus, W_s' and therefore dC/dt are continuous functions for the entire deposition range ($\tau_{bmax}^* < 1$). It is apparent that τ_{bc}^* is not a constant, as it is a function of the depth-averaged concentration, C . Hayter (1983) describes the method used to solve for τ_{bc}^* .

Deposition tests performed by Parchure (1984) in an annular flume using Lake Francis sediment in water with varying salinity were analyzed in order to determine the combined effect of salinity and bed shear stress on the settling rates of this sediment. Hayter (1983) described the empirical analysis in detail. The analysis yielded a power law relationship between W_s and S in Range I. The equations for W_s as a function of C are included in Section 8 and will not be repeated here. The effect of salinity on the deposition rate in Range IIB was included as well; again refer to Section 8.

Deposition of suspended cohesive sediment is simulated to occur when (1) the flow is decelerating, i.e., $\tau_b(t+\Delta t) < \tau_b(t)$, and (2) when $\tau_b(t+\Delta t) < \tau_{bmax}$. When these two conditions are satisfied at any node, the rate of deposition is calculated as follows. The value of τ_{bc}^* is evaluated using the procedure described by Hayter (1983). Inasmuch as the log-normal relationship was found not to be suitable for $\tau_b^* < 0.25$, the minimum τ_{bc}^* value is set equal to 0.25. The maximum allowable value for τ_{bc}^* is 1.00. The dry mass of sediment deposited per time-step per element, M_D , is determined according to

Table 5.2 Values of Deposition Rate Coefficients

Coefficient	Value	Sediment Type	Salinity (ppt)	CEC (meq/100 gm)
τ_{bmin}	0.04	Grangemouth Harbor, Scotland	NR	NR
(N m ⁻²)	0.06-0.10	NR	NR	NR
	0.18	Kaolinite	0	77
	0.15	Kaolinite	34	77
	0.12	50% mixture Kaolinite & San Francisco Bay mud	34	NR
	0.096	San Francisco Bay mud	34	24
	0.185	Kaolinite	0	13
	0.118	Atchafalaya	0	29
τ_{bmax} (N m ⁻²)	0.50-1.0	NR	NR	
	1.69	San Francisco Bay mud	34	24
n	1.33	San Francisco Bay mud	NR	NR
	1.1-2.2	Thames River	NR	NR
	<1.0	Atchafalaya Bay, La.	NR	NR

NR = not reported

$$M_D = \frac{d\bar{C}}{dt} \Delta t \bar{d}_e \quad (5.17)$$

where $\bar{d}_e = [d_e(t) + d_e(t + \Delta t)]/2$, d_e is the thickness of sediment deposited per time step,

and

$$\frac{d\bar{C}}{dt} = \frac{1}{2} \left[\left. \frac{dC}{dt} \right|_t + \left. \frac{dC}{dt} \right|_{t+\Delta t} \right] \quad (5.18)$$

in Range I and Range IIA, and

$$\frac{d\bar{C}}{dt} = \frac{\bar{C}}{4\Delta t} (1 - \bar{C}_{eq}^*) \left[\operatorname{erf} \left(\ln \left(\frac{\Delta t}{\bar{t}_{50}} \right) \frac{0.434}{\sqrt{2\pi} \bar{\sigma}_2} \right) + 1 \right] \quad (5.19)$$

in Range IIB. In equation 5.19, $\bar{\theta} = [\theta(t) + \theta(t+\Delta t)]/2$, where $\theta = C, t_{50}, C_{eq}^*, \sigma_2$ and τ_b^* . The last term is included because C_{eq}^* is a function of τ_b^* . Equation 5.19 was obtained by integration of equation 5.16 from $t=0$ to $t=\Delta t$. Section 5.3.1 describes the procedure for calculating the bed thickness formed by M_D . The sink term in the governing equation (equation 3.12) is given by equation 5.18 in Ranges I and IIA, and by equation 5.19 for Range IIB.

Under unsteady flows, the value of C_{eq} , which is the steady state value of the suspended sediment concentration found in laboratory deposition tests under steady flows, is assumed to be zero. Nevertheless, the laboratory determined log-normal relationship for dC/dt , as given by equation 5.19, is used for Range IIB for the following reasons. The time-step, Δt , used in the estuarial sediment transport problems is typically of the order $0.1 t_{50} < \Delta t < 10t_{50}$. Therefore, dC/dt (given by equation 5.19) is significantly greater than zero at time Δt . This implies that, after any time interval Δt , the suspended sediment concentration, $C(t+\Delta t)$, does not approach C_{eq} , but is assumed to be equal to the following:

$$C(t + \Delta t) = C(t) - \frac{d\bar{C}}{dt} \Delta t \quad (5.20)$$

where $d\bar{C}/dt$ is given by equation 5.19. Thus, for unsteady flow conditions, the rate of deposition is considered to be a function of C_{eq} . Such a consideration is required for a realistic interpretation of deposition results for the purpose of ascertaining the depositional rates in unsteady estuarial environments.

SECTION 6

DATA COLLECTION AND MODEL CALIBRATION

Delo (1988) summarizes procedures that may be used for determination of some of the empirical coefficients contained in expressions for the rate of sediment transport processes of erosion and deposition when limited information about field conditions is available. He also emphasizes that "the behavior of cohesive sediment does vary considerably in quantitative terms from one source to another. Therefore, it is crucial that the engineer appreciates that estimates based on the data presented herewith may well be in error by half an order of magnitude (or more)."

6.1 DATA COLLECTION AND ANALYSIS

6.1.1 Field Data Collection Program

A field data collection program for a sedimentation study should consist of four principal components: (1) hydrographic survey; (2) sediment sampling; (3) measurement of suspended sediment concentration, water temperature and salinity; and (4) determination of sediment settling velocity. The collection program required for modeling the hydrodynamic regime in an estuary is rather well known and will not be addressed in this report. For one reference, refer to Smoot and Novak (1969).

6.1.1.1 Hydrographic Survey

At least two sonar fathometers and a gamma-ray transmission densitometer should be used to measure the depths in the water body to be modeled. First, the entire water body should be surveyed simultaneously using, for example, a 30-kHz and a 200-kHz fathometer.

Parker and Kirby (1977) reported that the sediment-water interfaces of stationary suspensions in the Severn Estuary, England, were detected by a 200-kHz fathometer but not by a 30-kHz fathometer. In areas where stationary suspensions are determined to exist (by comparison of the 30-kHz and 200-kHz records), a gamma-ray transmission densitometer or a turbidity meter should be used to supplement the depth record obtained with the fathometers. A fathometer alone may not be capable of detecting the surface of stationary suspension for two reasons: (1) The acoustic detection of a dense suspension depends on the gradient of the bulk density at the surface of the suspension and not on the magnitude of the density. In mobile suspensions and in newly formed stationary suspensions, this density gradient is very small, and in most cases the surfaces of these suspensions will not be detectable. (2) As the stationary suspension undergoes consolidation, different levels of the suspension may become detectable to fathometers with different frequencies at different times, which makes the interpretation of such fathometer records a difficult and uncertain task (Parker and Kirby 1977).

A gamma-ray transmission densitometer obtains in situ measurements of the sediment bulk density profiles, and can be used, in addition, to determine the thickness of stationary suspensions and the location (i.e., vertical elevation with respect to geodetic datum) of the top of the settled bed, at which the bulk density is usually assumed to be 1300 kg/m^3 . A static cone penetrometer directly measures penetration resistance and indirectly measures the shear strength of the sediment. The densitometer has to be calibrated at the beginning and end of survey operations to determine the relationship between the radiation count rate and sediment density. Calibration is generally performed using liquids with different densities. The densitometer is penetrated and retracted in the sediment at a rate of approximately 2 to 3 mm/sec, during which the radiation count rate and probe penetration depth are continuously recorded. This system has been used from both ships and submersibles and has the capability of measuring in situ bulk sediment densities up to 1800 kg/m^3 , operating in depths up to 3.6 km, and penetrating one to two meters in cohesive sediment suspensions (Hirst *et al.* 1975).

There are three methods used to fix the boat position during hydrographic survey: (1) optical methods, (2) electronic methods, and (3) combined systems. Optical methods include double horizontal sextant angle and transit line, and theodolite intersections from shore. Electronic methods include two megahertz systems, microwave systems and range and bearing

systems. Combined systems use a theodolite to determine the bearing and a microwave system to determine the distance. A description of these three methods is given by Ingham (1975) and Dyer (1979).

6.1.1.2 Sediment Sampling Using Corers

Before the data collection period begins, at least two 10 to 12 cm diameter cores should be collected at each sampling station. There are four types of corers in common use today: gravity-corer, piston-corer, vibracorer and box-corer. The cores are used in determining the erosional and consolidation characteristics of the existing sediment bed.

6.1.1.3 Measurement of Suspended Concentration, Salinity and Temperature

The first item that must be considered is the time period over which data are to be collected for eventual use in the model. The time period will be contingent upon the desired results from the modeling effort. In tidal water bodies, data should preferably be collected over a minimum of 15 hours (assuming the tide is semi-diurnal) over three different tidal cycles: spring, mean and neap. It would be more desirable to have the data collection period span at least one week starting, for example, on a spring tide and finishing at the subsequent neap tide. The next consideration is the number of sampling stations and where they should be located in order to adequately monitor the spatial variations of the concentration of suspended sediment. Stations must be located at all exterior water boundaries (cross-sections) of the estuarial system to be modeled. The width of the boundary cross-section and the lateral variability of the depth should be considered when deciding upon the minimum number of stations to be located laterally across such a boundary. For example, stations would definitely be located at prominent features such as navigation channels. Additional stations should be located at all interior confluences and bifurcations, and at as many other interior locations as possible. It is recognized that the length of the data collection period and the number of stations are often less than desired due to economic and logistical considerations.

At each station, the location of the top of the sediment bed with respect to a geodetic or tidal datum must be determined using the previously described surveying methods. The water temperature, electrical conductivity (or salinity) and concentration of suspended sediment should be measured at least once every one-half hour for the duration of the collection period at each of the sampling stations. These measurements should preferably be made at a minimum of three

depths over the vertical: one-half to one meter below the water surface, mid-depth and one-half meter above the bottom (i.e., top of sediment bed). For locations where the water depth is greater than about 3 to 4 m, measurements should be made at additional depths over the vertical. Both the measurement and analysis of water temperature and electrical conductivity data are discussed by Dyer (1979). A description of various filtration procedures for determining the suspension concentration gravimetrically is given by Dyer (1979).

There are three general methods used to measure the suspension concentration: (1) water sampling, (2) optical methods and (3) gamma-ray densitometer measurements.

Water bottles and shipboard pumps are the most common water sampling devices. The NIO bottle has capacities for 1.25 to 7.1 liters. Other water bottles, such as the Van Dorn bottle, have capacities of up to 10 liters or more. The NIO bottle consists of a PVC tube open at both ends with hemispherical bings on spring loaded arms that close each end when struck by a brass messenger dropped down the support wire (Dyer 1979).

Shipboard pumps are used to pump water samples up to the vessel through an intake tape mounted on an instrument package. It is recommended that in situ separation of the water and sediment be performed on the vessel using the filter method (van Rijn 1979).

Instruments for optical determination of the concentration of suspended sediment include the transmissometer, the nephelometer, and the Secchi disc. Nephelometers are not very practical for use in estuaries since they are sensitive to very low concentrations only. Secchi discs can be used to estimate surface values only. Transmissometers, or electro-optical turbidity meters, have been used successfully to measure vertical turbidity profiles in, among others, the Severn, Maas, James and Rappahannock estuaries, and in the Upper Chesapeake Bay (Kirby and Parker 1977; Nichols *et al.* 1979). These meters can be used to detect both mobile and stationary suspensions as their operating range is usually 0.25 to 25 g/l. They have a rapid response time (100 Hz), which allows profiles in 30 m depths to be taken in 15 to 20 seconds.

Both Kirby and Parker (1977) and Nichols *et al.* (1979) used instrument arrays on which were mounted a gamma-ray transmission densitometer, at least one electro-optical turbidity meter, an electromagnetic current meter, a pressure transducer, and a water temperature and a water temperature and conductivity probe. In general, the optical turbidity meters would be used to

record the concentration profile for suspensions up to 25 g/l and the transmission densitometer used for denser suspensions.

6.1.1.4 Determination of Sediment Settling Velocity

An appropriate method to measure settling velocities is by using an instrument similar to the sampling tube developed by Owen (1971), in which undisturbed samples of suspended sediments are collected in situ in their natural state. The settling velocities of the aggregates are determined immediately thereafter through use of a bottom withdrawal sedimentation test. The major drawback of an Owen tube is the quiescent condition in the tube during withdrawal. Allersma (1980) gives a detailed description of an in situ suspended sediment sampler.

6.1.2 Laboratory Testing Program

The following physicochemical sediment and fluid properties should be determined using the collected sediment cores.

6.1.2.1 Properties of Undisturbed Sediment Cores

A gamma-ray densitometer may be used to determine the sediment density profile in the undisturbed cores still in the liner tubes as soon after the cores are obtained as possible. A description of this procedure is given by Whitmarsh (1971) and Kirby and Parker (1974). If this instrument is not available, the freeze-drying procedure used by Parchure (1980) and Dixit (1982) or the pumping method used by Thorn and Parsons (1977) may be used to determine the bulk density profile. The pumping method consists of removing by suction a thin layer, e.g., 3 cm, from the top of the core. This procedure is repeated, layer by layer, with each layer analyzed to determine the mean bulk density.

6.1.2.2 Properties of Original Settled Bed

The bulk density and bed shear strength profiles and the erosion rate constant for each layer need to be determined for the cores. The number of layers and the thickness of each are determined from the nature of the bed shear strength profile. The erosion rate constant for each layer and the shear strength profile can be determined, for example, in the rotating cylinder erodibility testing apparatus described by Sargunam *et al.* (1973). In order to use this apparatus, the core sample must be trimmed. The portion of each core that is sufficiently consolidated such that it can be trimmed and tested in the erosion apparatus may be defined to be the settled bed.

The thickness of this portion defines the location of the top of the settled bed. Soft, unconsolidated portions of each core are assumed to be new deposits.

6.1.2.3 Properties of New Deposits

For cores with soft, unconsolidated or partially consolidated sediment on top of the settled portion, the following method may be used to estimate the erosional and depositional characteristics of such new deposits. The new deposit samples from the cores at all the stations should be mixed and subjected to laboratory erosion and deposition tests described by Parchure (1980), Mehta and Partheniades (1973) and Hayter (1983) to determine: the settling velocity as a function of suspension concentration and salinity; the minimum and maximum depositional shear stresses τ_{bmin} and τ_{bmax} ; the variation of t_{50} and σ_2 with the bed shear stress τ_b ; the number of characteristic stationary suspension layers, and the thickness, dry sediment density and shear strength of each layer; the number of characteristic partially consolidated new deposit layers, and the thickness, dry sediment density, shear strength and resuspension parameters ϵ_o and α for each layer; and the variation of the bed shear strength τ_c with ρ_s . The variation of the bed density and shear strength profiles with salinity can be determined by performing the erosion tests at several salinities between 0 and 35 ppt. The relationship between ρ_s and τ_c also needs to be determined for the collected sediment samples. Both the bed shear strength and density profiles may be determined using the methodology described by Mehta *et al.* (1982a). These profiles can then be used to establish an empirical relationship between ρ_s and τ_c .

6.1.2.4 Aggregate Shear Strength and Density

The determination of the aggregate shear strength, τ_s , and the aggregate density, ρ_a , corresponding to each sediment-fluid mixture can be carried out through rheological diagrams of applied shear stress versus shearing rate (Krone 1963). An example of such a diagram is presented in Figure 6.1, with shear stress, τ_s , proportional to the dial reading on the viscometer and shearing rate proportional to the rotation rate of the outer cylinder of the viscometer. The mixture was stirred occasionally to offset the effects of settling during the experiment. On Figure 6.1, mixing is indicated by a change of symbol.

The number of aggregation orders possible for a suspension of a given sediment is equal to the number of linear segments on the rheological diagram with different slopes. Thus, in Figure 6.1 the sediment sample has two possible orders of aggregation. Each order of aggregation

corresponds to a given volume fraction of aggregates (volume occupied by the aggregates divided by the total volume of the suspension) that in turn can be shown to be related to the relative differential viscosity (the viscosity of the suspension divided by the viscosity of the suspended medium). Given the viscosity of the suspending medium, the relative differential viscosity is determined from the slope of the rheological diagram, and hence the volume fraction can be calculated. The density, ρ_a , is then computed from the volume fraction.

Krone (1978) postulated that each segment is related to a particular volume fraction and therefore to a different manner in which the sediment can aggregate, i.e., different order of aggregation. In addition, he found that as the order of aggregation increases, the interaggregate pore volume increases and the strength of these aggregates decreases because of limited bonding area among the lower order aggregates.

6.1.2.5 Fluid Composition

The pH, total salt concentration, and concentrations of ions such as Na^+ , Ca^{2+} , Mg^{2+} , K^+ , Fe^{3+} and Cl^- should be determined for both the pore fluid in the consolidated bed portion of one core and a sample of the suspending fluid.

6.1.2.6 Composition and Cation Exchange Capacity of the Sediment

The sediment contained in the consolidated bed portion of one core from each collection station should be thoroughly mixed so that a spatially homogeneous sample is obtained. A standard hydrometer analysis should be conducted on each co-prepared sample to determine the sediment particle size distribution and thereby the percentage by weight of clay, silt and fine to coarse in each sample. In preparing the samples for this analysis, the sediment must not be initially air-dried (to obtain the dry weight of the material used in the test), as it has been found that dried sediment will not completely redisperse when the dispersing agent is added (Krone 1962). For this reason, the total dry weight of the sample must be obtained after the test by evaporating off all the water in an oven set at approximately 50°C. The percentage of organic matter by weight should be determined through use of a method such as the Walkley-Black test (Allison 1965). In addition, it is recommended that X-ray diffraction analysis of the bulk sample, and $< 2 \mu\text{m}$ unglycolated and glycolated portions be conducted in order to determine the predominant clay and non-clay mineral constituents. Finally, the cation exchange capacity must be determined for each sample.

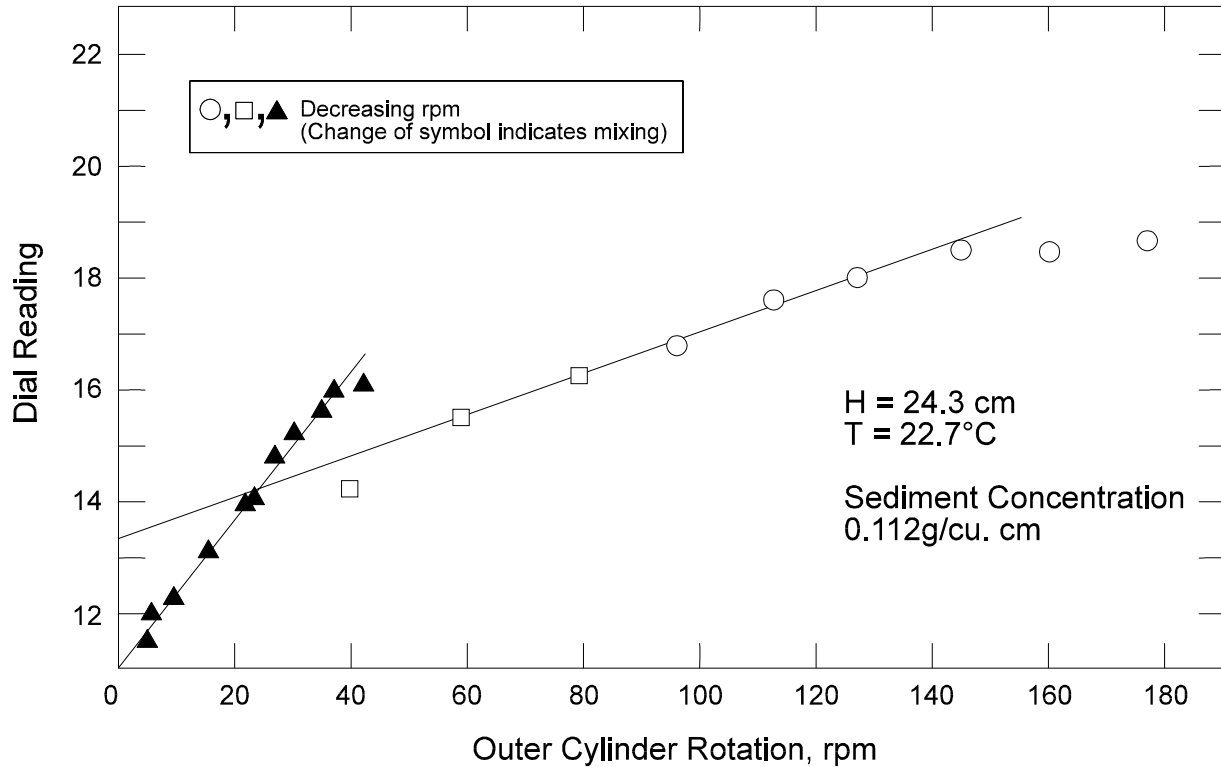


Figure 6.1 A Plot of Raw Viscometer Data Obtained from the U.S. Army Corps of Engineers Philadelphia District Sample (after Krone 1963).

6.2 MODEL CALIBRATION

Calibration of the HSCTM-2D modeling system is a two-step process involving first, calibration of the flow module HYDRO2D, and secondly, the sediment transport module CS2D. General guidelines are discussed below. While not comprehensive, the recommended procedures will provide the model user with sufficient background to initiate the first few iterations in the calibration process. Later iterations are often more site specific in nature.

6.2.1 Hydrodynamic Module

Calibration of the module HYDRO2D involves adjustments of the various internal and external frictional coefficients until a satisfactory match between model results and measured velocities and water surface elevations is obtained. This usually requires several runs of the module with different values of the eddy viscosity coefficient tensor for the internal frictional forces and the Chezy coefficient and wind shear coefficient for the external frictional stress at the bottom and water surface, respectively. Even for an experienced modeler, calibration will usually

require several iterations. Experience gained by this process will enable the modeler to at least qualitatively anticipate the effect of coefficient(s) adjustment(s) on module response. This should result in a reduction in the number of runs required to achieve calibration in future applications of the modeling system.

6.2.2 Sediment Transport Module

Calibration of the module CS2D, if necessary, may be accomplished through adjustment of the sediment dispersivity tensor, or more directly by adjustment of one of the coefficients in the sediment settling velocity model for shoaling problems or one of the coefficients in the erosion rate expressions for scour problems. The model should first be run using the built-in dispersion algorithm to calculate the dispersivity tensor and the coefficients in the deposition and erosion algorithms determined using the tests described in Section 6.1. Then, if necessary, the values of the appropriate coefficient(s) can be changed until a satisfactory match between model results and, for example, known shoaling rates is obtained. Again, this in general will require several runs of the model.

SECTION 7

HSCTM-2D USER INSTRUCTIONS

The user must be prepared to undertake the following four essential tasks -- (1) field measurements, (2) laboratory testing of sediment, (3) numerical modeling of hydrodynamics and sediment and contaminant transport, and (4) analyses of modeling system simulations -- when using HSCTM-2D to model a system. Brief discussions of the first two items are given in Section 6.1. Calibration of the modeling system is discussed in Section 6.2, and a description of the output from the modeling system is given in Section 7.4.

7.1 MODELING SYSTEM LIMITATIONS

A two-dimensional, depth-averaged modeling system such as HSCTM-2D can strictly be applied only to surface bodies of water, e.g., estuaries, harbors and basins (such as marinas), where the horizontal dimensions of the water body are at least one order of magnitude greater than the vertical dimension. Applications to partially mixed water bodies, especially highly stratified water bodies, should be made when only rough estimates of some sedimentary process (e.g., shoaling rate) are required.

Currently HSCTM-2D has the capability of simulating the transport and fate of only four constituents: salinity, one representative size or fraction of cohesionless sediment, one size fraction of cohesive sediment, and one inorganic contaminant. It is possible, however, to modify the model so that a greater number of constituents may be included.

Limitations of the numerical modeling system described herein come from four sources: (1) insufficient data, (2) poor quality data, (3) limitations of our understanding and representations of

processes such as dispersion, sediment erosion and deposition, and adsorption/desorption of contaminants, and (4) limitations of the numerical scheme used to solve the governing equations. The first two sources are attributed to the fact that, owing mainly to time and cost considerations, all the bathymetric, hydraulic, sediment and contaminant data required for use in a model such as CS2D are rarely, if ever, measured and/or collected in the body of water being modeled. In addition, the quality of the data is often questionable. Data requirements and the field collection and laboratory testing programs required to obtain these data are described in Section 6.1. The third and fourth categories are self explanatory. All these limitations are possessed by most numerical models.

The importance of experience in effectively using numerical models cannot be over emphasized. Experience gained through knowledge of the physical systems being modeled and repeated applications of the model will enhance the user's ability to choose the proper values of the various parameters, e.g., time-step size. The user will also gain the ability to anticipate the effect of changing the value of a particular parameter by a certain percentage on the model solution (i.e., model sensitivity).

7.1.1 Limitations of the Hydrodynamic Module

In addition to the previously mentioned limitation of two-dimensional, vertically averaged homogeneous flow, the hydrodynamic module HYDRO2D has the following additional limitations.

- The module will not accurately simulate supercritical flow.
- The model is based on a streamwise bottom slope that is mild and not steeper than (~1:10).

The following guidelines/recommendations should be following in using HYDRO2D.

- For stability, the mesh should be constructed with less than a 20% depth change among adjacent nodes.
- Set up boundary conditions where accurate data, sufficiently far away from the area of interest, are available.
- Elements that alternate between wetting and drying may be included. Note that if any of the nodes attached to an element is dry, the entire element is classified as dry. To maintain stability of the model, mesh boundaries paralleling flow lines where wetting and drying are expected to occur is recommended.

- The computed results should be compared to measured field data whenever possible.

7.2 USER INSTRUCTIONS

HSCTM-2D requires several files to operate. Two of them, a geometry file describing the mesh and a boundary condition file, can be generated by using SMS. The other files are described in Section 8.4.

The model includes two options for data specification: a default option in which default values (included in the program) are used for specified parameters and a non-default option in which all data must be specified by the user. The default option is of benefit when, due to insufficient data, all the required sediment related parameters (e.g., erosion/deposition rate coefficients) are not available to the modeling system user. As emphasized in this document, the default option should be used for qualitative analysis only. It will allow the user to make relative comparisons among various sites or designs. In creating the required input data files, the user should follow closely the data input instructions for both HYDRO2D and CS2D given in Sections 8.3 and 8.4. Sample input data sets included in Section 9 will assist the user in establishing these data files. The data sets accompanying the modeling system should be used to assist in constructing new data sets.

As indicated in Section 7.3, the HSCTM-2D modeling system may be operated in two different modes: (1) an uncoupled mode, in which first HYDRO2D is run to generate the flow field, and then CS2D is run to stimulate the sediment/contaminant transport, and (2) a semi-coupled mode, in which both models are operated in a semi-coupled manner in order to account for the effect of, for example, extensive sedimentation or scouring on the flow field. The first example problem described in Section 9 was run in the semi-coupled non-default mode, while the second was run using the uncoupled mode.

SMS can be employed for post-processing after HSCTM-2D is used to perform the hydrodynamic and sediment/contaminant transport analysis. HSCTM-2D outputs several "solution files" containing nodal water surface elevations and flow velocities, nodal suspended sediment concentrations, nodal bed elevation changes, nodal particulate contaminant concentrations on the surficial bed sediments, and residual error at each node of the mesh. These

solution files can be input by SMS to generate vector plots, color-shaded contour plots, and time-history diagrams.

7.3 DATA INPUT FOR MAIN PROGRAM OF HSCTM-2D

The format for the data input is given in Section 8.

7.4 SYSTEM DATA OUTPUT

7.4.1 Hydrodynamic Module

Output from the module HYDRO2D consists of the following: program control parameters; eddy viscosity coefficient; nodal connections and area for each element; (x, y) coordinates, bottom elevation, network slope, flow and water surface elevation boundary conditions, and the initial water depth at each node; initial nodal flow velocities, depth and water surface elevations; and nodal flow velocities, depth and water surface elevation at subsequent time steps. The node and element data and the initial conditions are optional output. Control for output printing is specified by the parameter IPRT (see Section 8). Specified output data may be stored on a disk file for use in CS2D if the modeling system is run in the uncoupled mode or stored on a disk file for use in the velocity vector plotting routine in SMS. An example of typical output for the semi-coupled mode is included in Section 9.

7.4.2 Sediment Transport Module

Output from the sediment transport modules in HSCTM-2D consists of the following data: sediment depositional properties; properties of unconsolidated new deposits, partially consolidated new deposits and the original settled bed; and initial nodal flow velocities, depths, suspension concentrations, and sediment dispersivity coefficients. Additional information can be obtained at specified time steps and for specified elements. At specified time steps, the output consists of: the nodal suspension concentrations, elemental bed shear stresses, bottom elevations, erosion and deposition rates and properties (e.g., layer thickness, average shear strength, and bulk and dry density) of all bed sections present in each element. The data printed at specified time steps (i.e., when $IFF(I,2) > 0$; see Section 9) are chosen by the value of $IFF(I,2)$, where I is the time step number. Specified output data (e.g., nodal suspension concentrations, change in nodal bed elevations) are stored on disk files for use by the contour plotting routine in SMS. For specified

elements, the following information is printed out at each time step: average velocity, suspension (surface erosion) rate, the flux of sediment eroded or deposited, and the bed elevation change in that time step. An example of typical output is included in Section 9.

Also included in the output data set are the following parameters: (1) the average amount of time sediment particles are in suspension for the entire model simulation. This parameter, t_{ave} , was conservatively estimated as follows:

$$t_{ave} = \frac{\sum_{i=1}^{NEC} \left[\sum_{j=1}^{NOCR} (\Delta t_{E-D})_j \right]_i}{NEC \cdot NOCR} \quad (7.1)$$

where NEC is the number of elements in which at least one erosion-deposition cycle occurred, NOCR is the number of erosion-deposition cycles which occur in the i th element over the entire simulation period, and $(\Delta t_{E-D})_j$ is the j th time period from occurrence of either redispersion or resuspension to occurrence of deposition in the i th element. This is an Eulerian approximation since it includes both temporal and spatial averaging. (2) The net change in the bed surface elevation (in meters) in each element over the simulation period (e.g., over a given number of tidal cycles). As stated in Section 5, only the partially consolidated and settled bed sections are considered in determining the bed elevation. (3) The net vertical mass-flux of sediment, which has units of kilograms per second, in each element over a given time interval. This is calculated as (a) the average vertical (upward) flux of sediment due to erosion in a particular element minus (b) the average vertical (downward) flux of sediment due to deposition in a particular element; thus, the net vertical flux is positive for a net upward flux and negative for a net downward flux. (4) The net downward (i.e., depositional) mass flux of sediment, which has units of kilograms per second, in each element over a given time interval. (5) The average thickness of the unconsolidated bed section (i.e., stationary suspension) in each element over a given interval of time.

7.4.3 Contaminant Transport Module

Output from the contaminant transport module in HSCTM-2D consists of the following data for specified elements at specified time steps: nodal dissolved and particulate contaminant concentrations, and nodal particulate contaminant concentrations on surficial bed sediments. The data printed at specified time steps (i.e., when $IFF(I,2) > 0$; see Section 9) are chosen by the value

of $IFF(I,2)$, where I is the time step number. Specified output data are stored on a disk file for use by the contour plotting routine in SMS.

SECTION 8

DATA INPUT REQUIREMENTS

This section describes the input data required to operate the modeling system HSCTM-2D. Any user of the system should become familiar with the descriptions given in this section, the user instructions given in Sections 7-9 and the limitations given in Section 7.1 before using HSCTM-2D.

Input data are read from both formatted (ASCII) and unformatted (binary) disk files. Standard FORTRAN 77 rules should be used for entering data for both integers and floating-point variables. Output from SMS may be written to a disk file, where it can be read during use of the modeling system.

8.1 GRID GENERATION

The grid should be set up so that node to node depth changes are less than 20%. Mesh boundaries should approximate flow boundaries in areas of wetting and drying. A dense mesh should be used where internal velocity gradients are expected, around flow obstacles, and where the mesh boundary exhibits high curvature. The size change from one element to the next, however, should be less than 50%.

The user may wish to obtain the SMS software. The SMS software and related documents can be obtained from Brigham Young University, Engineering Computer Graphics Laboratory, 368B CB, Provo, Utah 84602.

Use of SMS will enable a relatively quick (within a few hours or days) generation of a finite element mesh of the region being modeled and apply boundary conditions even for a large,

complex mesh (several thousand elements) of arbitrary shape. Errors can be detected and corrected in a few minutes. The user can then save information describing the mesh in a geometry file and one or more boundary condition files. A grid generated by hand rather than with a program such as SMS will require significantly more time (months compared to days).

HSCTM-2D will output one or more solution files containing the water surface elevation, flow velocity, contaminant or sediment concentration, sediment deposition rate and residual error at each node of the mesh. These solution files can be input by SMS for post-processing to produce vector plots, color-shaded contour plots, and time-history diagrams.

8.2 DATA INPUT FOR MAIN PROGRAM OF HSCTM-2D

8.2.1 Input/Output Filenames

The HSCTM-2D program reads a file named HSCTM.FIL for the name of each input, output and scratch file used by HSCTM-2D. The HSCTM.FIL also contains a code to tell if the file is formatted or unformatted and the logical unit number for the file. A sample HSCTM.FIL file is included with the distribution copy of the HSCTM-2D program.

HSCTM.FIL

I/O unit 49 = file 'HSCTM.FIL', form = FORMATTED

Format	Variable	Value	Description
I5	NFILES		Number of files to be opened by HSCTM-2D

The following set repeats for each file to be opened.

A32	FNAM		Full file name
* - free format	ICOD	0	Formatted
		1	Unformatted
		2	Transparent (unformatted) - for used with Lahey FORTRAN compiler
	LZP	see chart below	I/O logical unit number

Unit numbers identified in the HSCTM-2D program are defined below.

Unit		Description of File
2	INHEC	Boundary condition file (for HYDRO2D) generated by SMS
3	IOUT	Output file - generated by HYDRO2D
5	IN5	Input file containing sediment data (for CS2D)
8	LP	Output file - generated by CS2D
9	ND1	Scratch file
10	ND2	Scratch file
13		Sediment flux calculations
14		Suspended sediment concentration boundary conditions
15		Salinity boundary conditions
51	INT2	Sediment suspension concentrations - for post-processing with SMS
52	INT3	Nodal salinities - for post-processing with SMS
59	ISPRT	Summary print by node option
60	IGEON	Finite element grid - generated by SMS
61	IBUP	Alternate boundary conditions
62	IHOTO	Hotstart output file
63	IHOTN	Hotstart input file
64	IFINO	Hydrodynamic solution - for post-processing with SMS
72	LPDR2	Nodal bed elevation changes - for post-processing with SMS
73	LPCBP	Nodal bed contaminant concentrations - for post-processing with SMS

Title cards

I/O unit IN5

7X, A73	TITLE1		
7X, A73	TITLE2		
7X, A73	TITLE3		
34X, I1	NCON	1	HYDRO2D only
		2	HSCTM-2D
44X, I1	IDEFAU	0	Input all data
		1	Use default values

8.3 HYDRODYNAMIC MODULE - DATA INPUT

The data input format for the hydrodynamic module uses the HEC-style format as described in Appendix C. Data input to the program HYDRO2D consists of program operation data, grid geometry data, and both initial and boundary conditions data.

8.4 SEDIMENT/CONTAMINANT TRANSPORT MODULE - DATA INPUT

Input data requirements for CS2D consist of program operation data, grid geometry data, nodal velocities and salinities, initial and boundary conditions, parameters describing the erosional and depositional behavior of the cohesive sediment as well as the structure of the bed, and contaminant partition coefficients and decay rates. Input data are separated into 15 data sets. Each is described below.

A sample input file is included on the disk(s) with the program. The easiest way to set up an input file is to COPY the sample file and then make changes to the sample file. See the README file on the disk for the name of the sample sediment input file. The tables below give the format for variables that can be changed in the input. The program is set up to read an input file that includes title lines as in the sample file. If you set up a new input file and do not use the sample file as a template, be sure to maintain the same pattern.

8.4.1 Data Set A: Job Control Cards

Set A contains job control cards that specify input/output file numbers used in both reading and printing the different data sets, job title, problem options, output control, and parameters that specify how the initial nodal values of velocities, bottom elevations, dispersion coefficients, bed

profile, settling velocities, depths, suspended sediment concentrations and boundary conditions are determined. That is, initial values are either read from a formatted or unformatted data file, set equal to constants read in later data sets, or computed using user supplied routines. The problem option parameter specifies which one of three problem types is to be solved. The three types of problems that can be solved by CS2D are (1) steady state advection-dispersion of a conservative constituent, (2) unsteady advection-dispersion of a conservative constituent, (3) cohesive sediment transport.

Card A.1 I/O file numbers and equation solver used. Default value for input logical unit IN* is IN5 = 5. Default output logical unit is LP = 8. If the input logical unit is set equal to zero, the default value is used. This data set is read in Subroutine CS2D.

Format	Variable	Value	Description
7X,I3,12X,I3,12X,I3	INC		Logical unit for initial concentrations
	IND		Logical unit for diffusion coefficients
	INF		Logical unit for node point flow velocities
7X,I3,12X,I3,12X,I3	ING		Logical unit for settling velocities
	INSS		Logical unit for new nodal salinities
	INI		Logical unit for finite element grid
7X,I3,12X,I3,12X,I3	INB		Logical unit for boundary conditions
	INS		Logical unit for salinities
	NGC		Number of GC strings for specifying boundary conditions (number of places in the physical system where input and output occur)
5X,I5,9X,I6	NE		Number of elements in system
	NP		Number of nodes in system

Card A.2 Stop Control and Job Title.

34X, I1	NSTOP	0	Continue
		1	End of job

7X, A73	TITLE4	Title of HSCTM-2D job
---------	--------	-----------------------

8.4.2 Data Set B: Job Control Parameters

Card B.1 Job control parameters, input codes, and problem options.

7X, I3, 12X, I3, 11X, I4, 12X, I3	NOPT	Type of Problem	
		1	Steady state transport problem
		2	Unsteady transport problem
		* 3	Sediment transport problem
	ICODE	Output for non-sediment problems	
		* 0	Standard output
		1	Compares with analytic solution calculated in Subroutine EXACT
	NCYC		Number of time steps (Default=50)
	IVEL	Determines initial velocity field, i.e., at time step #1 (for unsteady problems only)	
		1	Velocity components in x and y directions are set equal to constants CONXY and CONYV read in Subroutine VELL
		2	Each nodal velocity read in from input file INF
		3	Velocity computed using user supplied routine in Subroutine VELL
		* 4	Velocities are calculated using the HYDRO2 hydrodynamic module
5		each nodal velocity component read in from unformatted input file INF	
7X, I3, 3(12X, I3)	ISOUR	Code to indicate if local sediment source or sink is located at any node.	
		* 0	no source/sink
		1	source/sink occurs at one or more nodes
	IDIF1	Initial diffusion coefficient values at each node	
		1	D_x and D_y are set equal to constants read in Subroutine DISPER
		2	Nodal diffusion coefficients are read in from file number IND
		* 3	Diffusion coefficients are calculated using user supplied procedure [NOTE: the procedure in the program is specific to the example problem]

	IBED	Initial bed profile		
		0	No sediment present on bed	
		* 1	Bed profile read in Subroutine ORGBED	
	ISET	Initial settling velocity at each node.		
		1	Set to a constant read in Subroutine SETVEL.	
		2	Each nodal settling velocity is read in from formatted file number ING.	
		* 3	Settling velocities are computed using settling velocity model in Subroutine SETVEL	
	7X, I3, 3(12X, I3)	ICONC	Initial suspended sediment concentrations.	
			* 1	Set to constant
			2	Read in from file number INC
3			Computed according to user supplied procedure in subroutine CONCIC	
INBC		Boundary conditions		
		* 1	Each value read in from formatted file number INB	
		2	Computed in Subroutine CONCBC using user supplied routine	
		3	Each value read in from unformatted file number INB. Boundary node array MFIX and Boundary condition array SPEC are both read in.	
IDRY		Code to indicate dry node (i.e., negative flow depth) problem.		
		* 0	No dry nodes will occur	
		1	Possible dry nodes	
ISZ		Temporal flow classification		
		* 0	Unsteady flow	
		1	Steady state flow	

8.4.3 Data Set C: Transient Problem Input

Transient control parameters are specified in Set C. Input data include time step size, degree of implicitness for the Crank-Nicolson type time-marching scheme used in CS2D, and transient code arrays that specify at which time steps during a dynamic simulation new values of one or more of the parameters listed under Data Set B are read in or calculated. One of the code arrays also specifies the type of output (e.g., nodal concentrations and/or discretized bed profiles), if any, desired at each time step.

Card C.1 Transient input

30X, F10.4	TETA	Degree of implicitness for Crank-Nicolson time marching scheme. (Default = 0.6667)	
		0	explicit
		1	implicit
16X, F9.1	DELT		Time step - [hour] (should be of the order 0.083 - 0.5 hr for sediment transport problems in estuaries)
16X, F9.2	TIM(1)		Start time - [hr]. (Default = 0.0)
I4	IOSTEP		Frequency of full output
I4	NSTIME		Time step number at which to start program

Card C.2 Information for FLUX Routine

I1, I10	IFLX	Flux routine switch	
		0	sedflux off
		1	sedflux on
	IFLXNP		Number of nodes in the FLUX string
5I10	IFLXNN		Node numbers of nodes in the flux string. If using SMS, the node numbers can be identified with that program. If there are less than 17 node nos., you need to know how the compiler handles this READ statement; e.g., when there are 5 nodes, the SALFORD compiler requires 1 line of input and 1 blank line.
5I10	IFLXNN		
5I10	IFLXNN		
2I10	IFLXNN		

Card C.3 Output control

43X, I7	NELE		number of elements for which time history will be written
20X, 5I5	NELH(J)		element numbers

8.4.4 Data Set D: Water and Sediment Properties

Set D specifies water temperature and nodal salinity values, properties of the cohesive sediment being modeled, and local sediment source/sink terms. Sediment properties include parameters specifying settling velocity and rate of deposition as functions of suspension concentration, salinity and equivalent sediment diameter, properties of both unconsolidated and partially consolidated beds (e.g., discretized bed density and shear strength profiles),

Card D.1 Water parameters. Read in Subroutine DENSTY

11X, F9.3	TEMPC		average water temperature [$^{\circ}$ C]
49X, I1	IS		determines how initial salinities are read in
		* 0	constant salinity for all nodes
		1	salinity for each node is read in

Card D.2 Constant salinity if IS = 0. Read in Subroutine DENSTY.

30X, F10.5	SW		value of constant salinity - [ppt]
------------	----	--	------------------------------------

Card D.3 If ISOUR.NE.O, read source/sink term at appropriate nodes. Reading stops for IT(J) < 0.

4(I10, F10.5)	IT(J)		node number
	TEMP(J)		local source/sink term - [kg/m ³]

Cards D.4 through D.16 are read in Subroutine SEDPRP.

Card D.4 Settling velocity parameters. If there is only one $W_s = KC^n$ relationship between $C = \text{CRCN1}$ and the concentration at which hindered settling begins, set $\text{CRCN3} = \text{CRCN2}$.

10X, F10.3	$\text{CRCN1} = C_1$		see equations for W_s below - $[\text{kg}/\text{m}^3]$. (Default = $0.30 \text{ kg}/\text{m}^3$)
10X, F10.3	$\text{CRCN2} = C_2$		see equations for W_s below - $[\text{kg}/\text{m}^3]$. (Default = $5.0 \text{ kg}/\text{m}^3$)
10X, F10.3	$\text{CRCN3} = C_3$		see equation for W_s below - $[\text{kg}/\text{m}^3]$. (Default = $5.0 \text{ kg}/\text{m}^3$)
40X, F10.5	GAC		density of sediment mineral - $[\text{kg}/\text{m}^3]$. (Default = $2650 \text{ kg}/\text{m}^3$)

Card D.5

10X, F10.4	$AA = A_1$		(Equation 8.1, 8.2)
10X, F10.4	$AB = A_2$		(Equation 8.3)
10X, F10.4	$AC = A_3$		(Equation 8.4)
10X, F10.4	B		(Equation 8.5)
10X, F10.4	FZ		(Equation 8.5)
10X, F10.4	AL		(Equation 8.4)

Card D.6

10X, F10.5	$WS1 = W_{s1}$		(Equation 8.1) - $[\text{m}/\text{s}]$
25X, F10.5	D		equivalent sediment particle diameter at t_{50} - $[\text{m}]$

Card D.7

10X, F10.5	$\text{EXPN1} = n_1$		m (Equation 8.2)
10X, F10.5	$\text{EXPN2} = n_2$		(Equation 8.3)

Card D.8

3(10X, F10.5)	EXPM1=m ₁		(Equation 8.1, 8.2)
	EXPM2=m ₂		(Equation 8.3)
	EXPM3=m ₃		(Equation 8.4)

Card D.9

10X, E10.5	WSK1=K ₁		(Equation 8.2) - [m/s]
10X, E10.5	WKS2=K ₂		(Equation 8.3) - [m/s]

For Range I and C < C₁ in Range II (SALIN = salinity):

$$W_s = AA * WS1 * SALIN^{**}EXPM1 \quad (8.1)$$

For CRCN1 < C < CRCN2:

$$W_s = AA * WSK1 * CNC(I,1)^{**}EXPN1 * SALIN^{**}EXPM1 \quad (8.2)$$

For CRCN2 < C < CRCN3:

$$W_s = AB * WSK2 * CNC(I,1)^{**}EXPN2 * SALIN^{**}EXPM2 \quad (8.3)$$

For C > CRCN3:

$$W_s = (WSK2 * CRCN2^{**}EXPN2 * SALIN^{**}EXPM2 * AB) * (1.0 - AY * CNC(I,1))^{**}5 / (1.0 - AY * CRCN3)^{**}5 \quad (8.4)$$

For C > C₁ in Range II:

$$T = A \log_{10}((T/T_{50}) * B * (SALIN^{**}F)^{**}(1.0 / SIG2)) \quad (8.5)$$

Card D.10 Properties of new deposits.

55X, I5	NLAYTM		number of layers formed by unconsolidated new deposits (UND) (default = 1)
55X, I5	NLAYT		number of layers formed by partially consolidated new deposits (PCND) (default = 5)
25X, F10.5	TAUBMN		τ_{bmin} - [N/m ²] (default = 0.10 N/m ²)
25X, F10.5	TAUMAX		τ_{bmax} - [N/m ²] (default = 1.0 N/m ²)

Parameters characterizing functional relationship τ_b^* and $\log_{10}(t_{50})$ and σ_2 at a salinity of 35 ppt:

Card D.11

5X, F10.2	A1		see equations for σ_2 below
5X, F10.2	S1		see equations for σ_2 below
5X, F10.2	A2		see equations for σ_2 below
5X, F10.2	S2		see equations for σ_2 below
5X, F10.5	C1		see equations for σ_2 below

Card D.12

5X, F10.2	A3		see equations for t_{50} below
5X, F10.2	S3		see equations for t_{50} below
5X, F10.2	A4		see equations for t_{50} below
5X, F10.2	S4		see equations for t_{50} below
5X, F10.5	C2		see equations for t_{50} below

NOTE: For

$$\tau_b^* < C1 : \quad \sigma_2 = S1 * \tau_b^* + A1 \quad (8.6)$$

$$\tau_b^* > C1 : \quad \sigma_2 = S2 * \tau_b^* + A2 \quad (8.7)$$

For

$$\tau_b^* > C2 : \quad t_{50} = 60 * 10^{(S4 * \tau_b^* + A4)} \quad (8.8)$$

$$\tau_b^* < C2 : \quad t_{50} = 60 * 10^{(S3 * \tau_b^* + A3)} \quad (8.9)$$

NOTE: The properties read in on Cards D.13-D.16 are determined from laboratory experiments (see Appendix B). These are the properties assigned to new deposits if/when deposition occurs during model simulation or initially if new deposits are present on top of the original settled bed, as specified in SET K.

Card D.13 et seq. Shear strength and dry sediment density unconsolidated new deposit layers. NLAYTM+1 pairs of values are read in starting at the bed surface and

proceeding down to the bottom of the bottom UND section. See Table for default values.

20X, F10.5, 30X, F10.5	SSM(I)		Bed shear strengths - [N/m ²].
	GADM(I)		Dry sediment densities - [kg/m ³].

Card D.14 et seq. Read for each NLAYTM

50X, 2F10.5	TLAYM(I)		Thickness of unconsolidated new deposit layers - [m]. (Default = 0.05)
-------------	----------	--	---

Card D.15 et seq. Shear strength and dry sediment density for partially consolidated new deposit layers. NLAYT+1 pairs of values are read starting at the top of these layers and proceeding downward. See Table for default values.

20X, F01.5, 30X, F10.5	SS(I)		Bed shear strengths - [N/m ²].
	GAD(I)		Dry sediment densities - [kg/m ³].

Card D.16 et seq. Thickness, ϵ_0 and α values for each partially consolidated layer. NLAYT pairs of values are read.

16X, F9.5, 15X, F10.5, 12X, F9.5	TLAY(I)		Layer thicknesses - [m]. (Default = 0.05 m)
	EPSILON(I)		ϵ - [kg/m ² /s]. (Default = 5×10^{-5} Kg/m ² /s)
	AFLA(I)		α - dimensionless. (Default = 2.0)

8.4.5 Data Set E: Initial Concentration Field

The initial concentration at each node must be specified for all unsteady problems. Data set E is read in Subroutine CONCIC. THE TYPE OF INPUT IS DETERMINED BY THE VALUE OF ICONC.

For ICONC = 1:

Card E.1 Initial concentration set at a constant at all nodes.

25X, F10.5	CINT		Initial concentration - [kg/m ³]. (Default = 0.10 kg/m ³)
------------	------	--	---

For ICONC = 2:

Card E.1 et.seq. Read in initial concentration for each node. Read from formatted file INC.
Reading stops for IT(J) < 0.

4(I10, F10.5)	IT(J)		Node number.
	TEMP(J)		Initial concentration - [kg/m ³].

For ICONC = 3: Compute initial concentrations at each node using user supplied model in Subroutine CONCIC.

8.4.6 Data Set F: Original Settled Bed Profile

This data set is only read if NOPT = 3 and if IBED is not zero. Otherwise the default bed condition will be a clean bed.

In Set F the original settled bed profile in every element (where a settled bed is present) is read in. The input parameters include the number of layers the settled bed profile is divided into, average pore water density, the thickness and erosion rate constant for each bed layer, and the discretized bed density and shear strength profiles. Also specified is the dry mass per unit surface area of soft new deposits found on top of the original settled bed for those elements where such exists. Data Set F is read in Subroutine ORGBED.

Card F.1

3I5, F10.5	NN		Element number. (Default = 1)
	NLA		Number of layers of original settled bed for element NN. (Default = 5).
	NM		If NM = 0, bed properties are read in for each element. IF NM ≠ 0, constant values are read in and used for all elements. (Default = 1)
	GWA		Average density of pore water in original bed - [kg/m ³]. (Default = 1000 kg/m ³)

Card F.2 et. seq. Shear strength and dry sediment density for original settled bed layers. NLA+1 pairs of values are read in starting at the top layer and proceeding downward. The first values are for the top of the original bed. See text for default values.

2F10.5	SSTO (NN,I)		Bed shear strengths - [N/m ²].
	GADO (NN,I)		Dry sediment densities - [kg/m ³].

Card F.3 et.seq. Thickness and value of M for all NLA settled bed layers. NLA pairs of values are read in.

2E10.3	THICKO(NN,I)		Thickness of Ith layer - [m]. (Default = 0.05 m)
	EROCON(NN,I)		M value for Ith layer - [kg/m ² /s]. (Default = kg/m ² /s)

Note: When NM ≠ 0, these cards are read in only once.

When NM = 0, repeat the set of cards [Card F.1, Card F.2 et.seq., Card F.3 et.seq.] for each element where a settled bed is present. End with Card F.1 where NN is less than 0 (but not = -10).

If a stationary suspension is present on top of the original settled bed, set NN=-10 at the end of the above set (i.e., after all Cards F.1, F.2 and F.3). For NN=-10, read the following cards. If IT(I) in Card F.4 is set equal to 5000, card F.4 is read only once, with specified dry sediment mass added to each element.

Card F.4 et.seq. Reading stops when IT(I) < 0.

I10, F10.5	IT(I)		Element number. (Default = 5000)
	TEMP(I)		Dry mass per unit area of soft unconsolidated sediment on top of settled bed - [kg/m ²]. (Default = 1.0 kg/m ²)

8.4.7 Data Set G: Initial Velocity Field

This data set is read in Subroutine VELL and is used only for unsteady problems. The value of IVEL determines the type of input.

The initial velocity field, defined by the two horizontal components of the depth-average flow velocity at each node, is specified in Set G. The x and y flow velocities may be set equal to constants, read from either a formatted or unformatted file, or HYDRO2D may be called to calculate the initial velocity field and depths of flow.

Card G.1 Velocities are set to constant values. Read if IVEL = 1. Read from file unit INF.

2(F10.5)	CONXV		Velocity component in the x-direction - [m/s].
	CONYV		Velocity component in the y-direction - [m/s].

Card G.1 Each nodal velocity component read in from formatted input file INF. Must be read in order for all NP nodes. Read if IVEL = 2. Read from file unit INF.

5X, 3E15.4	VEL(1,J)		Velocity component at node J in the x-direction - [m/s].
	VEL(2,J)		Velocity component at node J in the y-direction - [m/s].
	VEL(3,J)		Velocity component at node J in the z-direction - [m/s].

IVEL = 3 User supplied procedure in Subroutine VELL is used to calculate nodal velocities.

IVEL = 4 * HYDRO2D flow module is used to calculate nodal velocities.

IVEL = 5 Each nodal velocity component read in from unformatted input file INF.

	XVEL		
--	------	--	--

8.4.8 Data Set H: Initial Dispersion Coefficients

Data Set H is used with Subroutine DISPER to read in the initial dispersion coefficients or calculate those coefficients using the dispersion algorithm described in Section 5 of this manual. The value of IDIF determines the type of input. IDIF is either IDIF1 or IDIF(N) depending on the point in the program where Subroutine DISPER is called.

Card H.1 Dispersion coefficients are set to constant values. Read only if IDIF = 1.

2(F10.5)	CDIFL		Longitudinal dispersion coefficient - [m ² /s].
	CDIFT		Transverse dispersion coefficient - [m ² /s].

Card H.2 et.seq. Dispersion coefficients are read in node by node. Read if only IDIF = 2.
Reading stops for IT(J) < 0.

3(I5,2F10.5)	IT(J)		Node number.
	TEMP(1,J)		Longitudinal dispersion coefficient - [m ² /s].
	TEMP(2,J)		Transverse dispersion coefficient - [m ² /s].

IDIF = 3 * Dispersion coefficients D_{xx} , D_{xy} and D_{yy} are computed analytically using the dispersion algorithm described in Section 5.

8.4.9 Data Set I: Initial Settling Velocities

Data Set I is used with Subroutine SETVEL to read in the initial settling velocities or calculate them using the settling velocity model described in Section 5 of this manual.

The value of ISET determines the type of input. ISET is either ISET or ISVS(I) depending on the point in the program where Subroutine SETVEL is called.

For ISET = 1:

Card I.1 All settling velocities are set to constant. Read from file unit ING.

F10.5	CVSX		Settling velocity - [m/s].
-------	------	--	----------------------------

For ISET = 2:

Card I.2 et.seq. Settling velocity at each node is read in. Read from file unit ING. Stops reading if IT(J) < 0.

4(I10, F10.5)	IT(J)		Node number.
	TEMP(J)		Settling velocity - [m/s].

For ISET = 3: * Settling velocity model, for which parameters were read in SET D, is used to compute each nodal settling velocity.

8.4.10 Data Set J: Boundary Conditions

Concentration boundary conditions are specified in Set J. Depth-averaged suspended sediment concentrations are normally specified at all external water boundaries of the system being modeled. For any external node at which no concentration boundary condition is given, the normal diffusive flux is automatically set equal to zero. At least one node must have concentration boundary conditions specified. Data Set J is read in Subroutine CONCBC.

The value of INBC determines the type of input. INBC is also set equal to IFF(I,1) at one point in the program.

For INBC = 1:

Card J.1 et.seq. Node number and specified boundary condition. Read from file unit INB.

3(I10, F10.5)	IT(J)		Node number
	TEMP(J)		Specified concentration - [kg/m ³].

For INBC = 2: * Concentration computed according to user supplied procedure in Subroutine CONCBC.

For INBC = 3:

Card J.2 et.seq. Specified boundary conditions. Must be read in order for all NP nodes. Read from unformatted file INB.

	MFIX(J)		Equal to 1 for boundary node; 0 for all other nodes.
	SPEC(J,1)		Specified concentration at node J - [kg/m ³].

8.4.11 Data Set K: New Salinities

In Set K nodal salinity values are read in from either a formatted or unformatted file, or a constant salinity may be assigned to all nodes. The type of input is determined by the value of ISALC(J), for J=2,.....,NTTS. The logical unit for the input is INSS.

For ISALC(J) = 1:

Card K.1 Assign constant salinity value to each node.

30X, F10.5	SW		Constant salinity value - [ppt].
------------	----	--	----------------------------------

For ISALC(J) = 2:

Card K.2 New salinities for all nodes. Reading stops when IT(J) < 0.

3(I10, F10.5)	IT(J)		Node number.
	TEMP(J)		Salinity at jth node.

8.4.12 Data Set L: Dynamic Input

Dynamic input is specified in Set L that contains the required data to update the following parameters at the time steps specified in Set C: salinities, concentration boundary conditions, depths of flow, velocities, dispersion coefficients and settling velocities. If the code array value for a particular parameter at a given time step is zero, no input is required. If parameter update is required, the current value of the code array will determine the type of input.

The same subroutines that read initial values are used to read changes in these values during a dynamic run. The input code arrays in SET C tell the program if any new values should be read in at each time step. Note that the starting time is time step 1. The order of reading each set of data is given below.

DESCRIPTION	CODE ARRAY	INPUT CARD SET	SUBROUTINE
Salinities	ISALC(J)	SET K	
Concentration B.C.	IFF(J,1)	SET J	CONCBC
Velocities	IVOD(J)	SET F	CS2D
Dispersion Coefficients	IDIF(J)	SET E	CONCIC
Settling Velocities	ISVS(J)	SET J	DISPER

8.5 DATA MANAGEMENT

The large amount of data required to operate the CS2D modeling system in either the default or non-default mode necessitates careful preparation of the input data sets. The information contained in this section should be closely followed during the process. The flow chart of the main components of HSCTM-2D (in Appendix A) should be referred to in particular to assist the user in structuring the data sets for the various program options, whereas the flow charts and data input instructions for HYDRO2D and CS2D should be used to enter the correct data in the specified order and format. The data sets for the example problem described in Section 9 provide examples of proper data set organization. There exists (at present) no built-in or programmed assistance for inputting the required data at. The development of routines to make this operation "user friendly" is planned for future versions of the modeling system.

8.6 DEFAULT OPTION

The parameters for which default values are used when the default option is invoked (IDEFAU = 1) are indicated by asterisks in the listing in this chapter. Values of the default parameters are listed in Table 8.1. It is once again emphasized that the results obtained using the default option should be considered indicative of qualitative trends only, and used only for relative comparisons among different sites and/or designs.

Table 8.1
Default Values Used for Listed Parameters when Using Default Option

Parameter	Value	Parameter	Value
NOPT	4	AA	0.37
ICODE	0	AB	0.57
IVEL	4	AC	0.57
IELEV	0	B	0.47
IDIF1	3	FZ	-0.33
IBED	1	AL	-0.60
ISSET	3	WS1	0.00057
IDEP	0	D	0.000005
ICONC	1	EXP1	1.33
INBC	1	EXP2	1.33
IDRY	0	EXPM1	0.001
ISS	0	EXPM2	0.001
ISOUR	0	EXPM3	0.001
IS	0	ESK1	0.000001
ND1	9	WKS2	2.529-08
ND2	10	NLAYTM	5
NITI	4	NLAYT	5
NITN	3	TAUBMN	0.10
MBANA	0	TAUMAX	1.0
NSTART	1	A1	1.1
NCYC	50	S1	0.0
LI	0	A2	0.90
ITSI	3	S2	0.0
INC	5	C1	1.0
IND	5	A3	2.50
INE	5	S3	-0.04
INF	5	A4	2.20
ING	5	S4	-0.08
INH	5	C2	1.0
INI	5	SSM(I)	(.001, .005, .01, .03, .07, 10)
INB	5	GADM(I)	(5.,10.,15.,25.,35.,50.)
INS	5	TLAYM(I)	0.05
INSS	5	SS(I)	(.10.,.15.,.20.,.30.,.50)
ELVV	0.0	GAD(I)	(50.,60.,75.,90.,110.,125.)

Parameter	Value	Parameter	Value
XSCALE	1.0	TLAY(I)	0.05
YSCALE	1.0	EPSLON(I)	5.0E-05
DSET	0.0	AFLA(I)	5.0
DSETD	0.0	ORT(I)	50000.
TETA	0.6667	CRCN3	5.0
CRCN1	0.30	GAC	2650.0

SECTION 9

EXAMPLE PROBLEM

The utility of the HSCTM-2D modeling system is demonstrated by simulating the tidal flow and sediment transport in Winyah Bay, South Carolina. The portion of Winyah Bay modeled is shown in Figure 9.1. It must be emphasized that only a limited field study was conducted at this site, and therefore the results presented herein should be considered as demonstrative in nature only. A second example problem that demonstrates the contaminant transport capabilities of HSCTM-2D will be included in the second edition of this user manual.

Data used in modeling the flow and cohesive sediment transport, some of which were obtained during a limited two-day field study, included estuary geometry and bathymetry from NOAA navigation maps for Winyah Bay, and bathymetry of the Belle Isle marina from a post-dredge survey. Tides at the boundaries of the model grid were obtained using the TIDE1 Rise & Fall (TM) Software. The predicted tides were used for boundary conditions in the hydrodynamic module. A median sediment diameter of 50 μm , settling velocity of 10^{-5} m/s, and an average initial background suspension concentration of 10 mg/l were used. Spatially nonuniform, sinusoidally varying suspended sediment concentrations were used for the upstream and downstream open water boundary conditions for the sediment transport module. The slack tide (minima) concentrations at both boundaries were taken to be 10 mg/l, while maximum flood concentrations of 65 mg/l and 45 mg/l occurred at the upstream and downstream boundaries, respectively, and maximum ebb concentrations of 60 mg/l and 40 mg/l occurred at the upstream and downstream boundaries, respectively. These concentrations were representative of the suspension concentrations determined from water samples collected over two tidal cycles during the two-day field study. The finite element grid used to represent the portion

of Winyah Bay modeled in this study (see Figure 9.1) is shown in Figure 9.2. 918 elements and 2400 nodes were used in this grid.

The HSCTM-2D modeling system (in semi-coupled mode) was run for five days. Most of the output data are self explanatory. The new boundary conditions and the nodal velocities, flow depths and water surface elevations are printed at specified time steps. In addition, the nodal suspension concentrations, certain elemental averaged parameters (e.g., bed shear, bed elevation change, redispersion, resuspension and deposition rates), and the properties of the sediment bed in each element are printed at specified time steps. These bed properties include the numbers of layers of unconsolidated, partially consolidated, and settled bed sections which exist in each element, and the thickness, average shear strength, average bulk density, and average dry density of each layer.

Plots of the predicted velocity field during peak ebb flow are shown in Figures 9.3 and 9.4. These plots as well as Figures 9.2 and 9.5 were generated using SMS. Figure 9.3 shows scaled velocity vectors (1 cm = 2.0 m/s), whereas Figure 9.4 shows default length velocity vectors in proximity to the Belle Isle Marina. The latter plot shows the tide-induced circulation inside the marina. A plot of the predicted sedimentation contours at the end of the five day simulation is shown in Figure 9.5. Extrapolation of the predicted sedimentation inside the marina yields an annual average of 50 cm.

The following input data files are downloadable from the CEAM home page (as discussed in Section 2) along with the program files (hsctm.for and hsctm.h):

File Name	File Format	File Description
winyah.fil	ASCII	Contains list of input and output files (and associated unit numbers and file formats) for the Winyah Bay example problem.
winyah.inp	ASCII	Contains data sets described in Section 8.4.
winyah2.bin	binary	Contains finite element mesh (see Figure 9.2). The mesh was generated by the program GFGEN.
win-h.bc	ASCII	Contains input data for HYDRO2D described in Appendix C.
winyah.sbc	ASCII	Contains suspended sediment concentration boundary conditions.
winyah.sal	ASCII	Contains salinity boundary conditions.

winyah.hsi	binary	Contains hot start file for Winyah Bay example generated by running HYDRO2D for 72 hours.
------------	--------	---

The following table lists the output files generated by HSCTM-2D from the 5-day simulation of tide-induced flow and sediment transport in Winyah Bay.

File Name	File Format	File Description
winyah.out	ASCII	Contains output data from HYDRO2D.
wsed.out	ASCII	Contains output data from CS2D.
winyah.sol	binary	Contains hydrodynamic data that can be viewed using SMS (e.g., velocity vectors [see Figures 9.3 and 9.4], contour plots of velocities and water surface elevations).
sedconc.sol	binary	Contains suspended sediment concentrations at specified time steps. Use SMS to view contour plots.
salinity.sol	binary	Contains salinities at specified time steps. Use SMS to view contour plots.
deltabed.sol	binary	Contains bed elevation changes due to deposition and/or erosion. Use SMS to view contour plot. Figure 9.5 shows such a contour plot at the end of the 5-day simulation.
winyah.hso	binary	Contains hot start data output by HYDRO2D at end of simulation.

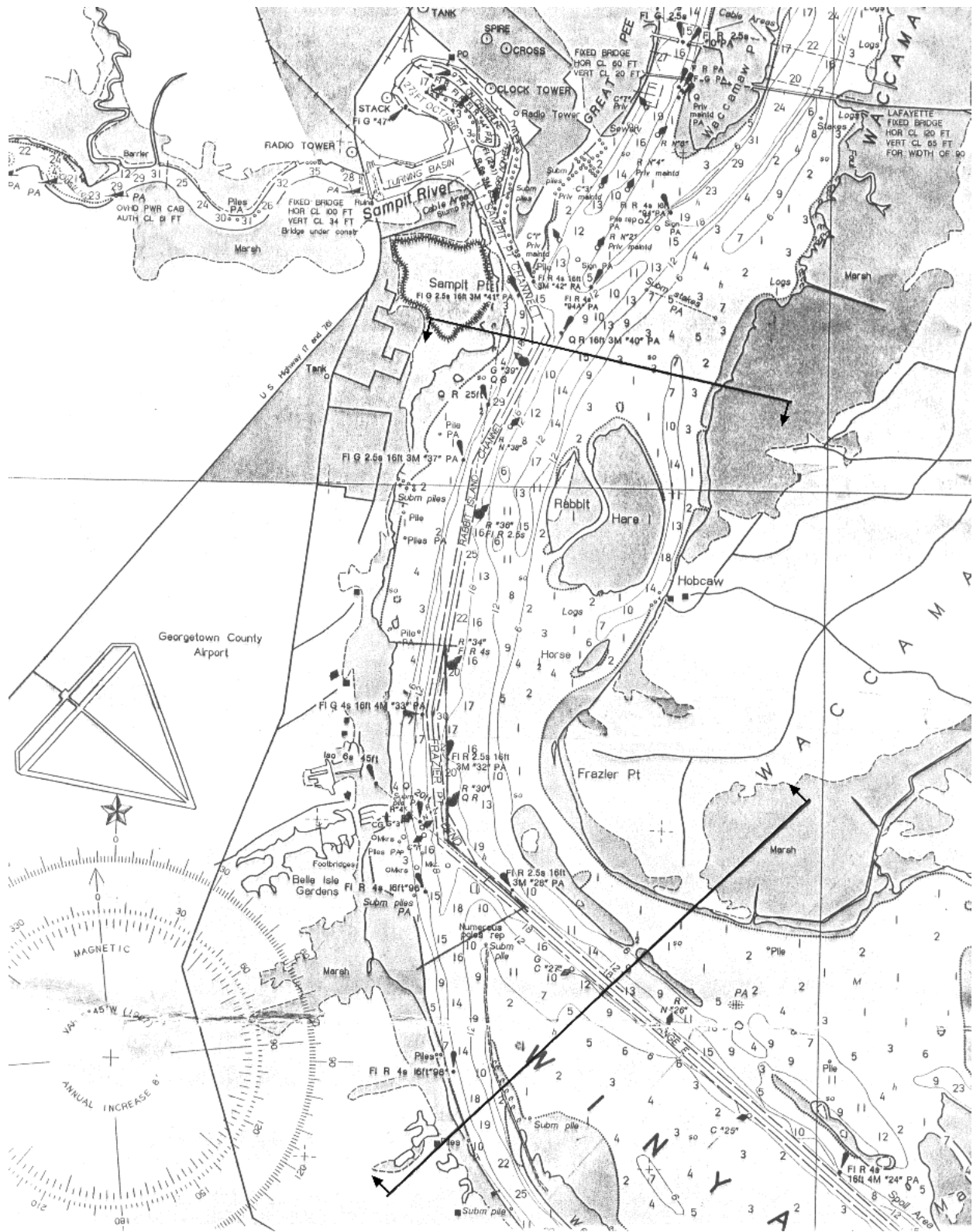


Figure 9.1 Reach of Winyah Bay, South Carolina modeled.

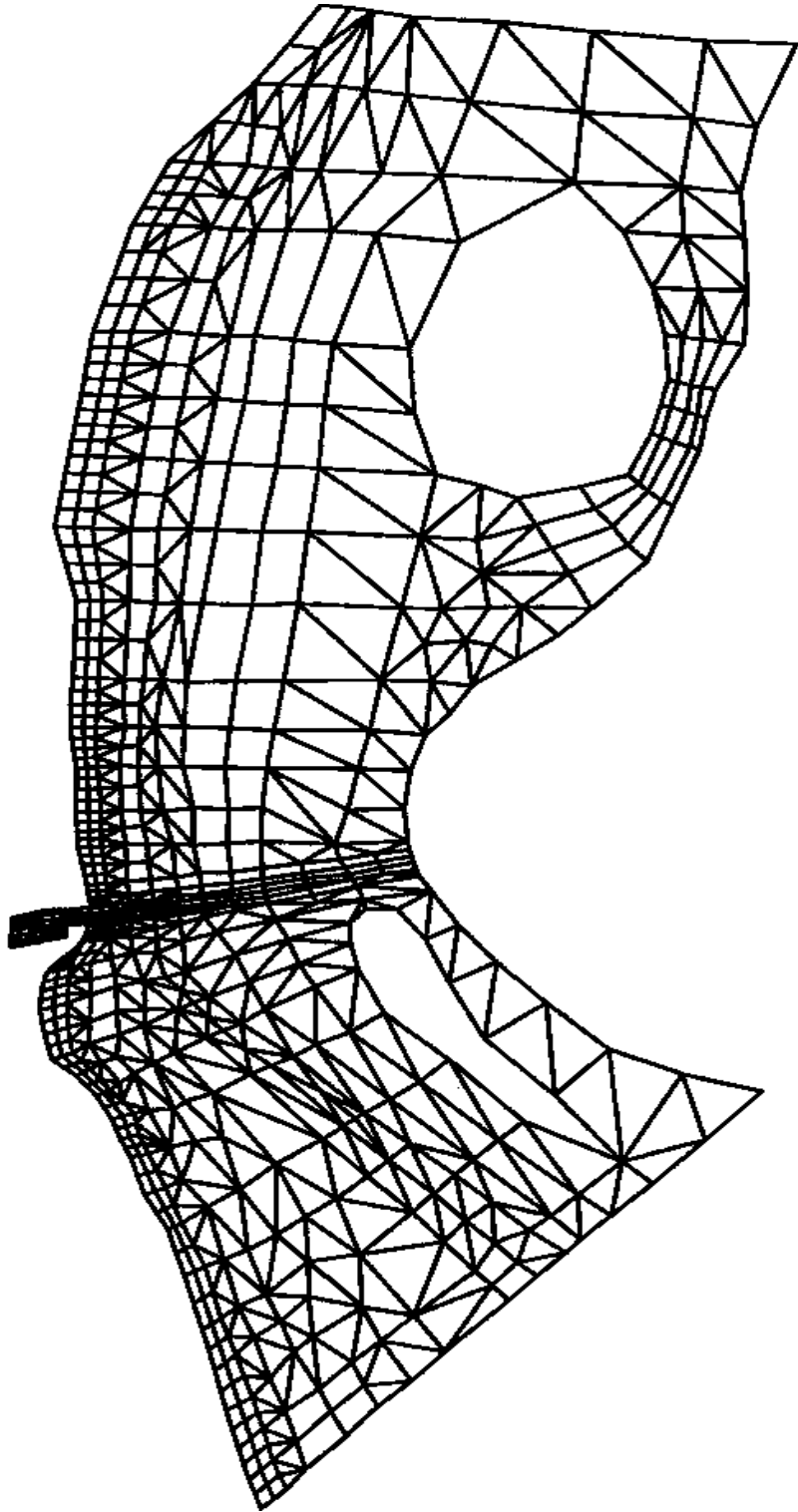


Figure 9.2 Finite Element Grid used in the HSCTM-2D Modeling

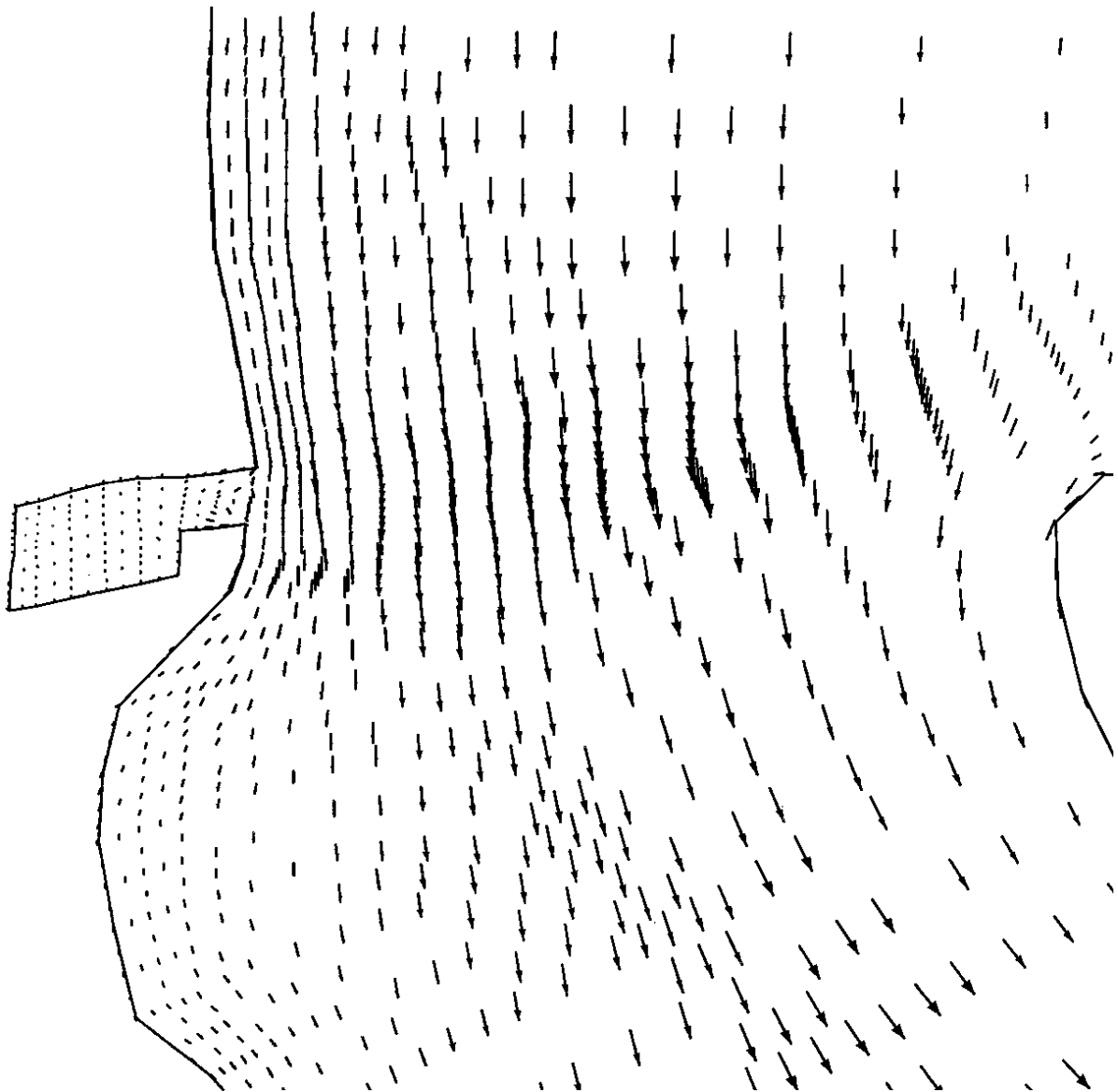


Figure 9.3 Velocity Vectors During Simulated Ebb Tide.

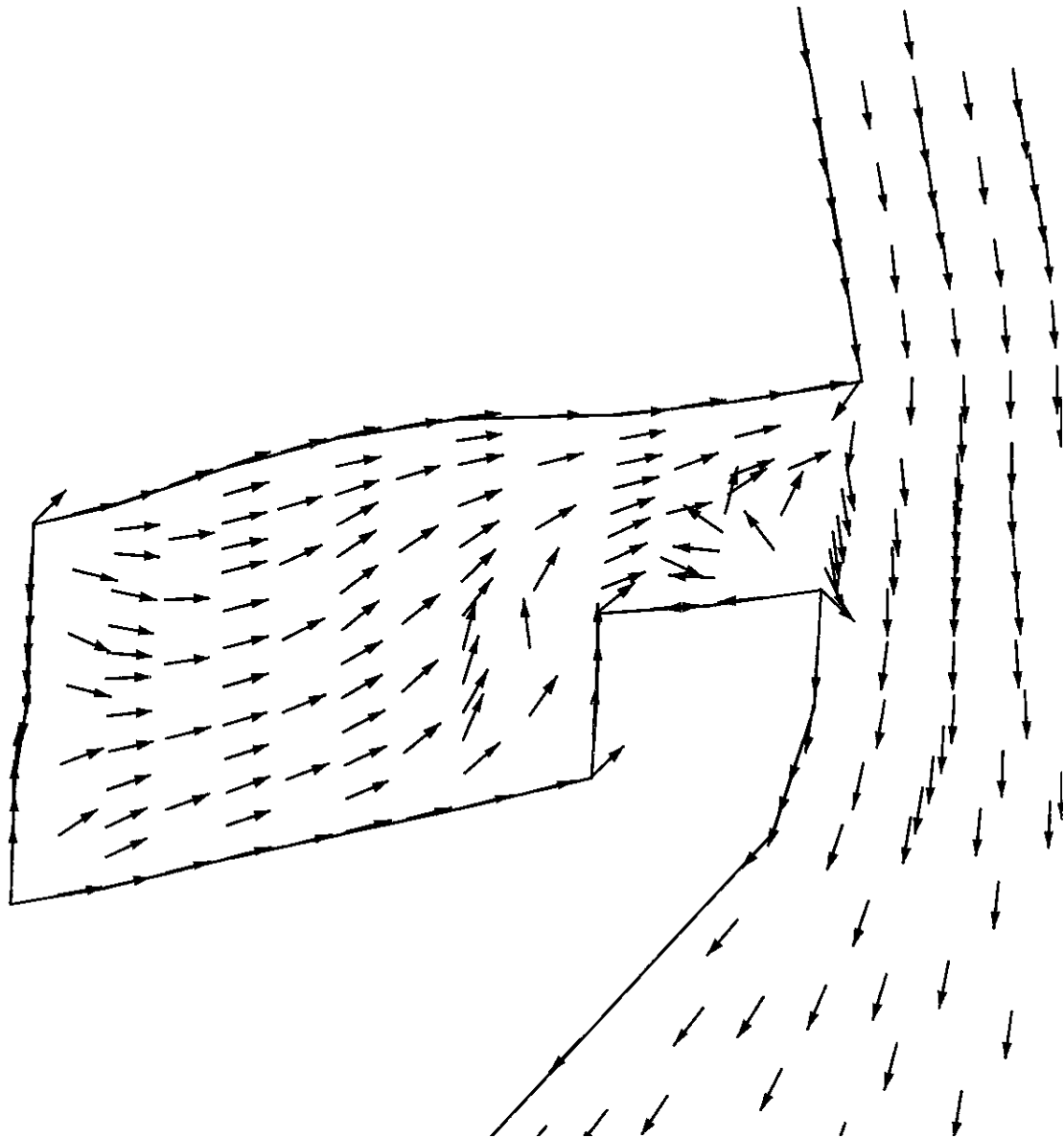


Figure 9.4 Constant Length (indicate flow direction only) Velocity Vectors in the Marina During Ebb Tide



Figure 9.5 Sedimentation Contours (mm) after 5 day Simulation

REFERENCES

Allersma, E., "Mud in Estuaries and Along Coasts," International Symposium on River Sedimentation, Beijing, P. R. of China, March, 1980.

Allison, L.E., Organic Carbon, Part II, American Society of Agronomy, Madison, Wisconsin, 1965.

Ariathurai, R., A Finite Element Model for Sediment Transport in Estuaries, Ph.d. Dissertation, University of California, Davis, California, 1974.

Ariathurai, R., and R.B. Krone, "Finite Element Model for Cohesive Sediment Transport," Journal of the Hydraulics Division, ASCE, Vol. 102, No. HY3, March, 1976, pp. 323-338.

Ariathurai, R., and K. Arulanandan, "Erosion Rates of Cohesive Soils," Journal of the Hydraulics Division, ASCE, Vol. 104, No. HY2, February, 1978, pp. 279-283.

Ariathurai, R., and A.J. Mehta, "Fine Sediments in Waterway and Harbor Shoaling Problems," International Conference on Coastal and Port Engineering in Developing Countries, Colombo, Sri Lanka, March, 1983.

Aris, R., "On the Dispersion of a Solute in a Fluid Flowing Through a Tube," Proceedings Royal Society of London, Series A, Vol 235, 1956, pp. 67-77.

Arulanandan, K., "Fundamental Aspects of Erosion of Cohesive Soils," Journal of the Hydraulics Division, ASCE, Vol. 101, No. HY5, March, 1975, pp. 635-639.

Arulanandan, K., P. Loganathan, and R.B. Krone, "Pore and Eroding Fluid Influences on Surface Erosion of Soil" Journal of Geotechnical Engineering Division, ASCE, Vol. 101, No. GT1, January, 1975, pp. 51-66.

Bain, A.J., Erosion of Cohesive Muds, M.S. Thesis, University of Manchester, United Kingdom, 1981.

Barnes, R.S.K., and J. Green, Editors, The Estuarine Environment, Applied Science Publishers, London, 1971.

Bauer, L., Water Quality and Heavy Metals in Sediments of Thirty-Six Florida Marinas, M.S. Project Report, Dept. of Environmental Engineering Sciences, University of Florida, Gainesville, 1981.

Been, K., and G.C. Sills, "Self-weight Consolidation of Soft Soils: An Experimental and Theoretical Study," Geotechnique, Vol. 31, No. 4, 1981, pp. 519-535.

Bellessort, B., "Movement of Suspended Sediments in Estuaries-Flocculation and Rate of Removal of Muddy Sediments," Tracer Techniques in Sediment Transport, International Atomic Energy Agency, Technical Report Series No. 145, 1973, pp. 31-40.

- Burt, T.N., and W.R. Parker, Settlement and Density in Beds of Natural Mud During Successive Sedimentation, Report IT 262, Hydraulics Research, Wallingford, United Kingdom, March, 1984.
- Christensen, B.A., Discussion of "Erosion and Deposition of Cohesive Soils," by Partheniades, E., Journal of the Hydraulics Division, ASCE, Vol. 91, No. HY5, September, 1965, pp. 301.
- Christensen, R.W., and B.M. Das, Hydraulic Erosion of Remolded Cohesive Soils, Special Report 135, Highway Research Board, Washington, D.C., 1973, pp. 8-19.
- Delo, E.A., Estuarine Muds Manual, Report 5R 164, Hydraulics Research, Wallingford, United Kingdom, February, 1988.
- Dixit, J.G., Resuspension Potential of Deposited Kaolinite Beds, M.S. Thesis, University of Florida, Gainesville, Florida, 1982.
- Dixit, J.G., A.J. Mehta, and E. Partheniades, Redepositional Properties of Cohesive Sediments Deposited in a Long Flume, UFL/COEL-82/002, Coastal and Oceanographic Engineering Department, University of Florida, Gainesville, Florida, August, 1982.
- Dyer, K.R., Estuaries: A Physical Introduction, John Wiley, London, 1973.
- Dyer, K.R., Editor, Estuarine Hydrography and Sedimentation, Cambridge University Press, Cambridge, United Kingdom, 1979.
- Dyer, K.R., Coastal and Estuarine Sediment Dynamics, John Wiley and Sons, London, 1986.
- Edzwald, J.K., J.B. Upchurch, and C.R. O'Melia, "Coagulation in Estuaries," Environmental Science and Technology, Vol. 8, No. 1, January, 1974, pp. 58-63.
- Einstein, H.A., and R.B. Krone, "Experiments to Determine Modes of Cohesive Sediment Transport in Salt Water," Journal of Geophysical Research, Vol. 67, No. 4, April, 1962, pp. 1451-1464.
- Elder, J.W., "The Dispersion of Marked Fluid in Turbulent Shear Flow," Journal of Fluid Mechanics, Vol. 5, 1959, pp. 544-560.
- Fischer, H.B., Longitudinal Dispersion in Laboratory and Natural Streams, Ph.D. Dissertation, California Institute of Technology, Pasadena, California, 1966.
- Fischer, H.B., "Mass Transport Mechanisms in Partially Stratified Estuaries," Journal of Fluid Mechanics, Vol. 53, Part 4, 1972, pp. 671-687.
- Fischer, H.B., "On the Tensor Form of the Bulk Dispersion Coefficient in a Bounded Skewed Shear Flow," Journal of Geophysical Research, Vol. 83, No. C5, May, 1978, pp. 2373-2375.

Fischer, H.B., J. Imberger, E.J. List, R.C.Y. Koh, and N.H. Brooks, *Mixing in Inland and Coastal Waters*, Academic Press, New York, 1979.

Grim, R.E., *Clay Mineralogy*, McGraw-Hill, New York, 1968.

Grimshaw, R.W., *The Chemistry and Physics of Clays*, Wiley-Interscience, New York, 1971.

Gust, G., "Observations on Turbulent-drag Reduction in a Dilute Suspension of Clay in Sea-water," *Journal of Fluid Mechanics*, Vol. 75, Part 1, 1976, pp. 29-47.

Hanzawa, H., and T. Kishida, "Fundamental Considerations of Undrained Strength Characteristics of Alluvial Marine Clays," *Soils and Foundation*, Japanese Society of Soil Mechanics and Foundation Engineering, Vol. 21, No. 1, March, 1981, pp. 39-50.

Hayter, E.J., *Prediction of the Movement of Cohesive Sediments in Estuarial Waters*, Ph.D. Dissertation, University of Florida, Gainesville, Florida, 1983.

Hayter, E.J., and A.J. Mehta, *Modeling of Estuarial Fine Sediment Transport for Tracking Pollutant Movement*, UFL/COEL-82/009, Coastal and Oceanographic Engineering Department, University of Florida, Gainesville, Florida, December, 1982.

Hayter, E.J. and A.J. Mehta, "Modeling Cohesive Sediment Transport in Estuarial Waters," *Applied Mathematical Modeling*, Vol. 10, August, 1986, pp. 294-303.

Hirst, T.J., M. Perlow, A.F. Richards, B.S. Burton, and W.J. van Sciver, "Improved In Situ Gamma-Ray Transmission Densitometer for Marine Sediments," *Ocean Engineering*, Vol. 3, No. 1, 1975, pp. 17-27.

Holley, E.R., "Unified View of Diffusion and Dispersion," *Journal of the Hydraulics Division, ASCE*, Vol. 95, No. HY2, March, 1969.

Holley, E.R., D.R.F. Harleman, and H. B. Fischer, "Dispersion in Homogeneous Estuary Flow," *Journal of the Hydraulics Division, ASCE*, Vol. 96, No. HY8, August, 1970, pp. 1691-1709.

Hood, P., "Frontal Solution Program for Unsymmetric Matrices," *International Journal for Numerical Methods in Engineering*, Vol. 10, 1976, pp. 379-399.

Hughes, P.A., "A Determination of the Relation Between Wind and Sea-Surface Drift," *Quarterly Journal of the Royal Meteorological Society*, London, Vol. 82, October, 1956, pp. 494-502.

Huebner, K.H. and E.A. Thornton, *The Finite Element Method for Engineers*, 2d ed. John Wiley & Sons, 1982.

Hunt, J.R., "Prediction of Ocean Particle Size Distribution from Coagulation and Sedimentation Mechanisms," *Advances in Chemistry Series No. 189 - Particles in Water*, M.D. Kavanaugh and J.O. Keckie, Editors, American Chemical Society, Washington, D.C., 1980, pp. 243-257.

Ingham, A.E., Editor, *Sea Surveying*, John Wiley & Sons, Chichester, United Kingdom, 1975.

Ippen, A.T., Editor, *Estuary and Coastline Hydrodynamics*, McGraw-Hill, New York, 1966.

Jobson, H.E., and W.W. Sayre, "Vertical Transfer in Open Channel Flow," *Journal of the Hydraulics Division, ASCE*, Vol. 96, No. HY3, March, 1970, pp. 703-724.

Kandiah, A., *Fundamental Aspects of Surface Erosion of Cohesive Soils*, Ph.D. Dissertation, University of California, Davis, California, 1974.

Karcz, I., and G. Shanmugam, "Decrease in Scour Rate of Fresh Deposited Muds," *Journal of the Hydraulics Division, ASCE*, Vol. 100, No. HY11, November, 1974, pp. 1735-1738.

Kelley, W.E., and R.C. Gularte, "Erosion Resistance of Cohesive Soils," *Journal of the Hydraulics Division, ASCE*, Vol. 107, No. HY10, October, 1981.

Kirby, R., and W.R. Parker, "Fluid Mud in the Severn Estuary and the Bristol Channel and its Relevance to Pollution Studies," *Proceedings of the International Chemical Engineers Exeter Symposium*, Exeter, United Kingdom, Paper A-4, 1973, pp. 1-14.

Kirby, R., and W.R. Parker, "Seabed Density Measurements Related to Echo Sounder Records," *Dock and Harbour Authority*, Vol. 54, 1974, pp. 423-424.

Kirby, R., and W.R. Parker, "The Physical Characteristics and Environmental Significance of Fine Sediment Suspensions in Estuaries," *Estuaries, Geophysics and the Environment*, National Academy of Sciences, Washington, 1977, pp. 110-120.

Kirby, R., and W.R. Parker, "Distribution and Behavior of Fine Sediment in the Severn Estuary and Inner Bristol Channel, U.K.," *Canadian Journal of Fisheries and Aquatic Sciences*, Vol. 40, Supplement Number 1, 1983, pp. 83-95.

Kranck, K., "Sedimentation Processes in the Sea," *The Handbook of Environmental Chemistry*, Vol. 2, Part A, O. Hutzinger, Editor, Springer-Verlag, Berlin, 1980, pp. 61-75.

Krone, R.B., *Flume Studies of the Transport of Sediment in Estuarial Shoaling Processes*, Final Report, Hydraulic Engineering Laboratory and Sanitary Engineering Research Laboratory, University of California, Berkeley, California, June, 1962.

Krone, R.B., *A Study of Rheological Properties of Estuarial Sediments*, Technical Bulletin No. 7, Committee of Tidal Hydraulics, U.S. Army Corps of Engineers, Vicksburg, Mississippi, September, 1963.

Krone, R.B., *A Field Study of Flocculation as a Factor in Estuarial Shoaling Processes*, Technical Report No. 19, Committee on Tidal Hydraulics, U.S. Army Corps of Engineers, Vicksburg, Mississippi, June, 1972.

Krone, R.B., "Aggregation of Suspended Particles in Estuaries," Estuarine Transport Processes, P. Kjerfve, Editor, the Belle W. Baruch Library in Marine Science, No. 7, University of South Carolina Press, Columbia, South Carolina, 1978, pp. 177-190.

Kruyt, H.R., Editor, Colloid Science, Vol. I, Elsevier, Amsterdam, New York, 1952.

Lambermont, J., and T. Lebon, "Erosion of Cohesive Soils," Journal of Hydraulic Research, Vol. 16, No. 1, 1978, pp. 27-44.

Lee, P.T., Deposition and Scour of Clay Particles Due to Currents, M.S. Thesis, Asian Institute of Technology, Bangkok, Thailand, 1974.

Mehta, A.J., Depositional Behavior of Cohesive Sediments, Ph.D. Dissertation, University of Florida, Gainesville, Florida, 1973.

Mehta, A.J., "Review of Erosion Function for Cohesive Sediment Beds," Proceedings of the First Indian Conference on Ocean Engineering, Indian Institute of Technology on Ocean Engineering, Indian Institute of Technology, Madras, India, Vol. 1, February, 1981, pp. 122-130.

Mehta, A.J., and E. Partheniades, Depositional Behavior of Cohesive Sediments, Technical Report No. 16, Coastal and Oceanographic Engineering Laboratory, University of Florida, Gainesville, Florida, March, 1973.

Mehta, A.J., and E. Partheniades, "An Investigation of the Depositional Properties of Flocculated Fine Sediments," Journal of Hydraulics Research, International Association for Hydraulics Research, Vol. 13, No. 14, 1975, pp. 361-381.

Mehta, A.J., and E. Partheniades, "Kaolinite Resuspension Properties," Journal of the Hydraulics Division, ASCE, Vol. 105, No. HY4, March, 1979, pp. 411-416.

Mehta, A.J., and E.J. Hayter, Preliminary Investigation of Fine Sediment Dynamics of Cumbarjua Canal, Goa, India, UFL/COEL-81-012, Coastal and Oceanographic Engineering Department, University of Florida, Gainesville, Florida, December, 1981.

Mehta, A.J., T.M. Parchure, J.G. Dixit, and R. Ariathurai, "Resuspension Potential of Deposited Cohesive Sediment Beds," Estuarine Comparisons, V.S. Kennedy, Editor, Academic Press, New York, 1982a, pp. 591-609.

Mehta, A.J., E. Partheniades, J. Dixit, and W.H. McAnally, "Properties of Deposited Kaolinite in a Long Flume," Proceedings of the Hydraulics Division Conference on: Applying Research to Hydraulic Practice, ASCE, Jackson, Mississippi, August, 1982b.

Migniot, P.C, "A Study of the Physical Properties of Different Very Fine Sediments and Their Behavior Under Hydrodynamic Action," *La Houille Blanche*, No. 7, 1968, pp. 591-620. (In French, with English abstract).

Mitchell, J. K., "Fundamental Aspects of Thixotropy in Soils," *Transactions of the ASCE*, Vol. 126, Pt. 1, 1961, pp. 1586-1620.

Mitchell, J.K., *Fundamentals of Soil Behavior*, John Wiley & Sons, New York, 1976.

Mitchell, J.K., A. Singh, and R.G. Campanella, "Bonding Effective Stresses and Strength of Soils," *Journal of the Soil Mechanics and Foundation Division, ASCE*, Vol. 95, No. SM5, September, 1969, pp. 1219-1246.

Nichols, M., R. Faas, and G. Thompson, *Estuarine Fluid Mud: Its Behavior and Accumulation*, Final Report, Virginia Institute of Marine Science, Gloucester Point, Virginia, April, 1979.

Officer, C.B., *Physical Oceanography of Estuaries*, John Wiley, New York, 1976.

Officer, C.B., "Physical Dynamics of Estuarine Suspended Sediments," *Marine Geology*, Vol. 40, 1981, pp. 1-14.

Okubo, A., "Effect of Shoreline Irregularities on Streamwise Dispersion in Estuaries and Other Embayments," *Netherlands Journal of Sea Research*, Vol. 6, 1973, pp. 213-224.

O'Melia, C.R., *Physicochemical Processes for Water Quality Control*, W.J. Weber, Editor, Wiley-Interscience, New York, 1972, pp. 61-109.

Owen, M.W., *A Detailed Study of the Settling Velocities of an Estuary Mud*, Report No. INT 78, Hydraulics Research Station, Wallingford, United Kingdom, September, 1970a.

Owen, M.W., *Properties of a Consolidating Mud*, Report No. INT 83, Hydraulics Research Station, Wallingford, United Kingdom, December, 1970b.

Owen, M.W., "The Effect of Turbulence on the Settling Velocities of Silt Flocs," *Proceedings of the Fourteenth Congress of I.A.H.R.*, Vol. 4, Paris, August, 1971, pp. 27-32.

Owen, M.W., *Erosion of Avonmouth Mud*, Report No. INT 150, Hydraulics Research Station, Wallingford, United Kingdom, September, 1975.

Owen, M.W., "Problems in the Modeling of Transport, Erosion, and Deposition of Cohesive Sediments," *The Sea VI, Marine Modeling*, E.D. Goldberg, I.N. McCave, J.J. O'Brien and J.H. Steel, Editors, Wiley-Interscience, New York, 1977, pp. 515-537.

Paaswell, R.E., *Causes and Mechanisms of Cohesive Soil Erosion: The State of the Art*, Special Report 135, Highway Research Board, Washington, D.C., 1973, pp. 52-74.

- Parchure, T.M., Effect of Bed Shear Stress on the Erosional Characteristics of Kaolinite, M.S. Thesis, University of Florida, Gainesville, Florida, December, 1980.
- Parchure, T.M., Erosional Behavior of Deposited Cohesive Sediments, Ph.D. Dissertation, University of Florida, Gainesville, Florida, 1984.
- Parker, W.R., and R. Kirby, "Fine Sediment Studies Relevant to Dredging Practice and Control," Proceedings of the Second International Symposium on Dredging Technology, BHRA, Paper B2, Texas A & M University, College Station, November, 1977.
- Parker, W.R., and R. Kirby, "Time Dependent Properties of Cohesive Sediment Relevant to Sedimentation Management-European Experience," Estuarine Comparisons, V.S. Kennedy, Editor, Academic Press, New York, 1982.
- Parker, W.R., and K. Lee, "The Behavior of Fine Sediment Relevant to the Dispersal of Pollutants," ICES Workshop on Sediment and Pollutant Interchange in Shallow Seas, Texel, United Kingdom, September, 1979.
- Partheniades, E., A Study of Erosion and Deposition of Cohesive Soils in Salt Water, Ph.D. Dissertation, University of California, Berkeley, California, 1962.
- Partheniades, E., A Summary of the Present Knowledge on the Behavior of Fine Sediments in Estuaries, Technical Note No. 8, Hydrodynamics Lab, M.I.T., Cambridge, Massachusetts, 1964.
- Partheniades, E., "Erosion and Deposition of Cohesive Soils," Journal of the Hydraulic Division, ASCE, Vol. 91, No. HY1, January, 1965, pp. 105-138.
- Partheniades, E., "Erosion and Deposition of Cohesive Soils," River Mechanics, Vol. II, H.W. Shen, Editor; Fort Collins, Colorado, 1971.
- Partheniades, E., "Unified View of Wash Load and Bed Material Load," Journal of the Hydraulics Division, ASCE, vol. 103, No. HY9, 1977, pp. 1037-1057.
- Partheniades, E., Kennedy, J.R., Etter, R.J., and Hoyer, R.P., Investigations of the Depositional Behavior of Fine Cohesive Sediments in an Annular Rotating Channel, Report No. 96, Hydrodynamics Lab, M.I.T., Cambridge, Massachusetts, 1966.
- Partheniades, E., Cross, R.H., and Ayoro, A., "Further Results on the Deposition of Cohesive Sediments," Proceedings of the Eleventh Conference on Coastal Engineering, ASCE, New York, 1968, pp. 723-742.
- Postma, H., "Sediment Transport and Sedimentation in the Estuarine Environment," Estuaries, Publication 83, G.H. Lauff, Editor, American Association for Advancement of Science, Washington, D.C., 1967, pp. 158-179.

- Preston, A., D. F. Jefferies, J.W.R. Dutton, B.R. Harvey, and A.K. Steele, "British Isles Coastal Waters: The Concentration of Selected Heavy Metals in Sea Water, Suspended Matter and Biological Indicators - a Pilot Survey," *Journal of Environmental Pollution*, Vol. 3, 1972, pp. 69-72.
- Richards, A.F., T.J. Hirst, and J.M. Parks, "Bulk Density - Water Content Relationship in Marine Silts and Clays," *Journal of Sedimentary Petrology*, Vol. 44, No. 4, 1974, pp. 1004-1009.
- Rosillon, R., and C. Volkenborn, *Sedimentacion de Material Cohesivo en Agua Salada*, Thesis, University of Zulia, Maracaibo, Venezuela, November, 1964.
- Sargunam, A., P. Riley, K. Arulanandan, and R. B. Krone, "Effect of Physico-chemical Factors of the Erosion of Cohesive Soil," *Journal of the Hydraulics Division, ASCE*, Vol. 99, No. HY3, March, 1973, pp. 553-558.
- Sayre, W.W., "Dispersion of Mass in Open Channel Flow," *Hydraulics Papers*, No. 3, Colorado State University, Fort Collins, Colorado, February, 1968.
- Sherard, J.L., R.S. Decker, and N.L. Ryka, "Piping in Earth Dams of Dispersive Clay," *ASCE Soil Mechanics and Foundation Conference*, Purdue University, Lafayette, Indiana, June, 1972.
- Smoot, G.F. and C.E. Novak, "Measurement of Discharge by Moving-Boat Method," Chapter A11 of *Book 3 Applications of Hydraulics*, U.S. Geological Survey Techniques of Water-Resources Investigations, Denver: U.S. Geological Survey, Books and Open-File Reports Section, 1969.
- Spangler, M.G., and R.L. Handy, *Soil Engineering*, Harper and Row, New York, 1982.
- Taylor, G.I., "Dispersion of Soluble Matter in Solvent Flowing Slowly Through a Tube," *Proceedings of the Royal Society of London, Series A*, Vol. 219, 1953, pp. 186-203.
- Taylor, G.I., "The Dispersion of Matter in Turbulent Flow Through a Pipe," *Proceedings of the Royal Society of London, Series A*, Vol. 223, May, 1954, pp. 446-468.
- Teeter, A.M., "Investigations on Atchafalaya Bay Sediments," *Proceedings of the Conference on Frontiers in Hydraulic Engineering*, ASCE, Cambridge, Massachusetts, August, 1983, pp. 85-90.
- Terzaghi, K., and R.B. Peck, *Soil Mechanics in Engineering Practice*, John Wiley and Sons, New York, 1960.
- Thorn, M.F.C., "Physical Processes of Siltation in Tidal Channels," *Proceedings of Hydraulic Modelling Applied to Maritime Engineering Problems*, ICE, London, 1981, pp. 47-55.
- Thorn, M.F.C., and J.G. Parsons, *Properties of Grangemouth Mud*, Report No. EX781, Hydraulics Research Station, Wallingford, United Kingdom, July, 1977.

Thorn, M.F.C., and J.G. Parsons, "Erosion of Cohesive Sediments in Estuaries: An Engineering Guide," Proceedings of the Third International Symposium on Dredging Technology, Paper F1, March, 1980.

van Olphen, H., An Introduction to Clay Colloid Chemistry, Interscience Publishers, New York, 1963.

van Rijn, L.C., Pump-Filter Sampler, Design of an Instrument for Measuring Suspended Sand Concentrations in Tidal Conditions, Research Report S 404-I, Delft Hydraulics Laboratory, The Netherlands, June, 1979.

Weckmann, J., Sediment Management of a Coastal Marina, M.S. Thesis, University of Florida, Gainesville, Florida, 1979.

Whitehouse, U.G., L.M. Jeffrey, and J.D. Debbrecht, "Differential Settling Tendencies of Clay Minerals in Saline Waters," Proceedings of the Seventh National Conference on Clays and Clay Minerals, 1960, pp. 1-79.

Whitmarsh, R.B., "Precise Sediment Density by Gamma-Ray Attenuation Alone," Journal of Sedimentary Petrology, Vol. 41, 1971, pp. 882-883.

Yeh, H.Y., Resuspension Properties of Flow Deposited Cohesive Sediment Beds, M.S. Thesis, University of Florida, Gainesville, Florida, 1979.

Zienkiewicz, O.C., The Finite Element Method in Engineering Science, McGraw-Hill, London, 1977.

APPENDIX A

HSCTM-2D STRUCTURE

A.1 SUBROUTINES IN HYDRO2D

A brief description of the subroutines used in HYDRO2D is given below.

Subroutine AGEN-	Generates specified total flow boundary conditions.
Subroutine BLINE-	Computes the coordinates and slopes of boundary mid-side nodes, and sets nodal no-slip or slip flow boundary conditions along solid boundaries.
Subroutine CHECK-	Computes the flow rate across specified cross-sections.
Subroutine COEFS-	Generates the element coefficient matrices for both triangular and quadrilateral elements.
Subroutine DEL-	Determines which nodes and elements are "dry"; these nodes and elements are eliminated from the system coefficient matrices.
Subroutine FRONT1-	Forms and solves the system matrix equation using the frontal elimination routine.
Subroutine INPUT-	Input data file for HYDRO2D is read in this routine.
Subroutine LOAD1-	Determines the equivalence between each node and particular degree of freedom (i.e., field variable) from the equation number in the system matrix.
Subroutine OUTPUT-	Prints out the nodal depth-average velocity components and flow depths at specified time steps where HYDRO2D is run to update the flow field.
Subroutine PREHYD	HEC style input reader for HYDRO2
Subroutine REWET-	Determines which previously "dry" or eliminated elements are now "wet" or covered with water, and adds these elements back into the system coefficient matrices.

- Subroutine SIZE - Computes the area of each element in the finite element grid.
- Subroutine STORM - Computes the temporal and spatial distribution of wind speed and direction of a storm as it moves over a model mesh.

A.2 SUBROUTINES IN CS2D

A brief description of the subroutines used in CS2D is given below.

- Subroutine BEDFOR - Forms the layered bed. Called from BEDMOD and ORGBED.
- Subroutine BEDMOD - Bed model
- Subroutine BEDSS - Calculates bed shear stress, friction velocity, elemental average velocity.
- Subroutine COMPAR - Compares steady state solution to analytical solution.
- Subroutine CONCBC - Sediment boundary conditions.
- Subroutine CONCIC - Initial sediment conditions.
- Subroutine DENSTY - Computes the water density at every node using the given water temperature, salinity and suspension concentration. The kinematic viscosity is also calculated as a function of water temperature.
- Subroutine DEPMAS - Computes the dry sediment mass deposited during the previous time step for every element where deposition is predicted to occur.
- Subroutine DEPSN - Computes the rate of deposition at each node where deposition is predicted to occur.
- Subroutine DISPER - Reads or computes (using the dispersion algorithm) the four components of the two-dimensional dispersion tensor for each node at every time step where the appropriate transient code array indicates that the values of the dispersion coefficients change.
- Subroutine DRYNOD - Determines at which nodes the water depth is less than DSET (see Card A.3). These nodes are eliminated from the finite element grid.
- Subroutine ELSTIF - Forms the element coefficient and load matrices. Modifies the element load matrix to account for specified boundary conditions.
- Subroutine EXACT - Computes analytical solution to steady state convection-diffusion problem.

Subroutine FRONT -	Forms and solves the system matrix equation at each time step for the nodal concentrations using the frontal elimination routine.
Subroutine ITERC -	Computes the thickness of the partially consolidated bed formed by the specified dry mass of sediment using an iteration procedure. Called by Subroutine BEDFOR.
Subroutine ITERM -	Computes the thickness of the stationary suspension formed by the specified dry mass of sediment using an iteration procedure. Called by Subroutine BEDFOR.
Subroutine INTERP -	Performs element to node interpolation.
Subroutine LOADX -	Forms the array NBC, which is used in solving matrix equations.
Subroutine LOAD2 -	Computes the bandwidth and number of equations.
Subroutine ORGBED -	Reads the original settled bed profile and the initial dry mass per unit bed surface area of new deposits on top of the settled bed for elements where such exist.
Subroutine RECORD -	Records the values at each time step of various parameters for the elements where time records are desired.
Subroutine RED -	Called by Subroutine FRONT to read data from the temporary (scratch) data file with unit number ND1.
Subroutine REDISP -	Computes the redispersion rate for unconsolidated new deposit layers (stationary suspension) when the flow is accelerating and the bed shear stress is greater than the shear strength of the suspension surface. Computations are made on an element-by-element basis.
Subroutine RESUSP -	Computes the resuspension rate for exposed partially consolidated bed layers or settled bed layers when the flow is accelerating and the bed shear stress is greater than the shear strength of the bed surface. Computations are made on an element-by-element basis.
Subroutine SEDPRP -	Reads the settling velocity, new deposit and consolidation properties of the cohesive sediment. Settling velocity parameters and the new deposit properties are printed out.
Subroutine SETVEL -	Reads, or computes using a built-in algorithm, the sediment settling velocity in Range I and for $C < C1$ in Range II as a function of the suspension concentration and salinity at each node for the time steps where the

appropriate transient code array indicates that a change in settling velocity occurs.

- Subroutine SHPFNS - Computes the isoparametric quadratic shape functions and their derivatives for quadrilateral elements with parabolic sides.
- Subroutine TSHAPE - Computes the isoparametric quadratic shape functions and derivatives for triangular elements with parabolic sides.
- Subroutine VELL - Reads, or computes using a user specified route or HYDRO2D, the depth-averaged components of the velocity in the x- and y-directions and the flow depth at each node for the time steps where the appropriate transient code array indicates that a change in the velocity occurs.
- Subroutine WRITER - Prints out the bed shear stress, bed elevation, erosion/deposition rates and the layer-by-layer bed properties for each element at each time step where the appropriate transient code array specifies.
- Subroutine WRT - Called by Subroutine FRONT to perform mass transfer of data to the temporary data file with unit number ND1.
- Function DENFUN - Computes the water density as a function of temperature and salinity.
- Function ERF - Computes the error function.
- Function ERFC - Computes the complementary error function.
- Function SIGFUN - Computes the values of σ_2 (given in eq. 3.28) as a function of τ_b .
- Function T50FUN - Computes the values of t_{50} (given in eq. 3.28) as a function of τ_b .

APPENDIX B

LABORATORY SEDIMENT TESTING PROGRAM

It is recommended that the following physicochemical sediment and fluid properties be determined using the collected sediment cores.

B.1 Properties of Undisturbed Sediment Cores

The gamma-ray densitometer may be used to determine the bulk sediment density profile in the undisturbed cores still in the liner tubes as soon as possible after the cores are obtained. A description of this procedure is given by Whitmarsh (1971) and Kirby and Parker (1974). If this instrument is not available, the freeze-drying procedure used by Parchure (1980) and Dixit (1982) or the pumping method used by Thorn and Parsons (1977) may be used to determine the bulk density profile. The pumping method consists of removing by suction a thin layer, e.g. 3 cm, from the top of the core. This procedure is repeated, layer by layer, and each layer is analyzed to determine the mean bulk density.

B.2 Properties of Original Settled Bed

The bulk density and bed shear strength profiles and the erosion rate constant for each layer need to be determined for the cores. The number of layers and the thickness of each are determined from the nature of the bed shear strength profile. The erosion rate constant for each layer and the shear strength profile can be determined, for example, in the rotating cylinder erodibility testing apparatus described by Sargunam *et al.* (1973). In order to use this apparatus, the core sample must be trimmed. The portion of each core that is sufficiently consolidated such that it can be trimmed and tested in the erosion apparatus is defined to be the settled bed. The thickness of this portion defines

the location of the top of the settled bed. Soft, unconsolidated portions of each core are assumed to be new deposits.

B.3 Properties of New Deposits

For cores with soft, unconsolidated or partially consolidated sediment on top of the settled portion, the following method may be used to estimate the erosional, depositional and consolidation characteristics of such new deposits. The new deposit samples from the cores at all the stations should be mixed and subjected to laboratory erosion, deposition and consolidation tests (described by Parchure (1980), Mehta and Partheniades (1973)) to determine: the settling velocity as a function of suspension concentration and salinity; the minimum and maximum depositional shear stresses τ_{bmin} and τ_{bmax} ; variation of t_{50} and σ_2 with the bed shear stress, τ_b ; the number of characteristic stationary suspension layers, and the thickness, dry sediment density and shear strength of each layer; the number of characteristic partially consolidated new deposit layers, and the thickness, dry sediment density, shear strength and the resuspension parameters ϵ_0 and α of each layer; the variation of $\bar{\rho}_\infty$ and $T_{dc\infty}$ with C_0 ; variation of $\rho(z)$ with T_{dc} ; variation of the bed shear strength, τ_c , with ρ . The variation of the bed density and shear strength profiles with salinity can be determined by performing the erosion tests at several salinities between 0 and 35 ppt. A brief description of laboratory tests which can be conducted in order to determine the above mentioned consolidation parameters is given next.

Laboratory tests to determine the consolidation characteristics of a cohesive sediment bed involve the measurement of the bed density profile. Various methods have been used for this purpose. Been and Sills (1981) measured the density profile of a clayey soil using a non-destructive x-ray technique. Methods which involve the destruction of the soil include, among others, the freeze-drying procedure used by Parchure (1980) and Dixit (1982), the pumping, or layer-by-layer sampling method used by Thorn and Parsons (1977), and the use of specially designed apparatuses (Parchure 1980). The latter consists of a 183 cm high, 30 cm diameter PVC cylinder, a bottom plate, and ten 1.27 cm diameter plastic tubes ranging from 1.27 to 12.7 cm in height glued to the bottom plate, concentric to the PVC cylinder. These cylinders are filled with a sediment suspension of known concentration, and the sediment is allowed to settle under quiescent conditions for a specifies

consolidation time. Following the procedure described by Parchure (1980), the bulk density profile can be determined.

The following parameters should be varied systematically in the laboratory tests in order to determine their effect on the rate of consolidation:

- (a) Consolidation time - it is recommended that the time allowed for the bed to consolidate before the density profile is measured be varied logarithmically from 0 to 72 hours (1 month).
- (b) Initial conditions - the initial suspension concentration, which determines the thickness and density of the initial bed.
- (c) Salinity - the salinity of the water should be varied from 0 (tap water) to 35 ppt.
- (d) Overburden - it is important that the effect of discretized to continuous additions of varying amounts of sediment (overburden) on top of the initial bed be determined in order to evaluate the effect of such overburden pressures on the consolidation rate of the lower bed layers.

The relationship between ρ and τ_c needs to be determined as well for the collected sediment samples. Both the bed shear strength and density profiles may be determined using the methodology described by Mehta *et al.* (1982a). These profiles can then be used to establish an empirical relationship between τ_c and ρ .

B.4 Fluid Composition

The pH, total salt concentration, and concentrations of ions such as Na^+ , Ca^{2+} , Mg^{2+} , K^+ , Fe^{3+} and Cl^- should be determined for both the pore fluid in the consolidated bed portion of one core and a sample of the suspending fluid.

B.5 Composition and Cation Exchange Capacity of the Sediment

The sediment contained in the consolidated bed portion of one core from each collection station should be thoroughly mixed so that a spatially homogenous sample is obtained. A standard hydrometer analysis must be conducted on each so-prepared sample to determine the sediment particle size distribution and thereby the percentage by weight of clay, silt and fine to coarse sand in each sample. In preparing the samples for this analysis, the sediment must not be initially air-dried (to obtain the dry weight of the material used in the test), as it has been found that dried sediment will not completely redisperse when the dispersing agent is added (Krone 1962). For this reason, the total

dry weight of the sample must be obtained after the test by evaporating off all the water in an oven set at approximately 50° C. The percentage of weight of organic matter should be determined through use of a method such as the Walkley-Black test (Allison 1965). In addition , it is recommended that x-ray diffraction analysis of the bulk sample, and < 2 µm unglycolated and glycolated portions be conducted in order to determine the predominant clay and non-clay mineral constituents. The cation exchange capacity must be determined for each sample.

APPENDIX C

DATA OUTPUT FOR HSCTM-2D AND

DATA INPUT FOR HYDRO2D

C.1 HSCTM-2D Binary Output File Format

Output binary files generated by HSCTM-2D are written by standard FORTRAN unformatted write statements. The variable types follow standard FORTRAN assignments, where variables are REAL, except for those beginning with the characters "I" through "N" which are INTEGER. The contents of each record for the primary binary results file from HSCTM-2D are described below.

Record 1.	MFLG IREC NP NE	
where	MFLG -	Model identifier flag (120-129 for HYDRO2D results) (135-139 for HYDRO2D hotstart file)
	IREC -	Version number of the HYDRO2D program
	NP -	Number of nodes in the mesh
	NE -	Number of elements in the mesh
Record 2.	IWRT1 (IBAN(i),i=1,1WRT1)	
where	IWRT1 -	Number of items contained in the banner array
	IBAN -	Integer interpretation of the banner character strings
Record 3.	IWRT2 IWRT3 (IREC(i),i=1,1WRT2) (FREC(I),I=1,1WRT3)	
where	IWRT2 -	Number of items contained in the IREC array
	IWRT3 -	Number of items contained in the FREC array
	IREC -	Integer flags which are set during execution
	FREC -	Floating point flags which are set during execution
Record 4.	IWRT4 (ITIT(i),i= 1,1WRT4)	
where	ITIT -	Integer interpretation of the title character string
Records 5-Last	TET NP	((VEL(j,k), j=1,3), k= 1,NP)
		(NDRY(k), k=1,NP)
	NE	(IMAT(k), k=1,NE)
		(WSEL(k), k=1,NP)
where	TET -	Simulation time, in decimal hours
	NP -	Number of nodes in the mesh
	VEL -	Array containing --> X-velocity, Y-velocity, and Depth
	NDRY -	Array containing wet/dry status for each node (1 = wet, 2 = dry, -1= About to become re-wet)
	NE -	Number of elements in the mesh
	IMAT -	Array containing each elements material type assignment
	WSEL -	Array containing water surface elevation for each node

C.2 Card Image Input Data Coding Instructions for HYDRO2D

This description of input data is written in the language for a standard eight-column format in which the first three columns are reserved for "Card Group" and "Data Type" alpha- characters, respectively. These three columns are considered to be field 0. The rest of field 1, columns 4 through 8, is read in several combinations of columns. The instructions use the following syntax: "O,Cxx" where the "O" refers to field 0, "C" to the column and the "xx" are column numbers.

Of the cards shown in the following table, Network (mesh) data are prepared by GFGEN, an accompanying program that reads the geometry file generated by SMS and generates a binary file containing the finite element mesh that is read by HSCTM-2D. The other cards are prepared here. The sequence of cards should be in the order shown in Table C.1. Input variables are summarized in Table C.2.

Either free field or the standard eight-column card fields are permitted with the default being to free field. In standard eight column fields, unneeded variables can be omitted, but in free field unneeded variables are delimited by commas. Card image input is given in section C.3 following the input instructions for each card.

The first set of "B" cards will be used for the steady-state solution. This group of cards should be terminated by an "END" card. Dynamic boundary conditions for each time-step will then either be added to the basic input (boundary condition) file separated by "END" cards, or in a separate alternate boundary condition input file. All specified boundary conditions hold from one time step to another unless they are specifically modified. The program does not permit new boundary conditions to be specified in mid-run nor does it allow a change in the types (e.g., stage, discharge) of boundary conditions.

Table C.1
HYDRO2D Data Card Summary

<u>Card</u>	<u>Content</u>	<u>Required</u>
T1 - T2	TITLE CARDS	NO
T3	TITLE CARD	YES
\$F	FORMATTED DATA SET	NO
\$M	MACHINE TYPE IDENTIFIER	YES
\$L	INPUT/OUTPUT FILE NUMBERS	NO
SI	SYSTEM INTERNATIONAL UNITS	NO
CA	SPECIAL CALCULATION VARIABLES	NO
CO	COMMENTS	NO
DE	WET/DRY BY ELEMENT	NO
DM	WET/DRY BY MARSH POROSITY	NO
EV	TURBULENT EXCHANGE AND MANNING'S N COEFFICIENTS	YES, if EX, EY and HN are not present
EX	TURBULENT EXCHANGE COEFFICIENTS, X-PLANE	NO
EY	TURBULENT EXCHANGE COEFFICIENTS, Y-PLANE	NO
FC	FLOW CONTROL STRUCTURES	NO
FD	FLUID DENSITY	NO
FT	FLUID TEMPERATURE	NO
G1	GEOMETRY, GENERAL GEOMETRY PARAMETERS	NO
GC	GEOMETRY, CONTINUITY CHECK LINES	NO
GE	GEOMETRY, ELEMENT CONNECTION TABLE	NO

(continued)

Table C.1 (continued)

<u>Card</u>	<u>Content</u>	<u>Required</u>
GN	GEOMETRY, NODAL COORDINATES, BOTTOM ELEVATIONS	NO
GT	GEOMETRY, ELEMENT TYPE (IMAT)	NO
GV	GEOMETRY, EDDY VISCOSITY TENSOR	NO
GW	GEOMETRY, 1-D CROSS SECTIONAL PROPERTIES	NO
GY	GEOMETRY, BOTTOM ELEVATIONS	NO
HN	HYDRAULICS, MANNING N-VALUES	NO
IC	INITIAL CONDITIONS, WATER-SURFACE ELEVATION	YES
LAT	LATITUDE	NO
TI	TIMING, NUMBER OF ITERATIONS COUNTER	YES
TO	TIMING FOR BINARY OUTPUT WRITE	NO
TR	TRACE PRINTOUT CONTROLS	YES
TRN	TRACE PRINTOUT NODE LIST	NO
TZ	TIMING, TIME ZERO	YES
BCC	BOUNDARY CONDITION CONTROL PARAMETERS	NO
BA	BOUNDARY, AZIMUTH OF FLOW	*
BS	BOUNDARY, CURRENT SPEED	*
BH	BOUNDARY, WATER-SURFACE ELEVATION	*
BQ	BOUNDARY, UNIT discharge	*

(continued)

Table C.1 (concluded)

<u>Card</u>	<u>Content</u>	<u>Required</u>
BRA	BOUNDARY, REFLECTION/ABSORPTION	*
BRC	BOUNDARY, RATING CURVE	*
BWC	BOUNDARY, WIND FORMULATION CONTROL	NO
BW	BOUNDARY, SURFACE WIND FIELD	NO
BWS	BOUNDARY, WINDSTORM	NO
BCN	BOUNDARY CONDITION SPECIFIED BY NODE	*
REV	REVISE THE COEFFICIENTS OR BOUNDARY CONDITIONS IN MIDTHME STEP	NO
END	END OF BC SPECIFICATIONS FOR TIME STEP	YES
STO	STOP THE SIMULATION	YES

* Specification of at least one type of boundary condition is required.

Table C.2
HYDRO2D Input Variables

<u>Variable</u>	<u>Description</u>	<u>Card</u>
AO	THE BOTTOM ELEVATION OF EACH NODE	GY,GN
AC1	MARSH POROSITY DEPTH SHIFT	DM
AC2	MARSH POROSITY DEPTH RANGE OVER WHICH THE SECTION REDUCES	DM
AC3	MARSH POROSITY, MINIMUM ACTIVE FRACTION OVER LOWER SECTION	DM
AC4	MARSH POROSITY, ABSOLUTE BOTTOM ELEVATION OF MARSH	DM
AC1X	CONSTANT FOR RATING CURVE	BRA,BRC
AC2X	MULTIPLIER FOR RATING CURVE	BRC
AC3X	BASE ELEVATION FOR RATING CURVE	BRC
AC4X	EXPONENT FOR RATING CURVE	BRC
ALFAK	ANGLE AT A NODE, IN DEGREES	BA
BETA	REFLECTION/ABSORPTION BOUNDARY COEFFICIENT	BRA
BETAL	STANDARD DEVIATION OF SPATIAL DISTRIBUTION FUNCTION IN DIRECTION OF STORM'S MOVEMENT	BWC
BETAT	STANDARD DEVIATION OF SPATIAL DISTRIBUTION FUNCTION IN DIRECTION OF TRANSVERSE TO STORM PATH	BWC
CORD	THE (X,Y) COORDINATES OF THE NODE	GN
DSET	THE WATER DEPTH AT WHICH A WET NODE IS CONSIDERED TO BECOME DRY	DE
DSETD	THE WATER DEPTH AT WHICH A DRY NODE BECOMES REWET	DE
DELT	LENGTH OF COMPUTATION TIME STEP	TZ

(continued)

Table C.2 (continued)

<u>Variable</u>	<u>Description</u>	<u>Card</u>
ELEV	THE AVERAGE INITIAL WATER-SURFACE ELEVATION OVER THE MESH	IC
FLD	ANY ALPHANUMERIC USER COMMENT	CO,END
FLZ3	FLOW CONTROL EQUATION, BASE FLOW	FC
FLZ4	FLOW CONTROL EQUATION, RELATIONAL COEFFICIENT	FC
FLZ5	FLOW CONTROL EQUATION, REFERENCE ELEVATION OR HEAD DIFFERENCE	FC
FLZ6	FLOW CONTROL EQUATION, EXPONENT	FC
FLZ7	FLOW CONTROL EQUATION, DIRECTION OF FLOW (RADIANSCOUNTERCLOCKWISE FROM + X-AXIS)	FC
HFX	HEAD SPECIFICATION ALONG A CONTINUITY LINE	BH
HMIN	INITIAL DEPTH FOR ONE DIMENSIONAL ELEMENTS	IC
IBUP	LOGICAL UNIT NUMBER FOR DYNAMIC BOUNDARY CONDITIONS INPUT TO HYDRO2D	\$L
IC1	CARD GROUP IDENTIFIER, ALL CARDS	ALL
IC3	DATA TYPE IDENTIFIER, SOME CARDS	SOME
ICON	CONTINUITY LINE NUMBER	BRA
ICOMID	(IVRSID) COMPUTER IDENTIFIER	\$M
IDEN	DYNAMIC COUNTER FOR INPUT OF VARIABLE (self count)	FD
ISTYPE	STORM REFERENCE POINT	BWS
DMN	NODAL MARSH POROSITY SWITCH	DM
IDNOPT	MARSH OPTION SWITCH	DM

(continued)

Table C.2 (continued)

<u>Variable</u>	<u>Description</u>	<u>Card</u>
IECHO	SWITCH TO CONTROL ECHO PRINTING OF CODED INPUT DATA RECORDS	TR
IGEON	LOGICAL UNIT NUMBER FOR GFGEN GEOMETRIC DATA FILE	\$L
IFINO	LOGICAL UNIT NUMBER FOR HYDRO2D TO WRITE RESULTS FOR TRANSFER TO STUDY	\$L
IFLZ1	FLOW CONTROL IDENTIFIER (IMAT > 904)	FC
IFLZ2	FLOW CONTROL TYPE (1-5)	FC
IHGEN	DYNAMIC COUNTER FOR INPUT OF NUMBER OF LINES ACROSS WHICH ELEVATION WILL BE SPECIFIED	BHL
IHOTN	LOGICAL UNIT NUMBER FOR FILE CONTAINING INITIAL CONDITIONS	\$L
IHOTO	LOGICAL UNIT NUMBER FOR HYDRO2D TO WRITE RESTART FILE	\$L
IMAT	THE ELEMENT TYPE (N-VALUE AND EDDY COEFFICIENTS)	GT,GE
IOPNID	MACHINE DEPENDENT OPEN STATEMENT CONTROLLER	\$M
OUT	LOGICAL UNIT FOR PRINTOUT	\$L
PRT	SWITCH TO PRINT ELEMENT INPUT DATA, INITIAL CONDITIONS AND N-VALUES	TR
IQGEN	DYNAMIC COUNTER FOR INPUT OF NUMBER OF LINES ACROSS WHICH TOTAL FLOW WILL BE SPECIFIED	BHL
ISPLPT	ALTERNATE PRINT FILE UNIT NUMBER	\$L
ISPRTN	DE-ACTIVATE PRINT SUMMARY BY NODE	TR
ISTGEN	DYNAMIC COUNTER FOR INPUT OF NUMBER OF LINES ACROSS WHICH AN ELEVATION-FLOW RELATIONSHIP WILL BE SPECIFIED	BQL
ITSI	NUMBER OF TIME-STEPS BETWEEN SUCCESSIVE FULL PRINTOUTS	TR

(continued)

Table C.2 (continued)

<u>Variable</u>	<u>Description</u>	<u>Card</u>
IWMX	WIND SPEED UNIT FLAG	BWC
IWIND	CONTROL FOR WIND FIELD INPUT:	BWC,BC
JCQ	CONTINUITY LINE NUMBER FOR TOTAL FLOW	BQ
JCH	CONTINUITY LINE NUMBER FOR HEAD BOUNDARY	BH
JCR	CONTINUITY LINE NUMBER FOR RATING CURVE	RC
LI	THE NUMBER OF ITERATIONS BETWEEN CHECKS FOR DRY NODE	DE
LINE	CORNER NODE NUMBERS FOR CONTINUITY CHECK	GC
LMT	TOTAL NUMBER OF CORNER NODES ON A GIVEN CONTINUITY LINE	GC
MBAND	RESTART IN MID-ITERATION FLAG	TZ
METRIC	SYSTEM INTERNATIONAL FLAG	SI
MND	PARAMETER - MAXIMUM NODE NUMBER - specified in HSCTM.H file.	
MCC	PARAMETER - MAX CONTINUITY CHECK LINES - specified in HSCTM.H file.	
MWDC1	MAXIMUM DEPTH SHIFT OF MARSH CHANNELS BELOW MEAN MARSH ELEVATION	DM
MWDC2	DEPTHS RANGE BETWEEN MARSH CHANNEL AND MAXIMUM MARSH ELEVATIONS	DM
MWDC3	FREQUENCY ASSOCIATED FOR LOWER SECTION	DM
MWDC4	MINIMUM DEPTH OF MARSH CHANNELS	DM
NBX	NUMBER OF NODES WITH BOUNDARY CONDITIONS SPECIFIED	G1,BCC

(continued)

Table C.2 (continued)

<u>Variable</u>	<u>Description</u>	<u>Card</u>
NCFLW	NUMBER OF FLOW CONTROL STRUCTURES	FC
NCYC	NUMBER OF TIME STEPS SIMULATED	TZ
NFIX	ARRAY CONTAINING LOGIC FLAGS FOR BOUNDARY CONDITION	BCN,BA-BH
NFIXH	REORDERING LIST	GO
NITI	NUMBER OF ITERATIONS FOR INITIAL SOLUTION - (OR STEADY STATE COMPUTATION)	TI
NITN	NUMBER OF ITERATIONS FOR EACH DYNAMIC COMPUTATION	TI
NJN	FLOW CONTROL STRUCTURE IDENTIFIER IMAT	FC
NJTI	FLOW CONTROLLER TYPE	FC
NMAT	THE NUMBER OF DIFFERENT SETS OF TURBULENT EXCHANGE COEFFICIENTS AND CHEZY AND/OR MANNING COEFFICIENTS	EX,EY
NOP	NODAL POINT-ELEMENT CONNECTION TABLE FOR HYDRO2D	GE
NREF	NODAL POINT REFERENCE FOR STORMS	BWS
NSID	DYNAMIC COUNTER FOR NUMBER OF ELEMENTS FOR WHICH ELEMENT INFLOW IS DESIRED	BQ
NSPLPT	ARRAY CONTAINING NODES FOR SPECIAL PRINT	TRN
NSTART	STARTING TIME-STEP NUMBER USED TO SKIP THROUGH BOUNDARY CONDITION DATA FOR RESTART	TZ
OMEGA	LATITUDE OF MESH (APPROXIMATE AVERAGE)	G1,LAT
ORT	EDDY DIFFUSION AND N-VALUE ARRAY BY ELEMENT TYPE	EX,EY HN,EV

(continued)

Table C.2 (continued)

<u>Variable</u>	<u>Description</u>	<u>Card</u>
QF	TOTAL FLOW ALONG A CONTINUITY LINE	BQ
QDIR	FLOW DIRECTION ALONG CONTINUITY LINE	BQ
QTOT	TOTAL DISCHARGE (CFS) CROSSING A CONTINUITY LINE	BQ
QVEC	THE UNIT DISCHARGE (CFS/FT)	BQ
RON	THE ARRAY OF NODAL FLUID DENSITY	FD
SIDF	ELEMENT INFLOW (PER UNIT AREA)	BQ
SPEC	ARRAY CONTAINING BOUNDARY CONDITION SPECIFICATIONS	BCN, BA-BH
SS1	LEFT SIDE SLOPE FOR ONE DIMENSIONAL NODES	GW
SS2	RIGHT SIDE SLOPE FOR ONE DIMENSIONAL NODES	GW
SSDCRT	STEADY STATE SATISFACTORY DEPTH CRITION	TI
SSWSE	STEADY STATE WATER SURFACE ELEVATION	BRC
TAX	WIND DIRECTION (DEGREES COUNTERCLOCKWISE FROM + X-AXIS)	BW
TBINRY	ARRAY CONTAINING USER SELECTED HOURS TO SAVE TO BINARY FINAL RESULTS FILE	TO
TEMP	AVERAGE INITIAL WATER TEMPERATURE	FT
TH	AZIMUTH OF X-DIRECTION OF AN ELEMENT FOR SPECIFYING EDDY DIFFUSION COEFFICIENTS	GE,GV
THETA	DIRECTION OF FLOW (RADIAN MEASURED COUNTERCLOCKWISE)	BQ,BRA BRC
THETAK	ORIENTATION OF STORM	BWS
THETAS	DIRECTION OF STORM TRACK	BWS

(continued)

Table C.2 (concluded)

<u>Variable</u>	<u>Description</u>	<u>Card</u>
TITLE	CHARACTER IDENTIFIER FOR THE RUN AND ALL OUTPUT FILES	T1-T3
TMAX	TOTAL TIME IN DECIMAL HOURS	TZ
TREF	HYDRO2D SIMULATION TIME OF STORM ARRIVAL AT 'NREF'	BWS
TWX	WIND SPEED	BW
UNOM	INITIAL VELOCITY FOR ONE DIMENSIONAL ELEMENTS	IC
USERCA1	USER SELECTED VARIABLE FOR TEMPORAL DERIVATIVE CALCULATION	CA
USDCRT	DYNAMIC SATISFACTORY DEPTH CRITON	TI
VWEC#	CURRENT SPEED (FPS) AT A NODE	BS
WC1	WIND CONTROL COEFFICIENT	BWC
WC2	WIND CONTROL COEFFICIENT	BWC
WC3	WIND CONTROL COEFFICIENT	BWC
WC4	WIND CONTROL COEFFICIENT	BWC
WIDTH	CHANNEL WIDTH FOR ONE DIMENSIONAL NODES	GW
WIDS	STORAGE WITH ASSOCIATED 1D NODE	GW
WINDMN	MINIMUM WIND SPEED (MPH)	BWS
WINDMX	MAXIMUM WIND SPEED (MPH)	BWS
XSCALE	SCALE FACTOR FOR X-COORDINATES	G1
ZMANN	MANNING N-VALUE ASSIGNED BY ELEMENT NUMBER	HN
ZSCALE	SCALE FACTOR FOR Z-COORDINATES	G1

C.3 Input Data Cards Description

T1-T3 Cards **Job Title** **T1-T2 - Optional**
T3 - Required

A 'T' card must be the first user input card in the boundary condition file for HYDRO2D. Any number of T1 and T2 cards may be used and sequence is not significant. Only one T3 card may be used, and it must be the last title card in the set. The program reads the "3" as meaning END OF 'T' CARDS.

<u>Field</u>	<u>Variable</u>	<u>Value</u>	<u>Description</u>
0, C1	IC1	T	Card group identifier
0, C2	IC3	1,2,3	
1-10	TITLE	Any	Any alpha-numeric data, up to 77 characters.

\$F Card **Formatted or Free Field Input** **Optional**

Card is required for formatted input data. Card must be left out for free field input.

<u>Field</u>	<u>Variable</u>	<u>Value</u>	<u>Description</u>
0, C 1-2	IC1	\$F	Card group identifier
			Specifies fixed field (formatted) run control input

\$L Card **I/O Data Logical Unit Numbers** **Required**

Card image data described in these pages are read from logical unit# 2 and the ECHO PRINT is (LU) 6.

<u>Field</u>	<u>Variable</u>	<u>Value</u>	<u>Description</u>
0, C 1-2	IC1	\$L	Card group identifier
1	NB		Logical unit for HOTSTART input
		0	Initial conditions for HYDRO2D will be coded in this data set.
		+	Initial conditions will be read from logical unit #63 - a HOTSTART is required.
2	NLL		Logical unit for HOTSTART output
		0	No HOTSTART file will be written.
		+	HYDRO2D will write a HOTSTART file on unit #62.

3	IFILE		Logical unit for GFGEN geometric data.
		0	All geometry will be coded in the HYDRO2D data set.
		+	GFGEN's geometric data will be opened in unit #60.
4	NOPT		The logical unit for HYDRO2D binary final results of hydraulic calculations.
		0	HYDRO2D will not save results
		+	HYDRO2D will write results for each time step on unit #64.
5	IBUP		The logical unit on which alternate dynamic boundary conditions will be input to HYDRO2D.
		0	No alternate BC file.
		+	Separate BC file will be read from unit #61.
6	IOUT		The logical unit for HYDRO2D standard printout.
		0	No full printout will be created
		+	Full printout will be created on unit #3.
7	ISPLPT		The logical unit for the summary print by node option.
		0	No special list of nodes printed
		+	Special printout created on unit #59. (TRN-card(s) required)

\$M-Card

Machine Identifier

Optional

<u>Field</u>	<u>Variable</u>	<u>Value</u>	<u>Description</u>
0, C 1-2	IC1	\$M	Card group identifier
1	ICOMID	+	Controller for record length and word size for front solver buffering. = 1 Micro with Definicon 032 Board Direct access record length unlimited and defined in terms of bytes. = 2 Prime Mini-Computer Direct access record length unlimited and defined in terms of small words (i.e., 2 bytes). = 3 Dec VAX Direct access record length. Limited to 32K bytes and defined in terms of long words (4 bytes) = 4 Apple MAC II using ABSOFT Fortran Definicon 020 Board, or Dec Vax to avoid short record limit. = 5 Cray or Cyber-205 Direct access defined for systems using 64 bit or 8 byte words and where record lengths are defined in bytes.

NOTE: If no \$M-card is supplied, ICOMID=4 by default.

CA Card **Special Calculation Variables** **Optional**

<u>Field</u>	<u>Variable</u>	<u>Value</u>	<u>Description</u>
0, C 1-2	IC1	CA	Card group identifier
1	USERCA1		Variable to calculate temporal derivative
		-,0 +	1.6 = default used if USERCA1 < 0 or if no CA-card is supplied. 1.5 = second order Taylor Series expansion.

CO Card **Comments** **Optional**

Comments may be supplied on this card anywhere within the run control input except as the first or last card types.

<u>Field</u>	<u>Variable</u>	<u>Value</u>	<u>Description</u>
0, C 1-2	IC1	CO	Card group identifier
1-10	FLD	A	Any alpha-numeric data

DE Card **Wet/Dry by Elemental Elimination** **Optional**

<u>Field</u>	<u>Variable</u>	<u>Value</u>	<u>Description</u>
0, C 1-2	IC1	DE	Card group identifier
1	DSET		Depth below which nodes are dry. If DSET = 0, Default is 0.275 ft or 0.084 m. NOTE: This variable is involved in the criterion for sufficient depth and velocity convergence to allow the code to advance to the next dynamic time-step before variable NITN on Toward is satisfied. If the maximum X- or Y-velocity change is less than 0.5 times DSET, and if the maximum depth change is less than DSET, the code advances to the next dynamic time-step.
2	DSETD		Depth above which nodes become active when rewetting. If DSETD=0, Default is 0.60 ft or 0.183 m
3	LI		Iteration frequency of testing for wetting and drying. Set LI=0 to prevent wet/dry testing. (default=0) Typically LI is a positive number which is a multiple of the interaction counter.

Set LI=99 or a large number to permit checking only at end of a time step

NOTE: Defaults are appropriately converted for SI units. If no DE-Card is present, defaults are used.

DM Card	Wet/Dry by Marsh Porosity (See Figure C.1 for parameter definition)		Optional
<u>Field</u>	<u>Variable</u>	<u>Value</u>	<u>Description</u>
0, C 1-2	IC1	DM	Card group identifier
0, C3	IC3	b N E T	Option 1: IDNOPT Option 2: For node = J Option 3: For element = J Option 4: For IMAT = J
1	J	-,0,+	For option 1, J = IDNOPT J = 0 Marsh option inoperative All DM Cards are ignored J = -1 Use given default values for all nodes J = -2 User specifies values for all nodes J = + User specifies values for all nodes > J For option 2, code the node number For option 3, code the element number For option 4, code the IMAT number
2	AC1	+	Depth shift (Default = 3.0 ft or 0.91 m)
3	AC2	+	Depth range over which section reduces (Default = 2.0 ft or .61 m)
4	AC3	+	Minimum active fraction over lower section (Default = .02)
5	AC4	+	Absolute bottom elevation of the marsh channels (optional)

DMb (DM blank) card is required, then optionally followed by DMT, DME, or DMN cards. If a node receives multiple assignments, the last assignment is processed.

NOTE: Defaults are automatically converted to metric if SI-card indicates SI units.

EV Card Turbulent Exchange Coefficients and Manning's N**Required
if HN, EX, or EY
not used**

Turbulent exchange coefficients should be coded by element type. In equation notation the value for E_{xx} , E_{xy} , E_{yx} , E_{yy} and Manning's n are coded on this card.

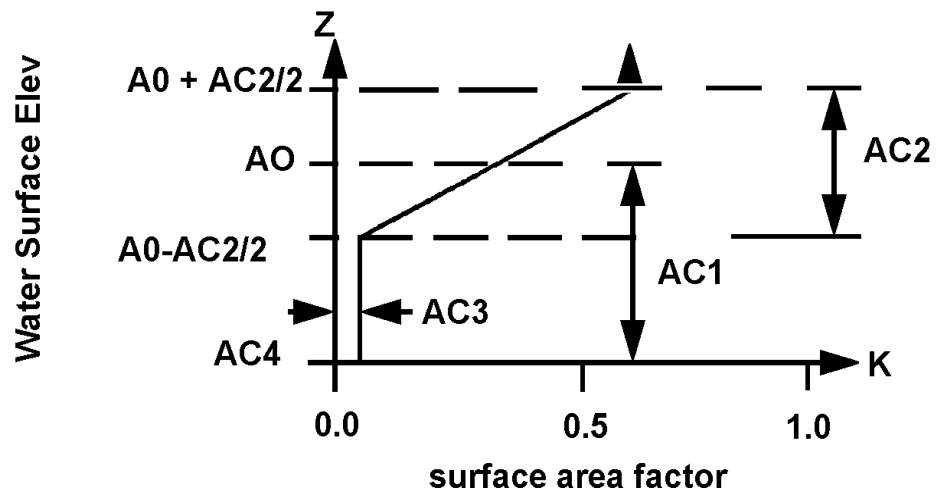
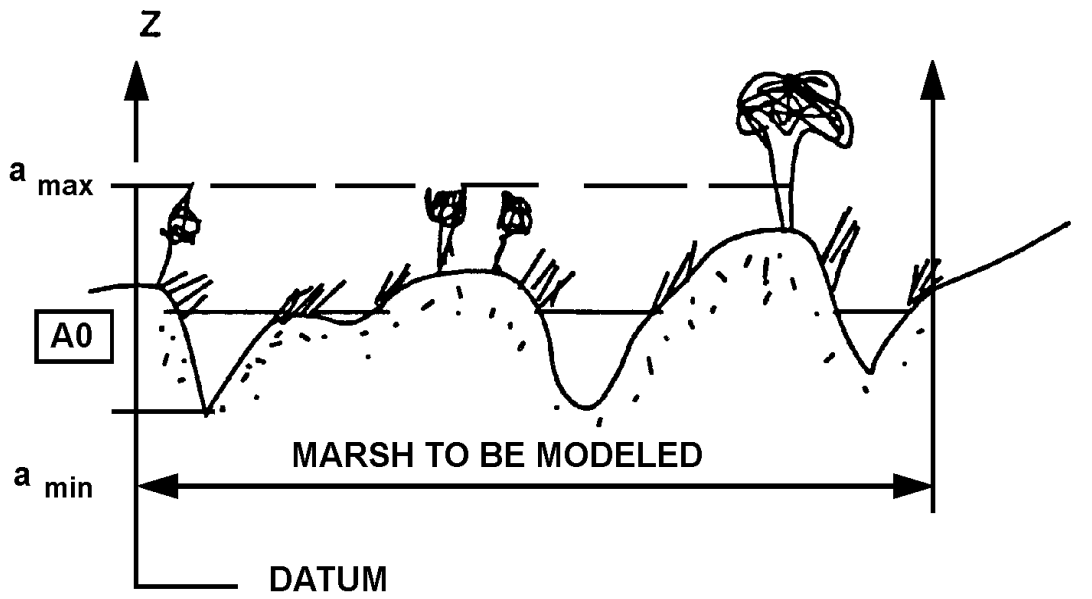
<u>Field</u>	<u>Variable</u>	<u>Value</u>	<u>Description</u>
0, C 1-2	IC1	EV	Card group identifier
1	J	+	Element type number for the set of turbulent exchange coefficients (IMAT)
2	ORT(J,1)	+	E_{xx} = x-momentum turbulent exchange in x-direction (lb-sec/ft ² or Pascal-sec for SI-units)
3	ORT(J,2)	+	E_{xy} = x-momentum turbulent exchange in y-direction (lb-sec/ft ² or Pascal-sec for SI-units)
4	ORT(J,3)	+	E_{yx} = y-momentum turbulent exchange in x-direction (lb-sec/ft ² or Pascal-sec for SI-units)
5	ORT(J,4)	+	E_{yy} = y-momentum turbulent exchange in y-direction (lb-sec/ft ² or Pascal-sec for SI-units)
6	ORT(J,5)	+	Manning's Coefficient (or Chezy if ORT(J,5) > 3.0)

Recall the formula for Peclet numbers (P), where P is recommended to be less than 20.

$$P = \frac{u \, dx}{E} \quad (1.94)$$

where:

- u = stream wise velocity (fps)
- dx = length of element in stream wise direction (ft)
- E = eddy viscosity (lb-sec/ft²)
- 1.94 required for non-SI calculation



- Where
- AO = bottom elevation from GFGEN ($AO = a$)
 - AC1 = bottom elevation offset
 - AC2 = transition range of the distribution ($a_{max} = AT$) ($a_{min} = AB$)
 - AC3 = minimum surface width factor
 - AC4 = optional override bottom elevation for a min (if not specified, $AC4 = AO - AC1$)

Figure C.1. Marsh Porosity surface assignments.

EX Card**Turbulent Exchange Coefficient, X-Velocity****Required
if EV not used**

Turbulent exchange coefficients should be coded by element type. In equation notation the value for E_{xx} and for E_{xy} are coded on this card. Values for E_{yx} and E_{yy} are coded on the EY-cards.

<u>Field</u>	<u>Variable</u>	<u>Value</u>	<u>Description</u>
0, C 1-2	IC1	EX	Card group identifier
1	J	+	Element type number for the set of turbulent exchange coefficients (IMAT)
2	ORT(J,1)	+	E_{xx} = x-momentum turbulent exchange in x-direction (lb-sec/ft ² or Pascal-sec for SI-units)
3	ORT(J,2)	+	E_{xy} = x-momentum turbulent exchange in y-direction (lb-sec/ft ² or Pascal-sec for SI-units)

EY Card**Turbulent Exchange Coefficient, Y-Velocity****Required
if EV not used**

Turbulent exchange coefficients should be coded by element type. In equation notation the value for E_{yy} and for E_{yx} are coded on this card. Values for E_{xx} and E_{xy} are coded on the EX-cards.

<u>Field</u>	<u>Variable</u>	<u>Value</u>	<u>Description</u>
0, C 1-2	IC1	EY	Card group identifier
1	J	+	Element type number for the set of turbulent exchange coefficients (IMAT)
2	ORT(J,3)	+	E_{yx} = y-momentum turbulent exchange in x-direction (lb-sec/ft ² or Pascal-sec for SI-units)
3	ORT(J,4)	+	E_{yy} = y-momentum turbulent exchange in y-direction (lb-sec/ft ² or Pascal-sec for SI-units)

END Card**End Card****Optional**

This card signals the end boundary condition input for a given timestep.

<u>Field</u>	<u>Variable</u>	<u>Value</u>	<u>Description</u>
0, C 1-2	IC1	EN	Card group identifier
0, C 3	IC3	D	Card type identifier
1-10	FLD	A	May be used for comments

FC Card	Flow Control Structures		Optional
<u>Field</u>	<u>Variable</u>	<u>Value</u>	<u>Description</u>
0, C 1-2	IC1	FC	Card group identifier
1	NJN	+	Flow controller identifier (imats >=904)
2	NJTI	+	Flow controller type
		= 1	Point source of flow, conditions are flow out equals flow in plus source (FLZ3), and equal total head at each node of the control element.
		= 2	Flow is a reversible function of head loss across the structure, conditions are flow out equals flow in, and flow $Q=FLZ3+FLZ4*(HN1-HN2-FLZ5)**FLZ6$ in the direction FU7, where HN1 and HN2 are water surface elevations at the nodes of the control structure element. Note that if HN1-HN2 is negative, the sign of the flow direction is reversed.
		= 3	Flow is a irreversible function of head loss across the structure, conditions are flow out equals flow in, and flow $Q = FLZ3 + BJ1*(HN1-HN2-FLZ5)**FLZ6$ in the direction FLZ7, where HN1 and HN2 are water surface elevations at the nodes of the control structure element. Note that if HN1-HN2-FLZ5 is negative, then Q=0.
		= 4	Flow is a function of water surface elevation, conditions are flow out equals flow in, and flow $Q = FLZ3 + FLZ4*(HN1-FLZ5)**FLZ6$ in the direction FLZ7, where HN1 is the water surface elevation at the first node of control structure element.
		= 5	Head loss is a function of flow conditions are flow out equals flow in, and flow $HN1-HN2 = FLZFLZ4-(Z)*-FLZ6$ in the direction FLZ7 where HN1 and HN2 are the water surface elevations at the nodes of the Control structure element.
3	FLZ3		Base flow
4	FLZ4		Relational coefficient
5	FLZ5		Reference elevation or head difference
6	FLZ6		Exponent
7	FLZ7		Direction of flow (radians, counterclock-wise from + x-axis)

FD Card	Fluid Density		Optional
<u>Field</u>	<u>Variable</u>	<u>Value</u>	<u>Description</u>
0, C 1-2	IC1	FD	Card group identifier

0, C3	IC3	b	Option 1: Universal assignment for all nodes
	N		Option 2: Assignment by individual node
1	J1	+	Node
2	RON(J1)	+	Fluid density at node J1 (slugs/ft ³ or kg/m ³ for SI-units)

NOTE: If no FD card is present, 1.935 slugs/ft³ is used. For SI-units, 998.46 kg/m³ is used.

FT Card	Water Temperature		Optional
<u>Field</u>	<u>Variable</u>	<u>Value</u>	<u>Description</u>
0, C 1-2	IC1	FT	Card group identifier
1	TEMP	+	Average initial water temperature (degrees Celsius)

NOTE: If no FT-card is present, 15° C is used.

G1 Card	Grid, General Geometry Parameters		Optional
<u>Field</u>	<u>Variable</u>	<u>Value</u>	<u>Description</u>
0, C 1-2	IC1	G1	Card group identifier
1	OMEGA	+	Local average latitude degrees, used in calculating the Coriolis forces.
		0	Default is OMEGA = 0 to turn off Coriolis.
2	XSCALE	+	Scale factor for X-coordinates.
		-,0	Default is 1.0
3	ZSCALE	+	Scale factor for Y-coordinates.
		-,0	Default is 1.0
4	NBX	0,+	Number of nodes with boundary conditions specified with BCN-Cards.
			Default NBX=0 and program will self-count.

NOTE: If no G1-Card is present, no Coriolis is applied, coordinate scale factors are 1.0, and BCN-cards are self counted.

GC Card**Continuity Check Line Calculation****Optional**

Flow continuity can be calculated at up to 100 lines across part or all of the grid. Up to 50 corner nodes per line. Prescribe the boundary line first since that line is used in calculating the percents displayed on all subsequent lines. Code corner nodes only. Code all lines in the same direction; otherwise, sign changes will occur in the printout. In general, code right to left when facing downstream. The first list should be the inflow boundary because it will be assumed to be 100%.

<u>Field</u>	<u>Variable</u>	<u>Value</u>	<u>Description</u>
0, C 1-2	IC1	GC	Card group identifier
1	LMT(K)	+	Total number of nodes to be listed for continuity line (K)
2	LINE(K,J)	+	Corner node number 1, ... total number.

If a continuation card is needed (> 8 numbers in formatted input), start in field 1 of next GC card (maximum of 50 nodes per check line).

GE Card**Grid, Element Connection Table****Optional**

The element connection table will usually be provided by the GFGEN pre-processor and will reside on logical unit 60. If so, this card should be omitted, unless small mesh revisions are required. Otherwise, code the Nodal Point-Element Connection Table.

<u>Field</u>	<u>Variable</u>	<u>Value</u>	<u>Description</u>
0, C 1-2	IC1	GE	Card group identifier
1	J	+	Element number
2-9	NOP(J,I)	+	Up to 8 node numbers for element J, listed counterclockwise around the element starting from any CORNER.
10	IMAT(J)	+	Element type (optional, may be specified on GT card)
11	TH(J)	-,0,+	Direction of eddy viscosity tensor (optional, may be specified on GV card) (Radians, counterclockwise from x-axis).
			For 1-D elements, the direction is automatically aligned with the orientation of the 1-D element.

NOTE: In order to place TH(J) on GE-card, you must be using free field input option. Otherwise, use the GV-card in combination with or without a GE-card.

GN Card**Grid, Nodal Point Coordinates****Optional**

The coordinate values read are multiplied by the appropriate scale factors, XSCALE and ZSCALE from G1-CARD, and will be in the proper X- (and Y-) and Z-coordinates (feet or meters) after transformation.

<u>Field</u>	<u>Variable</u>	<u>Value</u>	<u>Description</u>
0, C 1-2	IC1	GN	Card group identifier
0, C3	ISI	b	Option 1: Code X and Y coordinates only
		N	Option 2: Code X and Y coordinates and bed bottom elevations (as in GFGEN)
1	J	+	Node number
2	CORD(J,1)	-,0,+	X-coordinate
3	CORD(J,2)	-,0,+	Y-coordinate
4	AO(J)	+	Bottom elevation (option 2 only)
Continue for 1D nodes only:			
5	WIDTH	+	Channel width at zero depth for NODE
6	SS1	-,+	Left side slope at NODE
7	SS2	-,+	Right side slope at NODE
8	WIDS	+	Storage width associated with NODE at zero depth

GT Card**Grid, Element Types****Optional**

<u>Field</u>	<u>Variable</u>	<u>Value</u>	<u>Description</u>
0, C 1-2	IC1	GT	Card group identifier
1	J	+	Element number
2	IMAT(J)	0,+	Element type
3-10		+	Need as many (J, IMAT(J) sets) as GE Cards present. If > 4 sets, use continuation cards and start in Field 1.

NOTE: If HMIN and UNOM are specified with the elemental wet-dry option activated (DE card), then no wet-dry checks will occur first iteration. HMIN and UNOM are unused for fully 2D networks.

LAT Card		Local Latitude		Optional
<u>Field</u>	<u>Variable</u>	<u>Value</u>	<u>Description</u>	
0, C 1-2	IC1	LA	Card group identifier	
C3	IC3	T	Card type identifier	
1	IMAT	+	Element material type	
2	OMEGA	+	Latitude in degrees for the IMAT (Set OMEGA=0 to turn off Coriolis)	

NOTE: It desired you may fill the card with (IMAT, OMEGA) sets, or use more LAT Cards. Latitude (Coriolis) may be globally assigned on the G1-Card).

REV Card **Revise the Current Time Step** **Optional**

This card signals the HSCTM-2D model to solve for the current time step. However, additional iterations for the current time step will be made with revised boundary conditions and/or coefficients. See the examples below.

<u>Field</u>	<u>Variable</u>	<u>Value</u>	<u>Description</u>
0, C 1-2	IC1	RE	Card group identifier
1	IC3	V	Card type identifier
2-10	FLD	A	May be used for comments

Example:

```

T3
$M
$L
EV 1 500 500 500 500 0.03
TI 4 0 .01
BQL 6 50000. -1.2
BHL 7 100.
REV Now lower coefficients and increase Q for 2 iterations
TI 2 0 0.01
EV 1 300 300 300 300 0.027
BQL 6 75000. -1.2
REV Now lower coefficients more and increase Q
EV 1 150 150 150 150 0.025
BQL 6 100000. -1.2
END

```

STO(P) Card**Stop the HYDRO2D Simulation****Optional**

This card signals the end of all computation after the current time step has been completed.

<u>Field</u>	<u>Variable</u>	<u>Value</u>	<u>Description</u>
0, C 1-2	IC1	ST	Card group identifier
1	IC3	O	Card type identifier
2-10	FLD	A	May be used for comments

TI Card**Number of Iterations****Required**

<u>Field</u>	<u>Variable</u>	<u>Value</u>	<u>Description</u>
0, C 1-2	IC1	TI	Card group identifier
1	NITI	0,+	Number of iterations for initial solution
2	NITN	0,+	Number of iterations for each dynamic time-step(s)
3	SSDCRT	0,+	User specified criterion for satisfactory depth convergence during steady state. DEFAULT= DSET*0.5 from DE Card
4	USDCRT	0,+	User specified criterion for satisfactory depth convergence during unsteady (dynamic). DEFAULT = DSET*0.5 from DE Card

NOTE: If the user want the depth criterions to be based on 'DSET', then the DE-card must precede the TI-Card.

TO Card**Time for Saving the Binary Results Output File****Optional**

<u>Field</u>	<u>Variable</u>	<u>Value</u>	<u>Description</u>
0, C 1-2	IC1	TO	Card group identifier
1-10	TBINARY(J)	-,0,+	Time in decimal hour(s) at which the user wants to save final results to the binary file (Defined on \$L-card variable NOPT)
			Continue to list times until the card is full, then continue the list with another TO Card.

NOTE: If no TO Card is specified, all time steps are written to the binary file.

TR Card	Trace Printout Control			Required
<u>Field</u>	<u>Variable</u>	<u>Value</u>	<u>Description</u>	
0, C 1-2	IC1	TR	Card group identifier	
1	IPRT	0 1 2 3	Control for output printing: Node and element input data suppressed All input data printed except initial conditions Initial conditions from restart Manning's n-value table	
2	ITSI	+1 +2 +3 Etc. -1 -2 -3 Etc.	No. of iterations/time-steps between successive prints All iterations are printed Every other iteration Every third iteration Every time-step (last iteration only) Every other time-step (last iteration) Every third time-step (last iteration)	
3	IECHO	0 1 2	Switch to control HEC card input data echo No input data echo (default) Run control input is echoed Option 1 plus other diagnostics echoed	
4	ISPRTN	-, 0	Switch for print summary by node De-activate the option (even if TRN cards are present)	
5	ITRACE	0 1-2	Trace subroutine calls and controllers (for debug purposes only) No trace Degree of detail increases with the choice	

TRN Card	Nodal List for Special Summary Trace Printout			Optional
<u>Field</u>	<u>Variable</u>	<u>Value</u>	<u>Description</u>	
0, C 1-2	IC1	TR	Card group identifier	
C3	IC3	N	Card type identifier	
1-10	NSPLPT(J)	+	List of node numbers for special print summary List nodes until the card is full, then continue the list with another TRN card.	

2	ALFAK(J1)	+	The angle at node J1, in degrees or decimal of a degree, of the velocity vector (or unit discharge vector). Grid orientation is defined on GE-card.
3	J2	+	Another boundary node number (if desired)
4	ALFAK(J2)	+	The angle at node J2
5-10	etc.		Continue coding node and angles until the card is full, then use another BA-card.

NOTE: Either BC-cards or comparable data on BA through BRC cards is required.

BCC Card Boundary Condition Control Parameters Optional

The parameters on this card are necessary if and only if the user wishes to revise the boundary condition update parameters between dynamic time steps. If this card is present for steady state, the boundary condition parameters specified on previous cards (TZ, G1, and BW) will be overruled.

<u>Field</u>	<u>Variable</u>	<u>Value</u>	<u>Description</u>
0, C 1-2	IC1	BC	Card group identifier
0, C 3	IC3	C	Card type identifier
1	DELTA	+	The delta time step length in decimal hours (DELTA is revised only if the value > 0)
2	NBX	0,+	The number of nodes for which boundary conditions are specified on BCN cards. If zero, the program will self-count the number of BCN cards for this time step (if and only if END card is used)
3	IWIND	-,0,+	Control for wind field input. Please reference BW-blank card for IWIND values.

BCN Card Nodal Boundary Conditions Optional

The three required boundary conditions (BCN) parameters can be coded on this card type: U-velocity, V-velocity, and head. In addition, a five-digit number that tells the program the parameter type is coded as well as the nodal point number. Code one BCN set for each boundary node. Both corner and mid-side boundary nodes require boundary conditions.

<u>Field</u>	<u>Variable</u>	<u>Value</u>	<u>Description</u>
0, C 1-2	IC1	BC	Card group identifier
0, C 3	SI	N	Sets the BC at the specified node number

1	J1	+	The node or continuity check line number as indicated by the value of IC3
---	----	---	---

For Option 2:

2	SPEC(J1)	-,0,+	Water-surface elevation (ft or m) for node J1
---	----------	-------	---

For Option 3:

2	HFX(J1)	0,+	Water surface elevation (ft or m) for the continuity line J1
---	---------	-----	--

BQ Card

Boundary Discharge

Optional

This card type can be used instead of the BS-cards. The program will assign NFIX as 13x00 or 31x00 where the x denotes the values to be assigned by BH card data.

<u>Field</u>	<u>Variable</u>	<u>Value</u>	<u>Description</u>
0, C 1-2	IC1	BQ	Card group identifier
0, C 3	IC3	b	Option 1: Use the unit discharge in Field 2 and 3 for all boundary nodes equal to or greater than J1 in Field 1.
		N	Option 2: The node number i for inflow value.
		E	Option 3: The element number for element side inflow.
		L	Option 4: The continuity line number for inflow value.
1	J1	+	The node, element, or continuity line number as indicated by the value of IC3
Options 1 and 2 Only:			
2	QVEC	-,0,+	The unit discharge, (cfs/ft), at J1. The program will calculate QU- and QV-unit discharge vectors from QVEC by using the azimuth given on the BA-card. NFIX is automatically set to 3. The sign of the QU- and QV- is calculated from azimuth and grid orientation (BA-card).
Option 3 Only:			
2	SIDF	-,0,+	The element inflow per unit area or length as appropriate to the element.
Option 4 Only:			
2	QTOT	0,+	The total flow (cfs) crossing the continuity line
3	THETA	-,0,+	Direction of flow (radians measured counterclockwise from + x-axis). Note that the program adjusts the boundary directions to maintain parallel flow.

For BQ options 1 or 2, the card may be filled with node and QVEC paired values. FOR BQ option 3, the card may be filled with element and SIDF paired values. For BO option 4, the card may be filled with continuity line number, OTOT, and THETA groupings. However, if you prefer, one value per card is also permitted.

NOTE: Either BC-cards or comparable data on BA through BRC cards is required. If specifying discharge along a continuity line, the continuity line must extend from bank to bank.

BRA Card **Boundary, Reflection/Absorption** **Optional**

The special reflecting or non-reflecting rating curve which supplies a discharge to HYDRO2D using the following equation:

$$Q = A1 + A2 * (ELEV - E_o)$$

NOTE: E_o in this equation will be supplied after the steady state solution has been computed. Best results are obtained if this feature is only applied to a continuity line of a 1-D element.

<u>Field</u>	<u>Variable</u>	<u>Value</u>	<u>Description</u>
0, C 1-2	IC1	BR	Card group identifier
0, C 3	IC3	A	Data type identifier
1	ICON	+	Continuity line number
2	AC1X	-,0,+	A1 in the above eqn, Total Discharge ft ³ /sec or m ³ /sec
3	BETA	-,0,+	Reflection/Absorption coefficient used to calculate A2 in the above eqn, where BETA = 1 is Total Reflection at boundary BETA = 0 is Total Absorption at boundary
4	SSWSE	-,+	The steady state solution for the water surface elevation of the first node on the specified continuity line number. If this value is less than or equal to zero, HYDRO2D will incorporate the steady state solution before advancing to dynamic. If HOTSTARTING a dynamic run, the user must supply SSWSE with at least 4 significant figures past the decimal.
5	THETA	-,0,+	Direction of flow into the mesh (radians measured counterclockwise). Note that the boundary directions are adjusted to maintain parallel flow.
6	TAREA	0,+	Surface area of tidal storage area beyond the boundary. Used in defining standing wave flows.

$$TAREA = Velocity_{max} * Across / R_{max}$$

$$\text{where } R_{max} = \Delta WSELV / \Delta T * 3600$$

BRC Card**Boundary, Rating Curve****Optional**

The rating curve supplies a discharge to HYDRO2D using the following equation: $Q = A1 + A2*(ELEV-E0)**C$

<u>Field</u>	<u>Variable</u>	<u>Value</u>	<u>Description</u>
0, C 1-2	IC1	BR	Card group identifier
0, C 3	IC3	C	Data type identifier
1	JCR	+	Continuity line number
2	AC1X	-,0,+	A1 in the above equation
3	AC2X	-,0,+	A2 in the above equation
4	AC3X	-,0,+	E0 in the above equation
5	AC4X	-,0,+	C in the above equation
6	THETA	-,0,+	Direction of flow (radians measured counterclockwise from positive x-axis). Note that the boundary directions are adjusted to maintain parallel flow.

BS Card**Boundary Current Speed****Optional**

The magnitude of the velocity vector is coded on this card type. The input data program will convert BS data to U- and V- velocity components using the azimuth on the preceding BA-card. Sign of the component is calculated from its azimuth and the specified grid orientation (G1-Card). NFIX is assigned a value of 11x00 at each node having a BS value where the x denotes a value to be assigned by presence of BH-card data.

<u>Field</u>	<u>Variable</u>	<u>Value</u>	<u>Description</u>
0, C 1-2	IC1	BR	Card group identifier
0, C 3	ISI	b	Use the boundary condition (BC) in Field 1 for all boundary nodes equal to or greater than Field 3.
		N	The node number is coded for each BC value on this card
1	J1	+	Node number
2	WEC1	0,+	Current speed in fps at node J1. Sign will be determined from the azimuth of the vector
3	J2	+	Next node
4	VVEC2	0,+	Current speed at node J2, ft/sec or m/sec

BWC Card**Boundary, Wind Control Formulation****Optional**

The BWC card followed by a BW type card for wind speed and direction is required if a wind field is to be applied in HYDRO2D.

<u>Field</u>	<u>Variable</u>	<u>Value</u>	<u>Description</u>
0, C 1-2	IC1	BW	Card group identifier
1	IWIND	-,0,+	Control for wind field input IWIND = 0 no wind input IWIND < 0 wind field specified for all nodes using one line of input (BW-blank card) IWIND > 0 wind field specified at each node.
Type of Wind Formula			
		ABS(IWIND) = 1	Original formulation
		ABS(IWIND) = 2	Van Dorn Formula with user supplied coefficients
		ABS(IWIND) = 3	Wu Formula with user supplied coefficients
		ABS(IWIND) = 4	Safaie Formula with user supplied coefficients
		ABS(IWIND) = 5	Ekman Formula with default coefficients
		ABS(IWIND) = 6	Generic Formula with user supplied coefficients
		ABS(IWIND) = 7	Van Dorn Formula default coefficients
		ABS(IWIND) = 8	Wu Formula with default coefficients
2	IWMX	0,1	Flag to identify the units of the wind speed (recorded at height=10 m). IWMX = 0 for miles/hour IWMX = 1 for meters/second
Specify Field 3-6 as Needed			
3	WC1		Fields 3-6 will be the necessary coefficients required for the wind formulation as defined by the variable IWIND above.
4	WC2		
5	WC3		
6	WC4		

----- Special Instruction -----

If ABS(IWIND) = 2 Van Dorn

- WC1 = 10 meters, Anemometer height
- WC2 = Smooth water wind stress coefficient
- WC3 = Rough water wind stress coefficient
- WC4 = Critical wind velocity for wave formulation (m/s)

If ABS(IWIND) = 3 WU Formula

WC1 = 10 meters, Anemometer height
 WC2 = Wind stress coefficient
 WC3 = Air Density
 If WC3 > 0.0 units should be g/cm³,
 If WC3 < 0.0 default of 0.001226 g/cm³ used
 (Dry air at 1 atm pressure and 15°C)
 WC4 = unused

If ABS(IWIND) = 4 Safaie Formula
 WC1 = Charnock's constant
 If WC1 < 0.0 default of 0.0332 used
 WC2 = Dynamic roughness in cm (no default)
 WC3 = Acceleration due to gravity (affects wind formula only)
 If WC3 > 0.0 units should be cm/s²
 If WC3 < 0.0 default value of 979.965 cm/s² used
 WC4 = Air density
 If WC4 > 0.0 units should be g/cm³
 If WC4 < 0.0 default value of 0.001226 g/cm³ used
 (Dry air at 1 atm pressure and 15°C)

If ABS(IWIND) = 6 Generic Formula
 WC1 = 10 meter, Anemometer height
 WC2 = Wind stress coefficient (no default)
 WC3 = Empirical exponent (no default)
 WC4 = Air density
 If WC4 > 0.0 units should be g/cm³
 If WC4 < 0.0 default value of .001226 g/cm³ used
 (Dry air at 1 atm pressure and 15°C)

If ABS(IWIND) = 1, 5, 7 or 8 then WC1, WC2, WC3, and WC4 should all be zero

BWS Card		Boundary, Wind Storm (see Figure C.2 for explanation)		Optional
<u>Field</u>	<u>Variable</u>	<u>Value</u>	<u>Description</u>	
0, C 1-2	IC1	BW	Card group identifier	
0, C 3	IC3	S	Card type identifier	
1	ISTYPE	+	Storm reference point (3 = Center)	
2	NREF	+	Reference node for storm track	
3	TREF	+	Reference HYDRO2D simulation time for storm to arrive at node 'NREF'	
4	SSPD	+	Storm speed, mph	
5	WNDMAX	+	Maximum wind speed, mph	

6	WINDMIN	+	Minimum or base wind level, mph
7	THETAS	+	Direction of storm track, degrees counterclockwise from positive x-axis toward which the storm is moving
8	THETAT	+	Orientation of from (0,180 deg) relative to x-axis in degrees counterclockwise
9	BETAL	+	Standard deviation of spatial distribution function in the direction of the storm's movement
10	BETAT	+	Standard deviation of spatial distribution function in the direction transverse to storm path
11	DECAY	+	Exponential temporal decay for windspeed (hr^{-1})

NOTE: Each BWS-Card creates a storm, you may run multiple storms (presently dimensioned to 2)

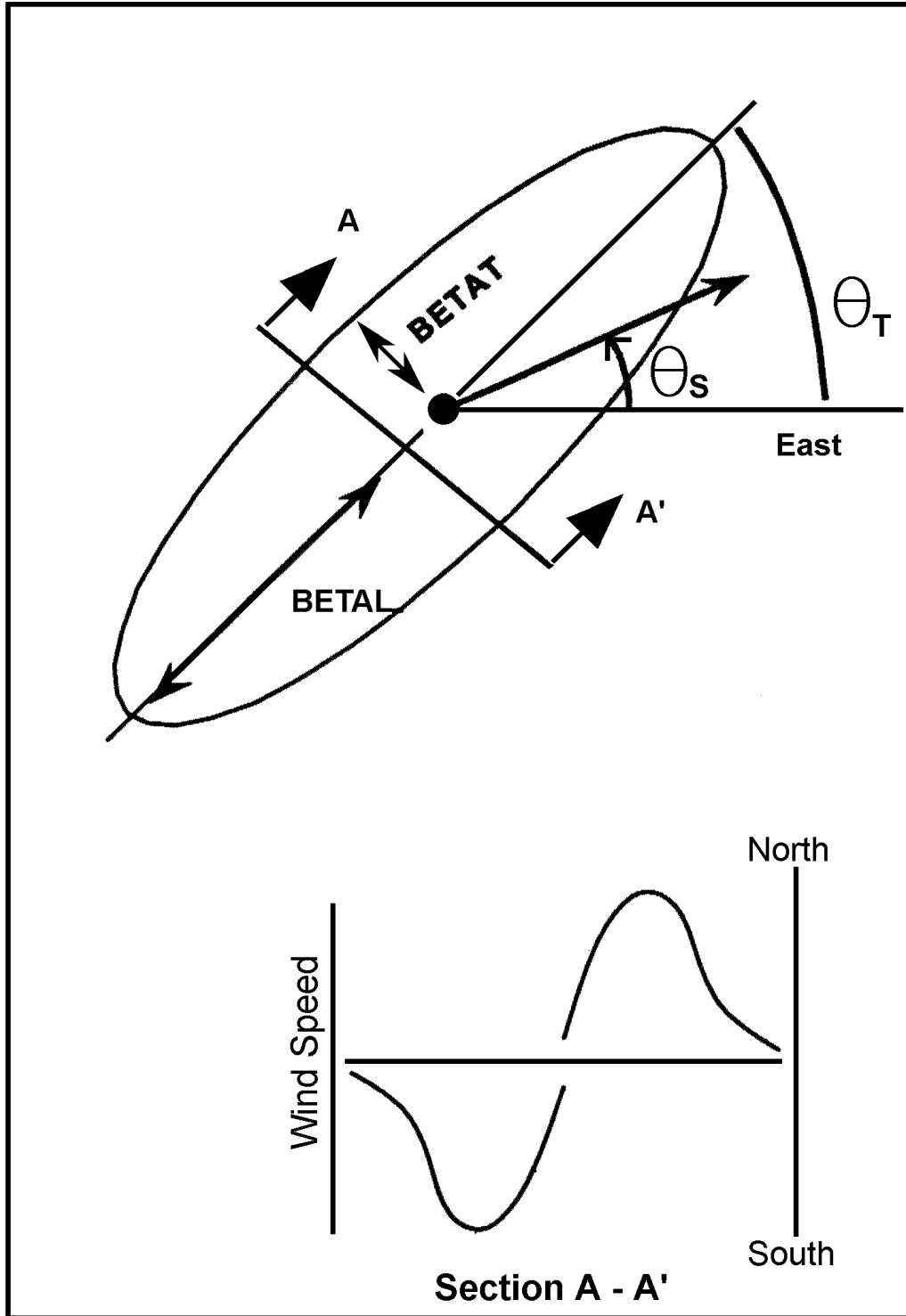


Figure C.2 Storm variable explanation.